QUIET CLEAN SHORT-HAUL EXPERIMENTAL ENGINE

(QCSEE)

Preliminary Analyses and Design Report

Volume I

October 1974

by

Advanced Engineering & Technology Programs Department

General Electric Company

Prepared For

National Aeronautics and Space Administration

NASA Lewis Research Center

Contract NAS3-18021

QUIET CLEAN SHORT-HAUL EXPERIMENTAL ENGINE

(QCSEE)

Preliminary Analyses and Design Report

Volume I

October 1974

FOREWORD

The Quiet Clean Short-haul Experimental Engine (QCSEE) Program is currently being conducted by the General Electric Company, Aircraft Engine Group under NASA Contract NAS3-18021. The preliminary design work was performed under the direction of the NASA Project Manager, Mr. Raymond J. Rulis, Lewis Research Center.

This report covers the preliminary design effort of under-the-wing (UTW) and over-the-wing (OTW) propulsion systems. Preliminary designs of experimental and flight versions of both propulsion systems were completed during the first six months of the contract, and an oral review of the designs was conducted at Lewis Research Center on June 25 and 26, 1974.

The preliminary design phase was approved by the NASA Project Manager on July 3, 1974, permitting the program to proceed through the detail design phase.

The report is covered in two volumes plus a separate appendix (Appendix B) containing information for government use only.

iii

TABLE OF CONTENTS

VOLUME I

TABLE OF CONTENTS (Continued)

VOLUME II

LIST OF ILLUSTRATIONS

LIST OF ILLUSTRATIONS (Continued)

xvii

LIST OF ILLUSTRATION (Continued)

LIST OF ILLUSTRATIONS (Continued)

LIST OF ILLUSTRATIONS (Continued)

LIST OF ILLUSTRATIONS (Continued)

LIST OF ILLUSTRATIONS (Continued)

LIST OF ILLUSTRATIONS (Concluded)

LIST OF TABLES

LIST OF TABLES (Continued)

LIST OF TABLES (Continued)

LIST OF TABLES (Continued)

LIST OF TABLES (Concluded)

SECTION 2.0

SUMMARY

The QCSEE Program has progressed through the planning and preliminary design phases, resulting in the definition of specific propulsion system configurations that are expected to meet all of the stated program objectives. This report describes the experimental propulsion systems to be built and tested in the program, as well as the ultimate flight systems that could grow out of the program in the post 1978 time period.

Certain compromises are planned to control cost of the experimental program. The contractor testing will be limited in duration with further testing to be conducted by NASA at Lewis Research Center. Also, material substitutions and "boiler plate" components are specified in certain areas to reduce program cost. However, these areas have been carefully selected such that these components will not adversely effect key technology areas.

2.1 PROGRAM OBJECTIVES

The major purpose of the QCSEE Program is to develop and demonstrate the technology required for propulsion systems for quiet, clean, and economically viable commercial short-haul aircraft. This comprehensive program includes the following objectives:

- To develop the propulsion system technology which will permit a short-haul aircraft, powered by four engines with a total installed thrust of 403,000 N (90,000 lb), to achieve the system noise goal of 95 EPNdB along a 152 m (500 ft) sideline and to minimize the ground area (footprint) exposed to objectionable noise levels.

- To demonstrate a propulsion system which will meet advanced pollution goals under all operating conditions.

- To develop the technology for very high bypass ratio engines with quiet low pressure ratio geared variable-pitch fans.

- To develop the technology required to meet propulsion system performance, control, weight, and operational characteristics.

- To develop the material, design, and fabrication technology for quiet propulsion systems which will yield engine designs which have an uninstalled thrust-to-weight ratio greater than 6 to 1; and installed thrust-to-weight ratios greater than 3.5 to 1.

- To develop the technology which will yield engine thrust response characteristics required for powered lift operations.

2

SECTION 1.0

INTRODUCTION

The Quiet Clean Short-haul Experimental Engine Program provides for the design, fabrication, and testing of experimental, high-bypass, geared turbofan engines and propulsion systems for short-haul passenger aircraft. The overall objective of the program is to develop the propulsion technology required for future externally blown flap types of aircraft with engines located both under-the-wing and over-the-wing. This technology encompasses the following elements:

- Variable-pitch and fixed-pitch fans
- Geared fans
- Low noise
- Low exhaust emissions
- High thrust-to-weight ratio
- Composite fan blades
- Composite fan frames
- Lightweight low drag nacelles
- Digital electric controls
- Thrust reverse means
- Rapid response
- Low fan pressure ratio, low fuel consumption cycles

- To provide the technology which will permit the design of quiet, efficient, lightweight thrust reversing systems for powered lift aircraft.

- To provide the technology to permit the design of integrated engine and nacelle installations which will be tolerant to aerodynamic distortion expected with operating flight conditions such as high cross-winds, large angles of attack, and side slip, and still provide good cruise performance.

- To provide the digital electronic engine control technology required to improve engine and fan pitch control, thrust response, operational monitoring, and to relieve the pilot's workload especially during powered lift flight operations in the terminal area.

2.2 SPECIFIC TECHNICAL OBJECTIVES

The following specific design objectives have been established for flight and experimental UTW and OTW propulsion systems:

2.2.1 Noise

The UTW and OTW experimental engines shall be designed to meet noise objectives on the basis of four-engined, 403,000-N (90,000-lb) thrust aircraft.

Takeoff and approach - 95 EPNdB @ 152 m (500 ft) SL

Max Reverse Thrust* - 100 PNdB @ 152 m (500 ft) SL

* 35% Max Forward thrust

The two conceptual flight design engines will meet these same noise objectives when installed on a typical short-haul commercial aircraft.

The design shall also minimize the acoustic footprints for both engines.

Methods for scaling engine noise, adjusting to flight conditions, and including wing/flap interaction effects are specified in Appendix A.

2.2.2 Pollution

The engines shall be designed to meet the exhaust emission standards specified for 1979 aircraft by the EPA.

2.2.3 Thrust-to-Weight

The experimental engines shall be designed to meet the following thrust and thrust-to-weight objectives.

3

	UTW		OTW	
	Uninstalled	Installed	Uninstalled	Installed
Thrust	81,000 N (18,300 lb)	77,200 N (17,400 lb)	93,200 N (21,000 lb)	90,000 N (20,300 lb)
Thrust/wt.	6.2	4.3	7.4	4.7

Uninstalled thrust includes all engine internal pressure losses up to the nozzle throat; installed thrust includes additional losses due to inlet ram recovery and core cowl scrubbing drag.

Uninstalled weight includes the dry weight of all engine components and engine accessories. Installed weight includes the following additions:

- Inlet and inlet anti-icing system
- Exhaust ducts, nozzles, and thrust reverser
- Fan duct and splitter
- Engine Mounts to interface with pylon
- Thrust Reverser and nozzle controls and hydraulic system
- Fire detection and extinguishing system
- Drains, vents, and oil cooler
- Instrumentation

Thrust/weight shall be representative of a flight engine design. This shall include analytical predicted flight weight of all boiler plate and nonflight design components.

2.2.4 Thrust Reversal

The UTW and OTW propulsion systems shall provide the following thrust reversal capability:

- Operation down to 5.144 m/sec (10 knots)
- Max. forward to max. reverse thrust transient in less than 1.5 seconds
- At least 35% static takeoff thrust in reverse
- Noise levels as specified in Section 2.2.1

2.2.5 Engine Bleed

The engines shall be capable of safely providing up to 13% engine core bleed.

2.2.6 Power Extraction

The engines shall be capable of supplying a minimum of 1640 W/4448 N (2.2 horsepower per 1000 lb) of installed thrust for customer takeoff power.

4

2.2.7 Dynamic Thrust Response

The engine thrust response shall be designed to meet an acceleration from 62% to 95% thrust in one second [sea level to 1830 m (6000 ft) altitude].

2.2.8 Distortion Tolerance

The engine shall be capable of satisfactory operation at inlet upwash angles of 0 to 50°, with 18 m/sec (35 knot) 90° crosswinds.

2.2.9 Oil Consumption

Engine oil consumption shall not exceed 0.906 kg/hr (2 lb/hr).

2.2.10 Dumping

No fuels or lubricants shall be dumped.

2.2.11 General Design Criteria

In addition to the specific objective listed above, the flight engines shall meet the following general criteria:

1. The propulsion system shall be designed for ground static, wind tunnel, and altitude chamber operation.

2. The propulsion system shall be designed for flight operation except in specific areas where nonflight hardware can be used to save costs.

3. Propulsion system characteristics, such as temperatures, specific fuel consumption, and overall pressure ratio shall be selected to be appropriate for sh t-haul commercial aircraft.

4. All propulsion system components shall be designed for life which is compatible with expected commercial short-haul operation.

5. The propulsion system control system shall be designed with digital logic and signal paths capable of interfacing with an aircraft on-board flight digital computer. The control system shall be designed to provide selectable programmed power management and failure indication and/or corrective action over the entire propulsion system operating envelope.

6. The propulsio systems shall be designed with the objective of achieving high performance, but it is not essential that hardware development be carried to the point where ultimate performance is achieved for the experimental propulsion systems. The Contractor

5

shall show that his analytical extrapolation of performance data to a fully developed propulsion system is reasonably accurate, and that deviations in performance do not significantly affect acoustic or pollution characteristics of the experimental propulsion systems.

Nacelles shall be designed with the following features:

1. . accurate representation of external and internal aerodynamic contours of flight nacelles.

2. Accurate acoustic representation of flight-type designs.

3. All electrical, fuel, oil, cooling, fire detection and prevention, control, and instrumentaion systems required to test the propulsion systems.

4. Convenient access for maintenance.

The propulsion systems shall be designed for the following maintenance features:

1. The engine shall be easily removable from the nacelle without requiring removal of the fan exhaust duct once it is installed.

2. The engine shall be capable of being trimmed on a test stand with no additional trimming required if installed on an aircraft.

3. Accessories shall be located for easy inspection.

4. Access to borescope ports shall be provided without requiring removal of any engine component.

5. Any propulsion system accessory shall be replaceable in 45 minutes.

6. Fans shall have an even number of blades, and blades shall be capable of rapid inspection and replacement.

7. Modular construction is desired to facilitate maintenance.

The propulsion systems shall be designed to perform within the flight maneuver forces envelope per MIL-E-5007C data December 30, 1965, paragraph 3.14, with the exception of conditions of catapult flight maneuver and precession rates.

2.3 OPERATING REQUIREMENTS

The foregoing specific objectives and general criteria are further amplified by the following propulsion system operating requirements.

6

2.3.1 Life and Duty Cycle

The engines shall be designed for a useful life of 36,000 hours over a 15 year period, based on the typical 403 km (250 mile) mission cycle shown in Table 2-I.

Table 2-I. Flight Duty Cycle.

Segment	Altitude		Mach No.	% Power	Time (Min)	% Time
	km	ft				
Start	0	0	0	–	0.5	1.11
Idle-Taxi	0	0	0	4–20	3.1	6.89
Takeoff	0	0	0–12	100	1.22	2.71
Climb	0–7.02	0–23K	0.3–0.5	Max. Cont	10.0	22.22
Cruise	6.41–7.63	21–25K	0.65–0.74	Max. Cr	14.0	31.11
Descent	7.02–0.3048	23–1K	0.7–0.4	F.I.	10.0	22.22
Approach	0.3048–0	1K–0	0.12	65	3.0	6.67
Reverse Thrust	0	0	0.12–0	Max. Rev	0.08	0.18
Idle-Taxi	0	0	0	4–20	3.1	6.89
					45.0	100

Cyclic life shall be based on 48,000 mission cycles plus 1000 ground checkout cycles to full power.

The engine shall be capable of operation throughout the flight envelope shown in Figure 2-1, unless the extremes adversely affect engine cost or weight. Consideration will be given to restricting the envelope should this occur. The combustor shall meet commercial relight requirements as shown on the flight envelope.

In addition to the above life objectives, the engine must be capable of meeting an alternate experimental engine life cycle including very high fan horsepower levels for short periods for fan mapping (Table 2-II).
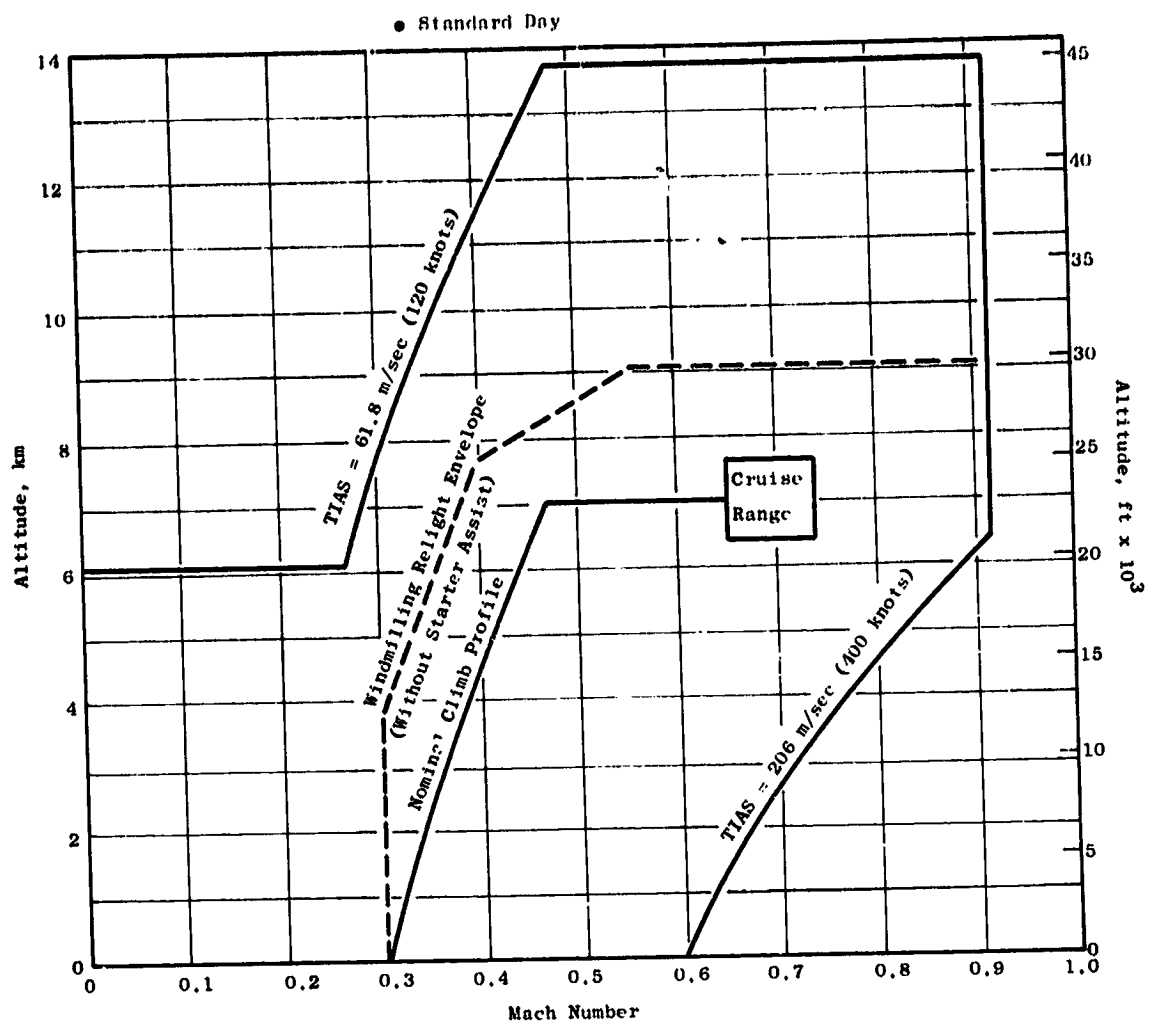
Figure 2-1. QCSEE Operating Envelope.

Table 2-II. Experimental Duty Cycle.			
% N_F	% Fan HP	Time, hr	% Time
105	100	1	0.04
100	140	1	0.04
100	130	15	0.56
100	110	15	0.56
100	100	150	5.59
90	80	500	18.64
75	50	1000	37.29
30	10	1000	37.29
		2682	100.0

2.3.2 Flight Maneuvers

The engine and its supports shall withstand without permanent deformation the conditions specified on Figure 2-2. The calculated weight of the engine shall be increased by the specified weight allowed for all engine-mounted accessories.

The engine and its supports shall be designed to not fail when subjected to static loads equivalent to 1.5 times the value specified above for metal parts and 3.0 times for composite parts.

The engine shall be capable of withstanding loads caused by seizure of either rotor with deceleration from maximum rpm to zero rpm in one second.

Composite parts shall be capable of withstanding unbalanced loads caused by loss of five adjacent composite fan blades at maximum rpm. Metal parts shall be capable of withstanding loss of one equivalent metal blade.

2.3.3 Flight Attitudes

The engine shall be capable of operating within the range of flight attitudes shown in Figure 2-3.

2.4 UTW EXPERIMENTAL PROPULSION SYSTEM

The UTW experimental engine system cross section is shown in Figure 2-4. The fundamental design criterion which established the unique shape of the engine is the fan cycle required to meet the noise objectives. Both the fan and core engine design pressure ratios were dictated by jet-flap noise constraints. The fan contains 18 composite variable-pitch blades with flight weight disk and blade supporting system. The fan is capable of pitch change from forward to reverse thrust through either flat pitch or stall pitch. Two

Flight

(0 to Max. Thrust)

$\ddot{\theta} = \pm 6 \text{ rad/sec}^2$

$\dot{\psi} = 0$

$\ddot{\psi} = 0$

$\dot{\theta} = \pm 1 \text{ rad/sec}$
or
S.L. = 4.0

Applicable to
Complete
Crosshatched
Area

$\dot{\theta} = 0$
S.L. = 1.5

Applicable to
Complete Rectangle
from 7 Up to
10 Down

Up

7
6
5
4
3
2

Aft   Fore

3

Down

1. Load factors and angular velocities and accelerations should be taken at or about the C.G. of the engine.

2. Side load factors (S.L.) act to either side.

3. $\dot{\theta}$ and $\ddot{\theta}$ are pitching velocity and acceleration.

4. $\dot{\psi}$ and $\ddot{\psi}$ are yawing velocity and acceleration.

5. Down loads occur during pull out.

6. Fore loads occur during arrested landing.

S.L. = 2.0

$\dot{\theta} = 0$

$\dot{\psi} = 0$

$\ddot{\theta} = \pm 14 \text{ rad/sec}^2$

$\ddot{\psi} = \pm 6 \text{ rad/sec}^2$

Up

4
3
2
1

Aft   Fore

4 3 2 1   1 2 3 4 5 6 7 8 9 10

Landing

(0 to Max. Nonaugmented Thrust)

2
3
4
5
6
7
8
9
10

Down

Figure 2-2.   QCSEE Design Loads.
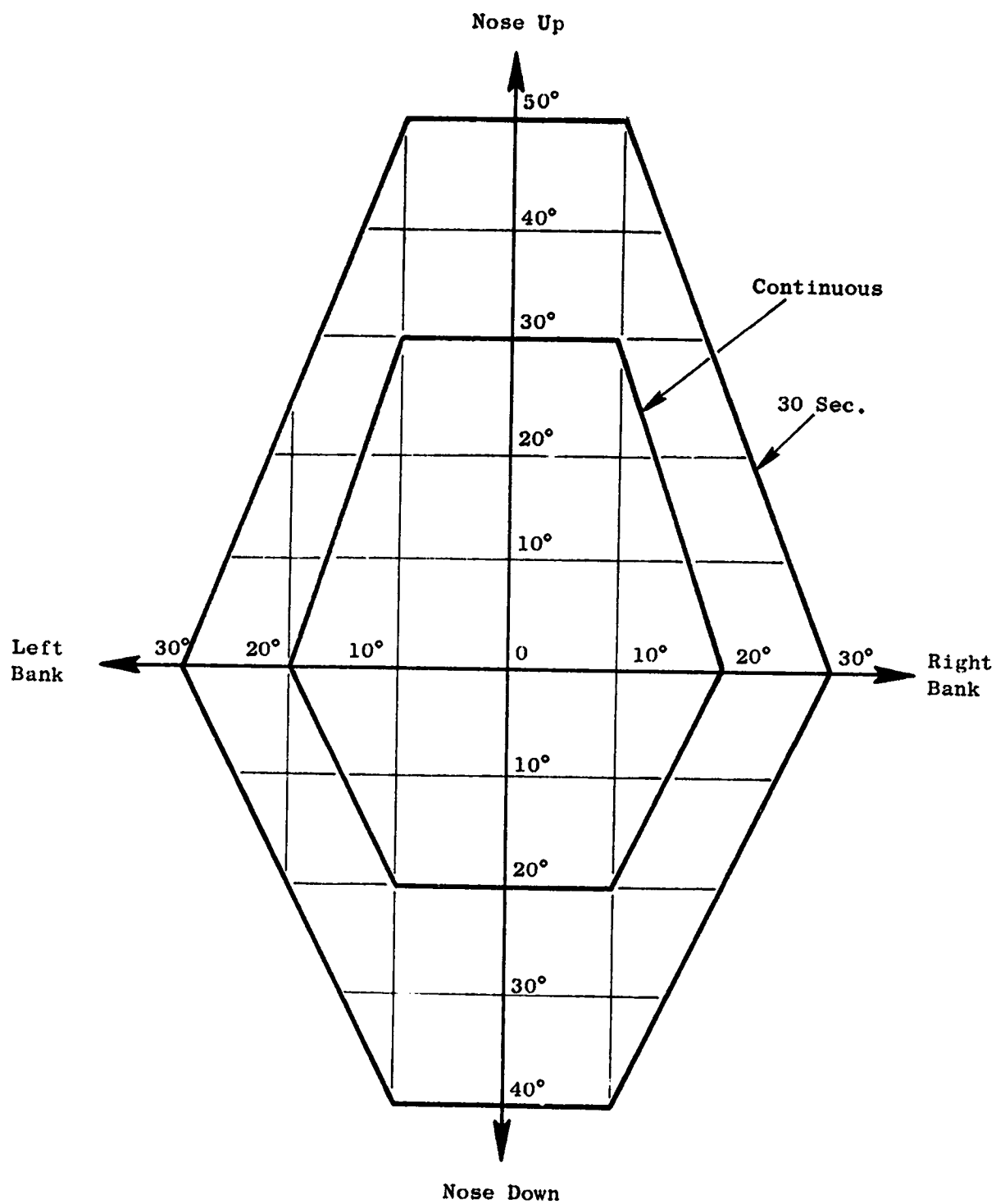
Figure 2-3. QCSEE Flight Attitudes.
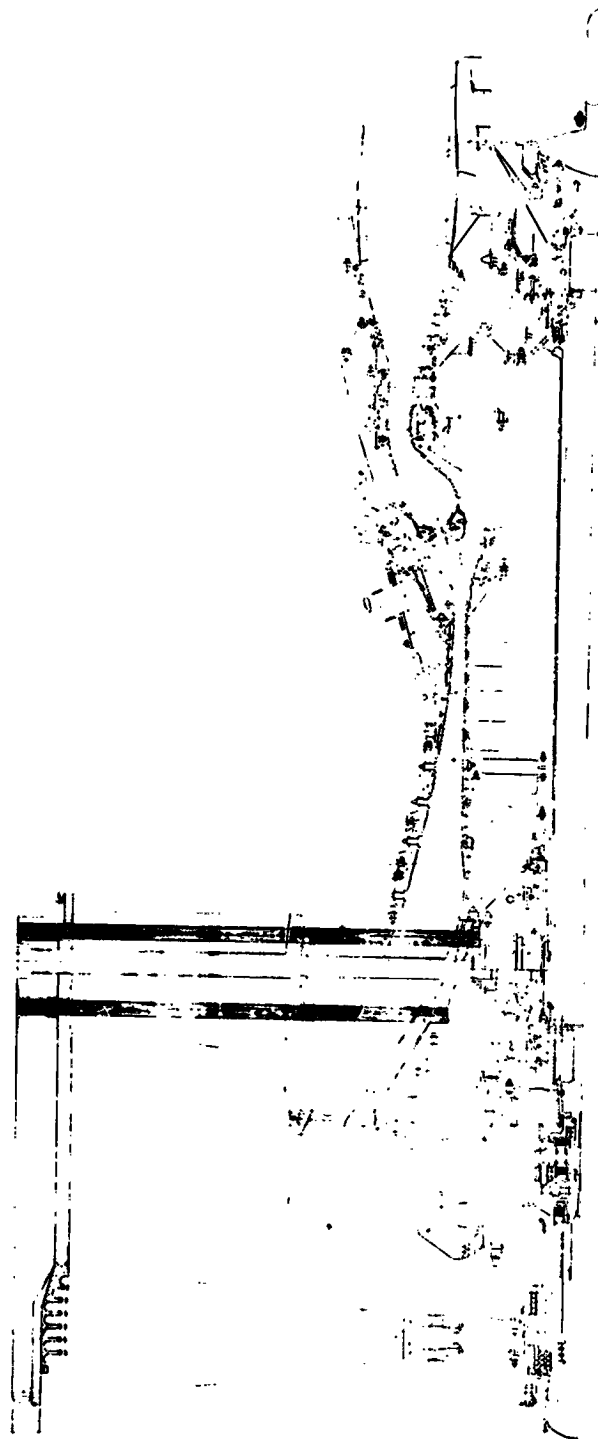
Figure 2-4. UTW Experiment . Engine System.

blade actuation systems, harmonic drive and alternate ball bearing screw types, are planned with motive power supplied by hydraulic motors. The actuation system is capable of providing 130°/sec pitch change velocity at takeoff power.

The fan frame is a flight-weight composite structure containing integral acoustic treatment, outer casing, containment, and fan tip treatment. Thirty-three integral outlet guide vanes also act as structural struts. The outer casing of the frame provides both inner and outer nacelle flow paths and also containment for failed airfoils. Core inlet flow path and mounts for the forward bearings, gears, radial drive, etc., are also integrally provided.

The reduction gear consists of a six-star epicyclic system having a ratio of 2.465 and a 100% power rating of 9890 kw (13,256 horsepower). The core engine and low pressure turbine, including the turbine frame and low pressure shaft, are F101 components with necessary modifications as described in Section 11.0.

Engine fuel flow, blade pitch angle, and exhaust nozzle area are controlled by a digital electric control, which modifies the fuel demand of a modified F101 hydromechanical control. Major engine accessories are mounted on a boiler plate gearbox on top of the fan frame.

The UTW experimental propulsion system consists of the engine as described above with added components to make up a complete nacelle package, as shown in Figure 2-5. The nacelle components include a lightweight composite hybrid inlet providing acoustic suppression by means of a high throat Mach number (0.79) and integral acoustic treatment. The composite fan duct, acoustic splitter, and core cowl are hinged from the pylon to provide access for engine maintenance. The core exhaust nozzle and nozzle plug are acoustically treated to reduce aft radiated noise. The fan exhaust nozzle is a variable-area, four-flap design capable of area change from takeoff to cruise, as well as opening to a flared position to form an inlet in the reverse thrust mode. The nozzle flaps are hydraulically actuated.

2.5 UTW FLIGHT PROPULSION SYSTEM

The UTW flight engine system cross section is shown in Figure 2-6. Differences from the experimental engine are primarily in material substitutions to save cost in this Program. For example, the following parts would be titanium rather than steel in a flight engine: fan shaft, gear carrier, and bearing support cones. The accessory gearbox would use a cast aluminum casing rather than fabricated steel, and several accessories such as oil tank, heat exchanger, filters, and pumps would be of optimized design rather than using available hardware. Several changes have also been postulated in the F101 core consistent with the lower QCSEE cycle compressor discharge pressure.

The UTW flight propulsion system cross section is shown in Figure 2-7. Bleed manifolding would be added for the cabin air conditioning and anti-icing systems and for any high-lift devices requiring engine bleed air. The flight system would include a flight-type fire detection and extinguishing system rather than test facility equipment.

13
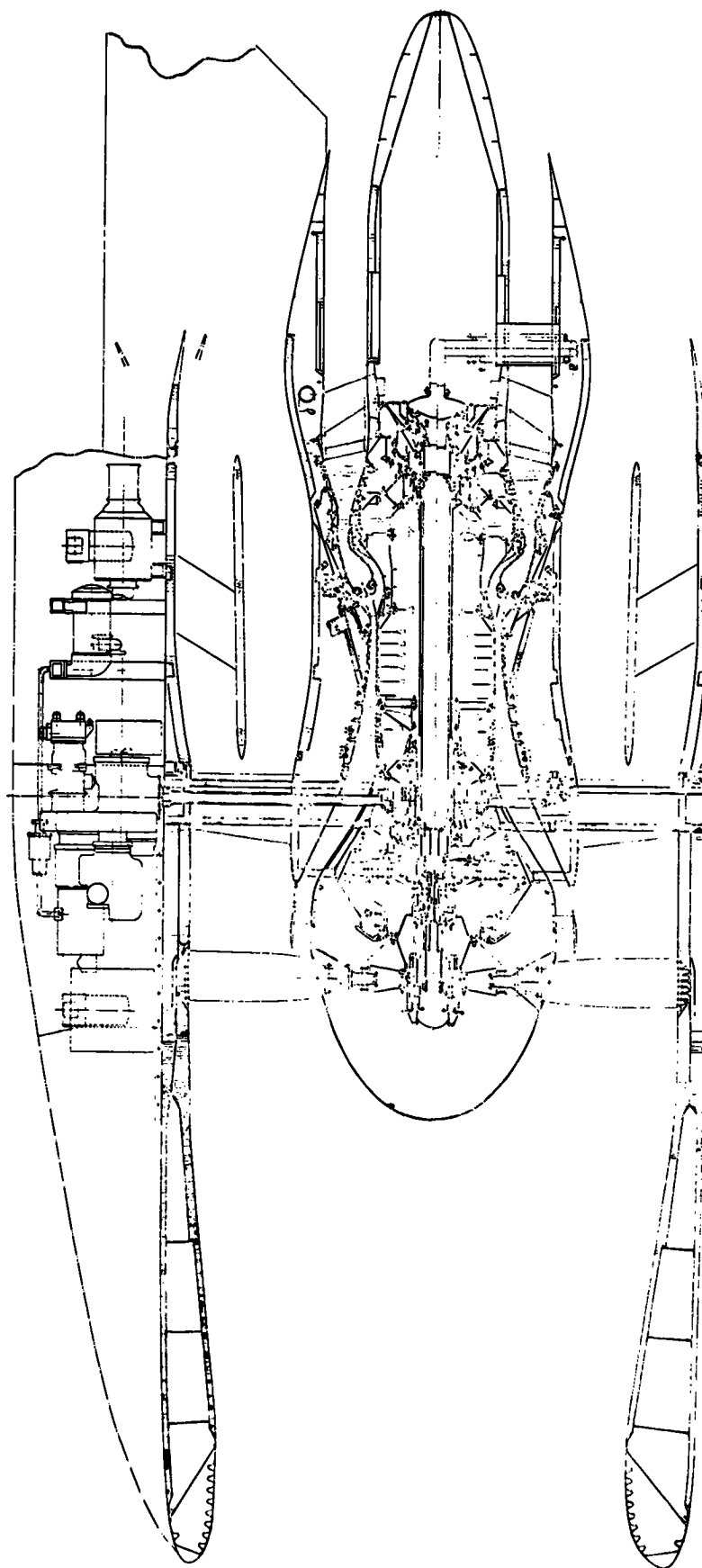
Figure 2-5. UTW Experimental Propulsion System.
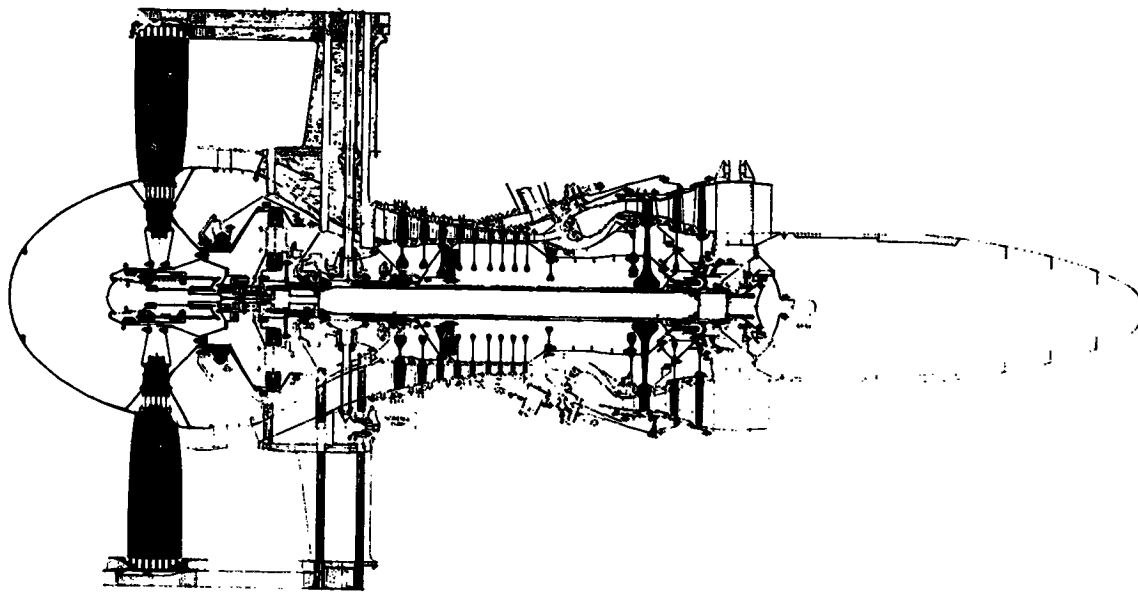
Figure 2-6. UTW Flight Engine System.
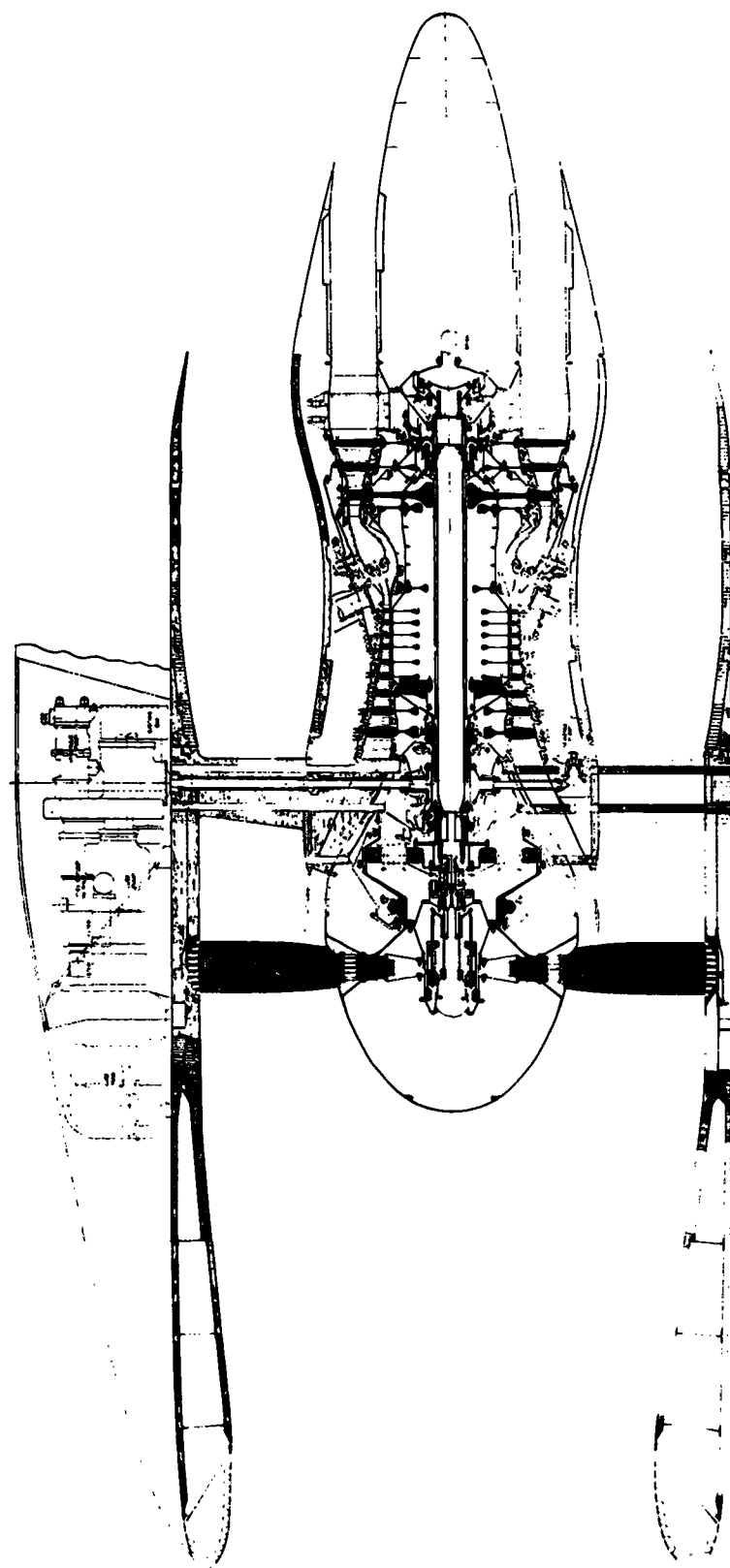
Figure 2-7. UTW Flight Propulsion System.

16

Both the experimental and flight UTW engines are top mounted from a pylon, with mounts on the fan frame and turbine frame. By opening bypass duct and core cowl, the engine and inlet can be removed from the pylon in the downward direction. A hinged accessory cover provides access to engine accessories located in front of the pylon.

2.6 OTW EXPERIMENTAL PROPULSION SYSTEM

The OTW experimental engine system cross section is shown in Figure 2-8. The fan contains 28 fixed-pitch titanium blades. The airfoil sections have been selected as suitable for composite construction in a flight configuration. The titanium fan disk incorporates a larger cross section than in a flight configuration because of greater weight of the metal blades.

The OTW fan frame is structurally identical to the UTW frame. Differences occur in the areas of the blade tip passage and the flow splitter to meet fan aero requirements.

The OTW reduction gear is similar to the UTW component, except that it contains eight star gears, has a gear ratio of 2.062 to match the higher rpm OTW fan to the F101 low pressure turbine, and is rated at 12,880 kw (17,214 horsepower).

The OTW control system is identical with that of the UTW engine except for different programmed schedules for the different cycle, deletion of the variable pitch function, and actuation of a target thrust reverser instead of flare nozzle.

The OTW experimental propulsion system is shown in Figure 2-9. In order to achieve a major cost saving by utilizing the same test cell, engine accessory system, and facilities, the OTW propulsion system is top mounted with the same accessory location as the UTW system. Thus the OTW experimental engine runs inverted compared to a flight installation. To reduce program cost, the nacelle components for the OTW system are of "boiler plate" construction with interchangeable acoustic treatment panels. Because of greater weight of these components, they are separately supported from the test stand with flexible joints at the fan frame interfaces. The OTW boiler plate nacelle components can also be used with the UTW flare nozzle to form a complete UTW installation. This will be done for initial UTW acoustic developmental testing.

The OTW propulsion system incorporates a "D -shaped nozzle to spread the exhaust flow over the wing flaps. Nozzle area is varied by means of doors at the sides of the nozzle. A target-type thrust reverser is incorporated, deflecting the jet efflux forward and upward. To avoid impingement of the jet on the test facility and instrumentation lines, the nozzle will be inverted to exhaust forward and downward in the initial experimental engine tests. The exhaust nozzle will be rotatable about the engine centerline such that it can be installed in the upright, inverted, or 90° attitude as required for subsequent NASA testing.

17
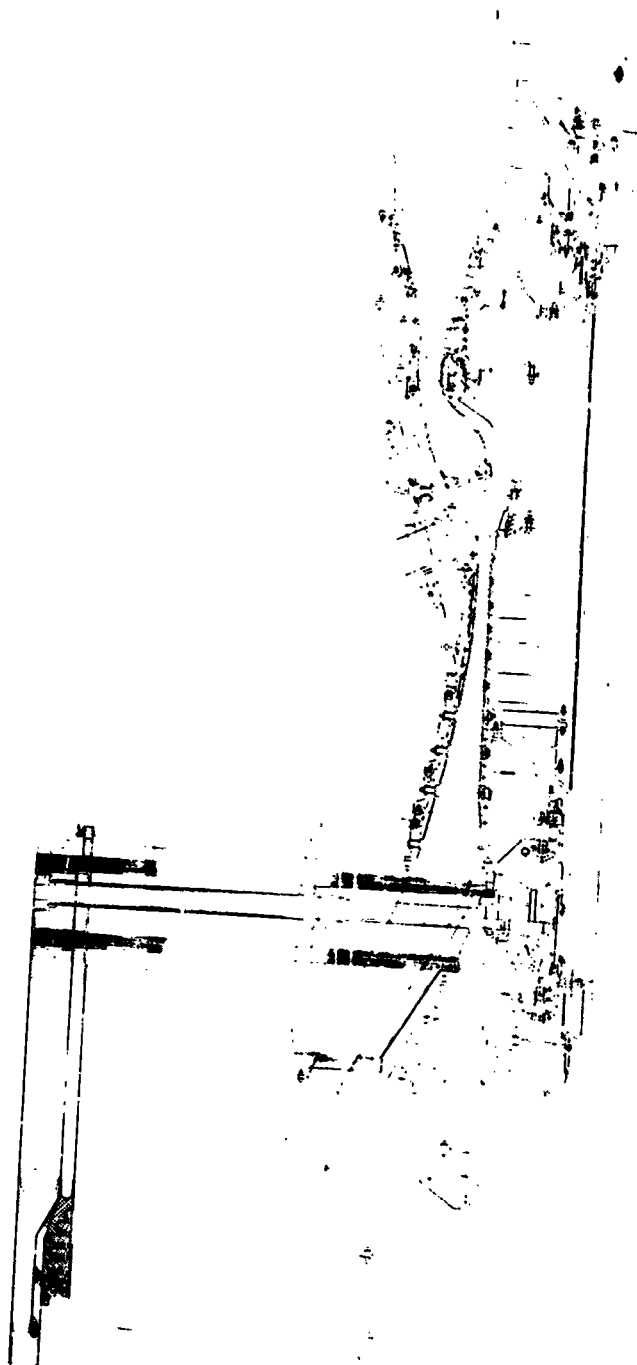
Figure 2-8. OTW Experimental Engine System.

13
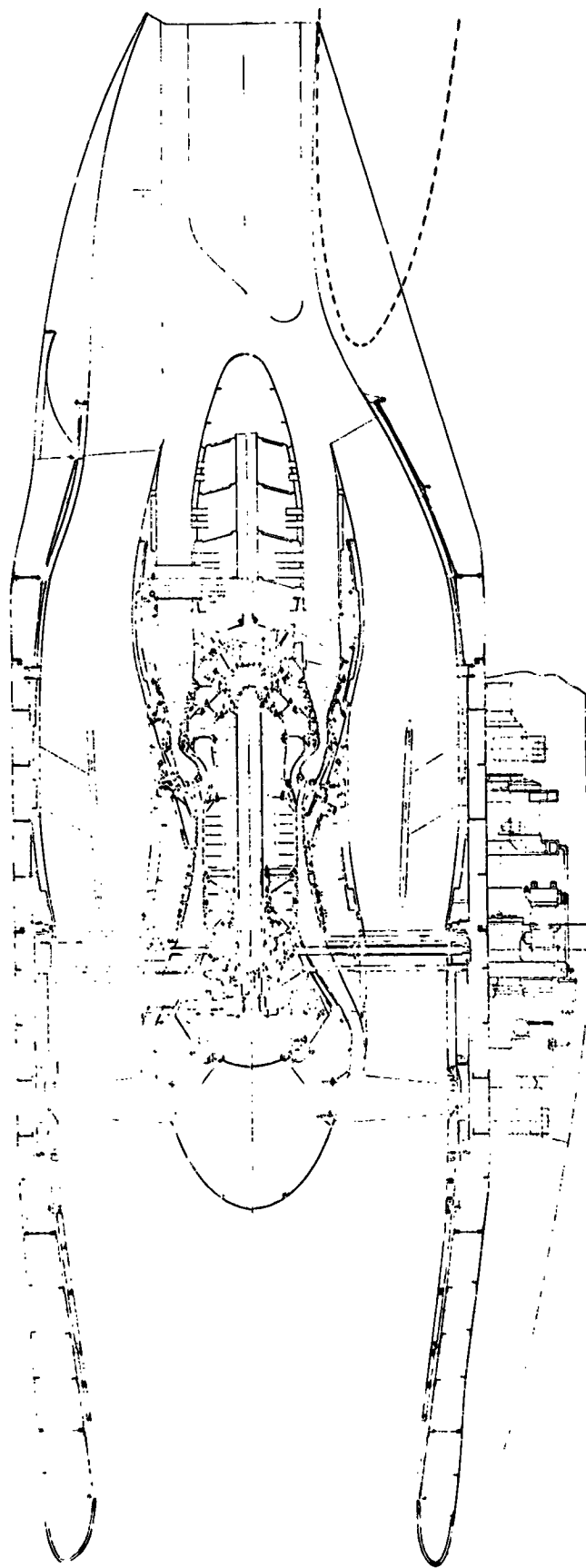
Figure 2-9. OTW Experimental Propulsion System.

2.7 OTW FLIGHT PROPULSION SYSTEM

The OTW flight engine system cross section is shown in Figure 2-10. Differences from the experimental engine are the same as those cited for the UTW system; and in addition, titanium fan blades would be replaced by composite blades, and the disk would be modified accordingly.

In the OTW flight configuration, accessories would be bottom mounted, fairing into the wing leading edge. Therefore, the lube scavenge pump, which is located in the bottom core cowl region in the top-mounted engines, can be moved to the accessory gearbox.

The OTW flight propulsion system cross section is shown in Figure 2-11. The D-shaped nozzle is located in its proper orientation for flow spreading over the wing surface, and the reverser discharges upward and forward. The nacelle components in the flight engine are composite materials with integral acoustic treatment. As in the case of the UTW system, the engine can be removed from the pylon by opening bypass duct doors and lowering the engine and inlet. Engine accessories are located ahead of the bottom pylon, with a hinged door for access.

20
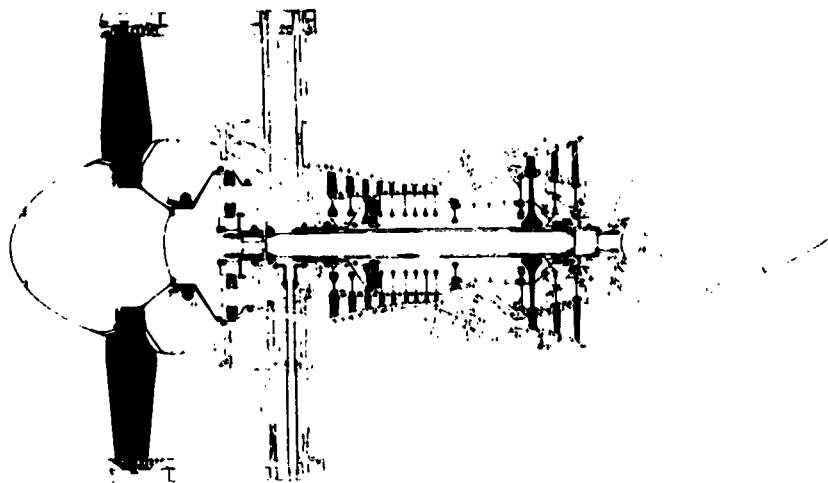
Figure 2-10. OTW Flight Engine System.
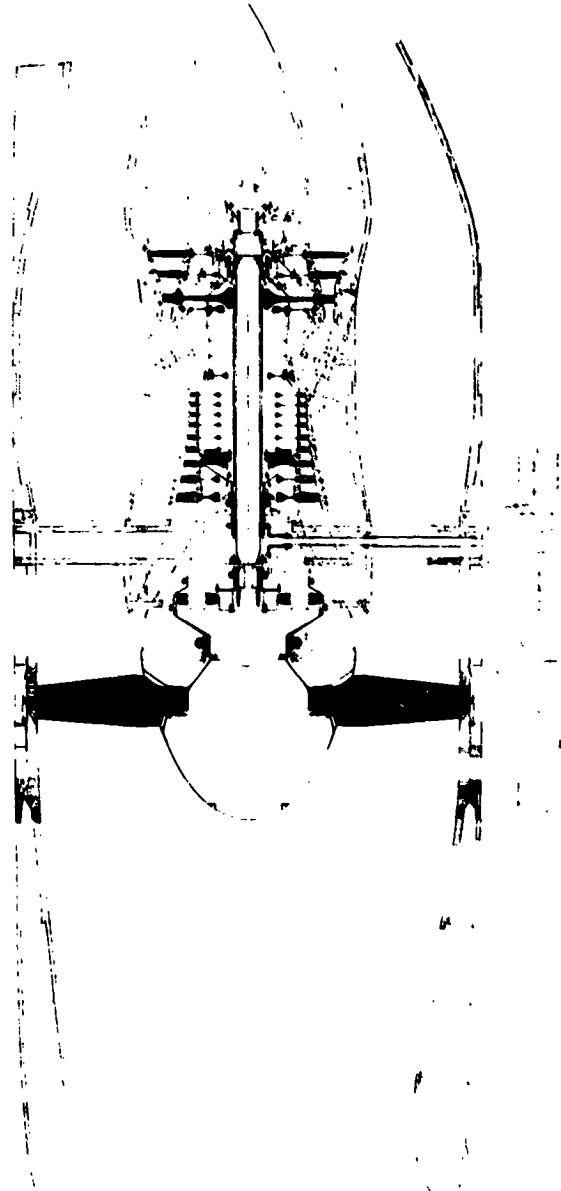
Figure 2-11. OTW Flight Propulsion System.

SECTION 3.0

ACOUSTIC DESIGN

3.1 SUMMARY

The preliminary acoustic design of both the UTW and OTW engines has resulted in configurations which meet takeoff, approach, and reverse thrust noise goals. Table 3-I summarizes the noise levels for each engine at the three design points.

Table 3-I. Summary of UTW and OTW Noise Levels.			
• 400.34 Kilonewtons (90,000 Lbs) Thrust			
• 4 Engines			
	Takeoff EPNdB	Approach EPNdB	Reverse Thrust PNdB
UTW	94.0	91.5	98.0
OTW	95.0	90.5	100.0
Goal	95.0	95.0	100.0

The noise levels have been obtained by estimating unsuppressed noise from existing test data of similar fan and core configurations, suppressing the dominant engine noise sources with the advanced technology concepts to be developed under the QCSEE program, and extrapolating these levels to inflight conditions. Jet/flap noise was added to the engine noise levels to obtain total system or aircraft noise levels.

The preliminary acoustic design effort has attempted to establish UTW and OTW engine configurations which have balanced suppression in the fan inlet, fan exhaust, and core. To establish the balanced system suppression, detailed predictions have been made for these 10 different noise sources:

1.	Fan inlet	6.	Gears
2.	Fan exhaust	7.	Flow
3.	Turbine	8.	Struts
4.	Combustor	9.	Splitter
5.	Compressor	10.	Jet/Flap

By defining the various sources which could represent noise floors, treatment is applied to the engine only to the extent which is beneficial to the total system.

Figure 3-1 summarizes the main acoustic features of the UTW engine. A high throat Mach number inlet (M = 0.79) is used to suppress inlet noise at takeoff. Wall treatment having a length equal to 0.74 fan diameters is added to provide inlet noise suppression at approach and in reverse thrust. The rotor-stator spacing is 1.5 tip chords. The vane-blade ratio was selected to reduce second harmonic noise. Exhaust suppression utilizes inner and outer wall treatment with varying thickness to obtain increased suppression bandwidth. A 101.6 cm (40 in.) splitter is required to obtain the desired aft suppression level. A major concern in the aft duct is noise generated by flow over the treated surfaces, struts and splitter. To keep these sources below the suppressed fan noise, the duct Mach number is limited to 0.45. Core suppression utilizes a low frequency side-branch resonator design for combustor noise reduction with thinner treated panels on the inner and outer walls to reduce the high frequency turbine noise. Treatment is also applied in the core inlet to reduce forward radiated compressor noise.

Figure 3.2 summarizes the main OTW engine acoustic characteristics. The inlet design is the same as the UTW inlet with the treatment panels selected to match the OTW spectrum. Due to more rotor blades with shorter chords, the rotor-chord spacing ratio exceeds that of the UTW engine since the vane design and axial location is common to both engines. This acoustic benefit, however, is offset to some degree by the lower vane-blade ratio of the OTW engine. In the exhaust duct a shorter splitter is utilized because of increased wall treatment length and wing shielding benefits. As in the UTW design, the duct Mach number is limited to 0.45. Core treatment incorporates the low and high frequency components used in the UTW engine.

3.2 DESIGN REQUIREMENTS

The noise requirements for both the UTW and OTW engine are specified as a total system or aircraft noise level at the operating conditions associated with takeoff and approach operation. A reverse thrust requirement is also specified for static aircraft conditions. These are shown graphically on Figure 3.3. Specific requirements are given in Tables 3-II and 3-III.

Takeoff noise requirement is 95 EPNdB maximum on a 152.4 m (500 ft) side-line with the aircraft at 61 m (200 ft) altitude and the engines at 100% thrust. Takeoff flap angle and aircraft speed are given in Table 3-II. Also shown in Table 3-II are inlet angle of attack and upwash angles which must be accounted for with regard to fan inlet noise generation and high Mach inlet suppression.

At approach, the noise requirement is the same as takeoff but the engine is operated at 65% thrust. Flap angles, defined in Table 3-II, however are increased for the powered-lift approach.

24

LOW FREQUENCY COMBUSTOR NOISE SUPPRESSOR

STACKED HIGH FREQUENCY TURBINE NOISE SUPPRESSOR

PHASED TREATMENT

$\overline{M}_N = 0.45$

101.6 cm (40") LONG SPLITTER

1.5 ROTOR/OGV SPACING
1.83 VANE/BLADE RATIO

TREATED L/D = 0.74

0.79 THROAT MACH NO.
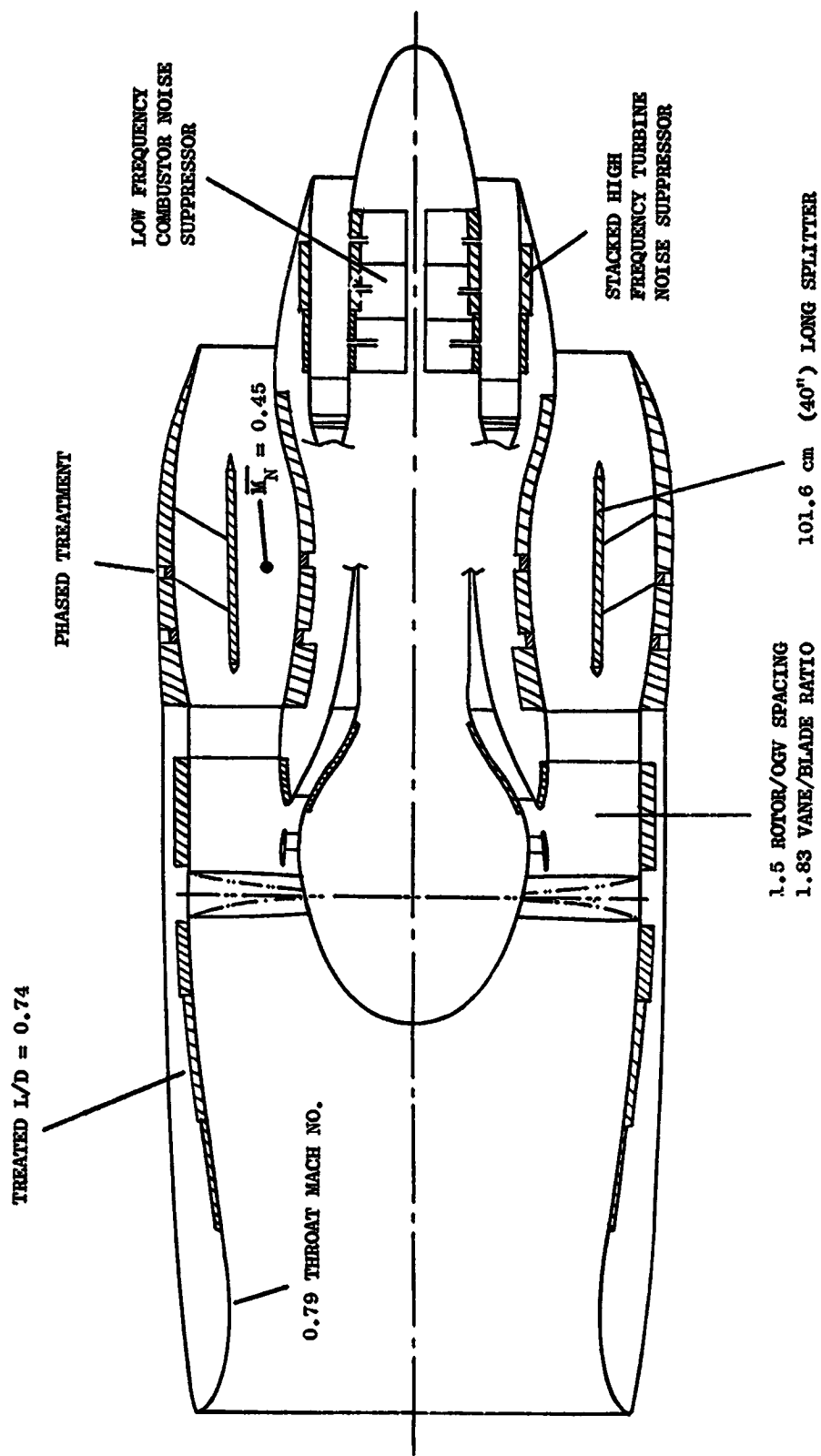
Figure 3-1. QCSEE UTW Engine.
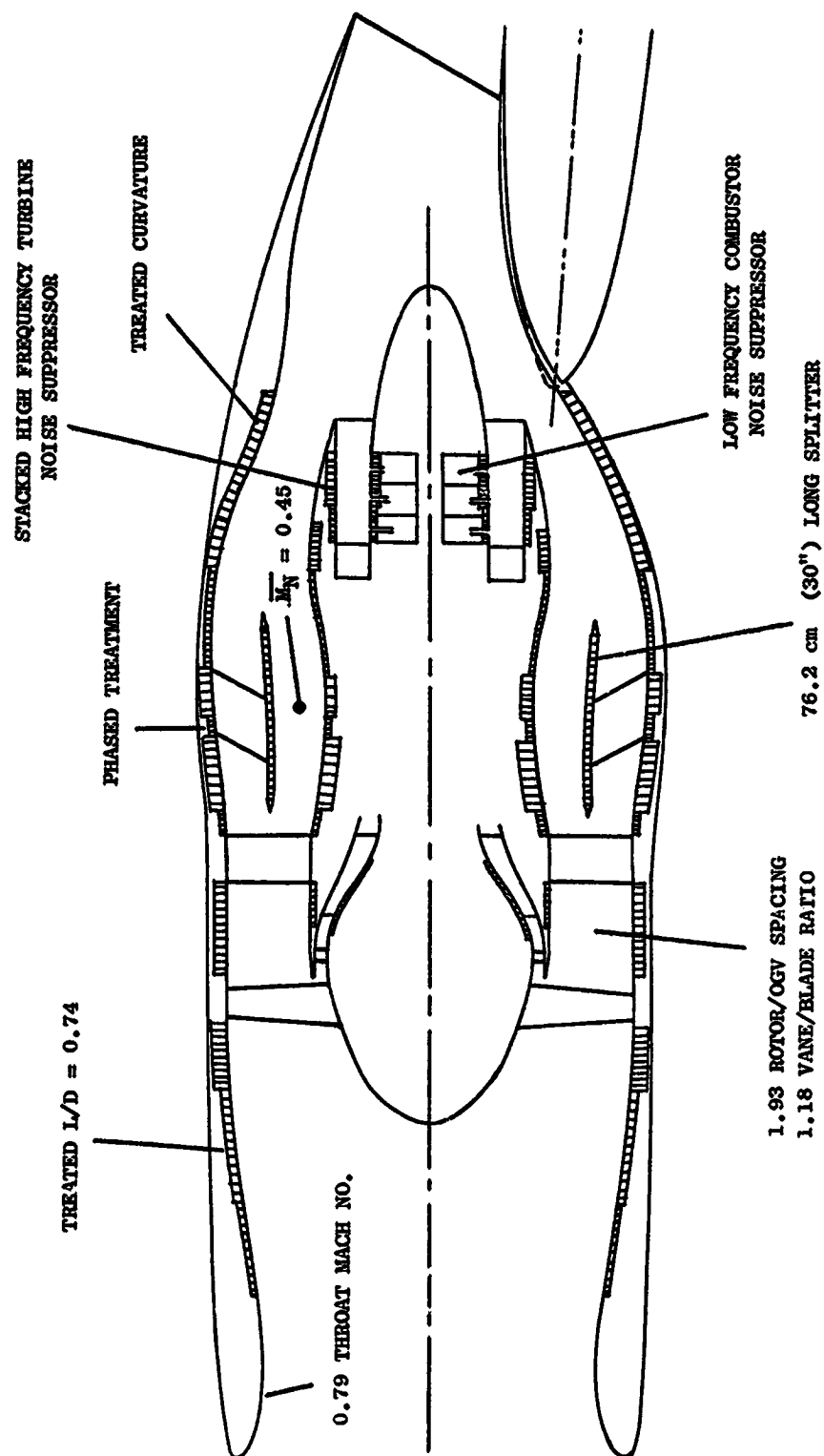
Figure 3-2. QCSEE OTW Engine – Preliminary Design.

STACKED HIGH FREQUENCY TURBINE
NOISE SUPPRESSOR

TREATED CURVATURE

LOW FREQUENCY COMBUSTOR
NOISE SUPPRESSOR

PHASED TREATMENT

$\overline{M_N}$ = 0.45

76.2 cm (30") LONG SPLITTER

TREATED L/D = 0.74

0.79 THROAT MACH NO.

1.93 ROTOR/OGV SPACING
1.18 VANE/BLADE RATIO

95 EPNdB

100% F_N
61 m (200 ft) Altitude

100 PNdB (R/T)
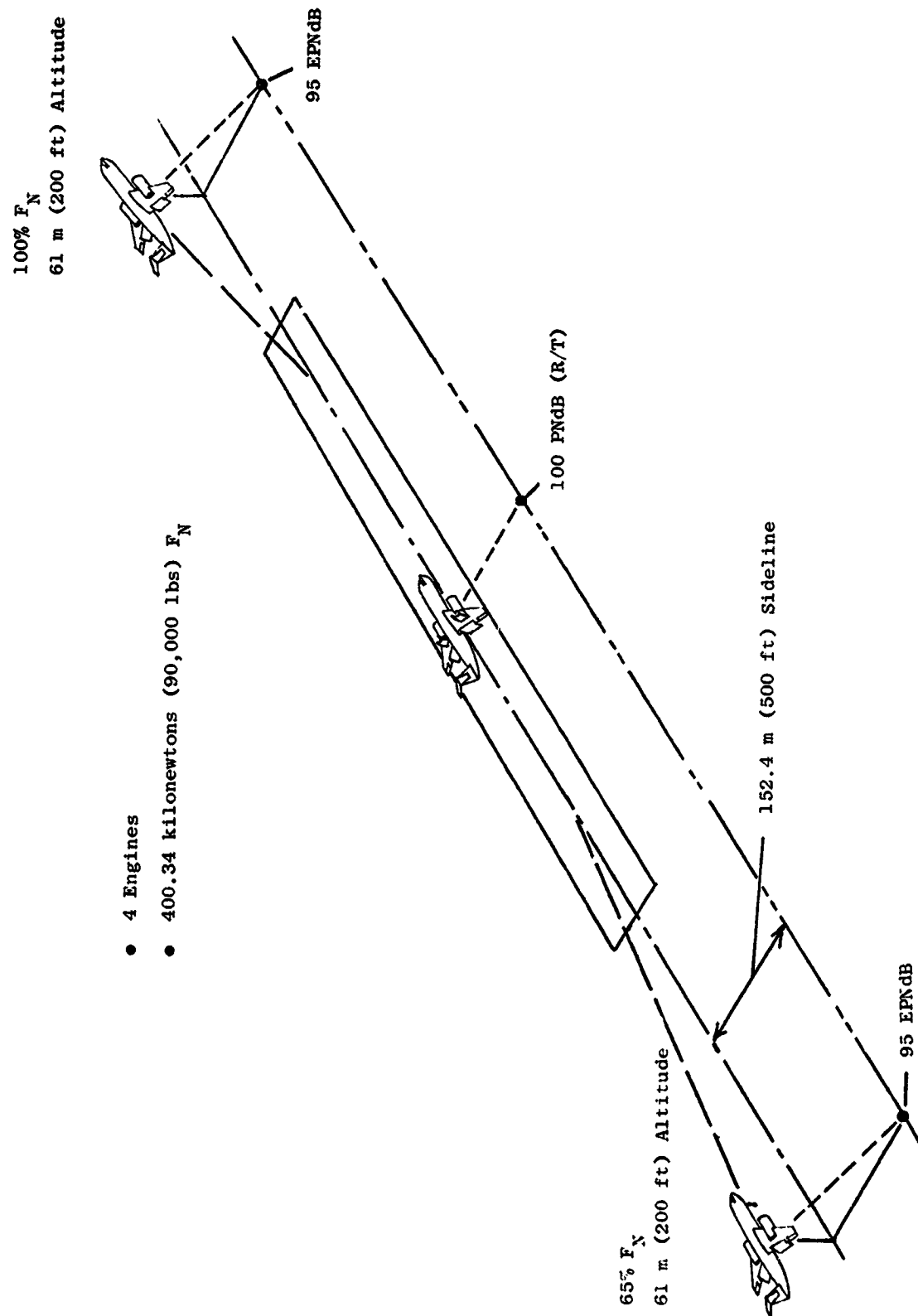
- 4 Engines
- 400.34 kilonewtons (90,000 lbs) F_N

152.4 m (500 ft) Sideline

65% F_N
61 m (200 ft) Altitude

95 EPNdB

Figure 3-3. QCSEE Acoustic Requirements.

27

Table 3-II. UTW and OTW Engine and Aircraft Flight Characteristics for Acoustic Calculations.

Flight Conditions	Takeoff	Landing
Aircraft Speed, m/sec (knots)	41.15 (80)	41.15 (80)
Flap Angle, radians (degrees)	0.524 (30)	1.047 (60)
Climb or Glide Angle, radians (degrees)	0.218 (12.5)	0.105 (6)
Angle of Attack, radians (degrees)	0.105 (6)	0.035 (2)
Upwash Angle, radians (degrees)	0.262 (15)	0.192 (11)
Installed Net Thrust, percent	100	65

Table 3-III. Propulsion System Reverse Thrust
             Static Test Conditions.

UTW Propulsion System

Fan Blade Position   Through Flat Pitch or Stall

Thrust   35% of SLS Takeoff

Flap Angle   0.524 radians (30°)

Aircraft Speed   0 m/sec (0 knots)

OTW Propulsion System

Thrust   35% of SLS Takeoff

Flap Angle   0.524 radians (30°)

Aircraft Speed   0 m/sec (0 knots)

Reverse thrust noise is limited to 100 PNdB maximum at full reverse thrust (35% of maximum forward) with the aircraft at static conditions. For the UTW engine, this can be accomplished by reversing the fan blades through either flat pitch or stall.

Since the engine noise levels are to be measured during static testing, a procedure for determining inflight noise levels from static data has been established as part of the contract. This procedure, see Appendix A, establishes the following:

1. Jet/flap noise calculation procedure
2. Extrapolation procedures
3. Doppler shift correction
4. Dynamic effect correction
5. In-flight cleanup and upwash angle correction
6. Relative velocity correction for jet/flap noise
7. Fuselage shielding and OTW wing shielding
8. PNdB to EPNdB calculation

This procedure has been used in all noise estimates for the UTW and OTW engines.

3.3 UTW PRELIMINARY DESIGN

3.3.1 System Acoustic Design Considerations (UTW)

Many features of the UTW QCSEE engine designs have been selected based on the low system noise requirements for a 100.085 kilonewton (22,500 lb) thrust engine installed in an under-the-wing configuration. The two major noise sources considered were the fan noise and the jet/flap noise. Forward radiated fan noise is primarily a function of fan tip speed (Figure 3-4, Appendix B). The data were normalized on the basis of fan inlet weight flow, a fan funda- mental tone of 3150 Hz, and a rotor-vane spacing of two chords. This correlation shows that unsuppressed fan noise in the inlet quadrant can be reduced with lower tip speed, and further, that tip speeds lower than 366 m/sec (1200 ft/sec) avoid the increased noise levels due to the multiple pure tones associated with supersonic tip speed fans. The lowest tip speed, 289 m/sec (950 ft/sec), consistent with the other engine cycle requirements, was therefore selected for the UTW fan.

Aft radiated fan noise levels have been correlated primarily with fan pressure ratio (Figure 3-5, Appendix B) In addition to controlling aft fan noise, the fan pressure ratio also determines the fan jet velocity. Since the jet/flap noise is proportional to the velocity to the sixth power, low fan pressure ratios result in rapidly reduced aft system noise levels. Since aft generated fan noise can be suppressed with acoustic treatment, the fan pressure ratio was selected primarily based on the need to achieve low levels of jet flap noise.

30

Fan source noise reduction features were selected to provide noise reduction at the source with minimum weight and performance impact.

Rotor-OGV spacing of 1.5 rotor chords was selected in order to reduce fan source noise levels and minimize the need for splitters in the fan inlet and exhaust. Wider rotor-OGV spacing would produce an additional reduction. The same reduction can also be achieved with a lengthened exhaust splitter with a smaller weight increase than the frame length required for additional spacing.

The variable-pitch fan also provides an additional degree of flexibility in optimizing the fan performance for minimum noise.

A vane-blade ratio of 1.83 has been selected to minimize the fan tone second harmonic level which makes a large contribution to the perceived noise levels.

Table 3-IV shows the major design features in the UTW Preliminary Design which impact the projected noise levels. The engine system trades discussed above have produced an engine preliminary design which meets the noise goals of the program as well as the performance and thrust-to-weight-requirements.

3.3.2 Takeoff Noise Constituents

Noise levels for the UTW engine are shown on Figure 3-6 in bar chart form. Unsuppressed noise is dominated by the fan in the forward and aft quadrants. Suppressed noise levels are balanced between the fan and jet/flap noise in the aft quadrant and are controlled by the jet/flap noise in the forward quadrant. The constituent levels shown are at the angle of maximum noise for the suppressed engine, thus in the forward quadrant, 1.4 radians (80°) is selected, since the dominant source, jet/flap noise, is a maximum at that angle. Fan inlet noise has been suppressed well below the jet/flap noise.

Gear noise and compressor noise are not shown as they were not contributing noise sources.

These constituent levels were obtained by the steps shown in Table 3-V. Calculations began with 61 m (200 ft) sideline unsuppressed levels which were extrapolated to the 152.4 m (500 ft) sideline, 61 m (200 ft) altitude condition and then adjusted for in-flight corrections per the Appendix A calculation procedure. Suppression was then added to obtain suppressed in-flight constituent levels in the forward and aft quadrants. These constituents were then summed to obtain maximum forward and aft PNdB levels which were converted to a single EPNdB level per the Appendix A procedure.

Table 3-IV. UTW Design Parameters.

Number of Fan Blades	18
Fan Diameter, cm (in.)	180.4 (71)
Fan Pressure Ratio	1.27
Fan Speed, rpm	3074
Fan Tip Speed, m/sec (ft/sec)	289.6 (950)
Number of OGV's	33
Fan Weight Flow, kg/sec (lb/sec)	405.5 (894)
Inlet Mach Number (Throat)	0.79
Rotor/OGV Spacing	1.5
Treatment Length/Fan Diameter	0.74
Fan Exhaust Area, m^2 ($in.^2$)	1.561 (2420)
Core Exhaust Area, m^2 ($in.^2$)	0.3315 (514)
Gross Thrust (Uninstalled), kN (lb)	81.4 (18,300)
Blade Passing Frequency, Hz	920
Core Weight Flow, kg/sec (lb/sec)	31 (69)
Fan Exhaust Velocity, m/sec (ft/sec)	198 (633)
Core Exhaust Velocity, m/sec (ft/sec)	232 (744)

- 100.085 kilonewtons (22,500 LBS) INSTALLED THRUST, SLS
- 152.4 m (500 FT.) SIDELINE, 61 m (200 FT.) ALTITUDE
- 41.15 m/s (80 KNOTS) AIRCRAFT SPEED
- EPNdB = 94
- GEAR AND COMPRESSOR, NONCONTRIBUTING CONSTITUENTS
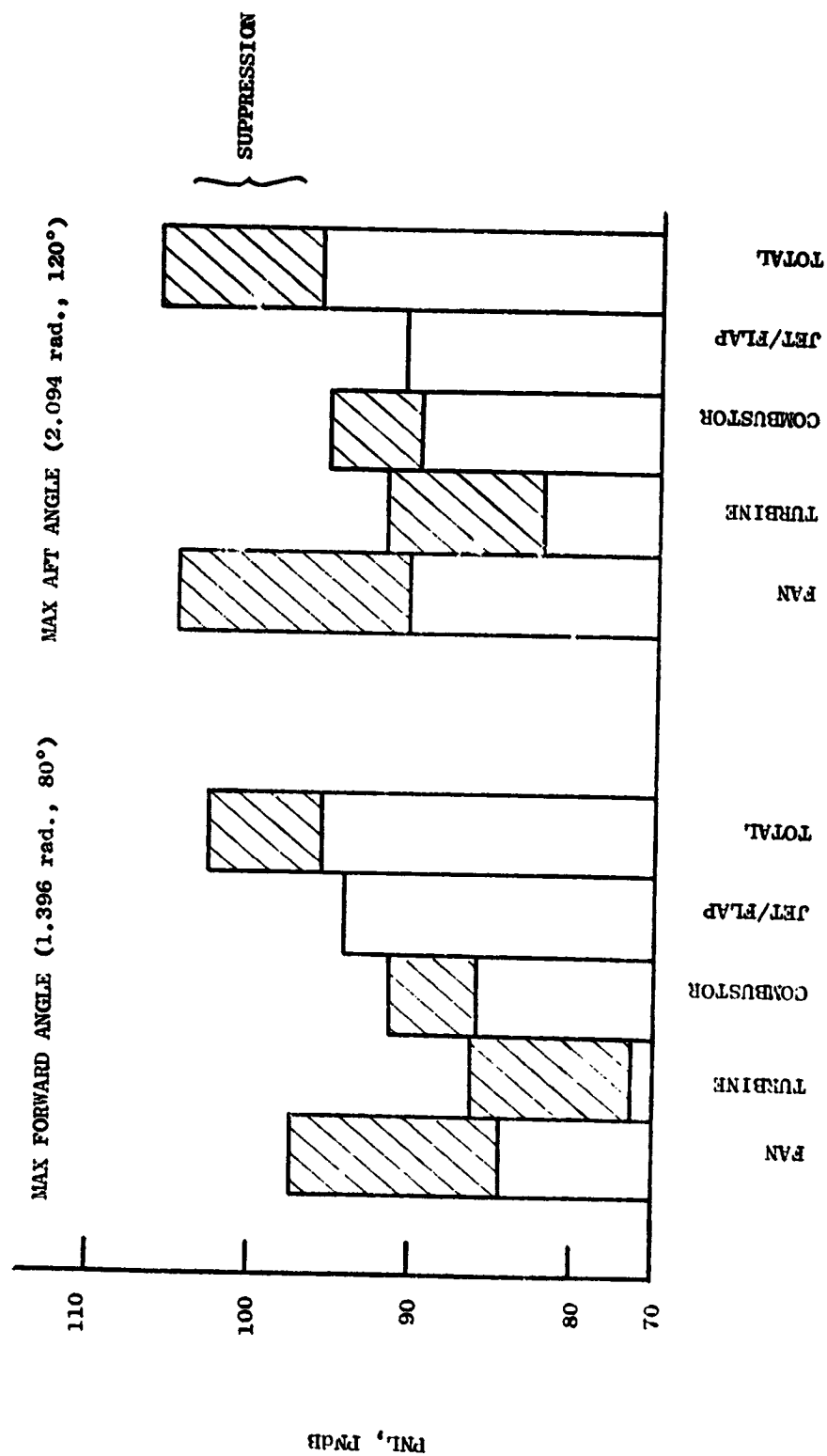
Figure 3-6. UTW Takeoff Noise Constituents.

33

Table 3-V. QCSEE UTW Noise Levels.

- Takeoff Power, 100,085 kilonewtons (22,500 lbs) F_N(Installed)

	(1.396 radians, 90°) Max. Forward Angle PNdB				(2.094 radians, 120°) Max. Aft Angle PNdB			
	Fan	Turbine	Combustor	Jet/Flap	Fan	Turbine	Combustor	Jet/Flap
Single Engine – Unsuppressed @ 61 m (200 ft) Sideline	107.5	94.1	95.5	100.1	112.3	100.1	99.5	97.8
Total Corrections – Appendix A Procedure	-10.1	-7.9	-4.2	-5.9	-7.5	-8.3	-5.2	-7.1
Corrected Level	97.4	86.2	91.3	94.2	104.8	91.8	94.3	90.7
Suppression	-13.0	-9.6	-4.5	-	-14.5	-9.6	-4.5	-
Suppressed System	84.4	76.6	86.8	94.2	90.3	82.2	89.8	90.7
Sum Constituents	95.8				96.0			

PNdB to EPNdB   94 EPNdB

34

3.3.3 Takeoff Suppression

Inlet

At takeoff, the forward radiated fan noise is suppressed by means of a high throat Mach number inlet. Various tests have been conducted on scale model fans with high throat Mach number inlets (Figure 3-7, Appendix B). These tests were conducted with low tip speed fans, below 305 m/sec (1000 ft/sec), and the results show varying degrees of suppression. At 0.79 Mach number, which was selected for the QCSEE design, suppression from 10 to 30 PNdB has been obtained; for QCSEE, a level of 13 PNdB reduction was applied to the forward fan noise. A detailed evaluation of these various data is currently in progress and a 50.8 cm (20 in.) simulator test program is planned in 1975 to select the proper high Mach inlet design.

Fan Exhaust

The procedure employed in designing the fan exhaust duct treatment involved both theoretical considerations and empirical experience. The design involved a series of iterational steps until the maximum suppression within the imposed constraints was attained. The sequence of steps followed in the treatment design procedure are given below.

1. #### Liner Segment Optimization

   - The unsuppressed source spectra at the desired conditions were obtained.

   - The source spectra were Noy-corrected.

   - The desired tuning frequencies, f_o, for the individual liner segments of the phased treatment were determined from the Noy-weighted spectra at the defined conditions.

   - Liner faceplate parameters were chosen in order to achieve a desirable (optimum, if possible) value of the resistance.

   - The required liner cavity depths were determined from optimum specific reactances at the chosen tuning frequencies given by[1]*

     $$x/\rho c = -0.77 \ H/\lambda_p$$

   where

   $x/\rho c$ = the specific reactance

   H = height of the duct, i.e., the distance between the two opposite walls lined with the same optimized liners.

---

*Superscript number refers to references listed at the end of this section.

35

ρ = density of air

$$\lambda_p = c(1 \pm M)/f_o \begin{cases} + \text{ exhaust mode} \\ - \text{ inlet mode} \end{cases}$$

and where

λ_p = wave length (including flow effects)

c = velocity of sound

M = Mach number

2. Transmission Loss

- At the tuning frequency, f_o, peak transmission loss (TL_o) per unit L/H of each liner segment was calculated as

$$TL_o = 7/(H/\lambda_o) \text{ in dB per unit L/H}$$

where

$\lambda_o = c/f_o$ is the wavelength at the tuning frequency

L = the liner panel length

- The effective maximum transmission loss, TL_{oe}, was estimated to be

$$TL_{oe} = 1.35 \, (0.8 \, TL_o)/(1 + M)$$

i.e., 80% effective treatment area was assumed. The factor 1.35 (1 + M) is estimated to account for the effect due to the difference between the actual flow Mach number, M, in the engine duct and that associated with acoustic duct test results at 0.35 Mach number.

Figure 3-8, Appendix B, shows maximum suppressions at observed tuning frequencies in laboratory experiments and engine tests and a predicted maximum suppression curve. Maximum suppression per unit of treated-length-to-duct-height ratio (L/H) is plotted as a function of the frequency parameter H/λ_o. Both engine data (exhaust duct only) and laboratory rectangular flow-duct data (including both exhaust and simulated inlet) are presented. The predicted curve is for the plane-wave mode in which the optimum impedance components are assumed to have been used for each frequency (Reference 1). The measured maximum suppressions correlate quite well with the predicted curve.

Each data point represents the maximum of a measured suppression versus frequency curve. The measured maxima are directly comparable with the prediction provided the treatment used in the test actually had the optimum impedance components at the values of H/λ_o reported, i.e., was appropriately tuned.

The close grouping of the data relative to the predicted curve, therefore, strongly suggests that in the exhaust duct the plane-wave mode is dominating current engine design. This approach suggests that an important way to obtain

36

higher peak suppression and thus greater treatment effectiveness is to include splitters and so to reduce H/λ_0.

The following procedure was used:

- Calculated suppression at the blade passing frequency (BPF) or its harmonics was increased by a factor of 10/7 to account for the observed enhanced suppression at these frequencies from engine and duct data relative to broadband noise.

- If the imposed limitations prevented the corresponding liner segments on two opposite duct walls from being tuned to the same frequency, i.e., in case of liner mismatch, the effective peak suppression of each segment was reduced by 35%.

- Suppression bandwidth appropriate to the value of the frequency parameter, H/λ_0, of each liner segment was applied to the effective maximum suppression of each liner segment and the respective suppression spectra were generated.

Suppression bandwidth plots are shown in Figure 3-9.

Empirical experience yields results confirming the suppression bandwidth curves. The bandwidth is given in terms of percentage of peak suppression (dB units) versus the ratio of frequency to maximum suppression frequency. The data are derived from duct test results in which the peak suppression as given in Figure 3-8, Appendix B, was achieved.

- Whenever warranted by the curvature of the duct, the suppression bandwidth included appropriate modifications due to curvature effect. The latter was based on experimental duct data. Figure 3-10, Appendix B, shows the effect of duct curvature on suppression bandwidth. The shown curvature effects are based on measured suppression enhancement in a treated curved duct as compared with the attenuation in a straight duct of the same dimensions and lined with equivalent treatment as the curved duct. The curved duct is also shown schematically in Figure 3-10.

- The total suppression spectrum (i.e., the sum of the suppression spectra of the constituent liner segments of the phased treatment) was constructed.

- The appropriate phasing effect spectrum was incorporated into the total suppression spectrum. The phasing effect is based on duct experimental results. A representative effect of phased (multi-element) treatment on suppression is illustrated in Figure 3-11.

- The suppressed spectra were obtained.

- The respective suppression ΔPNdB's were obtained from the unsuppressed and associated suppressed PNdL levels.
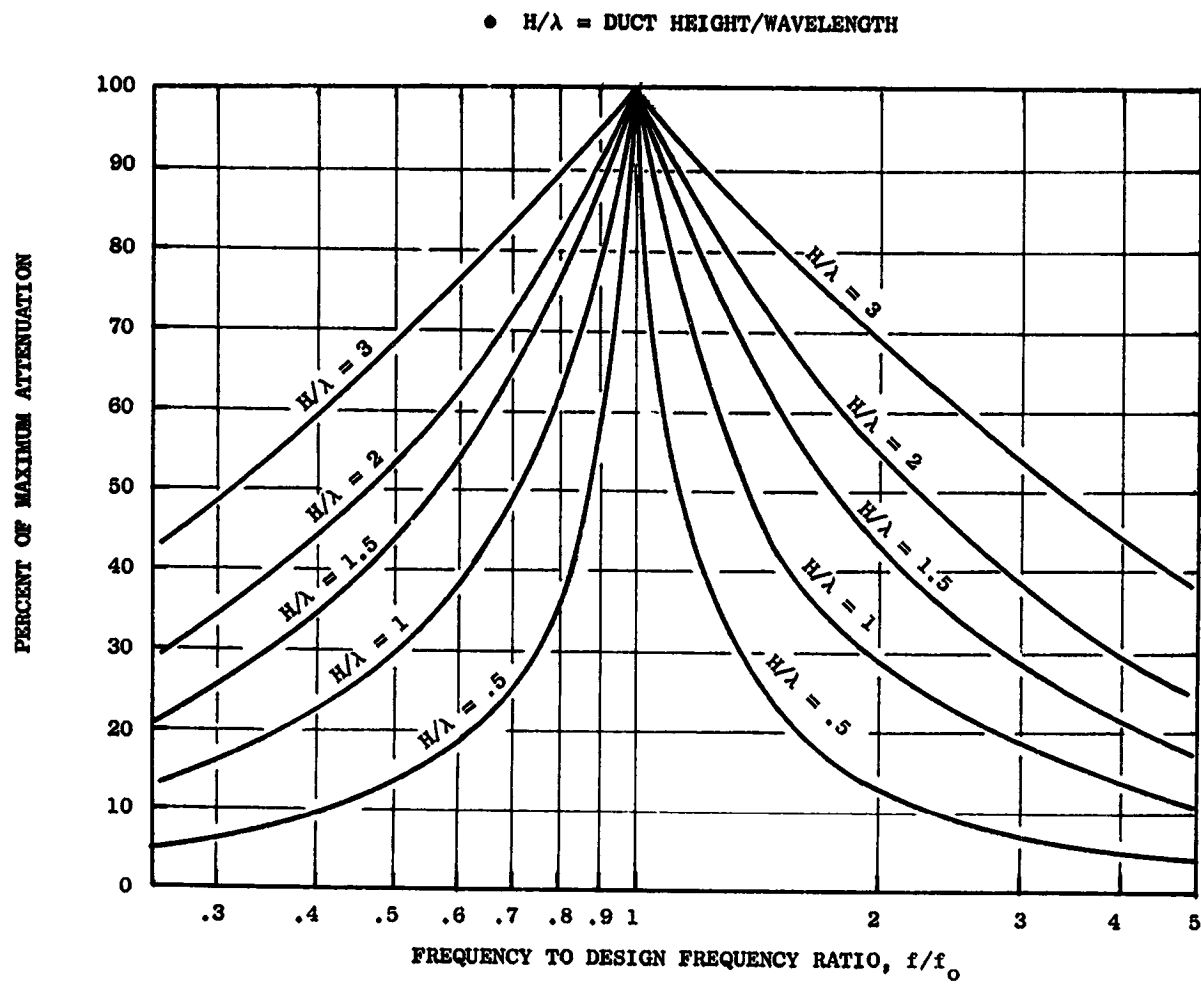
Figure 3-9. Suppression Spectrum Relative to Maximum Attenuation.
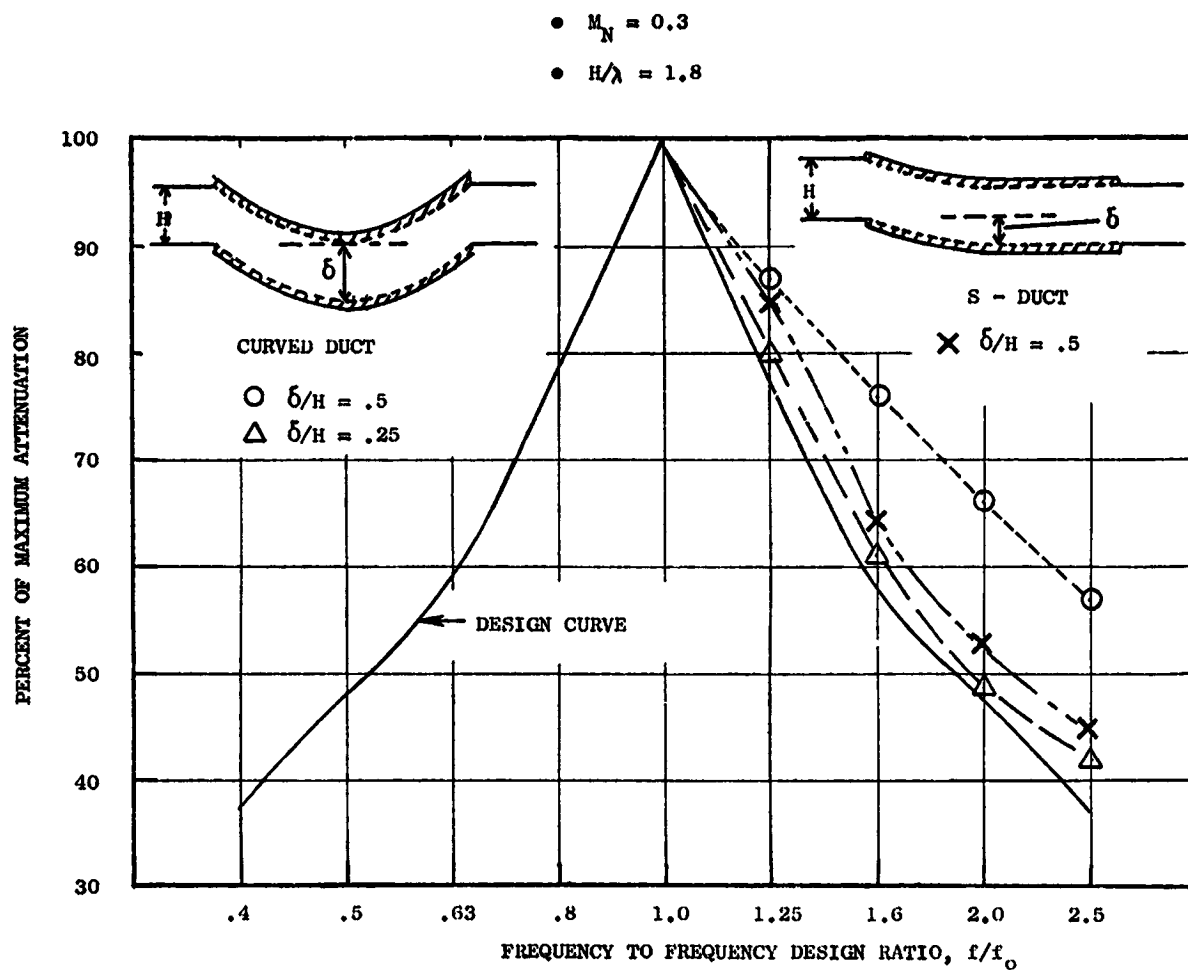
Figure 3-10. Effect of Duct Curvature on Suppression Bandwidth.
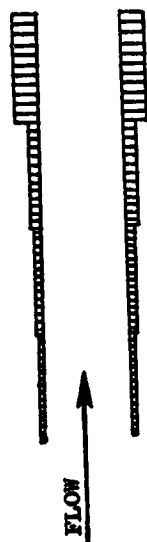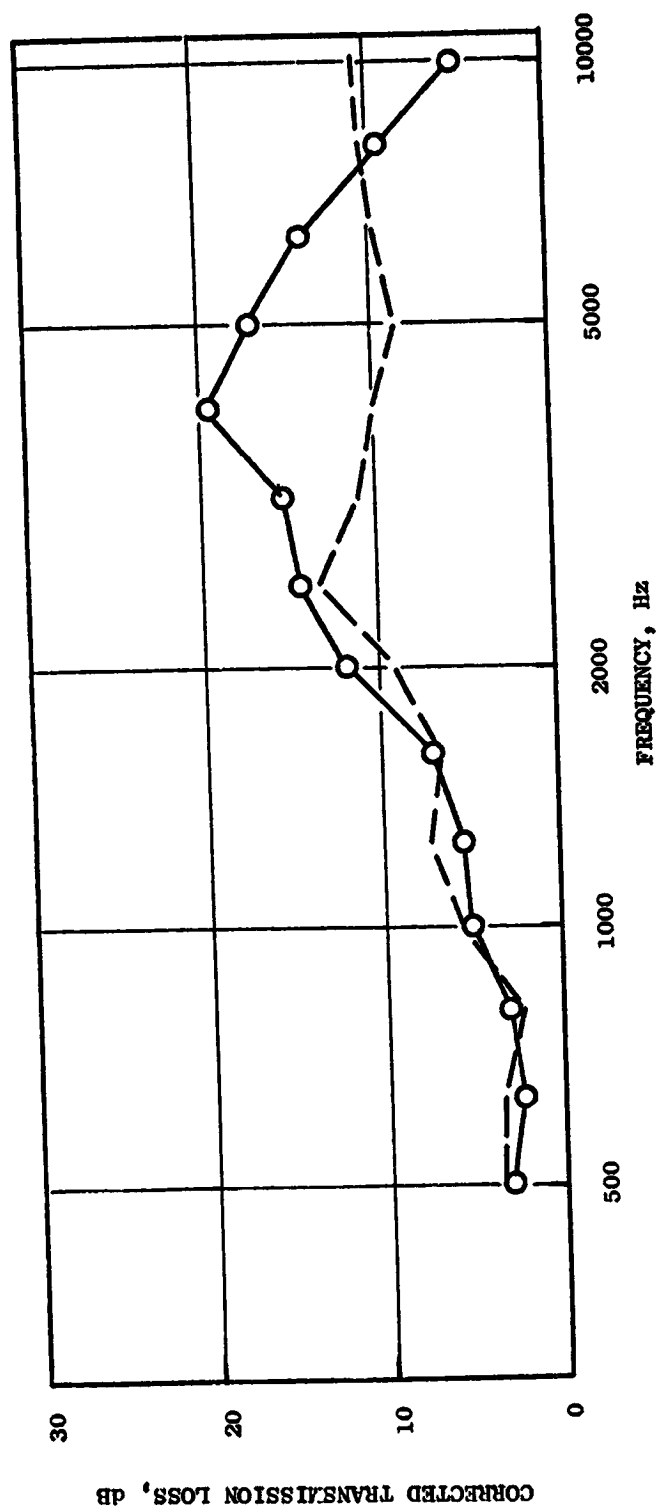
Figure 3-11. Typical Phased Treatment Test Results.

40

Figure 3-12 shows the maximum aft angle 152.4 m (500 ft) sideline, 61 m (200 ft) altitude unsuppressed, and Noy-weighted unsuppressed fan spectra of the UTW engine. Two SPL peaks are observed: one at the blade passing frequency of 1000 Hz and another at 2000 Hz, the 2nd harmonic.

The fan exhaust duct treatment configuration is given in Figure 3-13 with the respective liner depths, faceplate parameters, liner segment lengths, splitter length and thickness, and average duct heights defined.

Figure 3-14 shows suppression spectra ascribed to longitudinal liner segments as identified by the circled numbers. The sharply peaking suppression spectrum, 4, is due to the fan frame treatment which was assumed to be effective mainly at the blade passing frequency (BPF). The "total" suppression spectrum is the sum of all liner segment spectra. Also given is the "total" spectrum with curvature effect and the suppression spectrum which includes the former and phasing effect. The duct curvature and phased treatment are shown to increase the "total" suppression level at frequencies above 3000 Hz.

Figure 3-15 compares the unsuppressed, the suppressed, and Noy-weighted suppressed fan spectra on a 152.4 m (500 ft) sideline at the maximum aft angle. The suppressed spectra include the effects of curvature and phasing. The suppressed Noy-weighted spectrum is flat with respect to frequency which indicates a balanced treatment design.

Table 3-VI lists the respective fan exhaust duct suppressions in terms of ΔPNdB. The frame and wall treatment alone without the splitter and the beneficial effects of the duct curvature and phasing is predicted to produce a suppression of 6.2 PNdB. The curvature and phase effects enhance suppression by 1.0 PNdB. The 101.6 cm (40 in.) long treated splitter doubles the suppression to 14.5 ΔPNdB.

Table 3-VI.   UTW Fan Exhaust Duct Suppression.

- 152.4 m (500 ft) Sideline
- Takeoff
- Maximum Aft Angle (120°)

Condition	ΔPNdB
● Frame and Wall Treatment, Standard Design	6.2
● Above with Curved Duct and Phased Treatment	7.2
● Frame and Wall Treatment, Splitter, Curved Duct, and Phased Treatment	14.5
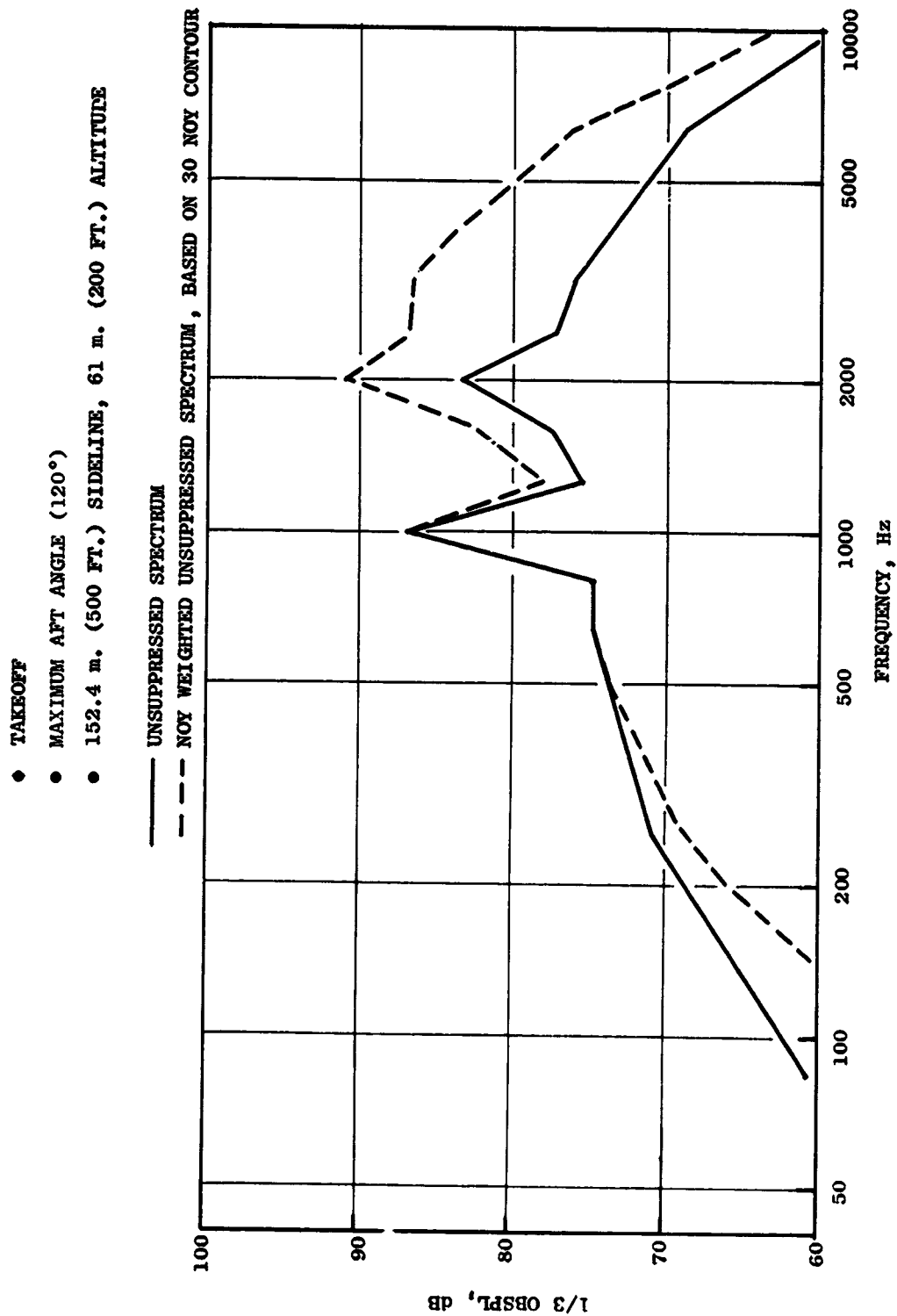
Figure 3-12. UTW Unsuppressed Fan Spectra.

- TAKEOFF
- MAXIMUM AFT ANGLE (120°)
- 152.4 m. (500 FT.) SIDELINE, 61 m. (200 FT.) ALTITUDE

UNSUPPRESSED SPECTRUM
--- NOY WEIGHTED UNSUPPRESSED SPECTRUM, BASED ON 30 NOY CONTOUR

1/3 OBSPL, dB

FREQUENCY, Hz

42

1.397 cm (.55") DEPTH

4.064 cm (1.6") DEPTH

2.54 cm (1") DEPTH

1.397 cm (.55") DEPTH

2.54 cm (1") DEPTH

1.397 cm (.55") DEPTH

2.54 cm (1") DEPTH

4.064 cm (1.6") DEPTH

35.6cm(14")

5.08cm(2")

30.5cm(12")

5.08cm(2")

35.6cm(14")

5.08cm(2")

25.4cm (10")

3.048 cm (1.2")

101.6 cm. (40")

43.2 cm(17")

17.8 cm(7")

STATION 264

STATION 200

OGV

SEGMENT ④ ① ② ③ ⑤ ⑥

FACEPLATE DIMENSIONS:

SEGMENT	THICKNESS	HOLE DIAMETER	OPEN AREA RATIO
④	.0813 cm (.032")	.0762 cm (.03")	10%
① ② ③ ⑤ ⑥	.0457 cm (.018")	.0813 cm (.032")	27%

Figure 3-13. UTW Fan Exhaust Duct Treatment.

43

● 101.6 cm (40") LONG SPLITTER
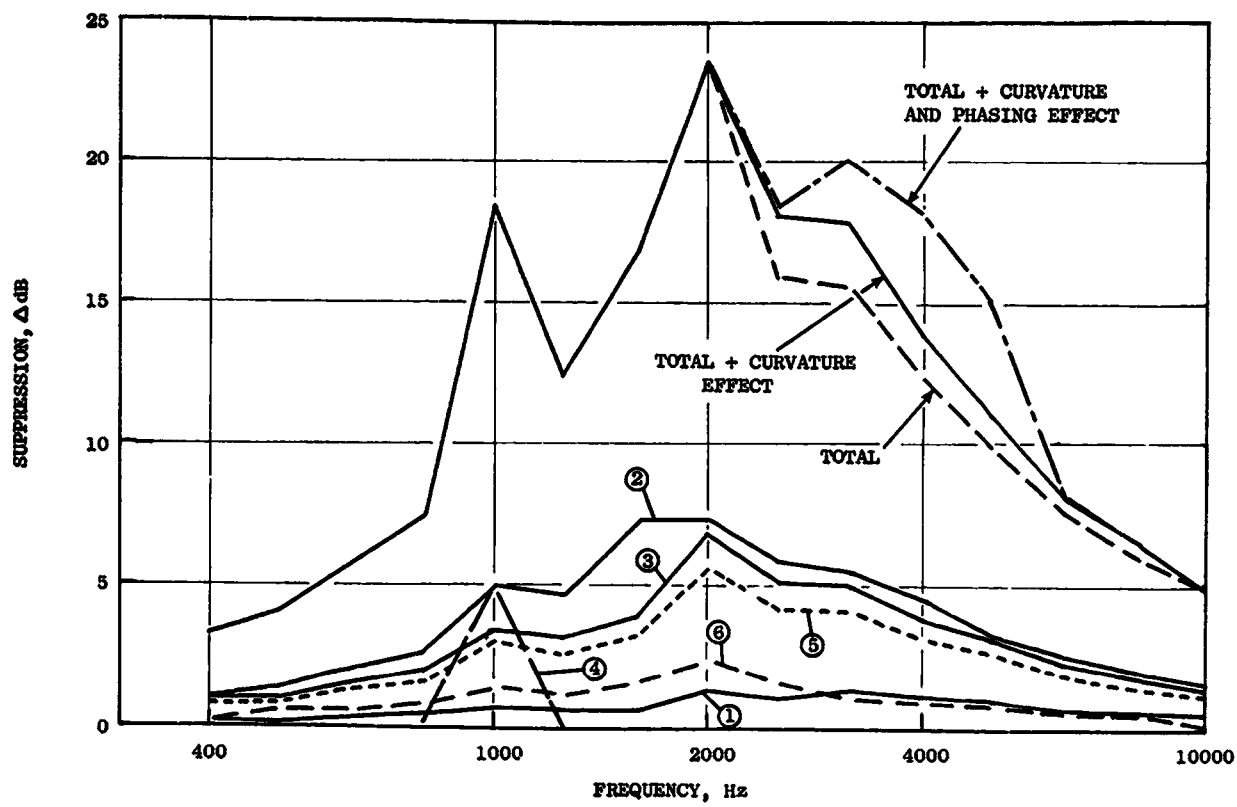
Figure 3-14. UTW Total and Segmented Fan Exhaust Duct Suppression.

44

● TAKEOFF

● MAXIMUM AFT ANGLE (120°)

● 152.4 m. (500 FT.) SIDELINE

—·— NOY WEIGHTED SUPPRESSED SPECTRUM, BASED ON 30 NOY CONTOUR

— — — SUPPRESSED SPECTRUM

——— UNSUPPRESSED SPECTRUM
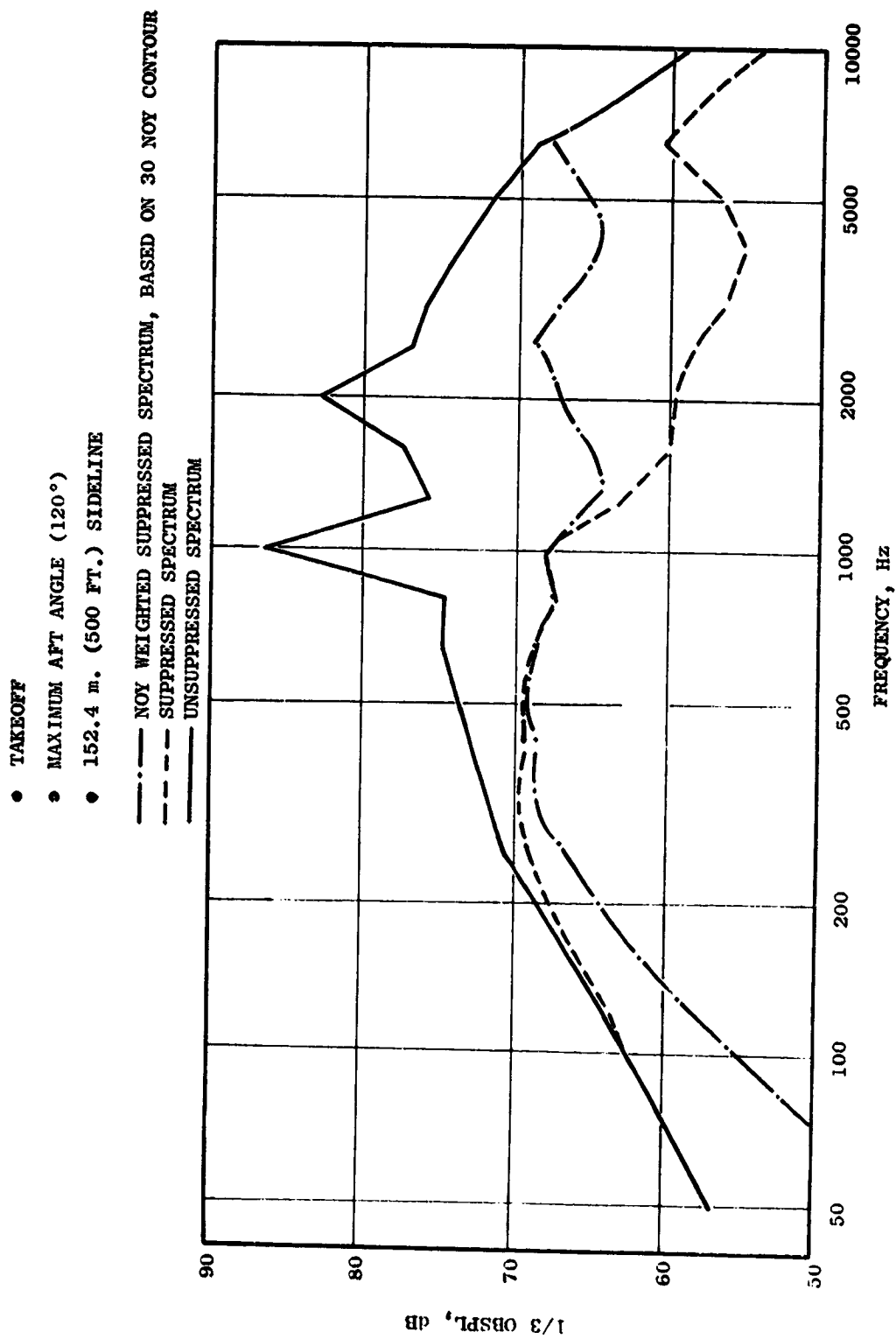
Figure 3-15.   UTW Suppressed and Unsuppressed Fan Spectra.

Suppressed Obstruction Noise and Flow Noise Regeneration

Part of the preliminary design study with respect to aft fan duct suppression involved the concern that the fully suppressed engine could exhibit noise floors which would prevent the treatment from being fully effective. The noise floors are strut noise, splitter trailing edge noise, and treatment flow regenerated noise.

The following models were used throughout the preliminary design to estimate the sound power levels for both the UTW and OTW engines.

The strut noise estimate is based on an overall power level (OAPWL) formulation, derived from a series of laboratory tests of obstructions in flow. The tests were performed under the core noise program (Reference 2). The over all strut noise power level is given by the following expression:

$$OAPWL = 16.8 + 10 \, Log \, (c \cdot t_{max} \cdot h \cdot u^5) + 4 \, Log \, C_D + 10 \, Log \, N \quad re: \quad 10^{-13} \, watts$$

where

c = chord, m (ft)

t_{max} = maximum strut thickness, m (ft)

h = strut length, m (ft)

u = upstream flow velocity, m/sec (ft/sec)

C_D = profile drag coefficient

N = number of struts

The spectral shape of the strut noise is shown in Figure 3-16. The suppression due to treatment aft of the six struts was applied in the UTW and OTW engines.

The splitter trailing edge noise estimate is based on a semiempirical formulation by I.L. Ver (Reference 3) and is as follows (for any 1/3-octave band):

$$PWL = 126 + 55 \, Log \, M + 10 \, Log \, A - 45 \, Log \, (P/100) + 7.5 \, Log \, (T/530)$$
(for T in ° R)

where

PWL = one-third-octave Power Level   re: 10^{-13} watt

and

M = surface Mach number

A = surface area, m^2 (ft^2)

P = percent open area of cross section of flow passage area

46
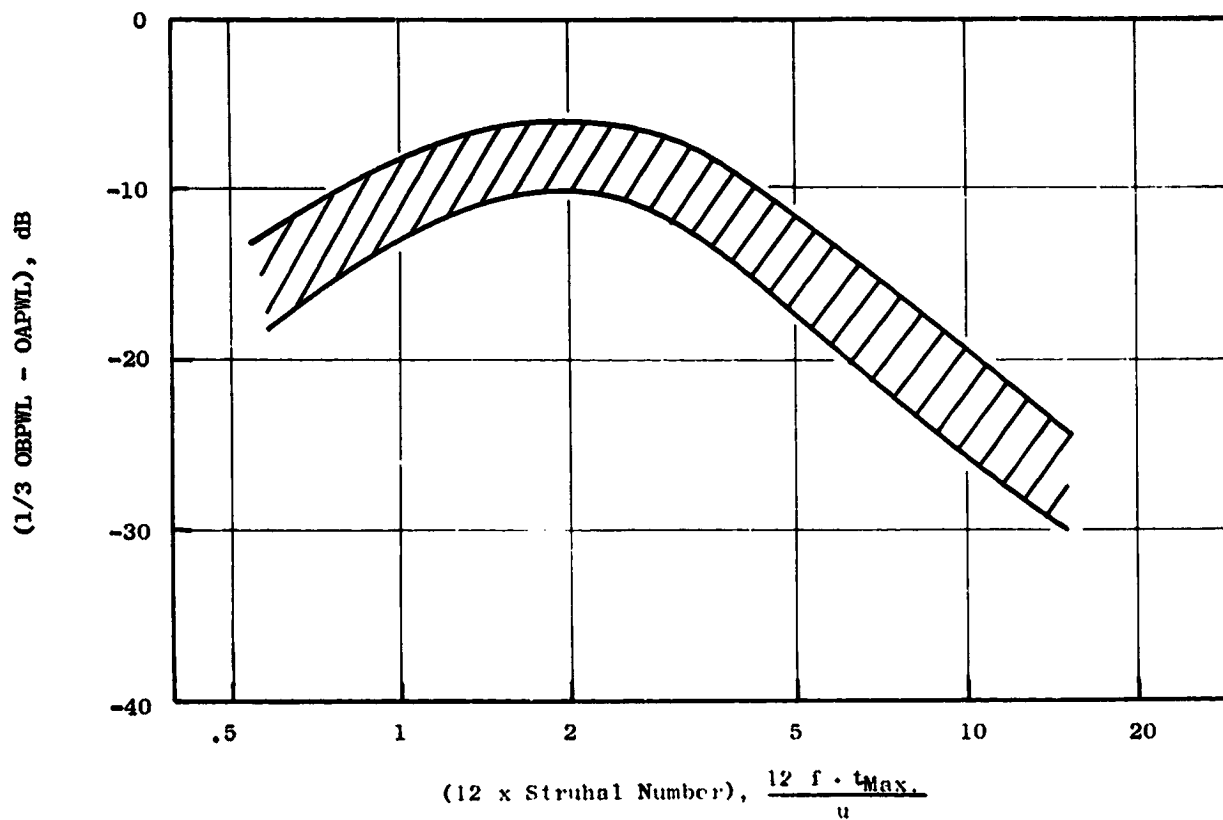
Figure 3-16. Normalized Spectrum of Strut Noise.

This prediction scheme is based on commercial silencer system noise floor data. Besides the flow Mach number and the radiating area (Face Area), the only other correlating parameter is the blockage or percent open area of cross section (P). The Ver-based estimate presents an upper limit, since commercial silencer trailing edges do not necessarily represent the best aerodynamic design and we have not applied any suppression due to treatment aft of the splitter trailing edge for this estimate.

The flow noise regenerated due to treatment is based on a model presented in Reference 3. The model, below, is under review in the course of this contract. An average turbulence scale of 2.5 cm (1 inch) has been used throughout this report. The attenuated flow regenerated noise floor level, p'(f), is given as follows:

$$p'(f) = [p(f)/2\beta] (1 - e^{-\beta L}) \text{ (watts/Hz·m)}$$

where

f = frequency, Hz

β = attenuation per unit length due to treatment (Neper/m)

L = treatment length (m)

The flow regenerated noise per unit length, p(f), is given by

$$p(f) = 1.6 \cdot M^3 \cdot \bar{u}^{-3} \cdot \rho \cdot A \cdot N^{-1} \cdot \delta^{-2} \cdot L^{-1} \times 10^{-7} \text{ (watt/ Hz·m)}$$

where

M = flow Mach number

$\bar{u}$ = flow mean velocity (m/sec)

ρ = density (kg/m^3)

A = scrubbing (treatment) area (m^2) per unit duct length

N = number of holes per unit area (m^{-2})

δ = turbulence scale (m)

All power level calculations involving obstruction or flow noise regeneration are based on a 10^{-13} watt reference level.

The sound pressure level floors for suppressed strut noise, splitter trailing edge noise, and attenuated treatment flow regenerated noise are shown in Figure 3-17. An average flow of 0.46 Mach number through the splitter section was assumed for these calculations. It is obvious that the suppressed engine spectrum is above these estimated floor levels.

48
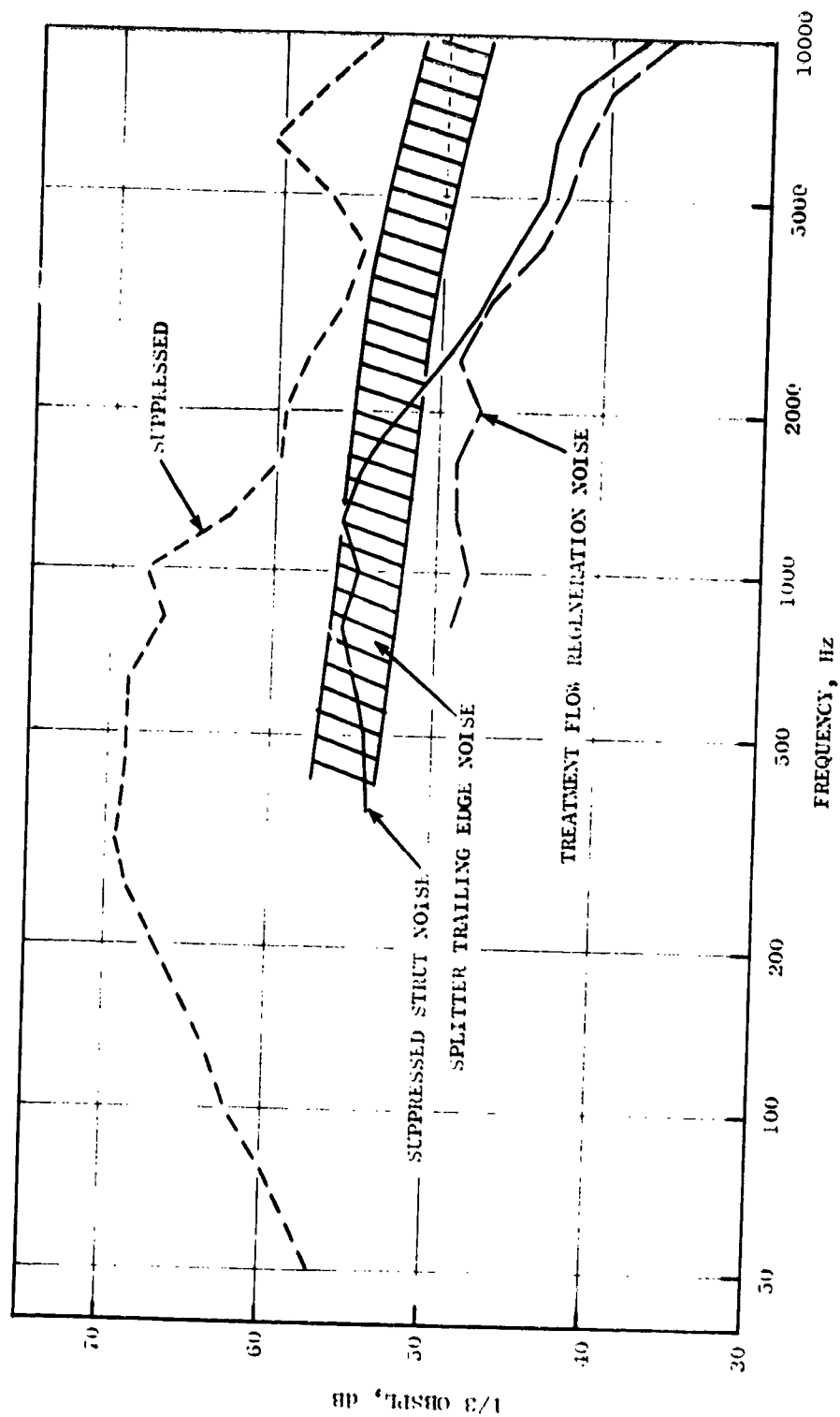
Figure 3-17. UTW Suppressed Fan and Flow Generated Noise Spectra.

49

The following values were assumed for the estimates shown in Figure 3-17.
Strut Noise:

Chord (c) = 25.08 cm (0.82 ft)

Max. Strut Thickness(t_{max}) = 1.58 cm (0.05 ft)

Strut Length (h) = 30.48 cm (1.0 ft)

Profile Drag Cooeff.(C_D) = 0.086

Number of Struts (N) = 6

Upstream Flow Velocity (u) = 161 m/sec (530 ft/sec)

Splitter Trailing Edge Noise:

Surface Area (A) = 4.63 m^2 (20.75 ft^2)

Percent Open Area of
Cross Section of Flow
Passage Area (P) = 92%

Temperature (T) = 294.3° K (530° R)

Trailing Edge Mach No. (M) = 0.48

Treatment Flow Regenerated Noise:

Number of Holes
per Unit Area (N) = 911,500 Holes/m^2 (84,400 Holes/ft^2)

Flow Mach No. = 0.46

Density (ρ) = 1.3 kg/m^3 (0.09 lb/ft^3)

$\hat{\beta}$ = 4.99 Nepers/m @ 2000 Hz

L = 1.064 m (42 in.)

$\bar{u}$ = 161 m/sec (530 ft/sec)

S = 2.54 cm (1.0 in.)

A = 10.8 m^2 (48.5 ft^2)

Core Exhaust

Takeoff core suppression requirements are based on the spectra shown in Figure 3-18. The core spectrum, a combination of both turbine and combustor spectra, shows peaks at 315 Hz and 5000 Hz when Noy weighted. The Noy-weighted combustor spectrum, not shown, yields two peaks, one at 315 Hz and the other at 2500 Hz. Therefore, the following core suppressor designs are based on these three tuning frequencies.

Table 3-VII shows a comparison of six suppressor designs based on current prediction methods and data. The ΔPNdB numbers are results from applying the suppression spectra shown in Figures 3-19 through 3-22 to the core spectrum and its components.
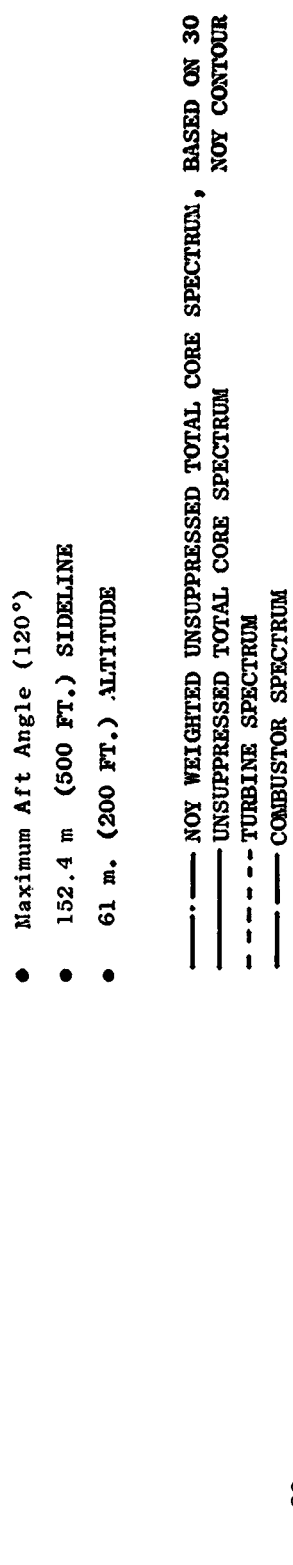
Figure 3-18. UTW Takeoff Unsuppressed Core Spectra.

51

Table 3-VII. Core Suppression.

- 152.4 m (500 ft) Sideline
- Takeoff

Treatment	PNdB Suppression		
	Core	Combustor	Turbine
1. Folded Quarter Wave (600 Hz; 2000 Hz) (600 Hz; 5000 Hz)	4.0 4.5	2.7 1.8	4.5 7.0
2. SDOF (4000 Hz)	4.3	2.3	8.4
3. Phased SDOF (2500 Hz; 5000 Hz) Without Phased Effect	4.4	2.6	8.5
4. Phased SDOF (2500 Hz; 5000 Hz) With Phased Effect	4.9	2.8	10.6
5. Side Branch Resonator (2500 Hz; 5000 Hz) Without Phased Effect	5.6	4.3	7.6
6. Side Branch Resonator (2500 Hz; 5000 Hz)	6.1	4.5	9.6

- 4000 Hz TUNING FREQUENCY
- 810.9 °K (1000 °F)
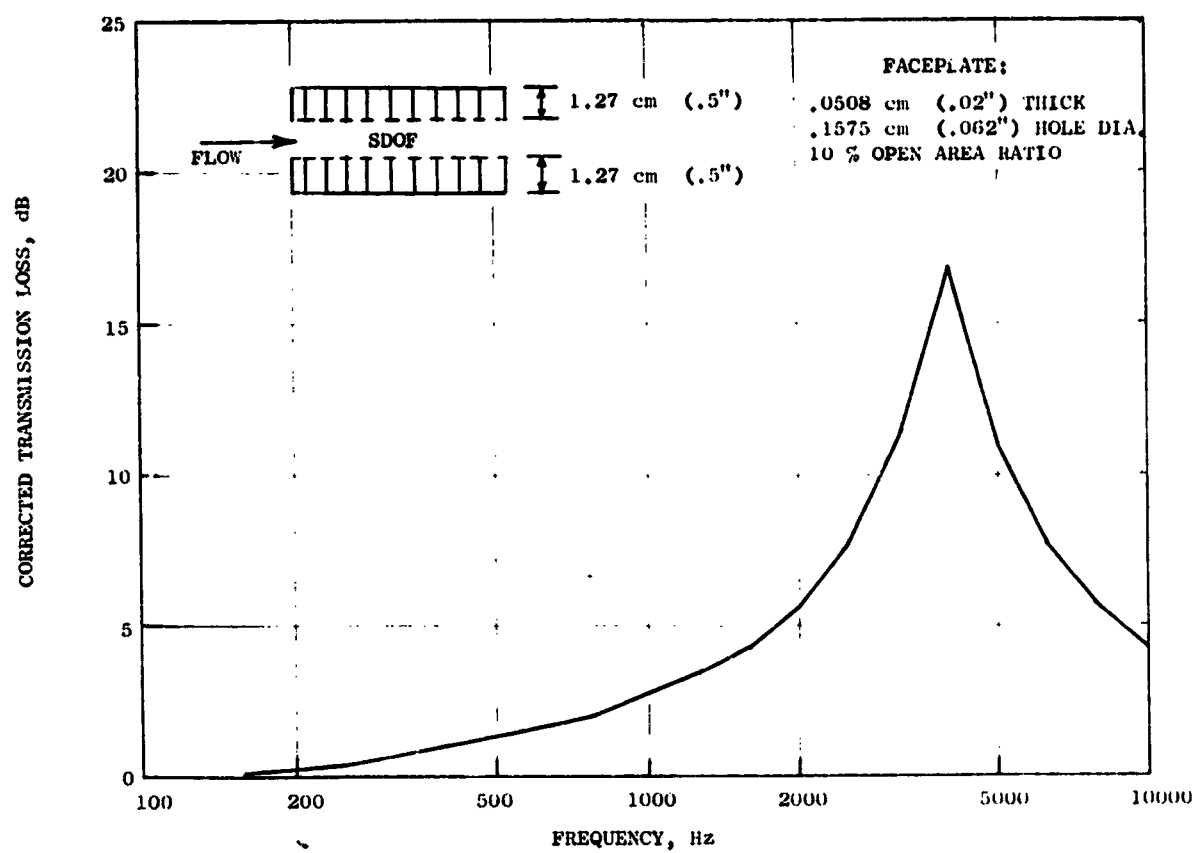
Figure 3-19.   SDOF Predicted Transmission Loss.

Figure 3-20. Predicted Transmission Loss of Phased SDOF.
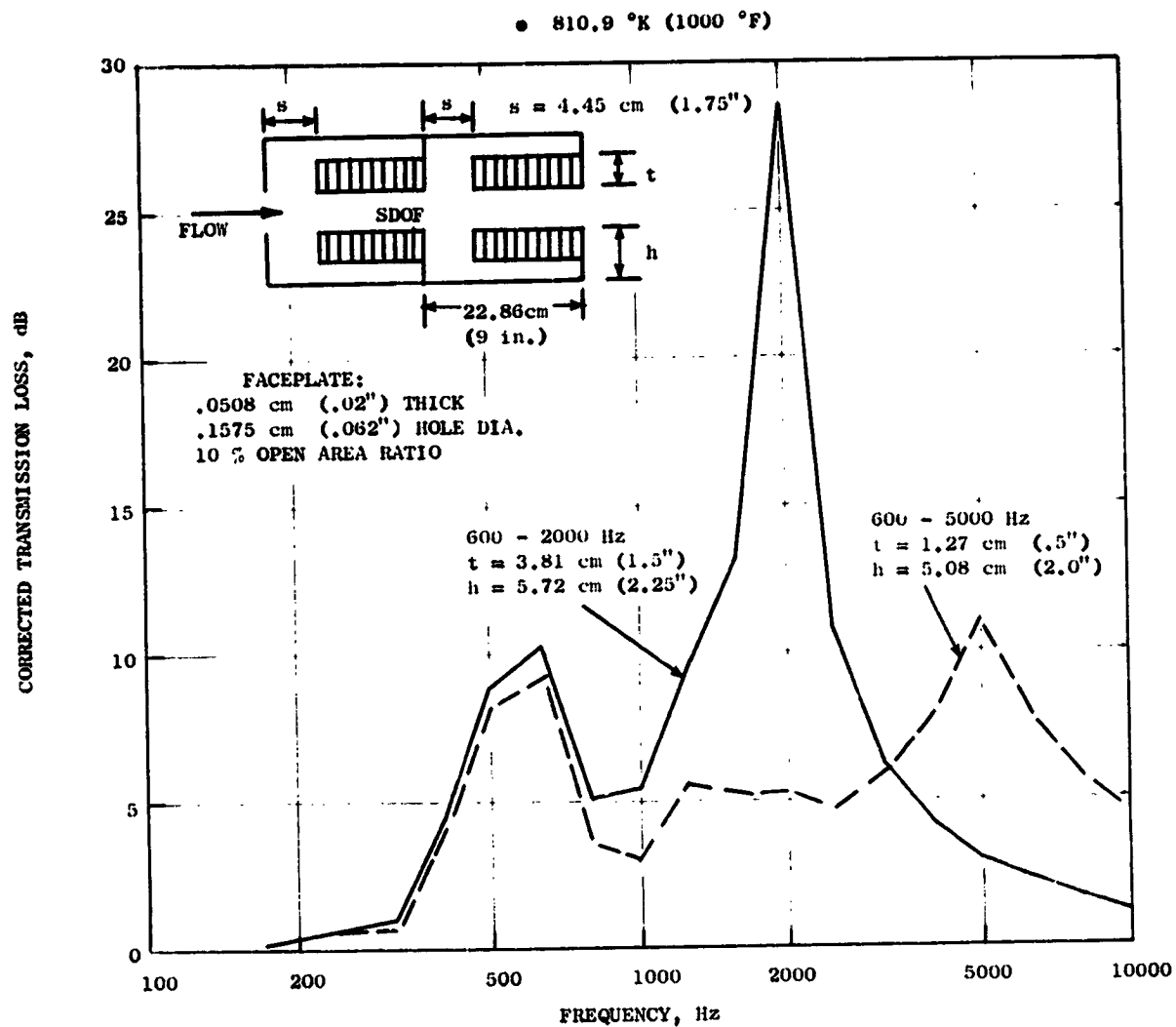
Figure 3-21. Folded Quarter Wave Predicted Transmission Loss.

- 2500 AND 5000 Hz TUNING FREQUENCIES
- 810.9 °K (1000 °F)

PHASED SDOF

FLOW

SIDE BRANCH RESONATOR

WITH PHASED EFFECT

WITHOUT PHASED EFFECT
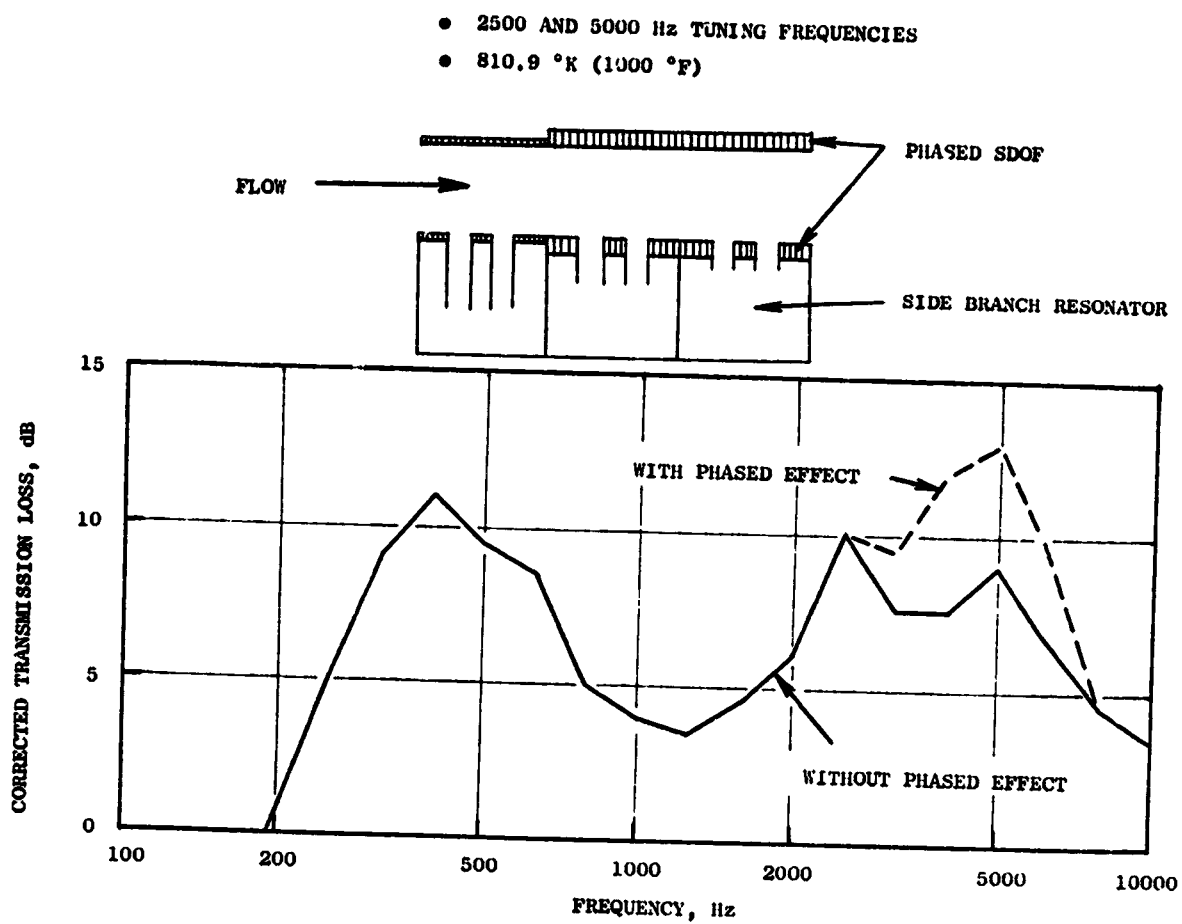
Figure 3-22. Predicted Transmission Loss of Side Branch Resonators with Phased SDOF.

The SDOF and phased SDOF suppression estimates shown in Figures 3-19 and 3-20 result from using Figure 3-8, Appendix B, to predict the peak attenuations and applying the proper bandwidths from Figure 3-9. All predictions are made at 540° C (1000° F) and at a Mach number of 0.4. The phase effect shown in Figure 3-20 is derived from test data with the effect shown in Figure 3-11. When SDOF and phased SDOF treatment are not used in conjunction with a low frequency suppressor design, an 80% effective area is used to account for pylons, joints, and mounting brackets in the engine duct.

The folded-quarter wave concept's predicted suppression shown in Figure 3-21 is scaled from rectangular duct data. The SDOF components' suppression is predicted in the same manner as above with a 60% effective area to account not only for the engine duct pylons, joints, brackets, but also the 20% open area required for the folded-quarter wave suppressors.

The most optimistic suppression shown in Figure 3-22 is for the side-branch resonator design, consisting of three side-branch resonators tuned for different low frequencies in combination with high frequency SDOF treatment. The suppression predictions, Table 3-VII, are based on side-branch resonator theory stating the transmission loss as:[4]

$$TL = 10 \, \mathrm{Log}_{10} \left[1 + \frac{\alpha + 0.25}{\alpha^2 + \beta^2 \, (f/f_o - f_o/f)^2} \right]$$

where

f = frequency, Hz

f_o = resonance frequency, $\left(c/2\pi\sqrt{A_o/V \times t'} \right)$ Hz

α = resonator resistance $(SR/A_o\rho c)$

β = resonator reactance $(Sc/\pi f_o V)$

S = area of main duct, m^2

R = flow resistance of resonator neck, mks rayls

V = volume of resonator, m^3

A = total resonator neck area, m^2

t' = equivalent length $(t + 0.8 \, A_o)$, m

ρ = gas density, kg/m^3

c = speed of sound, m/sec

t = neck length, m

Substituting the proper values for the variables at 540° C (1000° F) and for M = 0.4, the suppression for each side-branch resonator was super-imposed with the high frequency SDOF. Here again, the SDOF components' suppression is predicted using the method described previously and a 60% effective area to account for engine geometry and side-branch resonator 20% open area. Figure 3-23 shows the UTW installation of the side-branch resonator suppressor design.

Compressor Inlet

The compressor inlet treatment design is shown in Figure 3-24. The treatment was designed such that the depicted configuration would give a peak suppression value of 6 dB at 8000 Hz, the compressor first-stage blade passing frequency. The peak suppression estimate was made using Figure 3-8, Appendix B, having defined the L/H and H/λ_o parameters.

The second- and third-stage compressor tones were not considered to contribute to the total engine system noise level since their blade passing frequencies occur at 10,000 Hz or above in a low Noy weighted region.

3.3.4 Approach Noise Constituents

To obtain 65% thrust at approach, the UTW fan may be operated at a variety of engine speeds, blade angles, and nozzle area combinations. For the preliminary design, the engine speed was assumed to be 100% (to satisfy engine response requirements) which required a blade angle change of +8° (toward flat pitch) with a nozzle area equal to takeoff.

As blade angle varies, the fan source noise, forward and aft, changes. NASA QF9 reverse pitch fan data and General Electric 91.44 cm (36 in.) reverse pitch fan data (Reference 5) were used to define this variation in noise as shown on Figure 3-25, Appendix B). In the forward quadrant, the 91.44 (36 in.) data would predict a reduction in noise for a change in blade angle of 0.14 radians (+8°) while the QF9 data would increase slightly. For the preliminary design, an increase of 1 PNdB was assumed on the fan inlet noise. In the aft quadrant, both sets of data show a bucket-type curve which does not affect the noise between zero radian (0°) and 0.14 radian (8°). The fan aft noise levels were not changed for the 0.14 radian (8°) blade angle variation.

The approach noise constituents are shown on Figure 3-26. Jet/flap noise in the forward quadrant is the dominant source for the suppressed levels with fan inlet, exhaust, and aft jet/flap noise approximately 6 to 8 PNdB lower. Unsuppressed, the fan aft noise is dominant. Table 3-VIII gives the constituent levels, forward and aft from unsuppressed 61 m (200 ft) sideline to suppressed inflight totals forward and aft. The Appendix I corrections are similar to the takeoff condition.

58

FAN EXHAUST
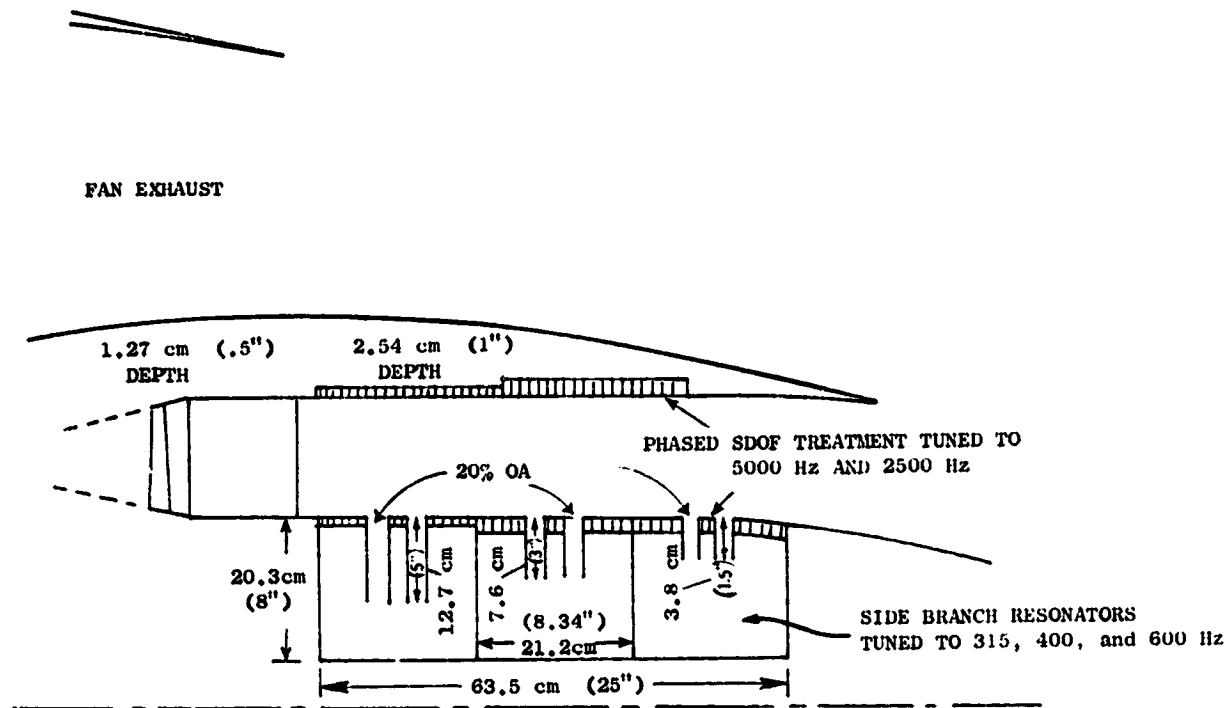
Figure 3-23. UTW Core Treatment (Conceptual Design).

● PEAK SUPPRESSION = 6 dB
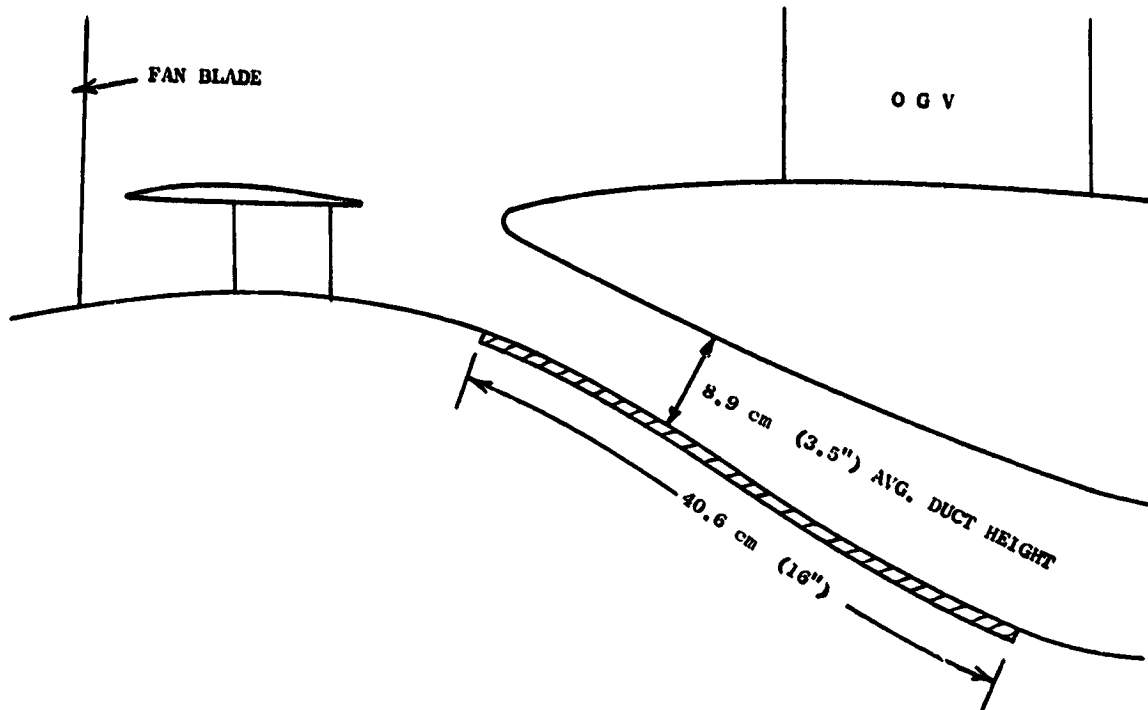
COMPRESSOR FIRST STAGE BPF

	TAKEOFF	APPROACH
UTW	8000 Hz	8000 Hz
OTW	8000 Hz	6300 Hz

SECOND AND THIRD STAGE TONES FALL INTO
HIGH FREQUENCY (10KHz AND ABOVE) LOW NOY
WEIGHTED REGION

FACE PLATE THICKNESS = .0254 cm (.01")
HOLE DIAMETER = .1143 cm (.045")
OPENAREA RATIO = .095
CAVITY DEPTH = .4572 cm (.18")
$L/H = 2.28$
$H/\lambda = 1.63$
PEAK TUNING FREQUENCY = 6300 Hz
FLOW MACH NUMBER = 0.4

Figure 3-24. QCSEE Compressor Treatment.

Figure 3-26. UTW Approach Noise Constituents.

- 65% THRUST AT AIRCRAFT SPEED
- 152.4 m (500 FT.) SIDELINE, 61 m (200 FT.) ALTITUDE
- 41.15 m/s (80 KNOTS) AIRCRAFT SPEED
- EPNdB = 91.5
- GEAR AND COMPRESSOR, NON-CONTRIBUTING CONSTITUENTS

Table 3-VIII. QCSEE UTW Noise Levels.

- Approach Power (65% Thrust @ A/C Speed)
- Takeoff Fan Speed
- Blade Angle = 0.14 radians (8°) Closed

	(1.047 radians, 60°) Max. Forward Angle PNdB				(2.094 radians, 120°) Max. Aft Angle PNdB			
	Fan	Turbine	Combustor	Jet/Flap	Fan	Turbine	Combustor	Jet/Flap
Single Engine - Unsuppressed @ 61 m (200 ft) Sideline	103.9	84.3	88.8	98.2	106.1	97.3	94.8	93.6
Total Corrections - Appendix A Procedure	-9.8	-7.8	-4.3	-5.9	-7.5	-8.0	-5.2	-7.1
Corrected Level	94.1	76.5	84.5	92.3	98.6	89.3	89.6	86.5
Suppression	-8.0	-9.6	-4.5	-	-14.5	-9.6	-4.5	-
Suppressed System	86.1	66.9	80.0	92.3	84.1	79.7	85.1	86.5
Sum Constituents	93.7				91.1			

PNdB to EPNdB   91.5 EPNdB

3.3.5 Approach Suppression

Inlet

The inlet treatment was designed using the procedure described in Section 3.3.7 to give maximum suppression for reverse thrust. The treatment configuration is shown in Figure 3-27.

Figure 3-28 depicts the approach maximum forward angle, 152.4 m (500 ft) sideline, 61 m (200 ft) altitude unsuppressed spectrum and the Noy-weighted unsuppressed spectrum. The unsuppressed spectrum is dominated by the peak at the BPF frequency. The Noy-weighted unsuppressed spectrum, however, is dominated by the second harmonic peak. Figure 3-29 shows the estimated suppression spectrum. The treatment as designed gives maximum suppression at 2 kHz, which corresponds to the peak in the Noy-weighted unsuppressed SPL spectrum. The resulting suppressed spectrum at the approach maximum forward angle 152.4 m (500 ft) sideline is shown in Figure 3-30.

Fan Exhaust

The fan exhaust duct suppression at 152.4 m (500 ft) sideline maximum aft angle is listed in Table 3-IX. The unsuppressed, suppressed, and Noy-weighted suppressed fan spectra at the maximum aft angle 152.4 m (500 ft) sideline are shown in Figure 3-31.

Table 3-IX.   UTW Fan Exhaust Duct Suppression.

- 152.4 m (500 ft) Sideline
- Approach
- Maximum Aft Angle (60°)

Condition	ΔPNdB
● Frame and Wall Treatment, Standard Design	6.1
● Above With Curved Duct and Phased Treatment	7.2
● Frame and Wall Treatment, Splitter, Curved Duct and Phased Treatment	14.5

The attained suppression, ΔPNdB, due to fan frame and assumed straight duct wall treatment is 6.1 dB. The estimated effect of duct curvature and of liner phasing increase the suppression to 7.2 PNdB. The suppression is more than doubled to 14.5 PNdB when the 101.6 m (40 in.) long treated splitter is included. The suppression increase is due to the additional treatment surface of the splitter and to the reduction in the duct height.

63

TREATMENT DEPTHS:

A = 1.524 cm (.6")
B = 1.905 cm (.75")
C = 2.413 cm (.95")

FACE PLATE THICKNESS = .051 cm (.02")
OPEN AREA RATIO = 0.10
HOLE DIAMETER = .102 cm (.04")

TREATED L/D = 0.74
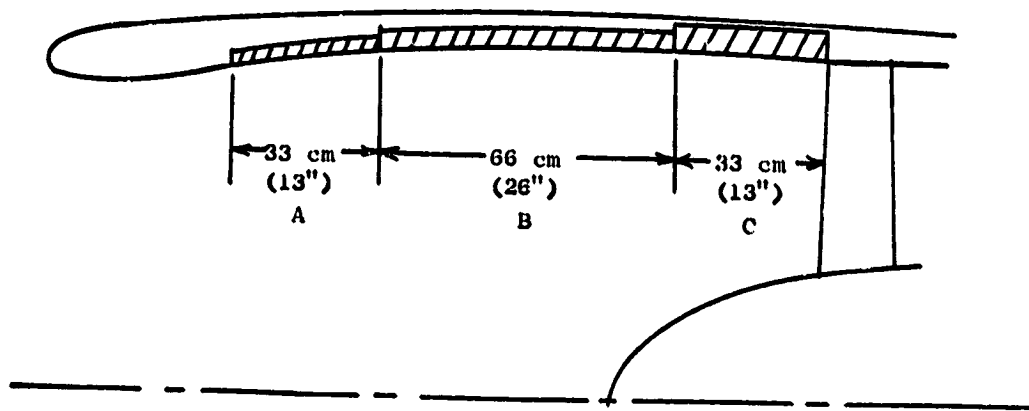
Figure 3-27. UTW Inlet Treatment Configuration.

Figure 3-28. UTW Unsuppressed Fan Spectra.

- APPROACH
- MAXIMUM FORWARD ANGLE (60°)
- 152.4 m. (500 FT.) SIDELINE, 61 m. (200 FT.) ALTITUDE
- 65% THRUST AT AIRCRAFT SPEED
- TAKEOFF RPM AND NOZZLE AREA
- BLADE ANGLE = .1396 RADIANS (8°)

--- NOY WEIGHTED UNSUPP. SPECTRUM, BASED ON 30 NOY CONTOUR
— UNSUPPRESSED SPECTRUM

65

- ROTOR 11 DATA SCALED TO QCSEE BLADE PASSING FREQUENCY
- TREATED L/D = 0.74
- APPROACH

	ROTOR 11	QCSEE
TREATED L/D	0.82	0.74
FAN TIP SPEED	298.7 m/s (980 FT/SEC)	289.6 m/s (950 FT/SEC)
BPF	8300 Hz	2000 Hz
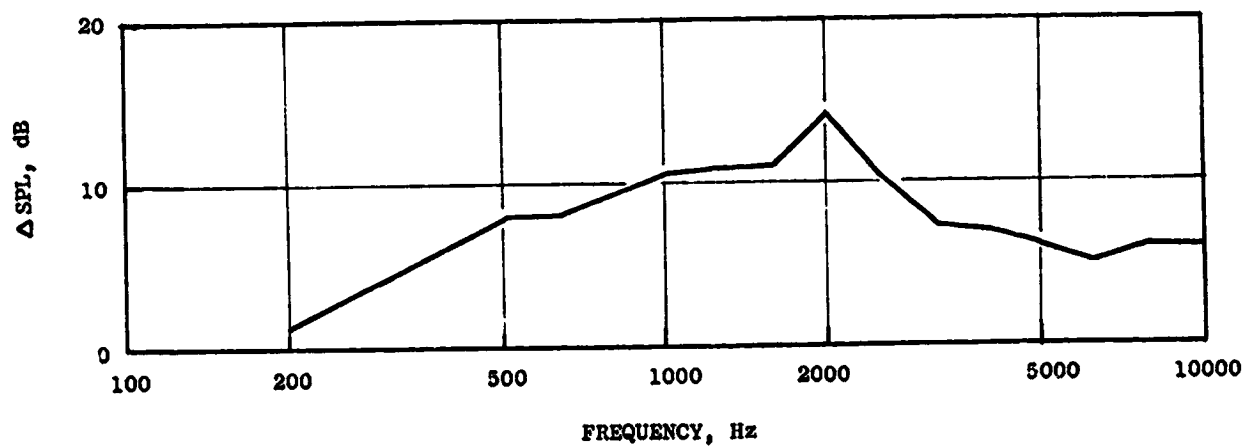
Figure 3-29. UTW Inlet Suppression.
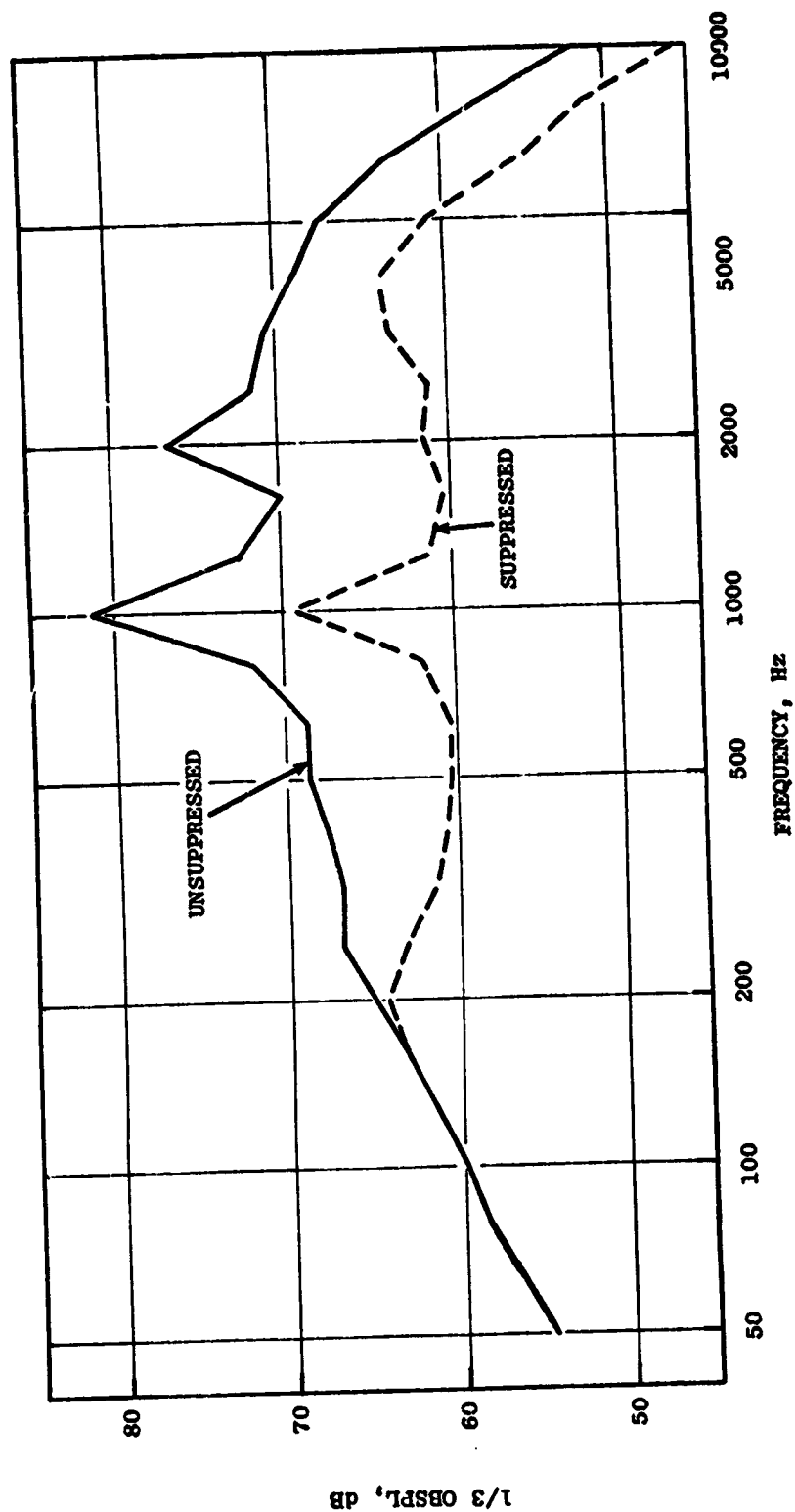
Figure 3-30. UTW Suppressed and Unsuppressed Engine Spectra.

67
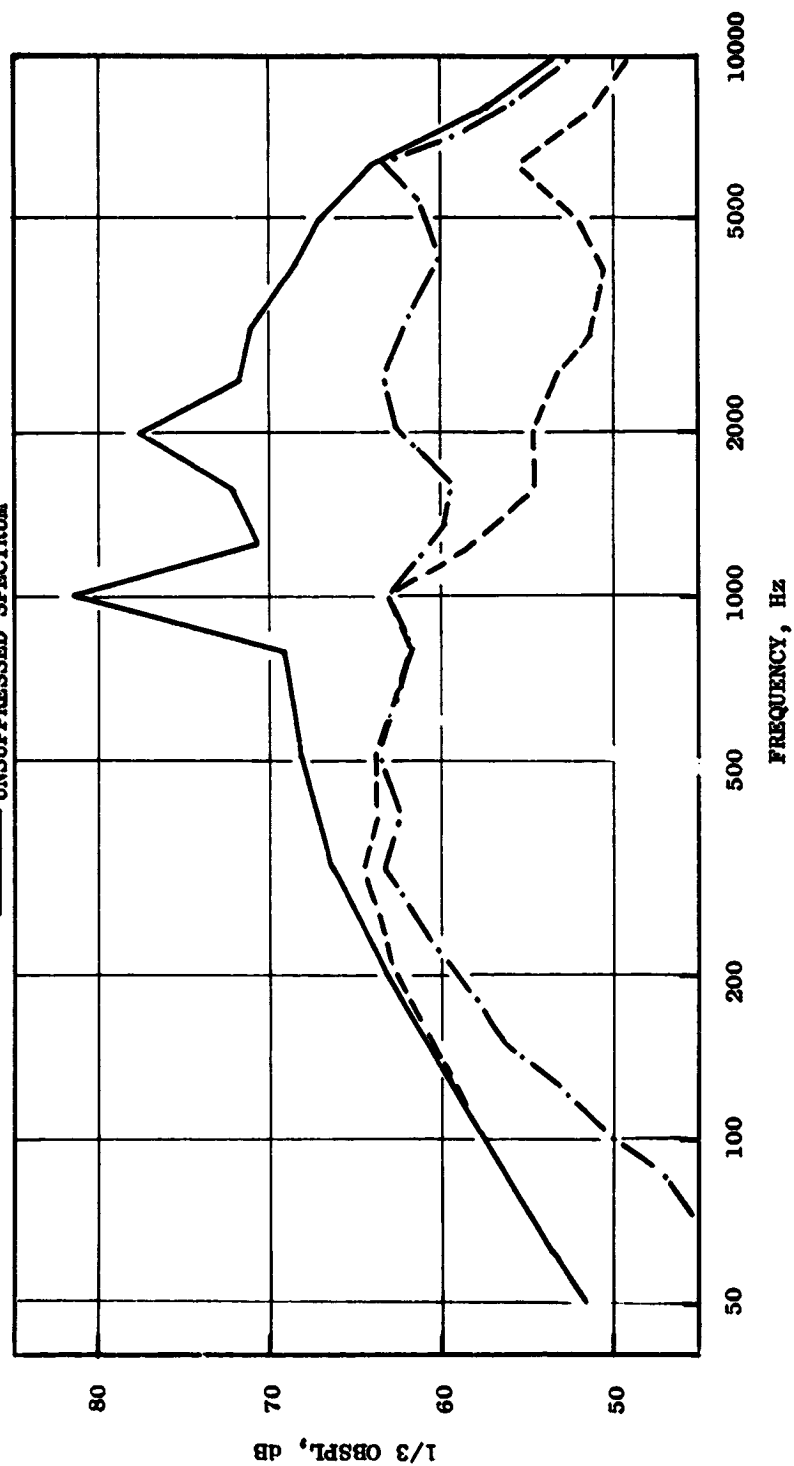
Figure 3-31. UTW Suppressed and Unsuppressed Fan Spectra.

Core Exhaust

At approach, the combustor and turbine spectra shapes change very little from the takeoff spectra shapes because of the relatively small core speed changes. Therefore, the suppression estimates for approach are the same as those at takeoff.

Compressor Inlet

The compressor inlet treatment design and suppression is the same as that described in Section 3.3.3.

3.3.6 Reverse Thrust Noise Constituents

The predicted noise constituents for the UTW engine operating in the reverse thrust mode are given in Figure 3-32. The constituents are for a single engine on a 152.4 m (500 ft) sideline at 90% fan speed, operating through stall, at 35% thrust.

The unsuppressed fan noise estimates were determined using QF9 data scaled to the UTW engine. The QF9 noise directivity was used to establish the relative unsuppressed noise levels at the maximum forward angle 1.05 radians (60°) and the maximum aft angle 2.09 radians (120°). The unsuppressed and suppressed fan noise for the UTW versus the QF9 levels are compared in Figure 3-33.

The turbine, combustor and jet/flap noise levels were determined using the same prediction methods as used for the forward mode noise estimates, with the pertinent engine cycle data as calculated for the engine reverse thrust mode operation. These constituent noise directivity patterns were assumed to have the same characteristics as for the forward thrust engine operation. The gear and compressor noise levels were estimated and found to be non-contributors to the total system suppressed noise level.

A breakdown of the noise constituents is given in Table 3-X. The corrections as defined in using the Appendix A procedure are given for each constituent along with the suppression levels. The maximum total noise found by summing the constituents is 98 PNdB at the maximum forward angle with the fan noise being the dominating noise source.

3.3.7 Reverse Thrust Suppression

The estimated fan noise suppression spectrum at the maximum forward angle is given in Figure 3-34. The suppression is for a treated-length-to-fan-diameter ratio of 0.74. The treatment was designed such that the maximum level of suppression could be achieved for the reversed thrust mode operation. The level of suppression for reversed thrust was established using the following procedure.

Figure 3-32. UTW Reverse Thrust Noise Constituents.

- 152.4 m (500 FT.) SIDELINE
- MAX PNdB = 98.0
- GEAR AND COMPRESSOR, NON-CONTRIBUTING CONSTITUENTS
- THRU STALL, 90% N_F

- 35% OF TAKEOFF THRUST
- 1.047 rad. (60°) ACOUSTIC ANGLE
- 152.4 m (500 FT.) SIDELINE
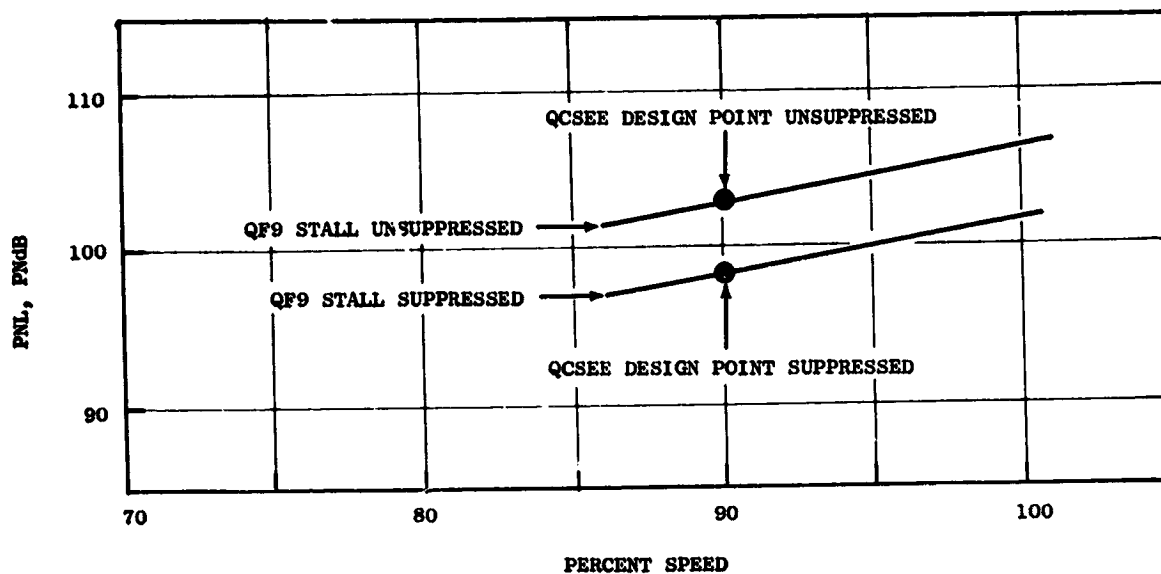
Figure 3-... UTW Reverse Thrust Fan Noise.

Table 3-X. QCSEE UTW Noise Levels.

- Reverse Thrust
- 90% Fan Speed
- Through Stall

	(1.047 radians, 60°) Max. Forward Angle PNdB				(2.904 radians, 120°) Max. Aft Angle PNdB			
	Fan	Turbine	Combustor	Jet/Flat	Fan	Turbine	Combustor	Jet/Flap
Single Engine – Unsuppressed @ 61 m (200 ft) Sideline	111.5	94.0	93.5	86.6	107.3	100.0	99.5	85.5
Total Corrections – Appendix A Procedure	-8.5	-17.5	-7.3	-7.1	-8.7	-10.7	-7.3	-7.1
Corrected Level	103.0	76.5	86.2	79.5	98.6	89.3	92.2	78.4
Suppression	-5.0	-9.6	-4.5	-	-9.3	-9.6	-4.5	-
Suppressed System	98.0	66.9	81.7	79.5	89.3	79.7	87.7	78.4
Sum Constituent=	98.0				92.7			
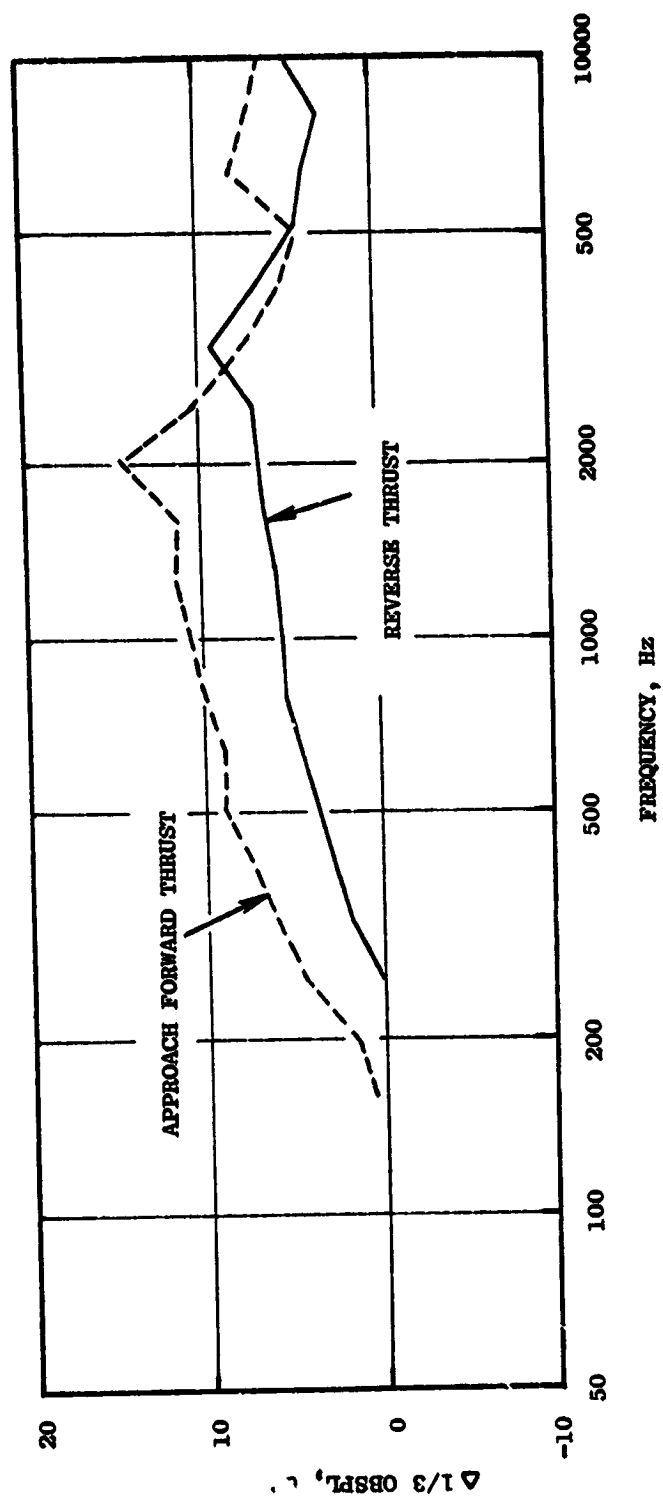
Figure 3-34. UTW Fan Inlet Suppression Spectra – Approach and Reverse Thrust.

73

1. The suppression spectrum was derived using measured fan suppression from Rotor 11 which had the same treatment-length-to-fan-diameter ratio (L/D) and the same fan tip speed as that of the UTW engine.

2. The suppression spectrum was then frequency shifted to the optimum tuning frequency of 3150 Hz found by Noy weighting the UTW reverse thrust maximum forward fan noise spectrum.

3. The level of suppression was then adjusted by applying the same percentage of peak suppression reduction as observed from acoustic duct test results. Figure 3-35 compares inlet and exhaust noise suppression levels at the fan exhaust and fan inlet Mach number as predicted for the UTW fan inlet at reverse thrust and forward thrust. The suppression bandwidths were not changed.

4. The approach noise suppression as shown was established by applying a frequency shift correction for the change in airflow direction and Mach number and increasing the peak suppression level to that measured for the given (L/D).

The suppression spectrum for the fan exlet was determined by adjusting the predicted fan exhaust suppression spectrum (as predicted for the exhaust treatment designed for takeoff at forward thrust Figure 3-14) to the reversed thrust conditions. This adjustment included corrections in peak frequency location and peak suppression levels due to the reversed flow direction as is illustrated in Figure 3-35.

No phasing effects were assumed, since laboratory experiments indicate that phased treatment is sensitive to treatment orientation. The exhaust duct treatment orientation was optimized for takeoff in the forward thrust mode. The peak suppression shifts from the 2000 Hz band to the 1250 Hz due to the reversed flow.

The combustor and turbine suppression estimates are the same as for the forward thrust conditions since the engine cycle parameters are not changed enough to produce significant changes in the unsuppressed spectral characteristics.

3.3.8 Effect of Constituents on System Noise

The primary constituents in the acoustic design are:

- Fan Inlet
- Fan Exhaust
- Core

Each has a significant development program defined to arrive at the design objectives. The levels for these three noise sources involves both unsuppressed noise estimates and suppression estimates. If either or both are different than the current evaluation, there will be an impact on the system EPNdB.

74
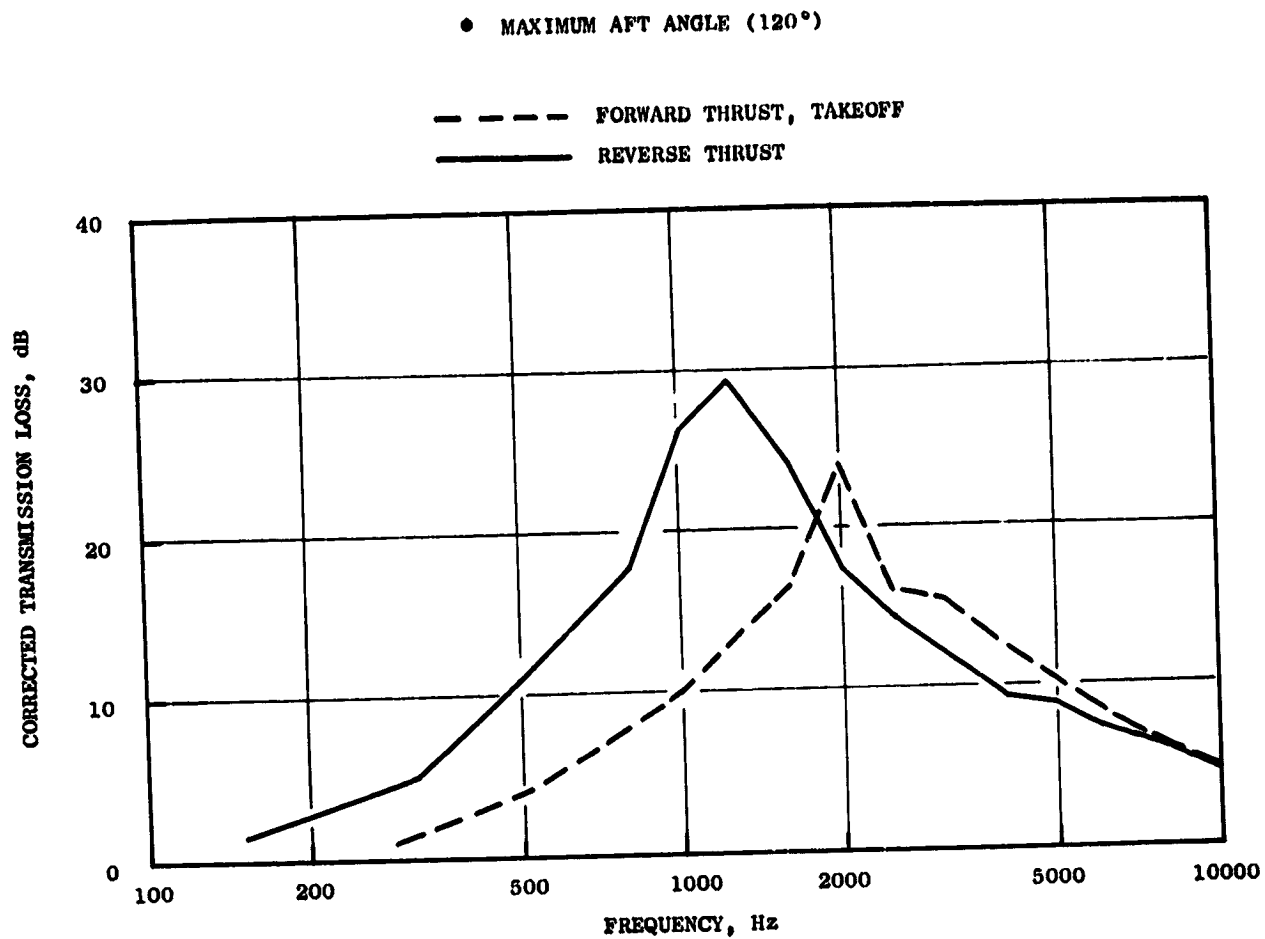
Figure 3-35. UTW Fan Exhaust Suppression Spectrum - Forward and Reverse Thrust.

Figure 3-36 is a carpet plot showing variations in the suppression level for each of the primary sources. The variation in suppression shown on the figures can also be interpreted as a variation in the unsuppressed noise level estimates with constant suppression.

The UTW design can vary all three source estimates and still meet the goal. For example, using Figure 3-36a with current core suppression estimates, the inlet level can be increased by 3 PNdB or the exhaust 2 PNdB and still meet 95 EPNdB. With the combustor and turbine levels increased by 2 PNdB, Figure 3-36b, the inlet noise can be increased 3 PNdB and the exhaust 0.5 PNdB.

With a 4 PNdB change in core noise, Figure 3-36c, the inlet and exhaust suppression must be increased significantly to meet the noise goal. Overall, Figure 3-36 shows the UTW design to be more sensitive to fan exhaust and core noise than to inlet noise.

3.4 OTW PRELIMINARY DESIGN

3.4.1 System Acoustic Design Considerations (OTW)

The fixed-pitch fan selected for the OTW engine also requires the selection of low noise design parameters as was done for the UTW engine. A fan tip speed of 350.5 m/sec (1150 ft/sec), less than 365.8 m/sec (1200 ft/sec) to ensure low inlet noise radiation, and a low fan pressure ratio (1.34) in order to keep aft radiated fan noise and OTW jet/flap noise to acceptable levels were chosen.

Tip speed and pressure ratio values are higher than those of the UTW engine since the OTW installation produces acoustic shielding for aft radiated noise.

Since a fan frame design common to the UTW engine is desirable, the Rotor-OGV spacing can be increased to 1.93 rotor chords with the shorter chord, higher blade number, fixed-pitch fan, which results in reduced fan source noise.

This advantage is to some extent offset by the reduction in the vane-blade ratio to 1.18 due again to the 33-element vane-frame with the 28-blade fixed-pitch fan. Since this design produces slightly higher tone levels and the acoustic treatment is more effective on tones, this effect is not a significant disadvantage. Table 3-XI lists the most salient engine design features which affect noise in the OTW design. This system like the UTW system produces an engine which is expected to meet the noise objectives as well as the weight and performance requirements.

3.4.2 Takeoff Noise Constituents

The constituent noise levels for the OTW propulsion system are given in Figure 3-37 in bar chart form. The unsuppressed engine is dominated in both the forward and aft quadrants by the fan noise. For the suppressed noise, the

76
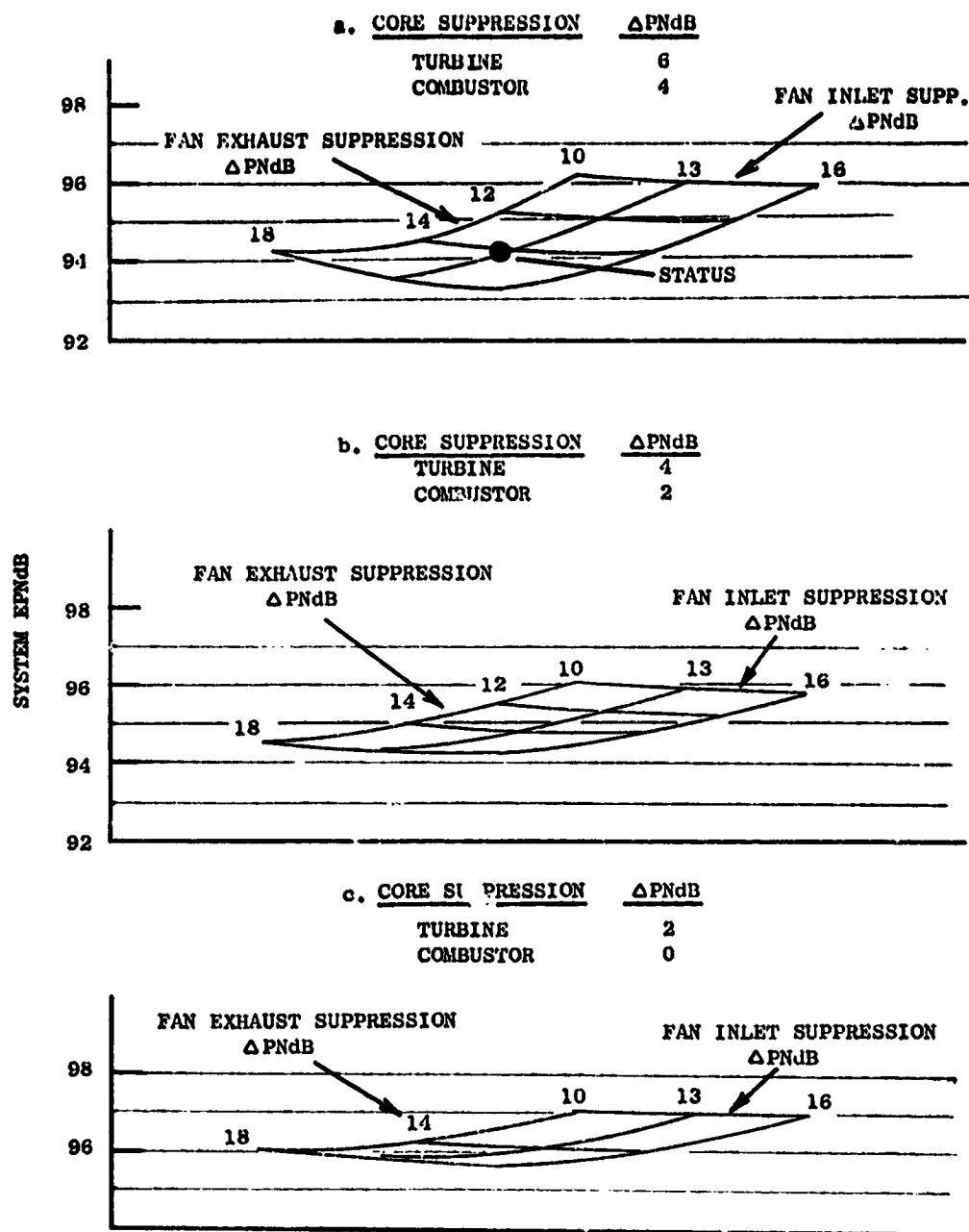
Figure 3-36. Effect of Constituent Suppression on System Noise - UTW.

Table 3-XI. OTW Design Parameters.

Number of Fan Blades	28
Fan Diameter, cm (in.)	180.4 (71)
Fan Pressure Ratio	1.34
Fan Speed, rpm	3778
Fan Tip Speed, m/sec (ft/sec)	350.5 (1150)
Number of OGV's	33
Fan Weight Flow, kg/sec (lb/sec)	405.5 (894)
Inlet Mach Number (Throat)	0.79
Rotor/OGV Spacing	1.93
Treatment Length/Fan Diameter	0.74
Exhaust Area, m^2 ($in.^2$)	1.747 (2708)
Gross Thrust (Uninstalled) kN (lb)	93.4 (21,000)
Blade Passing Frequency, Hz	1760
Exhaust Weight Flow, kg/sec (lb/sec)	402 (886)
Exhaust Velocity, m/sec (ft/sec)	231 (756)

Figure 3-37. OTW Takeoff Noise Constituents.

- 100.085 kilonewtons (22,500 LBS.) INSTALLED THRUST, SLS
- 152.4 m (500 FT.) SIDELINE, 61 m (200 FT.) ALTITUDE
- 41.15 m/s (80 KNOTS) AIRCRAFT SPEED
- EPNdB = 95
- GEAR AND COMPRESSOR, NON-CONTRIBUTING CONSTITUENTS

MAX FORWARD ANGLE (1.5705 rad., 90°)   MAX AFT ANGLE (2.094 rad., 120°)

SUPPRESSION

jet/flap is dominant, as a result of the highly suppressed fan inlet noise; thus, 1.40 radian (80°) is the maximum forward angle since the jet/flap noise peaks at that angle. As noted on Figure 3-37 the gear and compressor noise levels are not shown since they do not contribute to the total engine noise level.

The procedure outlined in Table 3-XII was followed in obtaining the constituent levels. Calculations start with the static unsuppressed single engine noise level on a 61 m (200 ft) sideline which is extrapolated to the 152.4 m (500 ft) sideline, 61 m (200 ft) altitude condition and then corrected for in-flight conditions using the Appendix A corrections. Suppressed levels were then obtained and the constituents were summed to obtain the in-flight maximum forward and maximum aft quadrant PNdB noise levels. These levels were converted to a single EPNdB value using Appendix A procedure.

3.4.3 Takeoff Suppression

Inlet

The OTW forward radiated noise is suppressed by a high throat Mach number inlet as described for the UTW system in Section 3.3.2. A level of 13 PNdB suppression was applied to the forward radiated fan noise level.

Fan Exhaust

The unsuppressed spectrum at the maximum aft angle, 152.4 m (500 ft) sideline, 61 m (200 ft) altitude is shown in Figure 3-38. Also shown is the Noy-weighted unsuppressed spectrum. The Noy weighting shifts the dominating peak from the 1600 Hz 1/3 octave band to the 3150 Hz 1/3 octave frequency band. This fact was taken into account in the treatment design.

The treatment combination as shown yielded the maximum ΔPNdB. Additional suppression at 3150 Hz would have required a significant increase in treatment length at the expense of the treatment optimized to 1600 Hz which reuslts in a lower overall ΔPNdB.

The OTW fan exhaust duct phased treatment arrangement is shown in Figure 3-39 with average duct height, liner design parameters, liner segment lengths, treated splitter length, and thickness defined. The suppression spectrum for the configuration is given in Figure 3-40. The "total" suppression with and without duct curvature and phasing effects is also shown. The circled numbers indicate the treated duct longitudal segments.

Suppression at the maximum aft angle, on a 152.4 m (500 ft) sideline is given in Table 3-XIII (in terms of ΔPNdB). The frame and wall treatment, assuming a straight duct, produces a ΔPNdB of about 6.7 dB. The duct curvature and phasing enhances suppression to 9.6 ΔPNdB. The treated 76.2-cm (30-inch) long splitter remoes an additional 5 dB and thus increases suppression to 14.5 PNdB.

80

Table 3-XII. OTW Noise Levels.

● Takeoff Power, 100.085 kN (22,500 lb)
  F_N(Installed)

	Max. Forward Angle PNdB (1.5705 radians, 90°)				Max. Aft Angle PNdB (2.094 radians, 120°)			
	Fan	Turbine	Combustor	Jet/Flap	Fan	Turbine	Combustor	Jet/Flap
Single Engine – Unsuppressed @ 61 m (200 ft) Sideline	114.9	96.5	98.5	101.0	115.9	100.8	101.5	98.1
(OTW Shielding)	–	(-5.0)	(-3.5)	–	(-5.0)	(-5.0)	(-3.5)	–
Total Corrections – Appendix A Procedure	-8.8	-13.6	-8.3	-6.6	-12.8	-13.9	-9.3	-7.6
Corrected Level	106.1	82.9	90.2	94.4	103.1	86.9	92.2	90.5
Suppression	-13.0	-9.6	-4.5	–	-14.5	-9.6	-4.5	–
Suppressed System	93.1	73.3	85.7	94.4	88.6	77.3	87.7	90.5
Sum Constituents				97.8				94.5
PNdB to EPNdB								95 EPNdB

81

Figure 3–38. OTW Unsuppressed Fan Spectra.

- TAKEOFF
- MAXIMUM AFT ANGLE (120°)
- 152.4 m. (500 FT.) SIDELINE, 61 m. (200 FT.) ALTITUDE

—·— NOY WEIGHTED UNSUPPRESSED SPECTRUM, BASED ON 30 NOY CONTOUR

——— UNSUPPRESSED SPECTRUM
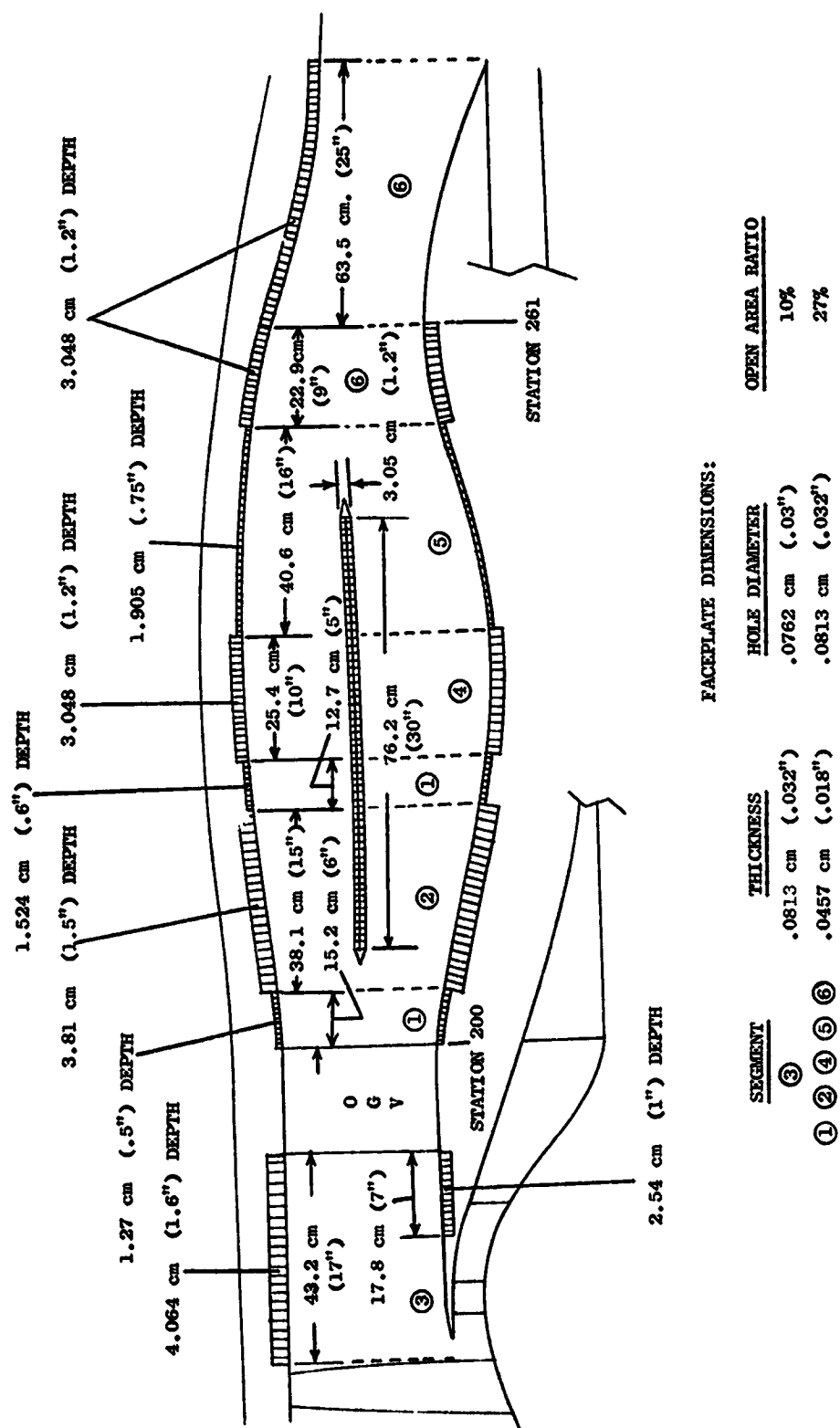
Figure 3-39. OTW Fan Exhaust Duct Treatment.

83
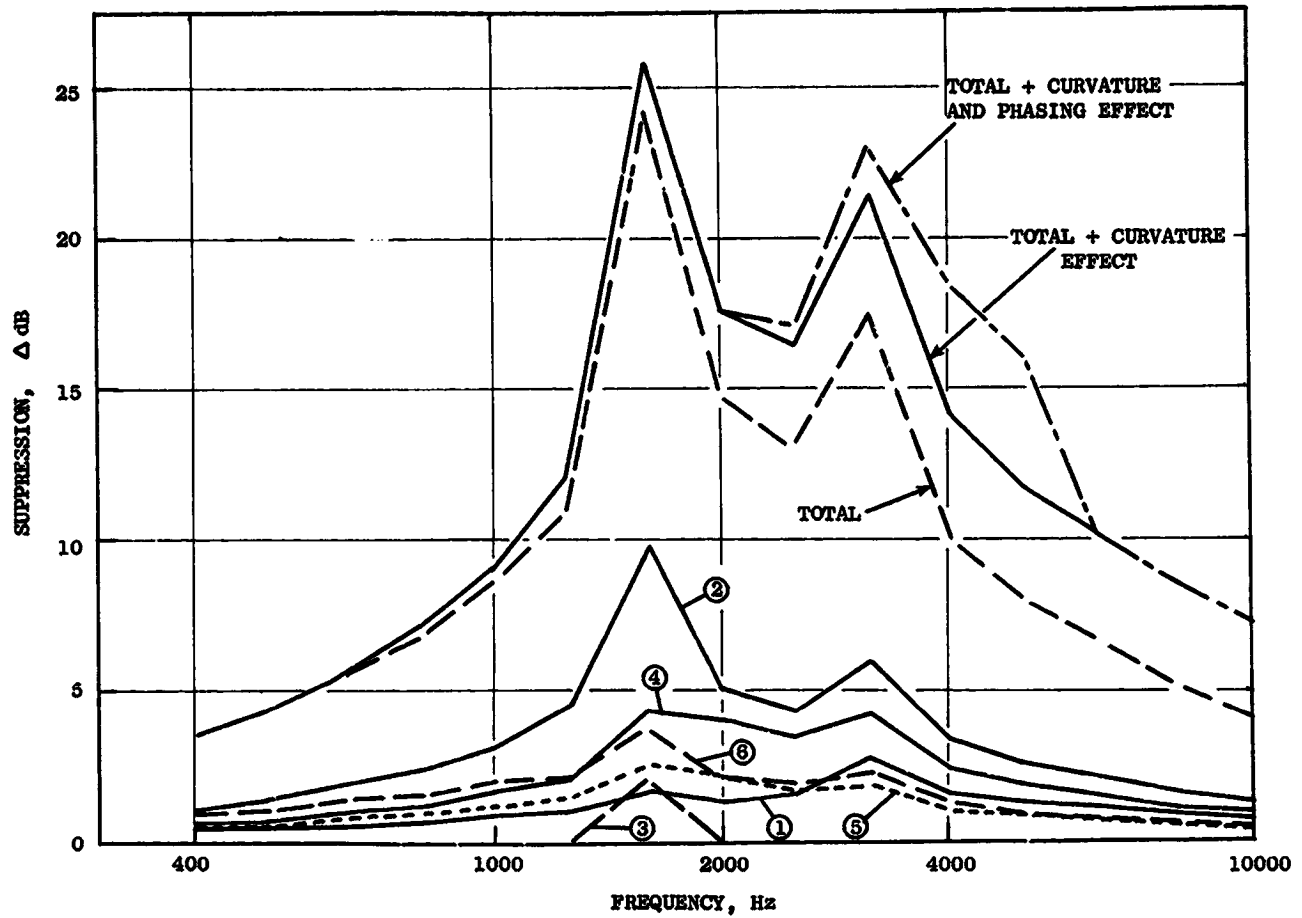
Figure 3-40. OTW Total and Segmented Fan Exhaust Duct Suppression.

Table 3-XIII. OTW Fan Exhaust Duct Suppression.

- 152.4 m (500 ft) Sideline
- Takeoff
- Maximum Aft Angle (120°)

Condition	ΔPNdB
• Frame and Wall Treatment, Standard Design	6.7
• Above with Curved Duct and Phased Treatment	9.5
• Frame and Wall Treatment, Splitter, Curved Duct and Phased Treatment	14.5

Suppressed Obstruction Noise and Flow Noise Regeneration in the Fan Exhaust Duct

The same procedures as described for the UTW estimates for the attenuated strut noise, splitter trailing edge noise, and flow regenerated (see Section 3.3.3) noise was adopted for the OTW exhaust system.

The suppressed engine noise spectrum level was found to be above the estimated floor noise levels as was found for the UTW engine in Section 3.2.2.

Core Exhaust

Figure 3-41 shows the OTW takeoff core spectrum to be very similar to the UTW spectrum, Figure 3-18, Section 3.3.3. Because of the small differences, the same core suppression is obtained for the OTW is described in Section 3.3.3.

Compressor Inlet

The compressors inlet treatment design is the same as presented in Section 3.3.3, Figure 35. The treatment was estimated to give a suppression of 6 dB for the compressor first-stage blade passing frequency.

3.4.4 Approach Noise Constituents

The approach noise constituents are shown in Figure 3-42 in bar chart form. The approach power setting is 65% of the available thrust at the given aircraft speed. Fan noise in both the forward and aft quadrants dominates the unsuppressed noise level. Jet/flap noise becomes the dominant source when the engine constituents are suppressed. Due to this dominance the forward quadrant noise is a maximum at 1.57 radians (90°) the jet/flap noise peak angle.

- MAXIMUM AFT ANGLE (120°)
- 152.4 m.(500 FT.) SIDELINE

— · — NOY WEIGHTED UNSUPPRESSED TOTAL CORE SPECTRUM, BASED ON 30 NOY CONTOUR
——— UNSUPPRESSED TOTAL CORE SPECTRUM
— · · — TURBINE SPECTRUM
——— COMBUSTOR SPECTRUM
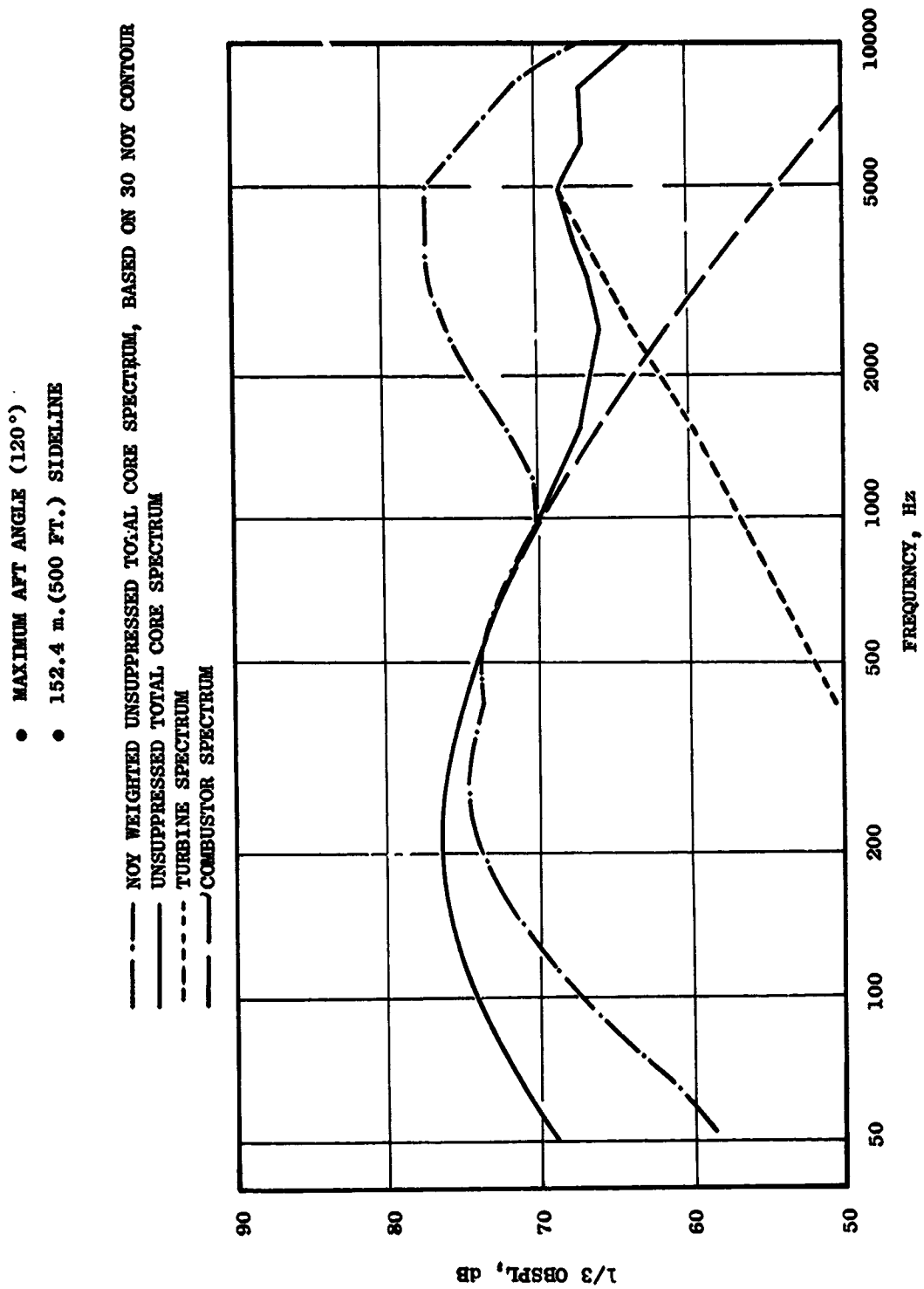
Figure 3-41. OTW Takeoff Unsuppressed Core Spectra.

Figure 3-42. OTW Approach Noise Constituents.

- 65% THRUST AT AIRCRAFT SPEED
- 152.4 m (500 FT.) SIDELINE, 61 m (200 FT.) ALTITUDE
- 41.15 m/s (80 KNOTS) AIRCRAFT SPEED
- EPNdB = 90.5
- GEAR AND COMPRESSOR, NON-CONTRIBUTING CONSTITUENTS

MAX FORWARD ANGLE (1.5705 rad., 90°)   MAX AFT ANGLE (2.094 rad., 120°)

87

Table 3-XIV gives the noise constituents for a single unsuppressed engine on a 61.0 m (200 ft) sideline. The corrections from using Appendix A procedure are also given and were used to calculate the in-flight noise levels. The suppressed constituent levels and the summed constituents, forward and aft, are also shown. These values were then converted to a single EPNdB value using Appendix A procedure.

3.4.5 Approach Suppression

Inlet

The inlet treatment design at approach is shown in Figure 3-43. The liner parameters, the treated-length-to-fan-diameter ratio (L_t/D_t) and the liner segment lengths are indicated. The inlet liner design and the associated suppression spectrum are based on Rotor 11 experience.

Figure 3-44 shows the fan inlet treatment suppression spectrum at approach. The resulting suppressed spectrum and the unsuppressed spectrum at the maximum forward angle on a 152.4 m (500 ft) sideline, 61 m (200 ft) altitude are depicted in Figure 3-45. The difference in levels of the suppressed and unsuppressed spectra noise levels is 10 PNdB, the suppression level applied in calculating the total engine suppressed noise level.

Fan Exhaust Duct Suppression At Approach

Table 3-XV summarizes the fan exhaust suppression for the OTW engine configuration at the maximum aft angle 152.4 m (500 ft) sideline, 61 m (200 ft) altitude. The fan frame and wall treatment with a standard design give a suppression of 6.7 PNdB. The addition of curvature and phasing effects increases the suppression of 9.5 PNdB. These effects with an acoustic splitter give a total of 14.5 PNdB, the value assumed in the calculation of the suppressed engine total noise level. The associated suppressed spectrum, the Noy-weighted suppressed spectrum, and the unsuppressed spectrum are shown in Figure 3-46.

Core Exhaust

At approach, the combustor and turbine spectra shapes change very little from the takeoff spectra shapes because of the relatively small core speed changes. Therefore, the same suppression estimates explained in Section 3.3.3 are used at approach.

3.4.6 Reverse Thrust Noise Constituents

To obtain reverse thrust on the OTW engine, the exhaust nozzle translates aft to form a target-type thrust reverser on top of the wing. The fan flow is then directed upward and forward to provide the desired reverse thrust.

For the preliminary design, it was assumed that an angle of 1.05 radians (60°) relative to the horizontal inlet axis would be required to obtain 35%

88

Table 3-XIV. OTW Noise Levels.

● Approach Power (65% Thrust at Aircraft Speed)

	Max. Forward Angle PNdB (1.5705 radians, 90°)				Max. Aft Angle PNdB (2.094 radians, 120°)			
	Fan	Turbine	Combustor	Jet/Flap	Fan	Turbine	Combustor	Jet/Flap
Single Engine - Unsuppressed @ 61 m (200 ft) Sideline	107.5	94.0	93.9	95.6	110.7	98.3	96.9	92.0
(OTW Shielding)	-	(-5.0)	(-3.5)	-	(-5.0)	(-5.0)	(-3.5)	-
Total Corrections - Appendix A Procedure	-9.9	-13.5	-8.3	-6.5	-12.8	-13.8	-9.3	-7.7
Corrected Level	97.6	80.5	85.6	89.1	97.9	84.5	97.6	84.3
Suppression	-10.0	-9.6	-4.5	-	-14.5	-9.6	-4.5	-
Suppressed System	87.6	70.9	81.1	89.1	83.4	74.9	83.1	84.3
Sum Constituents	92.6				89.3			

PNdB to EPNdB   90.1 EPNdB

TREATMENT DEPTHS:

A = 1.905 cm (.75")

B = 2.54 cm (1.0")

C = 3.81 cm (1.5")

FACE PLATE THICKNESS = .051 cm (.02")

OPEN AREA RATIO = 0.10

HOLE DIAMETER = .102 cm (.04")
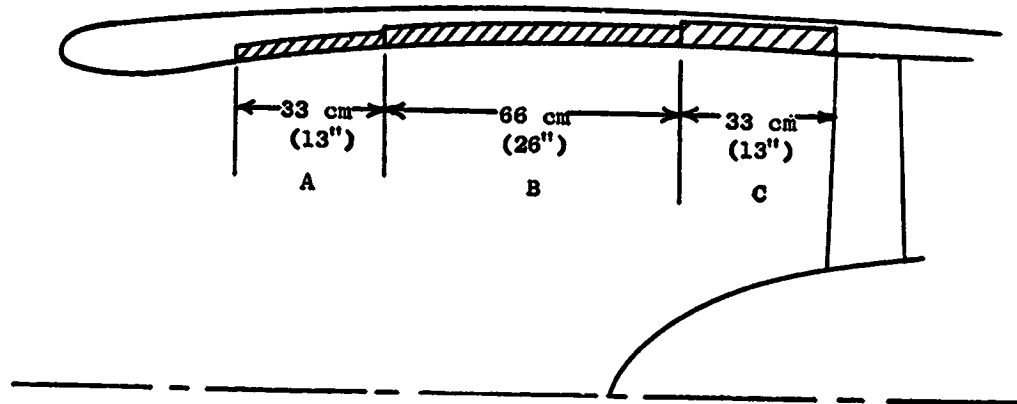
TREATED L/D = 0.74

Figure 3-43. OTW Inlet Treatment Configuration.

90

- ROTOR 11 DATA SCALED TO QCSEE BLADE PASSING FREQUENCY

- TREATED L/D = 0.74

- APPROACH

	ROTOR 11	QCSEE
TREATED L/D	0.82	0.74
FAN TIP SPEED	298.7 m/s (980 FT/SEC)	294.1 m/s (965 FT/SEC)
BPF	8300 Hz	1600 Hz
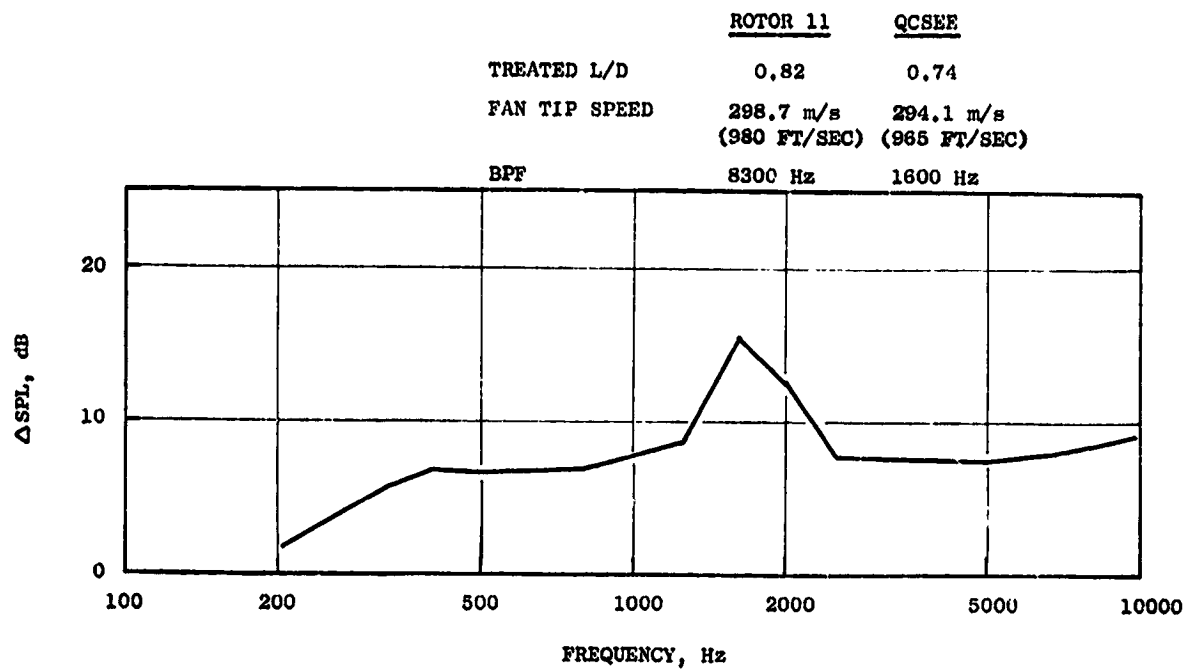
Figure 3-44. OTW Fan Inlet Suppression.

91

Figure 3-45. OTW Suppressed and Unsuppressed Engine Spectra.

- APPROACH
- MAXIMUM AFT ANGLE (120°)
- 152.4 m. (500 FT.) SIDELINE, 61 m. (200 FT.) ALTITUDE
- 65% THRUST @ AIRCRAFT SPEED

UNSUPPRESSED

SUPPRESSED

FREQUENCY, Hz

1/3 OBSPL, dB
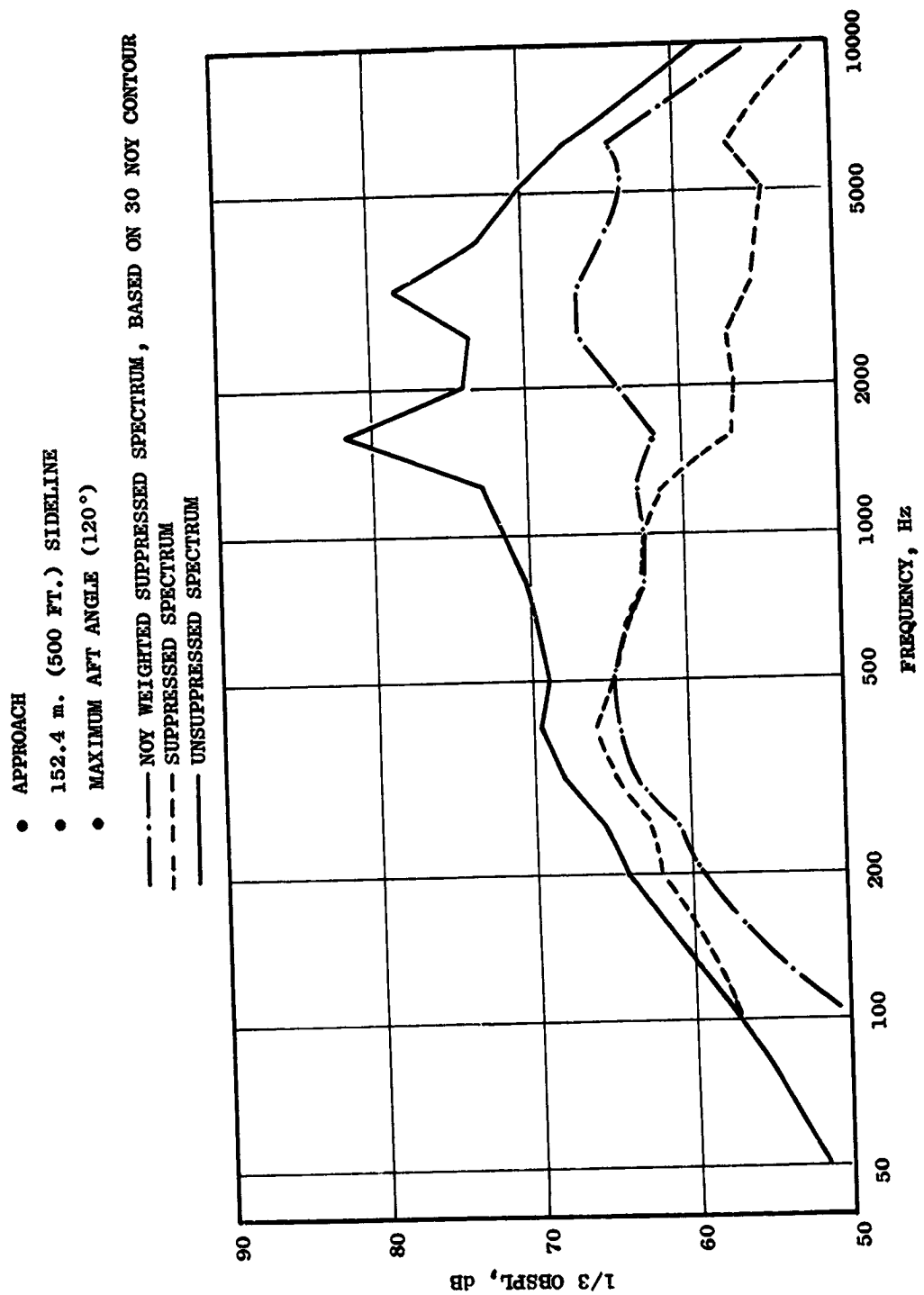
Figure 3-46. OTW Suppressed and Unsuppressed Fan Spectra.

Table 3-XV. OTW Fan Exhaust Duct Suppression.

- 152.4 m (500 ft.) Sideline

- Approach

- Maximum Aft Angle (120°)

Condition	ΔPNdB
• Frame and Wall Treatment, Standard Design	6.7
• Above with Curved Duct and Phased Treatment	9.5
• Frame and Wall Treatment, Splitter, Curved Duct and Phased Treatment	14.5

reverse thrust at 100% fan speed. This thrust axis was then assumed to be the new acoustic axis for the aft radiated engine noise constituents, fan, combustor, and turbine, thus causing them to peak in the forward quadrant.

Noise generated by the fan and core exhaust with the reverser door was estimated from scale model data of round jets interacting with semicylindrical target reversers. This was done by developing a ΔdB curve, Figure 3-47, between jet alone and jet plus reverser data as a function of jet velocity. Jet noise was then estimated for the reverser nozzle and a correction applied per Figure 3-47. The resulting constituent noise levels are shown on Figure 3-48 in bar chart form. Note that fan exhaust noise is now shown on the forward quadrant.

The fan inlet, fan exhaust, and jet/reverser noise are all contributing significantly to the total noise. Table 3-XVI gives the noise level developments and suppression levels.

3.4.7 Reverse Thrust Suppression

Suppression levels are the same as takeoff since the engine is operating at 100% speed.

3.4.8 Effect of Constituents on System Noise

As in the UTW design, the fan inlet, exhaust, and core noise are the three main contributors to the total system noise.

The OTW design, Figure 3-49, does not have as much acoustic suppression flexibility as the UTW design. From Figure 3-49, an increase in inlet noise would not be acceptable and would require a change in the inlet design such as more treatment or increased throat Mach number. Fan exhaust noise can increase significantly (4 PNdB) if inlet noise is reduced 1.5 PNdB.

94
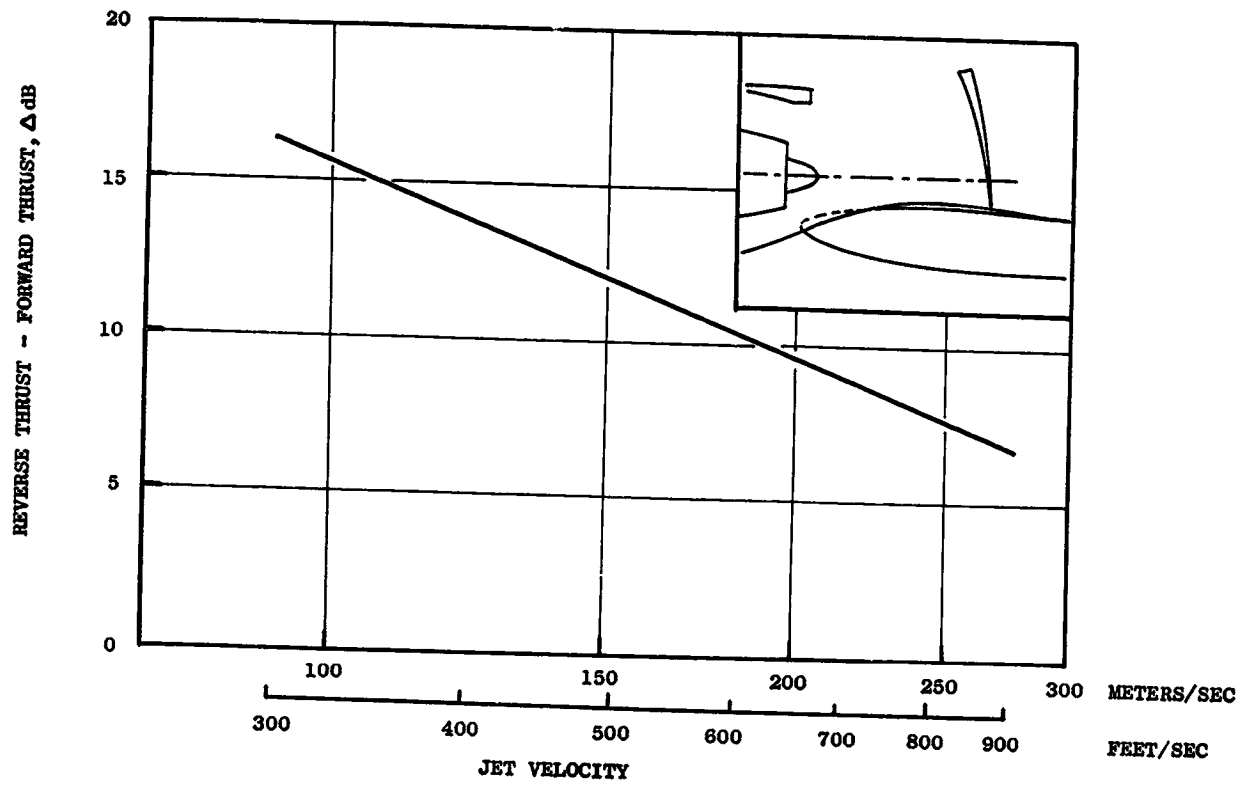
Figure 3-47. OTW Jet Noise Increase due to Thrust Reverser.
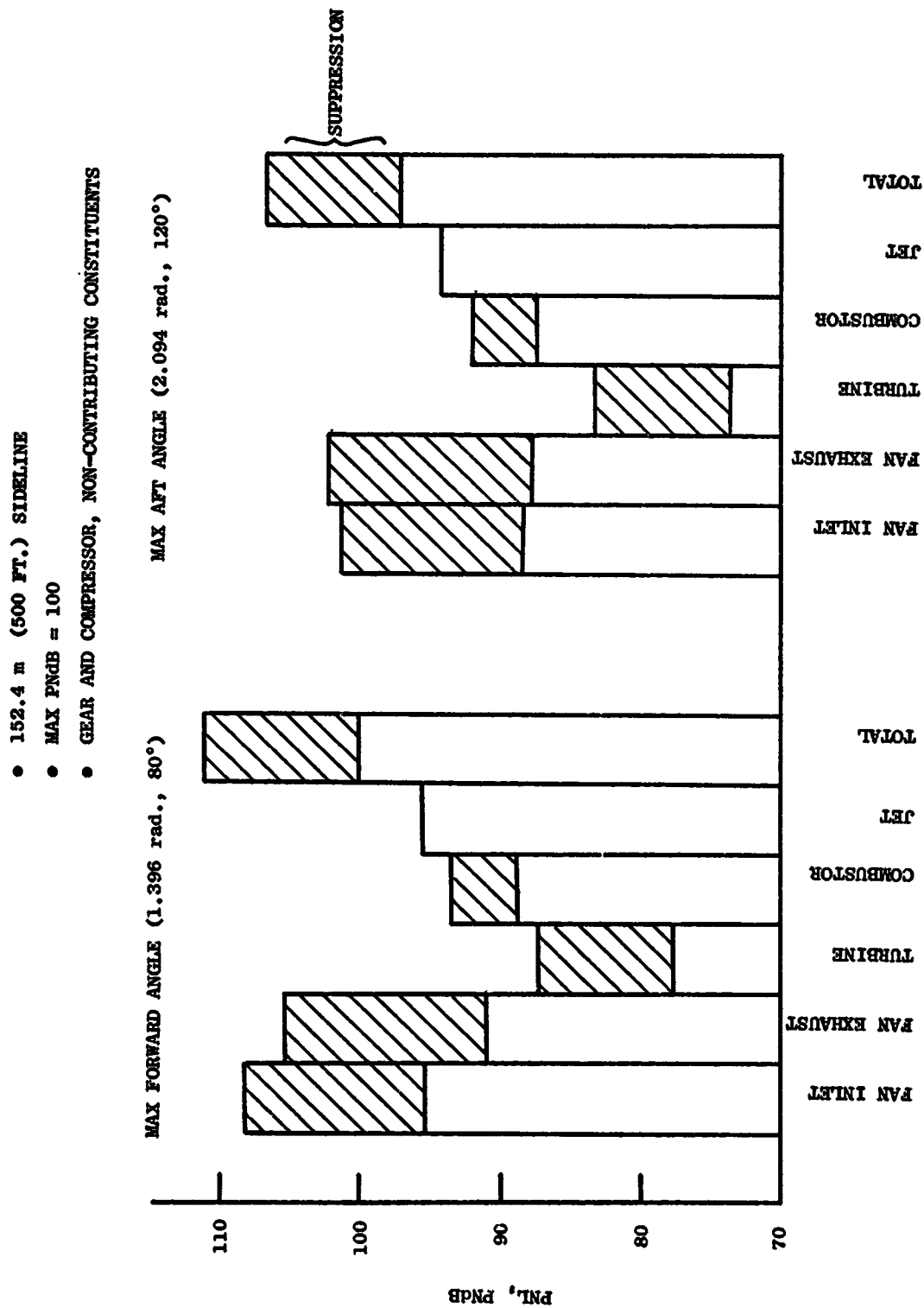
Figure 3-48. OTW Reverse Thrust Noise Constituents.

Table 3-XVI. OTW Engine Noise Level.

- Reverse Thrust
- 90% Fan Speed

| | (1.396 radians, 80°) Max. Forward Angle PNdB | | | | | (2.094 radians, 120°) Max. Aft Angle PNdB | | | | |
| | Fan | | Turbine | Comb. | Jet | Fan | | Turbine | Comb. | Jet |
	Inlet	Exhaust				Inlet	Exhaust			
Single Engine – Unsuppressed @ 61 m (200 ft) Sideline	115.4	112.7	96.1	99.4	101.5	108.4	109.5	92.0	97.9	99.7
Total Corrections – Appendix A Procedure	-7.1	-7.3	-8.9	-6.1	-5.9	-7.1	-7.3	-8.9	-6.1	-5.9
Corrected Level	108.3	105.4	87.2	93.3	95.6	101.3	102.3	83.1	91.8	93.8
Suppression	-13.0	-14.5	-9.6	-4.5	-	-13.0	-14.5	-9.6	-4.5	-
Suppressed System	95.3	90.9	77.6	88.8	95.6	88.3	87.7	73.5	87.3	93.8
Sum Constituents					100.0					97.0

- T/O POWER (100.085 kilonewtons (22,500 LBS.) $F_{N(INST.)}$)
- 152.4 m (500 FT.) SIDELINE, 61 m (200 FT.) ALTITUDE 41.15 m/s (80 KNOTS) AIRCRAFT SPEED
- STATUS JET/FLAP NOISE LEVEL
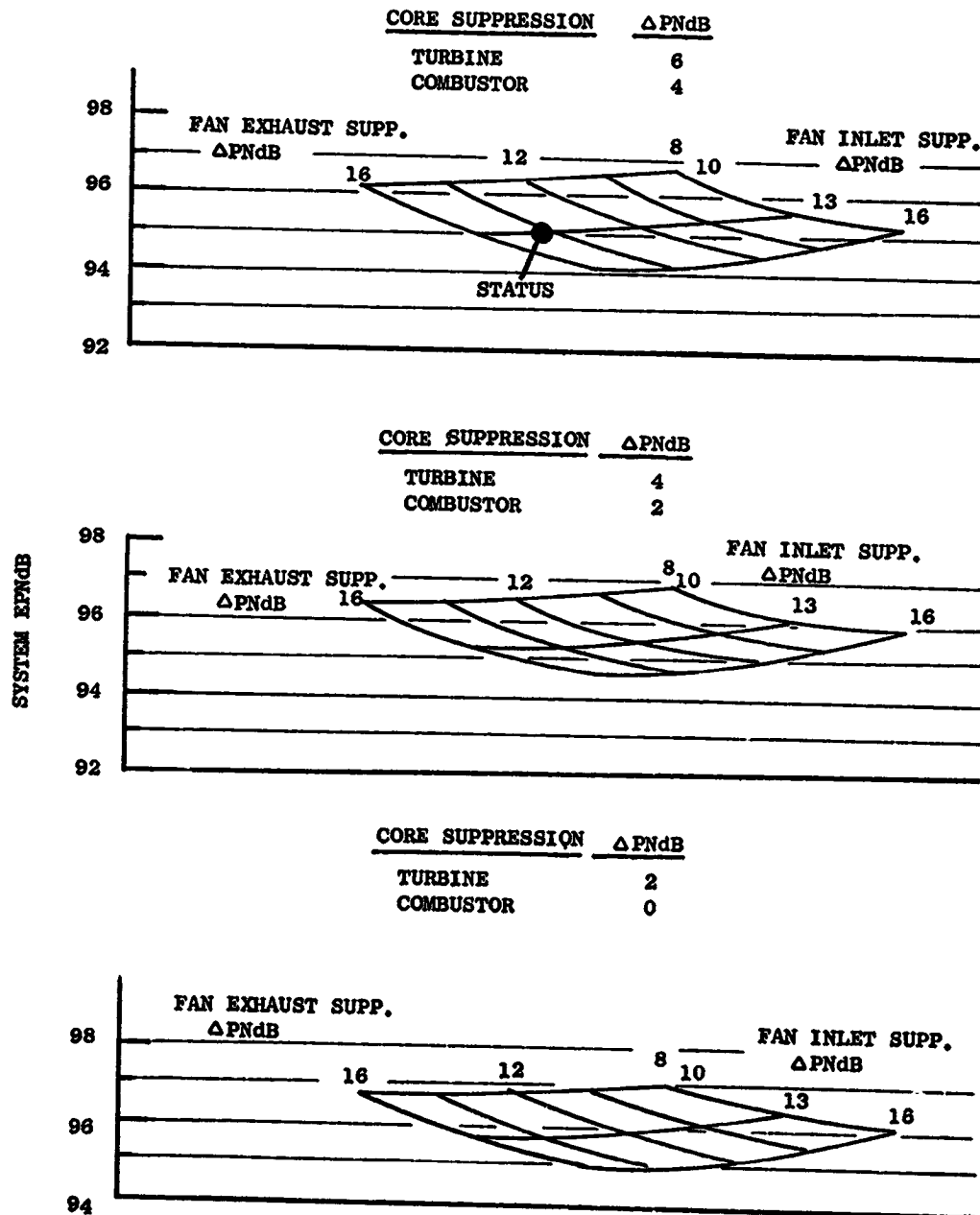
Figure 3-49. Effect of Constituent Noise Suppression on System Noise - OTW.

An increase in core noise of 2 PNdB, Figure 3-49b, would require a decrease in fan inlet and/or fan exhaust noise. An increase in core noise of 4 PNdB, Figure 3-49, would also meet 95 EPNdB with a decrease in fan inlet and/or fan exhaust noise.

Overall, Figure 3-49 shows the OTW design to be very sensitive to fan inlet noise and core noise.

3.5   EFFECT OF FIELD LENGTH ON ENGINE DESIGN

The following tables contain the results of a noise study which applied QCSEE UTW and OTW flight engines to a 914 m (3000 ft) runway aircraft.

Tables 3-XVII and 3-XVIII summarize the 610 m (2000 ft) versus the 914 m (3000 ft) runway aircraft application with respect to the system noise level adjustments. The aircraft definitions (including flap angle, aircraft velocity, and engine thrust levels) were provided by Douglas and Boeing. Each of these modifications provides a reduction in the system noise level, allowing the removal of the aft fan duct splitters from both treated nacelle configurations as defined to meet the noise requirements for a 610 m (2000 ft) runway application. The core nozzle treatment design was also modified and is shown in Figure 3-50. The very deep, low-frequency-type treatment was eliminated and the overall treatment length was reduced from approximately 62 cm (25 in.) to 51 cm (20 in.).

Tables 3-XIX through 3-XXII give the system noise constituents and corrections that are required for both the UTW and OTW engines at takeoff and approach. With the existing assumptions, predictions show that the suppressed noise levels are 0.6 to 0.8 EPNdB under the noise requirements at takeoff for the UTW and OTW systems, respectively.

Table 3-XVII. UTW - Effect of Runway Length on Noise.

	610 Meter (2000 Foot) Runway	914 Meter (3000 Foot) Runway	Resultant Noise Level Changes due to Increased Runway Length
Flap Angles, radians (degrees)			• Lower jet/flap noise (-1.8 PNdB on T/O and app.)
Takeoff	0.52 (30)	0.29 (16.9)	
Approach	1.05 (60)	0.815 (46.7)	• More favorable jet/flap V_R Noise directivity (-1.0 PNdB on max. forward angle at T/O)
Aircraft Velocity, m/sec (knots)			• Increased jet/flap V_R effect (additional -1.9 PNdB on T/O, -0.7 PNdB on app.)
Takeoff	41.15 (80)	62.86 (122.2)	
Approach	41.15 (80)	50.05 (97.3)	• More favorable PNdB to EPNdB conversion (additional -1.8 EPNdB on T/O, -0.9 EPNdB on app.)
Thrust (SLS, Installed)*			• All sources scaled down to lower thrust (-0.7 PNdB on T/O, -0.9 PNdB on app.)
Takeoff	100,000 N (22500 lbs)	82,200 N (18500 lbs)	
Approach	65,000 N (14625 lbs)	50,100 N (11230 lbs)	

Acoustic Configuration Changes:

• Remove aft fan duct splitter (fan aft suppression reduced by 7.8 PNdB)

• Simplify core nozzle treatment (comb. suppression reduced by 1.7 PNdB)
 (turb. suppression reduced by 0.3 PNdB)

Resultant 610 m (3000 ft) runway status (Appendix A corrections)
 Takeoff = 94.4 EPNdB
 Approach = 90.2 EPNdB

*Thrust requirements based on airframer's studies of 914 m (3000 ft) runway A/C and Appendix A.

Table 3-XVIII. OTW - Effect of Runway Length on Noise.

	610 Meter (2000 Foot) Runway	914 Meter (3000 Foot) Runway	Resultant Noise Level Changes
;ap Angle, radians (degrees)			• Lower jet/flap noise (-0.3 PNdB on T/O, -0.2 PNdB on app.)
Takeoff	0.52 (30)	0 (0)	
Approach	1.05 (60)	0.70 (40)	
Aircraft Velocity, m/sec (knots)			• Increased jet/flap V_R effect (additional -1.2 PNdB on T.O, -0.4 PNdB on app.)
Takeoff	41.15 (80)	58.13 (113)	• More favorable PNdB to EPNdB conversion (additional -1.5 EPNdB on T/O, -0.7 EPNdB on app.)
Approach	41.15 (80)	47.84 (93)	
Thrust (SLS, Installed)			• All sources scaled down to lower thrust (-0.6 PNdB on T/O, -1.7 PNdB on app.)
Takeoff	100,000 N (22500 lbs)	(19008 lbs)	
Approach	65,000 N (14625 lbs)	(9504 lbs)	

Acoustic Configuration Changes:

• Remove aft fan duct splitter (fan aft suppression reduced by 7.8 PNdB)

• Simplify core nozzle treatment (comb. suppression reduced by 1.7 PNdB)
      turb. suppression reduced by 0.3 PNdB)

Resultant 610 m (3000 ft) runway status (Appendix A corrections)
    Takeoff - 94.2 EPNdB
    Approach = 89.0 EPNdB

1.27 cm (0.5") Depth   3.81 cm (1.5") Depth

2.54 cm (10")   2.54 cm (10")

1.27 cm (0.5") Depth   3.81 cm (1.5") Depth

UTW AND OTW CORE NOISE SUPPRESSOR CONFIGURATION

FOR 914 METER (3000 FT.) RUNWAY VERSION

Figure 3-50. UTW and OTW Core Noise Suppressor Configuration.

Table 3-XIX. QCSEE UTW Noise Levels.

- Takeoff Power, 80.74 kN (18,150 lb) Installed Thrust
- 914 m (3000 ft) Runway

	(1.396 radians, 80°) Max. Forward Angle PNdB				(2.094 radians, 120°) Max. Aft Angle PNdB			
	Fan	Turbine	Combustor	Jet/Flap	Fan	Turbine	Combustor	Jet/Flap
Single Engine Unsuppressed @ 61 m (200 ft) Sideline	107.5	94.1	95.5	97.3	112.3	100.1	99.5	96.0
Total Corrections – Appendix A Procedure	-10.8	-8.6	-4.9	-8.5	-8.2	-9.0	-5.9	-9.7
Corrected Level	96.7	85.5	90.6	88.8	104.1	91.1	93.6	86.3
Suppression	-13.0	-9.3	-2.8	--	-6.7	-9.3	-2.8	--
Suppressed System	83.3	76.2	87.8	88.8	97.4	81.8	90.8	86.3
Sum Constituents	92.6				99.4			

PNdB to EPNdB   94.4 EPNdB

Table 3-XX. QCSEE UTW Noise Levels.

- Approach Power, 49.94 kN (11,230 lb) Installed Thrust
- 914 m (3000 ft) Runway
- Takeoff Fan Speed, Blade Angle 0.139 radians (8°) Closed

	(1.074 radians, 60°) Max. Forward Angle PNdB				(2.094 radians, 120°) Max. Aft Angle PNdB			
	Fan	Turbine	Combustor	Jet/Flap	Fan	Turbine	Combustor	Jet/Flap
Single Engine Unsuppressed @ 61 m (200 ft) Sideline	102.4	84.3	88.8	96.4	106.1	97.3	94.8	91.8
Total Corrections – Appendix A Procedure	-10.7	-8.7	-5.2	-7.5	-8.4	-8.9	-6.1	-8.7
Corrected Level	91.7	75.6	83.6	88.9	97.7	88.4	88.7	83.1
Suppression	-8.0	-9.3	-2.8	–	-6.7	-9.3	-2.8	–
Suppressed System	83.7	66.3	80.6	88.9	91.0	79.1	85.9	83.1
Sum Constituents	91.1				93.5			

PNdB to EPNdB   90.2 EPNdB

Table 3-XXI. QCSEE OTW Noise Levels.

- Takeoff Power, 84.52 kN (19,000 lb) Installed Thrust
- 914 m (3000 ft) Runway

	Max. Forward Angle PNdB (1.074 radians, 60°)				Max. Aft Angle PNdB (2.094 radians, 120°)			
	Fan	Turbine	Combustor	Jet/Flap	Fan	Turbine	Combustor	Jet/Flap
Single Engine Unsuppressed @ 61 m (200 ft) Sideline	115.9	87.8	95.5	99.7	115.9	100.8	101.5	97.8
Total Corrections – Appendix A Procedure	-9.4	-14.2	-8.9	-8.4	-13.4	-14.5	-9.9	-9.4
Corrected Level	106.5	73.6	86.6	91.3	102.5	86.3	91.6	88.4
Suppression	-13.0	-9.3	-2.8	–	-6.7	-9.3	-2.8	–
Suppressed System	93.5	64.3	83.8	91.3	95.3	77.0	88.8	88.4
Sum Constituents	96.5				97.8			

PNdB to EPNdB

94.2 EPNdB

Table 3-XXII. QCSEE OTW Noise Levels.

- Approach Power, 54.94 kN (12,350 lb) Installed Thrust
- 914 m (3000 ft) Runway

	(1.571 radians, 90°) Max. Forward Angle PNdB				(2.094 radians, 120°) Max. Aft Angle PNdB			
	Fan	Turbine	Combustor	Jet/Flap	Fan	Turbine	Combustor	Jet/Flap
Single Engine Unsuppressed @ 61 m (200 ft) Sideline	107.5	94.0	93.9	95.4	110.7	98.3	96.9	91.8
Total Corrections - Appendix A Procedure	-11.6	-15.2	-10.0	-8.6	-14.5	-15.5	-11.0	-9.8
Corrected Level	95.9	78.8	83.9	86.8	96.2	82.8	85.9	82.0
Suppression	-10.0	-9.3	-2.8	-	-6.7	-9.3	-2.8	-
Suppressed System	85.9	69.5	81.1	86.8	89.5	73.5	83.1	82.0
Sum Constituents	90.6				91.6			

PNdB to EPNdB   89.0 EPNdB

REFERENCES

1. Cremer, L., Acoustica, Volume 3, Beiheft, 1953.

2. "Identification of Component Noise Sources," Core Engine Noise Control Program, FAA-RD-74-125, Volume I, General Electric Aircraft Engine Group.

3. "Prediction Scheme for Self Generated Noise of Silencers," INTER-Noise 72 Proceedings, Washington, D.C., October 4-6, 1972.

4. Beranek, L.L., "Noise and Vibration Control," McGraw Hill Book Company, 1971.

5. "Aero-Acoustic Design and Test of a Multiple Suppressor for .914 M Diameter Lift Fan," NASA Report CR-121108.

SECTION 4.0

EMISSION CONTROL

4.1 SUMMARY

Studies were performed to define the combustor design for the two QCSEE engines. A prototype version of the F101 MQT combustor design was selected because this advanced combustor design has demonstrated excellent performance characteristics in development tests. C_xH_y, CO, NO_x, and smoke emissions level predictions have been prepared for the two QCSEE engines based on existing F101 engine and combustor component test data. These estimates indicate that both the OTW and UTW engines will meet the EPA requirements for smoke and NO_x emissions with the use of an unmodified F101 MQT-type combustor. However, because of the relatively low cycle pressure ratios of the two engines, their predicted C_xH_y and CO emissions levels exceed the applicable standards. Thus, methods of reducing the levels of these two emissions must be incorporated into the two QCSEE engines.

Several approaches for obtaining these needed reductions in the two engines have been identified based on the results of emissions control technology development programs, including the NASA Experimental Clean Combustor Program, which are underway at General Electric. These approaches involve modifications of the operating conditions within the combustor at engine idle power, since virtually all of the C_xH_y and CO emissions are produced at this engine operating mode. These approaches are:

- Increased compressor discharge pressure (CDP) bleed air extraction at idle.

- Circumferential sector fuel staging at idle

- Flat pitching the fan at idle to permit higher core engine speeds (UTW engine only)

All of these approaches appear to be suitable for use in the QCSEE engines, without compromising any other combustor performance requirements. With suitable combinations of these approaches, the emissions levels of the two QCSEE engines are expected to be in compliance with the program emissions level goals. Development tests of a QCSEE engine combustor are planned to permit the final selections of the most appropriate combination of these approaches for use in the two QCSEE engines.

4.2 EXHAUST EMISSIONS DESIGN GOALS

The target maximum emissions levels to be demonstrated with the two QCSEE engines are the Environmental Protection Agency (EPA) defined emissions standards, which become effective January 1, 1979, for Class T2 aircraft turbine engines. Engines in this EPA-defined category are all engines with a rated thrust of 35,580 N (8000 lb) or greater. These standards set maximum limits on the quantities of C_xH_y, CO, NO_x, and smoke emissions that can be discharged by engines.

108

The Class T2 engine standards in the three categories of gaseous emissions are shown in Table 4-I. The standards are defined in terms of pounds of emission per 1000 pound thrust-hours for a prescribed takeoff-landing mission cycle. This prescribed cycle is shown in Table 4-II. The intent of these standards is to limit the quantities of these exhaust constituents that can be discharged within and around airports.

Table 4-I. EPA Gaseous Emissions Standards for Class T2 Engines.

- Effective Date: January 1, 1979

- Standards*:

C_xH_y	(Pounds Per	0.8
CO	1000 Pound	4.3
NO_x	Thrust-Hours Per Cycle)	3.0

*As numerically and dimensionally expressed by the EPA.

Table 4-II. EPA Gaseous Emissions Standards - Turbojets and Turbofans.

- EPA Index Expressed As: Pounds Emission Per 1000 Pound Thrust-Hours, For a Prescribed Cycle

- Prescribed Cycle For Class T2 Engines:

Mode	% Power	Time (Minutes)
Taxi-Idle	Ground Idle	19.0
Takeoff	100	0.7
Climbout	85	2.2
Approach	30	4.0
Taxi-Idle	Ground Idle	7.0

The smoke standards are expressed in terms of the SAE ARP 1179 Smoke Number. The maximum allowable smoke number is dependent on rated engine thrust, as shown in Figure 4-1. For the UTW engine and the OTW engine, the smoke number standards are 25 and 24, respectively, as shown in Figure 4-1. Also shown in Figure 4-1 are the standards for several other General Electric commercial engines.
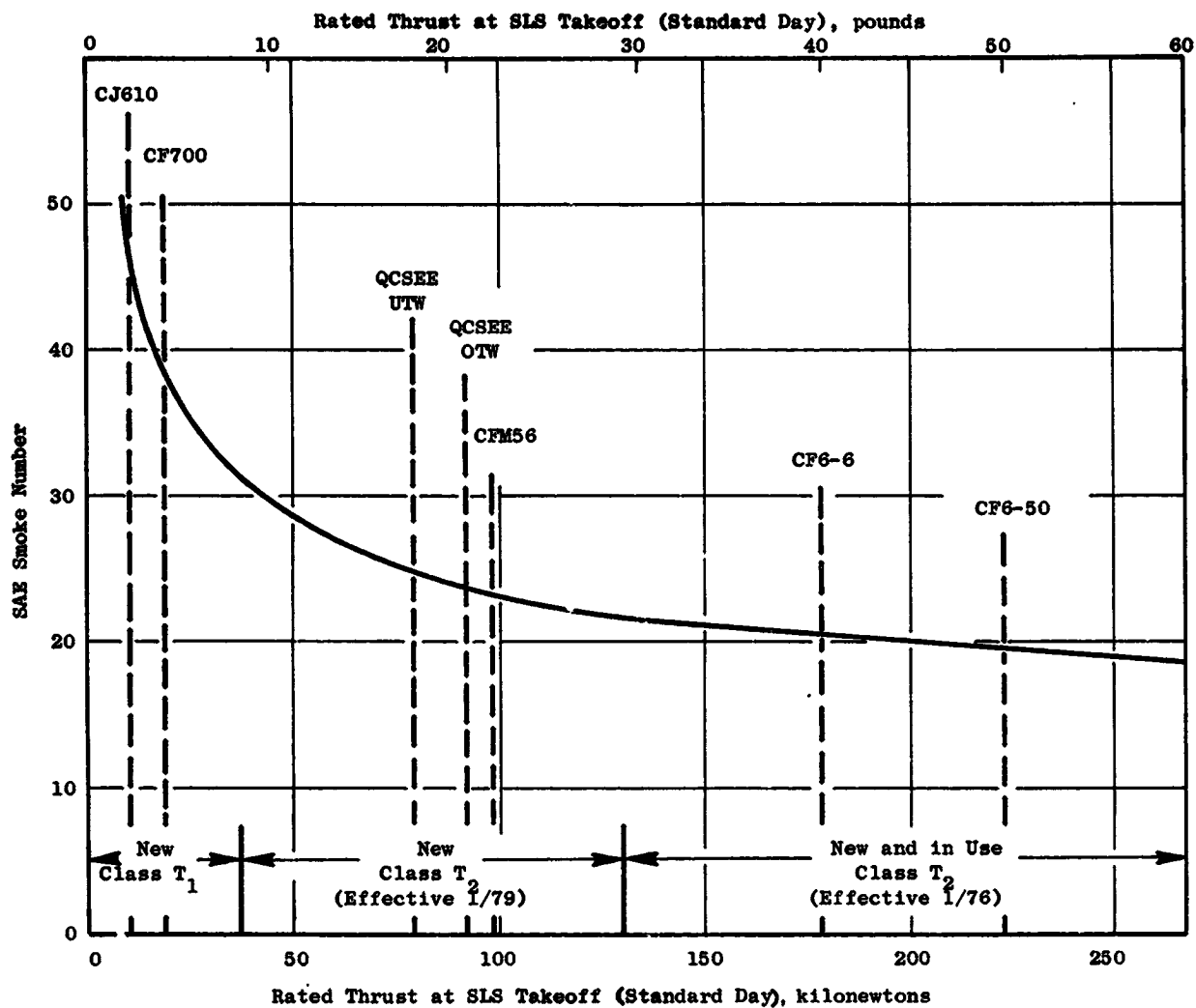
Figure 4-1. EPA Smoke Emission Standards.

4.3 SELECTED COMBUSTOR DESIGN FOR QCSEE ENGINES

A prototype version of the F101 MQT engine combustor will be used in both the UTW engine and the OTW engine. A cross sectional drawing c this QCSEE combustor design is presented in Figure 4-2.

This combustor design is aerodynamically and functionally the same as that of the actual F101 MQT engine combustor design, which is currently being developed. It differs from the F101 MQT engine combustor design only in some mechanical design details because this combustor is intended for use in the F101 PFRT core engines that will be used in the QCSEE program rather than in the F101 MQT core engine. As such, some of its mechanical mounting design features are slightly different from those being defined for the F101 MQT engine combustor. Development tests of this prototype version of the F101 MQT engine combustor are currently in progress as a part of the F1 engine program.

The F101 MQT engine combustor features an advanced central fuel injection dome design, as illustrated in Figure 4-3 (Appendix B). Earlier development versions of the F101 engine combustor, including the PFRT engine combustor, utilizing a three-stage carbureting scroll cup dome concept; Figure 4-4 (Appendix B) compares these two dome designs. Overall, excellent performance capabilities, including good altitude relight and exit temperature performance characteristics, have been obtained with this PFRT engine combustor design. The PFRT combustor configuration is shown in Figure 4-5. One of the key attractive features of this combustor is its short length; its length-to-dome-height ratio is only 2.78. The short length of this combustor may be seen in Figure 4-6. Thus, this combustor design is highly compact and has a high combustion space rate, at rated SLS takeoff operating conditions.

The operation of the carbureting scroll cups, which make up the dome, involves premixing of the fuel with a small amount of the combustor airflow upstream of the flow areas that meter the airflow into the combustor dome. This premixing design feature has been found in extensive development efforts carried out during the past few years, to be a possible area of concern. Tests have shown that, at some unique combustor operating conditions where the inlet air temperatures are high, the fuel is hot and the fuel flows are relatively low, fuel decomposition can occasionally occur in the premixing scroll. Any carbon deposits within the scroll resulting from this fuel decomposition tend to restrict the entry of the fuel-air mixtures into the combustor dome. This type of situation could possibly lead to fuel spillage out of the scroll intake and into the air upstream of the dome.

To eliminate this area of possible concern, efforts to develop a central fuel injection swirl cup design for use in the F101 engine were initiated in 1972. The intent of these efforts was to retain all of the attractive design and performance features of the PFRT engine combustor design, including low pressure fuel injection, but to eliminate the premixing feature. As a result of these efforts, the central fuel injection design shown in Figures 4-3 and 4-4 (Appendix B) was developed. This basic design approach was recently selected for use in the F101 MQT engine combustor. In order to incorporate the
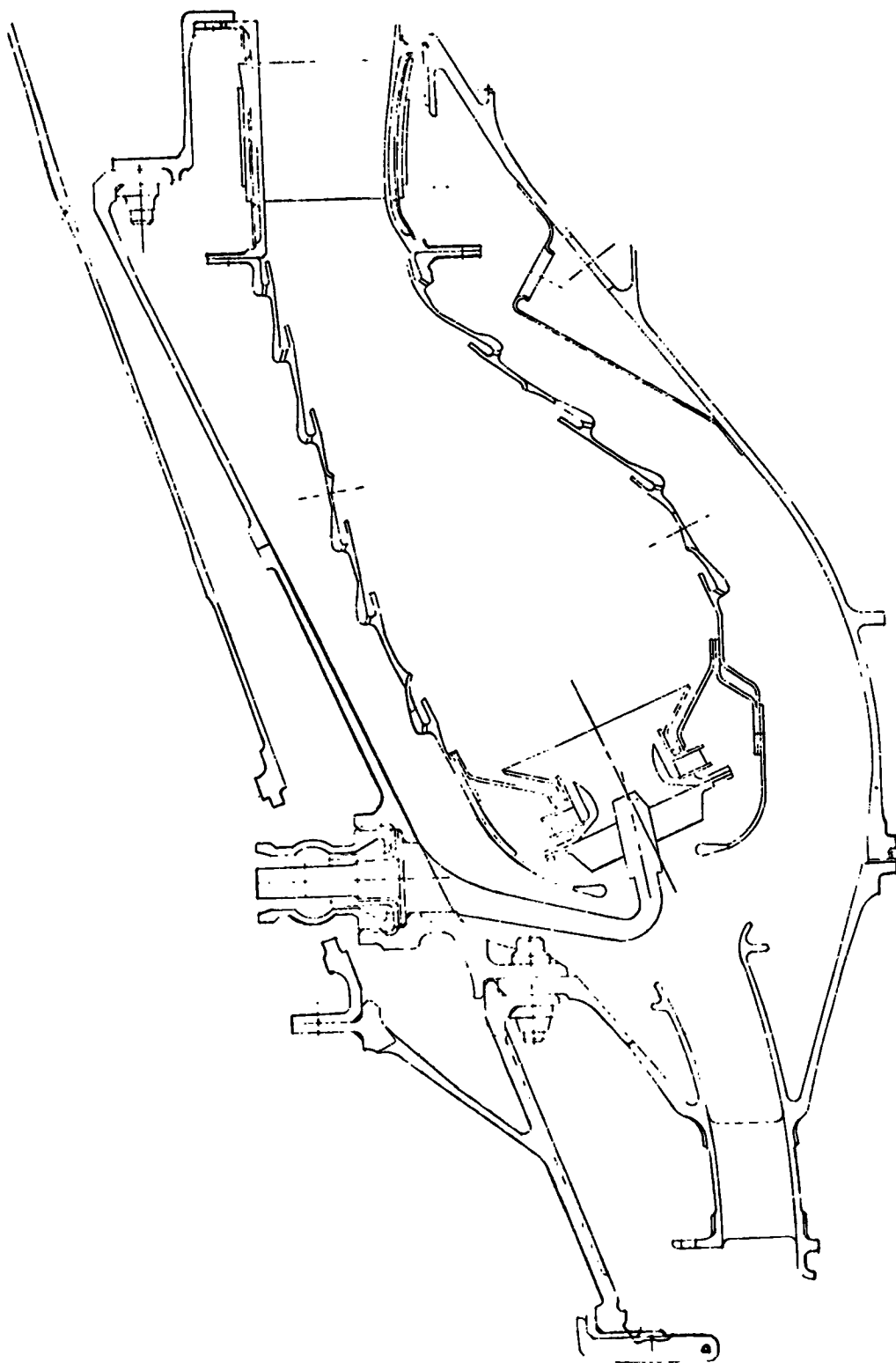
Figure 4-2. QCSEE Engines Combustor.
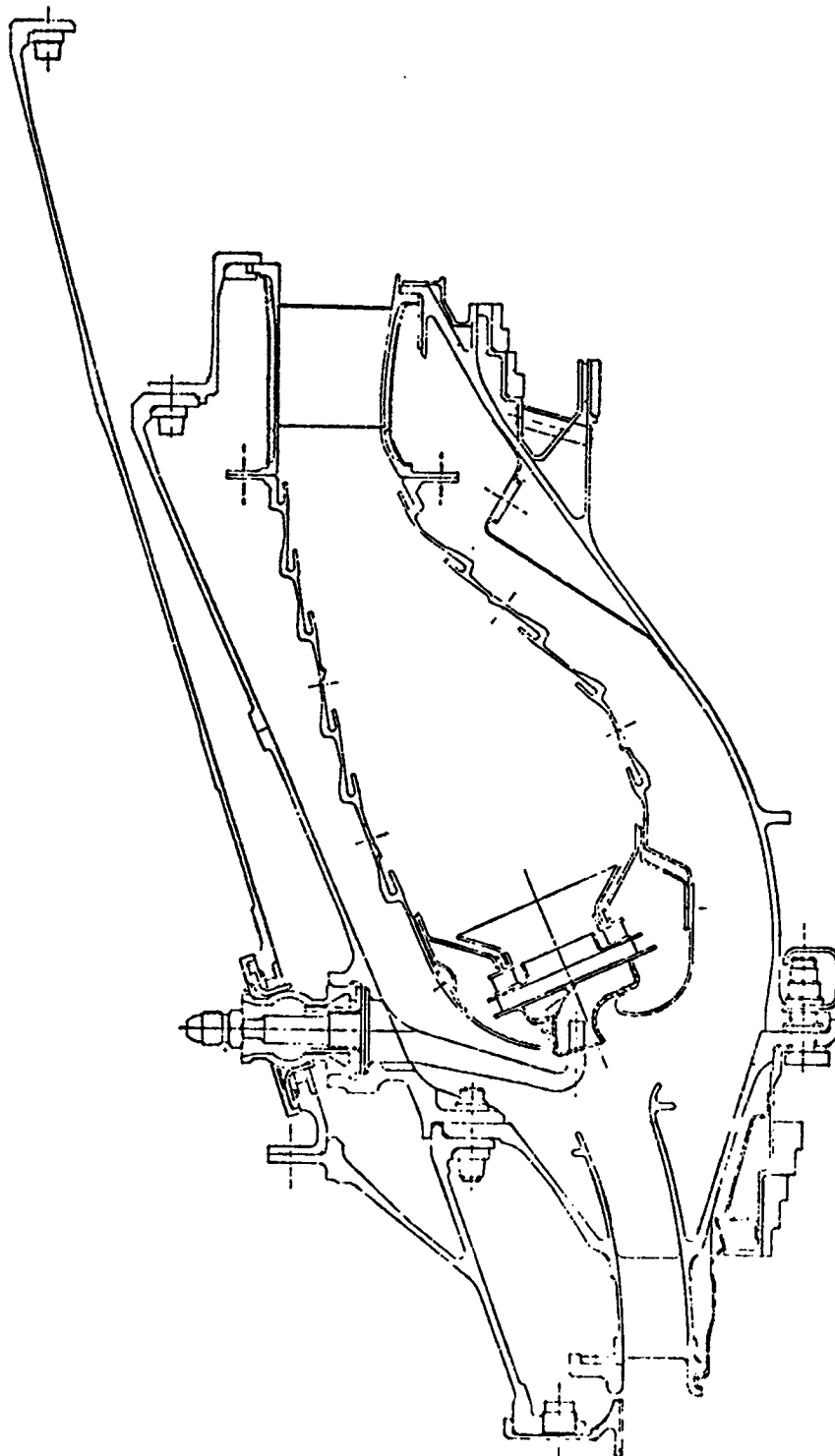
Figure 4-5. F101 PFRT Engine Combustor.
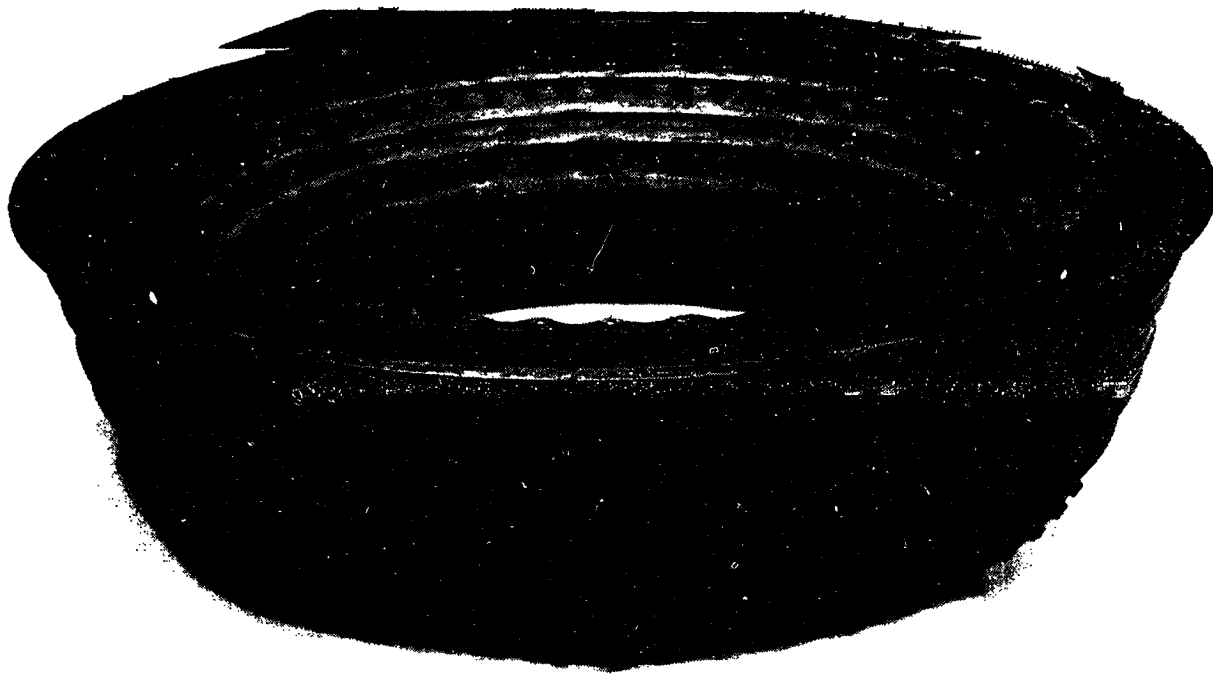
Figure 4-6. F101 PFRT Engine Combustor.

latest combustor design technology into the QCSEE engines, this design approach was also selected for use in the QCSEE engines combustor. This central fuel injection combustor design is identical in size to that of the PFRT combustor design and uses the same machined ring cooling liners.

Illustrations of the main features of this central fuel injection combustor dome design, as illustrated in Figure 4-3 and 4-4 (Appendix B). Fuel is introduced downstream of the combustor airflow pressure drop (primary air swirlers) by a centrally located fuel injector in each swirl cup assembly. High energy airflow from the diffuser is introduced through the primary air swirler located around the fuel injection source. This air serves to initially atomize the fuel and carries it to the primary cup exit. At this point, the secondary air swirler introduces air which rotates in a direction opposite to that of air from the primary swirler, as in the carbureting scroll swirl cup design. Fuel leaving the downstream edge of the primary cup venturi enters the shear region created by the mixing boundaries of the counter-rotating flows and the high aerodynamic shear stress imposed on the fuel produces very fine atomization and highly effective fuel-air mixing.

Extensive development testing of this central fuel injection combustor design has been conducted to perfect its operating characteristics. Excellent performance, including low exit temperature pattern and profile factors (Figure 4-7) and acceptable altitude relight capabilities (Figure 4-8, Appendix B) have been demonstrated in these tests.

One of the key accomplishments of these development efforts was the attainment of the altitude relight performance shown in Figure 4-8. This flight map is, of course, representative of a military engine application. The QCSEE engines, on the other hand, will operate over a commercial engine flight map, similar to that of the CF6-50 engine. The windmilling of the CF6-50 engine is shown in Figure 4-9 (Appendix B), where it is compared with the F101 engine flight map. A commonly employed parameter for evaluating ignition severity is PT/V_{ref} where P and T represent the combustor inlet pressure and temperature and V_{ref} the combustor reference velocity. Regions of low PT/V_{ref} on the windmilling map represent the most difficult areas to achieve ignition. The F101 combustor has demonstrated relight capability with PT/V_{ref} values down to 7.4 atmospheres °K seconds/meter (60(psi °R)/fps), which is also the minimum PT/V_{ref} encountered in the CF6-50 envelope, as is shown in Figure 4-9. Therefore it is expected that the QCSEE engines combustor will meet the anticipated altitude relight requirements. Further assessments of the QCSEE engines combustor relight capabilities will be made as the windmilling characteristics of these engines are better defined.

4.4 PREDICTED UTW AND OTW ENGINES EMISSIONS CHARACTERISTICS - WITH UNMODIFIED F101 MQT COMBUSTOR

4.4.1 Smoke Emissions

As noted previously, the QCSEE engines combustor features a central fuel injection dome design. This design uses swirl cups which introduce large amounts of the combustor airflow around each fuel injector, providing very effective fuel

115
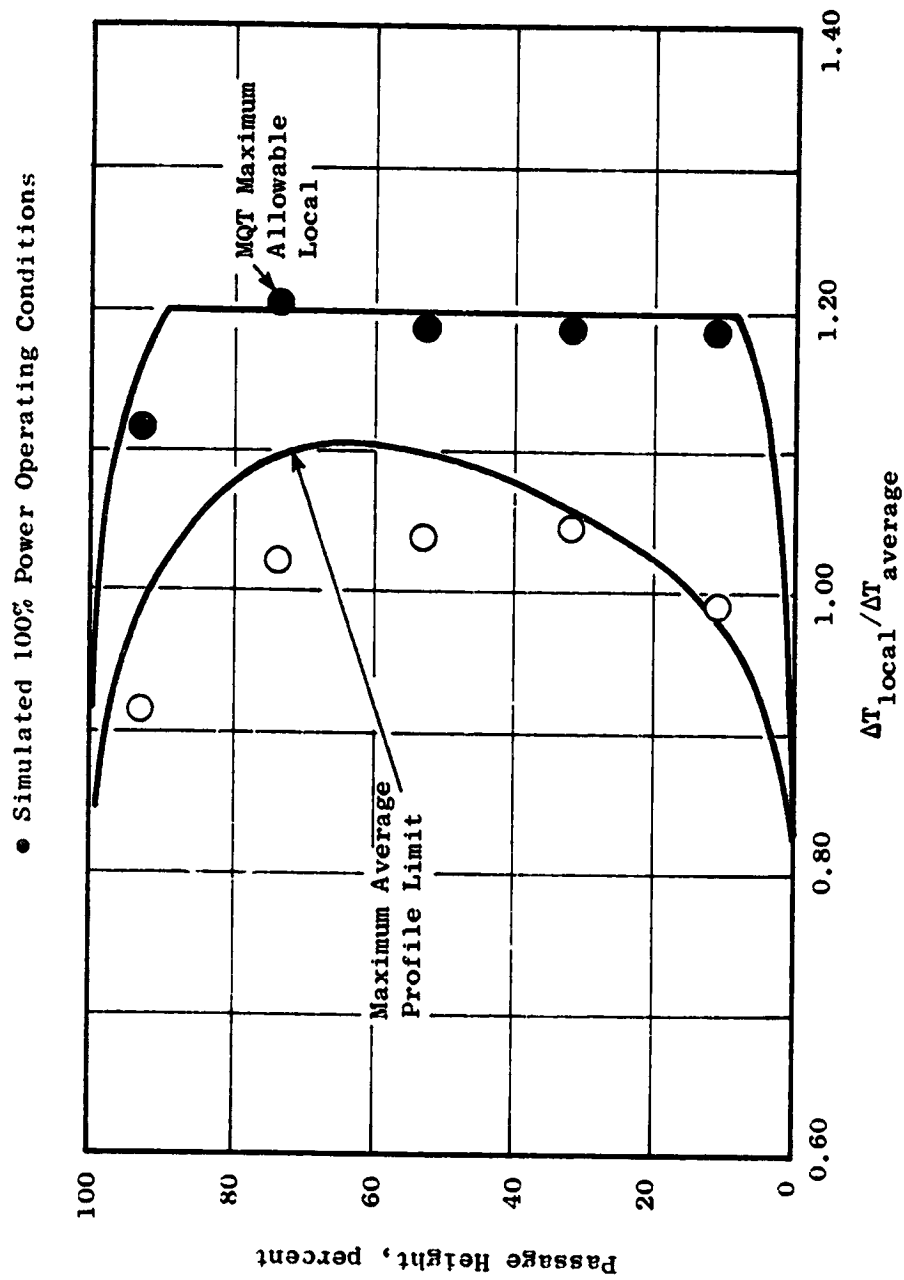
Figure 4-7. F101 Central Fuel Injection Combustor Exit Temperature Characteristics.

116

atomization and fuel-air mixing. Relatively uniform primary zone fuel-air mixtures are, thereby, achieved within short axial distances downstream of the fuel injectors. Designs of this type have demonstrated low smoke levels.

Estimates of : smoke emission levels of the QCSEE engines (Table 4-V) have been made based on data obtained in F101 PFRT engine tests and on F101 PFRT and prototype MQT combustor component tests. The peak smoke-emissions characteristics of current General Electric commercial engines are similar (Figure 4-10, Appendix B). As shown, both QCSEE engines are predicted to have low smoke levels which satisfy the EPA standards with margin.

4.4.2 Gaseous Emissions

Estimates of the gaseous emissions characteristics of the two QCSEE engines have been made based on the use of F101 PFRT engine test data and associated combustor component data. The combustor operating conditions in the QCSEE engines are, of course, considerably different from those of the F101 engines because of the engine cycle pressure ratio difference. The F101 combustor emissions indices were, therefore, adjusted to the combustor operating conditions of the QCSEE engines at the various engine operating modes of interest. Basically, these adjustments involve the use of corrections, developed at General Electric, of the emissions indices with combustor inlet air temperature and pressure. The resulting estimates are shown in Figure 4-11. For comparative purpose, the key emissions indices of the F101 PFRT engine are:

	Grams Per Kilogram of Fuel
C_xH_y at idle	1
CO at idle	17
NO_x at takeoff	24

The emissions indices of the F101 MQT engine are forcasted to be essentially the same.

Using these estimated emission indices, the emissions levels in terms of the EPA-defined parameter can be calculated. A copy of the computer summary sheet showing these calculations for the UTW and OTW engines are presented as Tables 4-III and 4-IV, respectively. Comparisons of these calculated emissions levels with the EPA standards are presented in Table 4-V for C_xH_y, CO, and NO_x emissions, respectively. As shown, both of the QCSEE engines are expected to meet the NO_x emission standard. However, reduction in the C_xH_y and CO emissions levels of the QCSEE engines will be required.

In part, the low predicted NO_x emissions levels of the F101 engine combustor in the QCSEE engines application are due to the relatively low cycle pressure ratios of these engines. The same basic combustor is used in the CFM56 engine which has a higher cycle pressure ratio that is similar to that of the CF6-6 engine. The CFM56 NO_x emissions levels (Figure 4-12, Appendix B) are lower than those of the CF6-6 engine because of the advanced and short length design features of the F101 combustor. Thus, the low predicted NO_x emissions

117
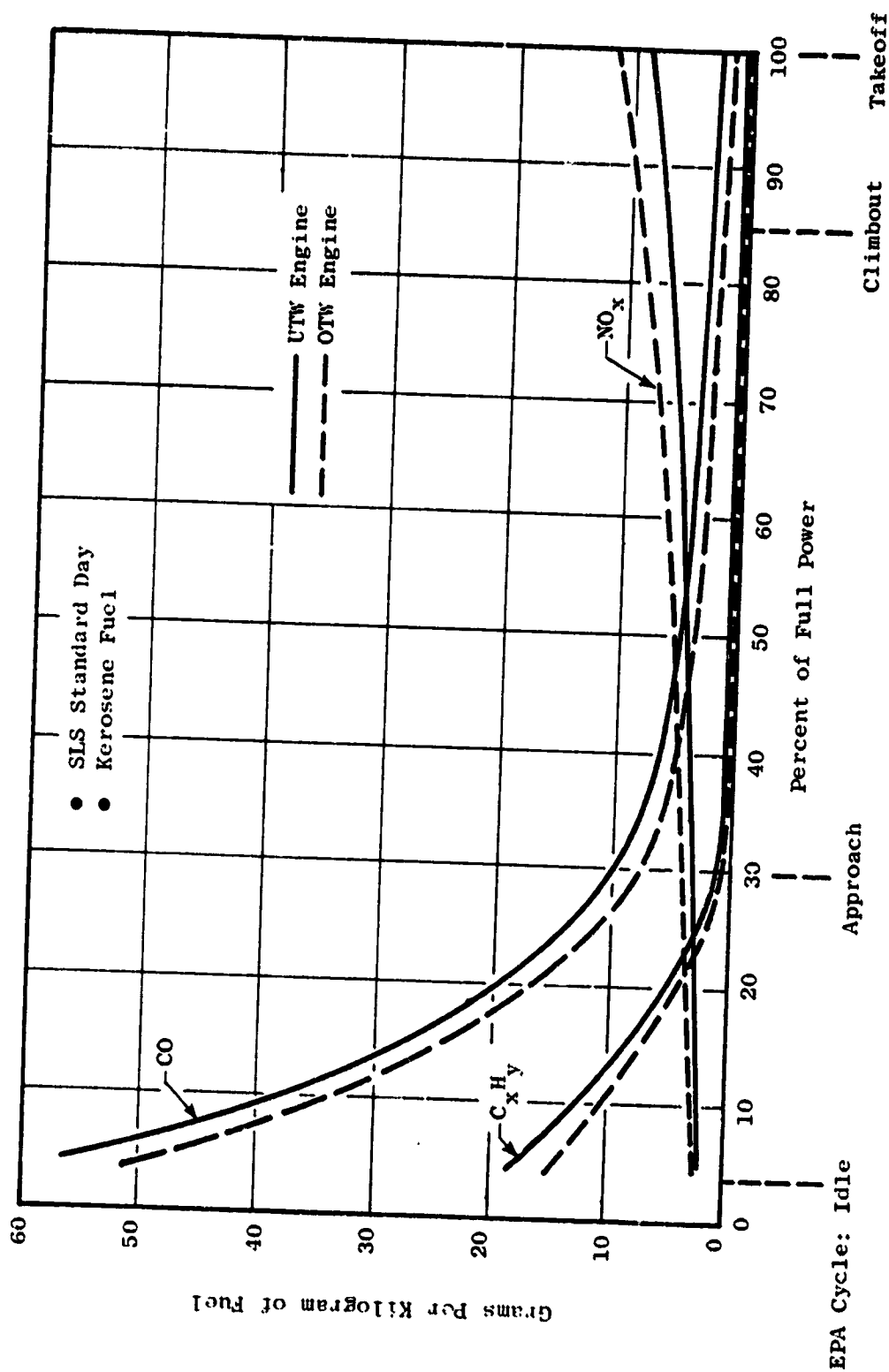
Figure 4-11. Estimated Gaseous Exhaust Emission Characteristics of QCSEE Engines, Based on F101 PFRT Engine and Combustor Test Data.

Table 4-III. Emissions Calculations Using Prescribed EPA Landing-Takeoff Cycle.

Date - 6/11/74
Engine Performance Source - QCSEE UTW SLS/STD Day OP Line Tech Requirements
Emissions Data Source - F101 Engine And Component Tests
Fuel Type - JP4 or JP5
Engine Class - T2

Engine Parameters	***************EPA Cycle Condition***************			
	Idle	Takeoff	Climb	Approach
Time (Minutes).............	26.00	.70	2.20	4.00
Percent Power..............	4.46	100.00	85.00	20.00
Thrust, Kilonewtons (1b)..	3.360	81.402	69.192	24.421
	(816)	(18300)	(155555)	(5490)
Fuel Flow, Kilograms/hr(pph)	302	2561	2091	730
	(666)	(5647)	(4610)	(1610)
Emissions Parameters				
Hydrocarbons				
Gm/Kilogram Fuel (1b/100lb)	18.000	.030	.050	.260
Kilogram/hr (1b/hr)	5.438	.077	.1043	.190
	(11.988)	(.167)	(.280)	(.419)
Kilograms (1b)	2.356	.001	.004	.013
	(5.195)	(.002)	(.008)	(.028)
% of Total Kilograms (1b)	99.267	.038	.162	.033
Carbon Monoxide				
Gm/Kilogram Fuel (1b/1000lb)	57.000	2.500	3.300	9.600
Kilogram/hr (1b/hr)	17.219	6.403	6.900	7.011
	(37.962)	(14.117)	(15.213)	(15.456)
Kilograms (1b)	7.462	.075	.253	.467
	(16.450)	(.165)	(.558)	(1.080)
% of Total Kilograms (1b)	90.870	.905	3.064	5.661
Oxides of Nitrogen				
Gm/Kilogram Fuel (1b/1000lb)	2.000	8.200	6.900	3.700
Kilogram/hr (1b/hr)	.604	21.003	14.428	2.702
	(1.332)	(46.305)	(31.809)	(5.957)
Kilograms (1b)	.253	.245	.529	.180
	(.557)	(.540)	(1.166)	(.397)
% of Total Kilograms (1b)	21.530	20.151	43.505	14.813

Summary   **EPA Parameter************************

(1b Emission/1000 1b Thrust-Hr-Cycle)[1]

	Calculated Level	1979 Standard	% Reduction Required
Hydrocarbons.......	3.48	.80	77.02
Carbon Monoxide....	12.11	4.30	64.49
Oxides of Nitrogen.	.178	3.00	.00

[1] As dimensionally expressed by the EPA.

Table 4-IV. Emissions Calculations Using Prescribed EPA Landing-Takeoff Cycle.

Date - 6/11/74
Engine Performance Source - QCSEE OTW SLS/STD Day OP Line Tech Requirements
Emissions Data Source - F101 Engine And Component Tests
Fuel Type - JP4 or JP5
Engine Class - T2

| | **************EPA Cycle Condition************** | | | |
Engine Parameters	Idle	Takeoff	Climb	Approach
Time (Minutes)............	26.00	.7ᴦ	2.20	4.00
Percent Power.............	3.81	100.00	85.00	30.00
Thrust, Kilonewtons (1b)..	3.559	93.417	79.404	28.024
	(800)	(21001)	(17851)	(6300)
Fuel Flow, Kilograms/hr (pph)	305	3228	2608	862
	(672)	(7116)	(5750)	(1900)
Emissions Parameters				
Hydrocarbons				
Gm/Kilogram Fuel (16/100016)	15.000	.020	.030	.190
Kilogram/hr (1b/hr)	4.536	.064	.078	.164
	(10.000)	(.142)	(.172)	(.361)
Kilograms (1b)	1.981	.001	.003	.011
	(4.368)	(.002)	(.006)	(.024)
% of Total Kilograms (1b)	99.272	.038	.144	.547
Carbon Monoxide				
Gm/Kilogram Fuel (1b/10001b)	51.00	1.700	2.300	7.800
Kilogram/hr (1b/hr)	15.545	5.487	6.00	6.722
	(34.272)	(12.097)	(13.225)	(14.820)
Kilograms (1b)	6.736	.064	.220	.448
	(14.851)	(.141)	(.485)	(.988)
% of Total Kilograms (1b)	90.197	.857	2.945	6.001
Oxides of Nitrogen				
Gm/Kilogram Fuel (16/10001b)	2.000	11.300	8.900	4.200
Kilogram/hr (1b/hr)	.610	36.474	23.212	3.620
	(1.344)	(80.411)	(51.175)	(7.980)
Kilograms (1b)	.264	.425	.851	.241
	(.582)	(.938)	(1.876)	(.532)
% of Total Kilograms (1b)	14.823	23.877	47.759	13.541

Summary   ********************************EPA Parameter*************************

(1b Emission/1000 1b Thrust-Hr-Cycle)[1]

	Calculated Level	1979 Standard	% Reduction Required
Hydrocarbons.........	2.64	.80	69.71
Carbon Monoxide......	9.88	4.30	56.49
Oxides of Nitrogen...	2.36	3.00	.00

[1] As dimensionally expressed by the EPA.

120

Table 4-V. Predicted QCSEE Engines Emissions Characteristics.

- With F101 MQT Combustor
- Based on 4% Power at Idle

Emission	1979 Standard[1]	UTW		OTW	
		With F101 Combustor, as Is	With Added Features[2]	With F101 Combustor, as Is	With Added Features[2]
C_xH_y (Pounds per 1000 Pound Thrust-Hours Per Cycle)	0.8	3.5	0.7	2.6	0.5
CO	4.3	12.1	5.5	9.9	4.4
NO_x	3.0	1.8	1.9	2.4	2.6
Smoke (SAE SN)	22 to 24	15.0	15.0	15.0	15.0

(1) As numerically and dimensionally expressed by the EPA

(2) Low Emissions Design/Operating Methods

- Single Sector (180°) Burning - At Idle
- High CDP Bleed Air Extraction - At Idle

121

levels of the QCSEE engines are due to the use of the basically low NO_x emissions characteristics of the F101-type combustor design, as well as to their lower cycle pressure ratios.

The predicted C_xH_y and CO emissions levels of the QCSEE engines are higher than those of the CFM56 engines (Figures 4-13 and 4-14, Appendix B). This is associated with their lower cycle pressure ratios and primarily result from the lower combustor inlet air temperatures and pressures at idle of the QCSEE engine cycles. The F101 engine combustor has, however, relatively favorable C_xH_y and CO emissions characteristics, as is indicated by comparing the C_xH_y and CO emissions levels of the CFM56 and CF6-6 engines. Accordingly, the predicted QCSEE engines C_xH_y and CO emissions levels are comparable to those of the CF6 engines, in spite of the lower QCSEE engines cycle pressure ratios.

4.5 PERTINENT EMISSIONS REDUCTIONS DESIGN TECHNOLOGY

As is discussed in the preceeding section, features to reduce the C_xH_y and CO emissions levels of both the UTW and OTW engines are needed.

The CO and C_xH_y emissions are, of course, products of inefficient combustion. As illustrated in Figure 4-11, these emissions are primarily produced at idle and other low power operating conditions. These emissions mainly occur at these operating conditions because the combustion efficiencies (degree to which the available chemical energy of the fuel is converted to heat energy) of most present day engines at these low engine power operating conditions are not optimum and are typically in the 90 to 96% range. At higher engine power settings, the combustion efficiency levels of most engines are generally well in excess of 99% and, therefore, virtually all of the fuel is converted to the ideal combustion products, carbon dioxide and water, at these operating conditions. The somewhat reduced combustion efficiency performance of most existing aircraft turbine engines at idle and other low engine power operating conditions is due to the adverse combustor operating conditions that normally prevail at these engine operating conditions. At the low engine power operating conditions, the combustor inlet air temperature and pressure levels are relatively low, the overall combustor fuel-air ratios are generally low, and the quality of the fuel atomization and its distribution within the primary combustion zone is usually poor because of the low fuel and air flows. In any given engine, all of these adverse combustor operating conditions are rapidly eliminated as the engine power setting is increased above idle power levels and, accordingly, its combustion efficiency performance is quickly increased to near-optimum levels.

To meet the CO and C_xH_y emissions standards defined by the EPA for Class T2 aircraft engines, combustion efficiency values at the ground idle operating conditions of 98.8% or higher are required. For example, in the case of the QCSEE engines, CO and C_xH_y emissions levels of about 25 and 5 grams per kilogram of fuel, respectively, are required at idle to meet the EPA standards. This combination of emissions levels is equivalent to a combustion efficiency value of 98.9%. Thus, significant improvements in the combustion efficiency performance levels, which are typical of present day engines at the ground idle operating conditions, are required to meet these EPA standards.

Based on combustion chemical kinetics considerations, these required significant improvements in combustion efficiency performance at idle appear to be obtainable in engine combustors, providing that improved control of the various processes which occur in the primary combustion zones of the combustors can be attained at idle operating conditions. CO is formed in combustors as a result of the combustion of near-stoichiometric or over-stoichiometric fuel-air mixtures in the primary zone because it is a thermochemical equilibrium product resulting from the combustion of such mixtures. Even in combustors designed to have relatively lean primary zone fuel-air mixtures at all operating conditions, relatively rich mixtures generally exist locally within the primary zone, since the fuel-air mixing process is not instantaneous. Considerable amounts of CO can be generated as a result of the combustion of these localized rich primary zone mixtures. At idle, any CO that is so generated is not rapidly consumed and, therefore, can escape from the combustion zones of the combustor. Therefore, to obtain low CO emissions levels at idle operating conditions in any given combustor, very precise control of the equivalent ratios in the primary combustion zone and in the dilution zone immediately downstream, and of the associated residence times in these zones is essential.

Unlike CO, the C_xH_y emissions are not thermochemical equilibrium combustion products. Moreover, combustion chemical kinetics data show that vaporized hydrocarbons, and any partially oxidized hydrocarbons, are consumed much more rapidly than CO. Thus, as long as these constituents reside in a flame zone for even a very brief time period, they are largely consumed. One of the products of this consumption process may be CO, depending on the flame zone stoichiometry and other factors. Thus, at idle operating conditions, relatively low C_xH_y emissions levels should be obtainable, based on these combustion chemical kinetics considerations, providing that the fuel is properly vaporized and mixed to some degree with air within the primary combustion zone. Thus, in any given combustor, the primary causes of this category of idle power emissions appear to be associated with its fuel injection characteristics. In particular, coarse fuel atomization may result in large numbers of large fuel droplets which can escape from the primary zone before they are fully vaporized. In many present-day combustors, the fuel atomization quality tends to be relatively coarse at the low engine power operating conditions because of the low fuel flows associated with these engine operating conditions. Also, the fuel spray pattern of a given combustor may be such that some of the fuel is directed into the relatively cold air streams used to cool the combustor liners and other parts. At idle, any fuel that is so entrained by these cooling air streams tends to be carried out of the primary combustion zone as unreacted fuel. Accordingly, to obtain reduced C_xH_y emissions levels as well as low CO emission levels, very effective fuel atomization at idle is an important need. The effective atomization is needed both to facilitate rapid and satisfactorily controlled fuel-air mixing in the primary combustion zone and to prevent fuel droplets from escaping from the primary zone.

At General Electric, investigations to identify and develop means of reducing CO and C_xH_y emissions levels at idle by providing improved fuel atomization and improved control of the primary combustion zone fuel-air ratios at idle have been underway for the past several years. For the most part, these investigation have been primarily conducted with CF6 engine combustors, which have already developed low smoke emission characteristics.

A major objective of these annular combustor development investigations has, therefore, been to retain these already developed low smoke emission characteristics. One of the major development programs of the kind, which is currently underway, is the NASA Experimental Clean Combustor Program. To date, some promising methods of obtaining significant reductions in the CO and C_xH_y emissions levels of these combustors have been identified in these programs.

Results from these investigations (Figure 4-15, Appendix B) have shown reductions in the C_xH_y and CO emissions level with improved fuel atomization at idle. Modest reductions were obtained by the use of fuel nozzles which were modified so that all of the fuel was delivered at idle through the primary orifices of these dual orifice nozzles. However, significant reductions in both C_xH_y and CO emissions levels were obtained with airblast fuel injection techniques, as compared to the levels obtained with the more conventionly used spray nozzle atomization techniques. With the airblast methods, the fuel is injected at low pressure and is atomized in swirl cup devices by a portion of the combustor airflow. Since the fuel atomization process is primarily dependent on the air kinetic energy, rather than on fuel pressure, very effective fuel atomization and fuel-air mixing are attained with these airblast fuel atomization methods over wide ranges of engine operating conditions, including idle. This type of fuel injection process is already embodied in the design of the QCSEE engines combustor.

One relatively simple means of obtaining more optimum primary zone fuel-air ratios at idle, without adversely affecting combustion performance characteristics at high power operating conditions, is to extract and dump overboard increased amounts of compressor discharge airflow when operating at idle. This approach results in increased fuel-air ratios throughout the combustor. Tests of a CF6-6 engine, in which various amounts of compressor discharge airflow were extracted, were conducted. The results (Figure 4-16, Appendix B) illustrated the beneficial effects of increasing the primary combustion zone fuel-air ratio, at a constant fuel flow rate. The use of increased bleed air extraction also results in small, but beneficial, increases in primary zone gas residence time, which are the result of the lower air mass flows through the combustor. Significant CO and C_xH_y emissions levels reductions were obtained in these investigations. Since many advanced engines have provisions for extracting large amounts of compressor discharge airflow, this concept appears to be an attractive one.

Still another means of obtaining the higher primary zone fuel-air ratios is to use fuel injection staging techniques at idle operating conditions. In this type of approach, fuel is valved to only selected fuel nozzles, or fuel injectors, instead of to the full complement of nozzles. This approach not only results in higher primary zone fuel-air ratios in the portions of the combustor annulus where the fuel is concentrated, but also results in improved fuel atomization since the same fuel flow is being delivered through fewer fuel nozzles and the fuel nozzle pressure drops are thereby increased. Various forms of such fuel injection staging can be considered, depending on the nature of the combustor design. Some fuel injection staging techniques that can be conveniently used in conventional annular combustors are illustrated in Figure 4-17. Tests of these fuel staging approaches were conducted in a CF6-50 combustor.

124
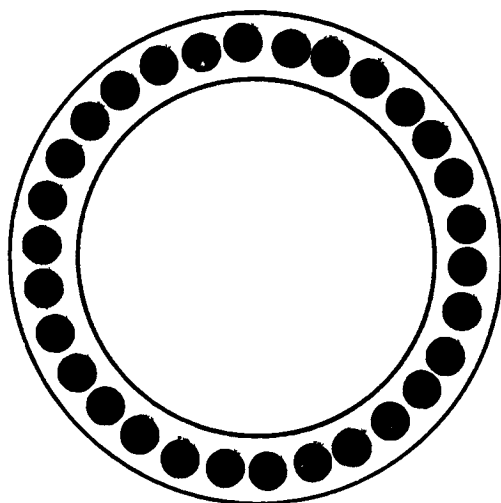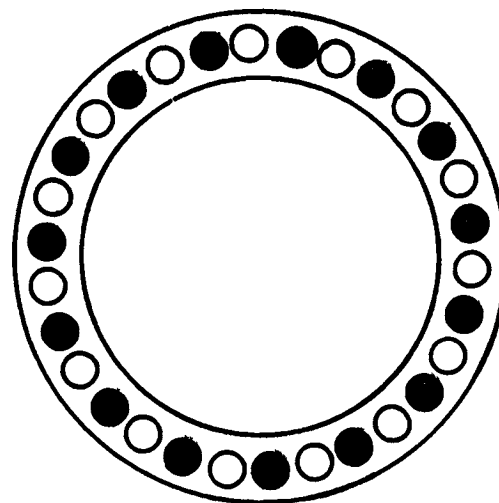
All Nozzles Fueled

Alternate Nozzles Fueled
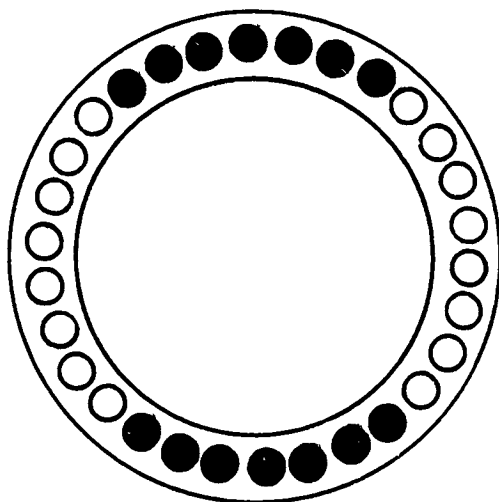
Opposing Sectors Fueled
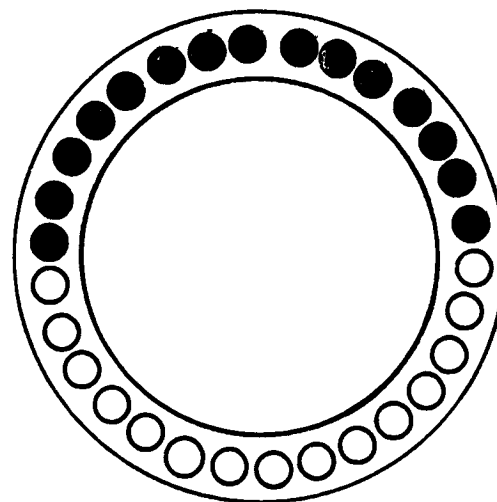
Single Sector Fueled

Figure 4-17. Fuel Staging Methods at Idle in the CF6 Engine.

The results (Figure 4-18, Appendix B) showed that the use of alternately fueled nozzles did not result in any reductions in the CO and C_xH_y emissions levels of this combustor. This finding appears to be due to the fact that, although repetitive locally enrichened primary zone fuel-air mixtures annulus were formed, excessive quenching of the combustion products apparently occurred in the several interface regions between these localized mixtures and the alternate nonfueled airstreams. However, the use of circumferential sector staging, in which the fuel was supplied to groups of adjacent nozzles, was found to be highly effective. With this latter type of staging, the designed en- richened fuel-air mixtures in the fueled zones were obtained and, at the same time, the number of boundaries between fueled and nonfueled regions was mini- mized. With the fuel stages to a single 3.14 radian (180°) sector, the lowest CO and C_xH_y emissions levels were obtained, since only two such boundaries existed with this fuel staging pattern. (Circumferential fuel staging of this kind, thus, appears to be an attractive approach for use at idle to obtain much reduced CO and C_xH_y emissions levels.) Further studies are, therefore, underway to assess the practicality and suitability of applying this approach in advanced engines.

Accordingly, based on the results obtained to date in these General Electric and other investigations, it appears that significant reductions in the CO and C_xH_y emissions levels of advanced combustors can be obtained by approaches involving improved fuel atomoization and primary zone stoichiometry control at idle. In general, these approaches can be used without adversely affecting either the combustion performance or the smoke and NO_x emission characteristics of these combustors at the high engine power operating condi- tions. In some instances, the use of these approaches can be accompanied by small increases in NO_x emissions levels at the low engine power operating conditions, but the NO_x emissions levels at these engine operating conditions are still quite low.

4.6 PREDICTED UTW AND OTW EMISSIONS CHARACTERISTICS - WITH ADDED EMISSIONS CONTROL FEATURES

Based on the above described results, the following C_xH_y and CO emissions reductions techniques have been selected for possible use in the QCSEE engines:

- Sector Fuel Staging - at Idle

- Increased CDP Bleed Air Extraction - at Idle

- For the UTW engine only, increased core engine speed to increase the combustor inlet air temperature and pressure and its fuel-air ratio. If this approach were to be used, the same idle engine thrust level would be maintained at the required low level (4% of rated thrust) by feathering the variable pitch fan.

Estimates have been made of the emissions characteristics of the two QCSEE engines (Table 4-V) with the first two of these emissions control methods in- corporated into the engines. These estimates are based on the results of the

above-described investigations with CF6 engine combustors. As shown in Table 4-V, the use of these features in the OTW engine is expected to result in emissions levels at or very close to the standards. For the UTW engine, the predicted CO emission level is still somewhat above the prescribed standard. The use of increased core engine speed at idle, with flat pitching of the fan, appears to be needed in the case of this engine. Studies of the CO emission level reduction obtainable with this approach are in progress. It is expected that with this added feature, the CO emission level can be reduced to the target value.

Development tests with a full-annular QCSEE engine combustor are planned to evaluate the effects of these various C_xH_y and CO emissions control methods. Based on the results of these tests, the final selection of the techniques to be incorporated into the UTW and OTW engines will be made.

SECTION 5.0

ENGINE CYCLE AND PERFORMANCE

5.1 SUMMARY

The QCSEE engine cycles were defined to meet requirements of externally
blown flap short-haul aircraft with under-the-wing and over-the-wing engine
installations. The UTW engine has a separated flow cycle, utilizing a single-
stage, variable-pitch, gear-driven fan. The OTW cycle has a mixed-flow cycle
with a single-stage, fixed-pitch, gear-driven fan. Both experimental and
flight-type engines are defined, with several major components used in common,
including the core engine. Objective thrust levels for the UTW engine are
81,402 N (18,300 lb) thrust uninstalled at sea level static, and 17,793 N
(4000 lb) thrust uninstalled at cruise, Mach 0.8, 9144 m (30,000 feet). For
the OTW engine the objective thrust is 93,413 N (21,000 lb) uninstalled, at
sea level static, and 21,129 N (4750 lb) uninstalled at cruise. Preliminary
design cycle and performance data are presented for these flight conditions
as well as for the noise rating conditions, 41.2 m/sec, 61 m (80 knots, 200 ft)
sideline.

5.2 CYCLE SELECTION CRITERIA

The QCSEE engine cycles were defined to be representative of propulsion
systems for powering externally blown flap types of short-haul aircraft, with
engines located under-the-wing (UTW) or over-the-wing (OTW). Primary constraints
include low-noise and low exhaust emissions. The particular UTW and OTW cycles
defined under this program were also selected to allow common usage of several
major propulsion system components. These components include:

- Inlet

- Fan frame

- Fan bypass duct

- Core engine

- Low pressure turbine

- Turbine frame

An inlet throat Mach number of 0.79 is required at maximum power at the
noise rating condition [41 m/sec, 61 m (80 knots, 200 ft) sideline], thus
establishing the airflow at that condition for both cycles. Ram recovery
characteristics of the selected inlet are shown in Figure 5-1. In Figure 5-2,
the corrected airflow characteristics are shown as a function of flight Mach
number. Also shown is the inlet throat Mach number for 406 kg/sec (894 lb/sec)
corrected airflow, selected as the limiting value for initial control mode
purposes.

128
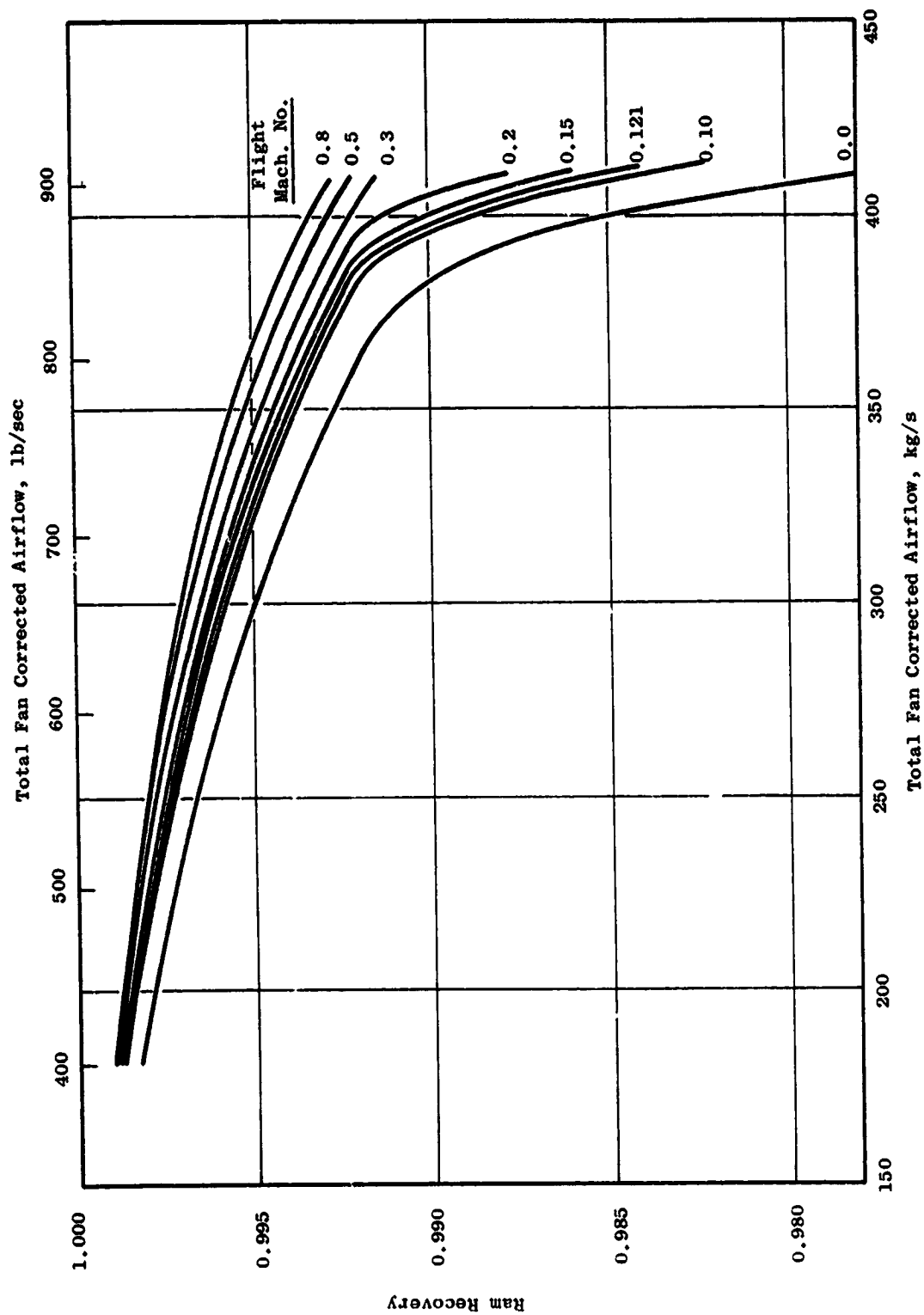
Figure 5-1. QCSEE Ram Recovery Characteristics.

129
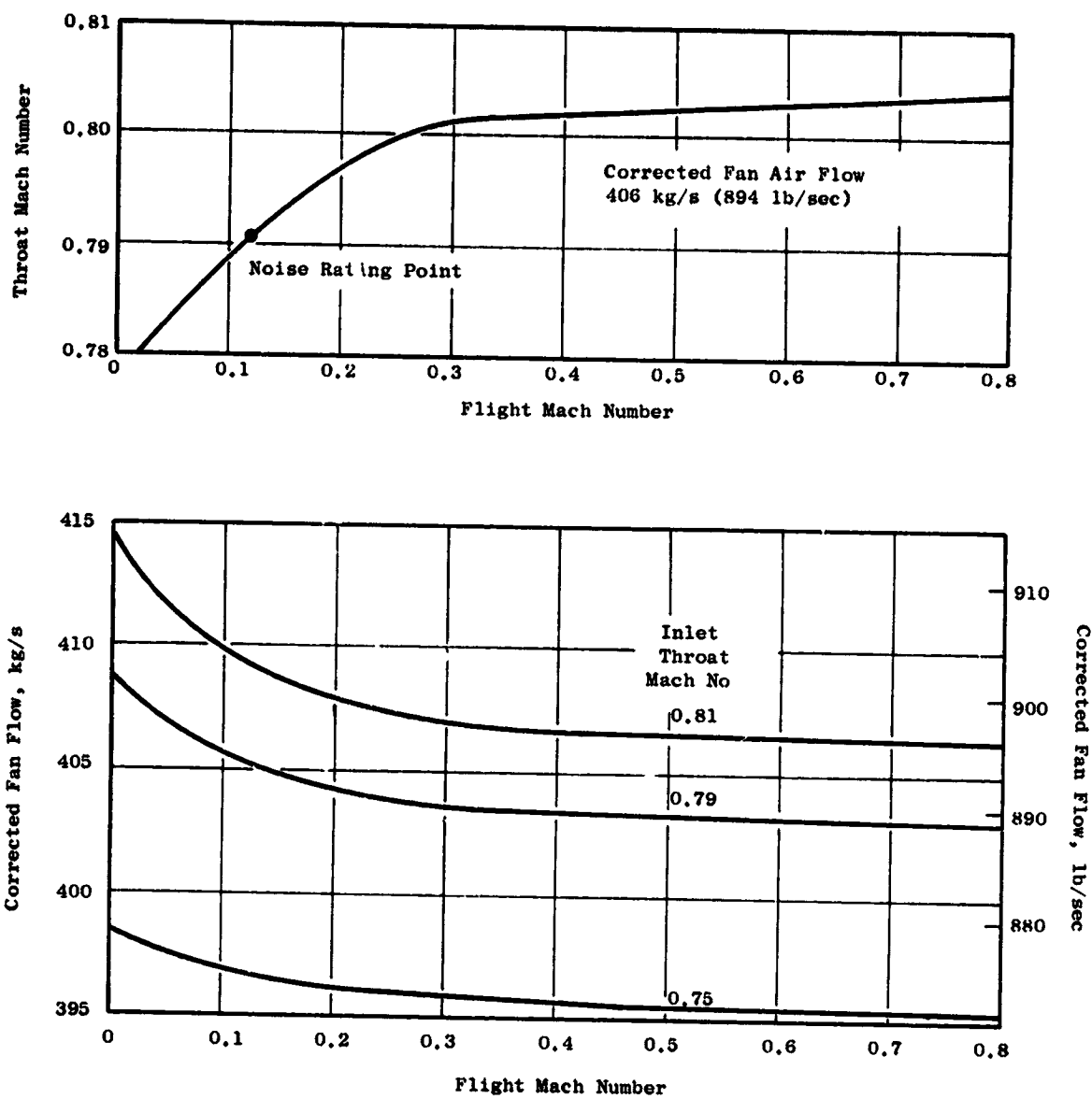
Figure 5-2. QCSEE Inlet Characteristics.

Performance objectives for the engines are summarized in Table 5-I. As shown in the table, the UTW engine has an uninstalled thrust at takeoff of 81,402 N (18,300 lb) and the OTW engine has 93,413 N (21,000 lb) thrust. At cruise, the UTW has 17,793 N (4000 lb) thrust; the OTW 21,129 N (4750 lb). Because noise constraints ·⁴· ted fan and core exhaust velocities for both the UTW and OTW systems, and a common inlet (fan tip diameter) and core are used, the two types of systems differ significantly in fan pressure ratio, turbine inlet temperature, overall pressure ratio, and thrust levels. The UTW engine has a separated-flow cycle with the fan hub pressure ratio lower than the fan bypass stream pressure ratio. The OTW engine has a mixed-flow cycle and has reverse stratification of the fan, the hub pressure ratio being higher than that of the bypass stream.

The experimental engines are based on utilization of PFRT F101 core engine components, while the flight engines are based on MQT level F101 cores.

Both engines utilize gear-driven fans, with the gear ratios selected to match the LP turbine, used in common, to the particular fan design. The UTW gear ratio is 2.4648; the OTW ratio is 2.0617. The UTW fan has a lower design pressure ratio and a corrected tip speed limit at takeoff of 290 m/sec (950 ft/sec). The OTW fan has a lower gear ratio because it has a higher design pressure ratio and higher tip speeds than the UTW.

Reverse thrust capability is achieved on the UTW by rotating the fan rotor blades so that air is pumped through the fan in the reverse direction to normal flow. The objective reverse thrust level, as shown in Table 5-I, is 35% of static takeoff thrust. On the OTW engine a conventional target-type thrust reverser is utilized.

5.3 UTW EXPERIMENTAL ENGINE AND SYSTEM PERFORMANCE

The UTW propulsion system incorporates a single-stage, variable-pitch, gear-driven fan. The fan and core streams exhaust through separate exhaust nozzles, with the fan nozzle being variable. PFRT level F101 core engine components are utilized. The cycle provides 81,402 N (18,300 lb) thrust uninstalled, at sea level static conditions, flat rated to a 305° K (90° F) day. Installed, with effects of ram recovery and scrubbing drags allowed for, the thrust level is 77,399 N (17,400 lb) at sea level static. At the Mach 0.8, 9144 m (30,000 ft) flight condition, the thrust level uninstalled is 17,793 N (4000 lb).

Parasitic and cooling flows for the UTW engines are shown in Figure 5-3. Flow quantities are included in the figure for both experimental and flight engines.

Internal cycle parameters and performance for the UTW experimental engine are shown in Table 5-II (see cycle nomenclature Table 5-III and station designations Figure 5-4). The first four columns in Table 5-II show the sea level static and 0.8 Mach number cruise rating points corresponding to the objective levels presented in Table 5-I. The installed data include effects of inlet ram recovery and the following drag terms:

Table 5-I. QCSEE Performance Objectives.

	UTW		OTW	
Takeoff, SLS, 90° F Day				
Uninstalled net thrust,[1] N (lb)	81403	(18300)	93413	(21000)
Uninstalled SFC, kg/Ns (lb/hr)/lb	9.6×10^{-6}	(0.34)	1.0×10^{-5}	(0.36)
Turbine rotor inlet temperature, °K (°F) (max)	1611	(2440)	1678	(2560)
Bypass ratio (approximate)	11.8		10.2	
Cycle pressure ratio (approximate)	13.7		15.5	
Installed net thrust,[1] N (lb)	77399	(17400)	90299	(20300)
Takeoff, SLS, Standard Day				
Uninstalled net thrust,[1] N (lb)	81402	(18300)	90299	(20300)
Uninstalled SFC, kg/Ns (lb/hr/lb)	9.3×10^{-6}	(0.33)	9.9×10^{-6}	(0.35)
Turbine rotor inlet temperature, °K (°F) (max)	1533	(2300)	1650	(2510)
Cruise, (Mach 0.8, 30000 feet) Standard Day				
Uninstalled net thrust,[1] N (lb)	17793	(4000)	21129	(4750)
Reverse Thrust				
35% of static takeoff thrust N (lb) (min)	28491	(6405)	32695	(7350)

[1] No bleed or power extraction
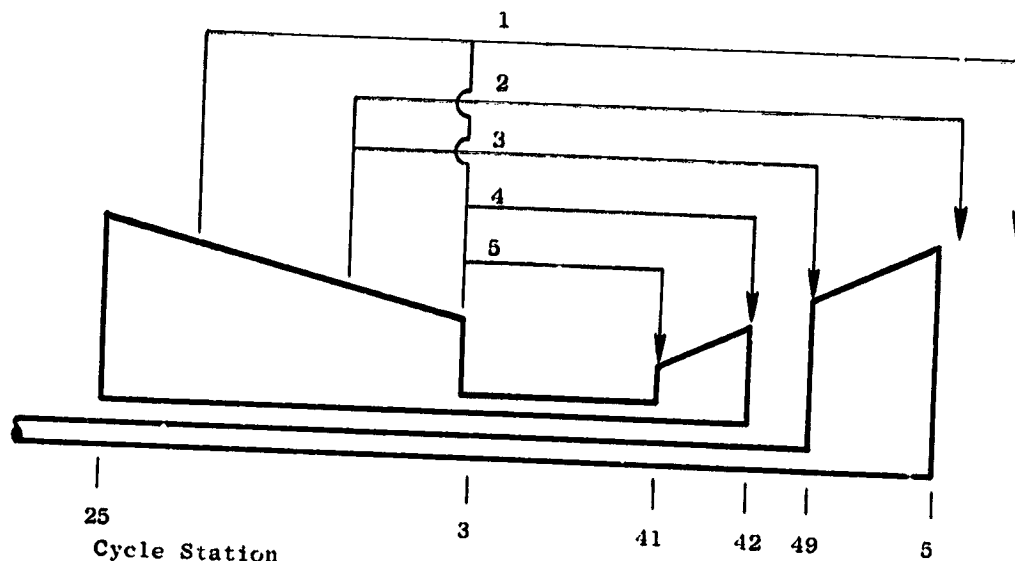
		Source	Sink	Quantity Exper. Engine ($\% W_{25}$)	Flight Engine
1	Balance Piston, LP Shaft & Rear Bearing Cooling	Stg. 3 & CDP	LP Disc	2.11	1.33
2	LP Turbine Rotor Disc & Dove-tail Cooling	Stg. 5	LP Disc	1.84	1.00
3	LP Turbine Nozzle Vane & Band Cooling	Stg. 5	LP Rotor Inlet	0	0.50
4	CDP Seal Leakage, HP Turbine Rotor Cooling	CDP	HP Disc	5.46	4.80
5	HP Nozzle Vane & Band Cooling (Nonchargeable)	CDP	HP Rotor Inlet	11.0	9.56

Figure 5-3. UTW Cooling Flow Schematic.

133

Table 5-II. UTW Experimental Engine Performance.

	①	②	③	④	⑤	⑥	⑦	⑧	⑨	⑩
ALT	0	0	0	30000	30000	200	200	200	200	200
XM	0	0	0	0.8	0.8	0.121	0.121	0.121	0.121	0.121
DTAMB	+31	0	+31	+18	+18	0	0	0	0	0
FN	18300	18300	17400	4000	3841	13831	8990	8990	8990	8990
SFC	0.319	0.309	0.336	0.737	0.758	0.391	0.385	0.391	0.410	0.407
W14Q2	11.84	11.89	11.76	11.36	11.34	12.05	12.46	13.31	13.74	11.93
PAMB	14.696	14.696	14.696	4.364	4.364	14.59	14.59	14.59	14.59	14.59
ERAM11	1.0	1.0	0.982	1.0	0.993	0.988	0.994	0.992	0.993	0.994
XM11	-	-	0.778	-	0.804	0.790	0.557	0.625	0.694	0.556
T1	549.67	518.67	549.67	484.92	484.92	519.48	519.48	519.48	519.58	519.48
P1	14.696	14.696	14.430	6.657	6.610	14.563	14.657	14.642	14.626	14.658
XNL	3157	3067	3157	3316	3316	3054	2503	2587	2722	3054
PCNLR	94.53	94.53	94.53	105.72	105.71	94.05	77.11	79.69	83.84	94.05
W2AR	894.0	894.0	894.0	894.0	894.0	894.0	743.7	798.4	843.6	742.1
W2A	868.4	894.0	852.7	418.8	415.9	885.2	741.2	794.8	838.9	739.5
P13Q12	1.272	1.272	1.277	1.391	1.391	1.260	1.171	1.156	1.147	1.170
E12D13	0.865	0.865	0.867	0.849	0.849	0.862	0.873	0.842	0.782	0.789
P23Q2	1.204	1.204	1.203	1.213	1.218	1.202	1.131	1.141	1.156	1.201
E2D23	0.792	0.792	0.793	0.787	0.787	0.791	0.800	0.798	0.786	0.796
ROPDEG	T/O	T/O	T/O	Cr	Cr	T/O	T/O	T/O	T/O	App
W14	800.8	824.6	785.9	384.9	382.2	817.4	686.1	739.3	782.0	682.4
T14	595	561	596	542	542	561	547	546	546	550
P14	18.69	18.69	18.43	9.26	9.20	18.35	17.16	16.93	16.77	17.14
P18Q14	0.986	0.986	0.986	0.988	0.988	0.986	0.989	0.987	0.985	0.989
P18	18.43	18.43	18.18	9.16	9.09	18.09	16.97	16.71	16.51	16.96
A18	2499	2499	2541	1870	1871	2568	2568	2929	3250	2568
AE18	2422	2422	2463	1840	1840	2489	2492	2844	3157	2492
V19	699	650	649	1042	1042	633	527	499	477	527
FG19	16576	16584	15779	13266	13113	15989	11192	11407	11547	11114
T23	587	554	587	520	521	555	543	545	548	555
P23	17.69	17.69	17.37	8.07	8.05	17.50	16.58	16.70	16.91	17.60
P25Q23	0.982	0.983	0.982	0.981	0.981	0.983	0.988	0.988	0.988	0.989
T49	2203	2098	2221	2159	2151	2071	1770	1780	1810	1801
P49	54.61	54.53	54.19	27.28	27.05	52.97	39.67	40.13	41.46	41.77
E49D5	0.906	0.905	0.905	0.895	0.895	0.906	0.899	0.903	0.908	0.915
P49Q5	3.25	3.25	3.25	4.48	4.51	3.21	2.53	2.56	2.64	2.65
XNL49	7781	7558	7781	8174	8173	7526	6170	6377	6709	7526
P8Q5	0.980	0.980	0.980	0.962	0.961	0.981	0.988	0.988	0.987	0.987
W8	69.28	70.92	68.46	34.71	34.50	69.33	56.03	56.51	57.93	58.19
T8	1690	1605	1705	1552	1544	1587	1422	1425	1438	1427
P8	16.45	16.44	16.32	5.86	5.77	16.17	15.50	15.49	15.52	15.57
A8	541	541	556	541	556	556	556	556	556	556
AE8	515	515	531	497	508	328	531	537	545	533
V9	803	781	779	1231	1196	744	540	540	551	561
FG9	1724	1716	1653	1324	1279	1599	938	945	989	1012
FRAM	0	0	0	10590	10514	3715	3110	3335	3521	3104

Table 5-III. Separated Flow Turbofan Nomenclature.

ALT	Altitude - feet
XM	Flight Mach number
DTAMB	Temperature increment from standard day ambient temperature
FN	Net thrust - lbs
SFC	Specific fuel consumption - lbs/hr/lb
W14Q2	Bypass ratio
PAMB	Ambient pressure - psia
ERAM11	Ram recovery
XM11	Engine inlet throat Mach number
T1	Fan inlet total temperature - deg R
P1	Fan inlet total pressure - psia
XNL	Fan physical speed - rpm
PCNLR	Percent fan corrected speed
W2AR	Engine inlet total corrected flow - lbs/sec
W2A	Engine inlet total flow - lbs/sec
P13Q12	Fan bypass pressure ratio
E12D13	Fan bypass adiabatic efficiency
P23Q2	Fan hub pressure ratio
E2D23	Fan hub adiabatic efficiency
ROPDEG	Fan rotor pitch setting, takeoff (T/O), approach (App), cruise(Cr), reverse (Rev)
W14	Bypass duct total flow - lbs/sec
T14	Bypass duct total temperature - deg R
P14	Bypass duct inlet total pressure - psia
P18Q14	Bypass duct pressure ratio
P18	Bypass duct jet nozzle throat total pressure - psia
A18	Bypass duct jet nozzle throat actual area - sq in
AE18	Bypass duct jet nozzle throat effective area - sq in
V19	Bypass duct jet nozzle exit velocity - ft/sec
FG19	Bypass duct gross thrust - lbs
T23	Fan hub discharge total temperature - deg R
P23	Fan hub discharge total pressure - psia
P25Q23	Intercompressor transition duct pressure ratio

Table 5-III. Separated Flow Turbofan Nomenclature (Concluded).

XNH	HP compressor physical speed - rpm
PCNHR	Percent HP compressor corrected speed
W25R	HP compressor corrected inlet air flow - lbs/sec
W25	HP compressor inlet air flow - lbs/sec
P3Q25	HP compressor pressure ratio
E25D3	HP compressor adiabatic efficiency
P3Q2	Overall cycle pressure ratio
T3	HP compressor discharge total temeprature - deg R
P3	HP compressor discharge total pressure - psia
P4Q3	Combustor pressure ratio
E36D4	Main combustion efficiency
T4	HP turbine 1st stage nozzle inlet total temperature - deg R
W41	HP turbine rotor inlet gas flow - lbs/sec
T41	HP turbine rotor inlet total temperature - deg R
E41D42	HP turbine adiabatic efficiency
P41Q42	HP turbine pressure ratio
T42	HP turbine discharge total temperature - deg R
W49	LP turbine rotor inlet total gas flow - lbs/sec
T49	LP turbine rotor inlet total temperature - deg R
P49	LP turbine rotor inlet total pressure - psia
E49D5	LP turbine adiabatic efficiency
P49Q5	LP turbine pressure ratio
XNL49	LP turbine physical speed - rpm
P8Q5	Primary exhaust duct pressure ratio
W8	Primary jet nozzle throat total gas flow - lbs/sec
T8	Primary jet nozzle throat total temperature - deg R
P8	Primary jet nozzle throat total pressure - psia
A8	Primary jet nozzle throat actual area - sq in
AE8	Primary jet nozzle throat effective area - sq in
V9	Primary jet nozzle exit velocity - ft/sec
FG9	Primary stream gross thrust - lbs
FRAM	Ram drag - lbs

Note: In reverse mode the fan cycle stations are assumed consistent with
direction of flow so that location on engine is reversed (i.e. duct
exit is conventional Station 1, inlet throat is conventional Station 18).

Station	Description
0	Free Stream Air Conditions
1	Inlet/Engine Interface
2	Fan Inlet
23	Fan Hub Discharge
25	HP Compressor Inlet
3	HP Compressor Discharge (Stator Exit)
4	Combustor Discharge
41	HP Turbine Rotor Inlet
42	HP Turbine Discharge
49	LP Turbine Rotor Inlet
5	LP Turbine Discharge
8	Primary Exhaust Nozzle Throat
9	Primary Exhaust Nozzle Discharge
12	Fan Inlet
13	Fan Tip Discharge
14	Bypass Duct Inlet
18	Bypass Exhaust Nozzle Throat
19	Bypass Exhaust Nozzle Discharge

Figure 5-4. Station Disignations - Separated Flow Turbofan Cycle.

- Fan flow scrubbing loss along the core casing.

- Fan flow scrubbing on the engine portion of the pylon.

- Core flow scrubbing on the center plug.

A corrected fan flow of 406 kg/sec (894 lb/sec) was used to set engine maximum power. At the approach flight condition (41 m/sec, 80 knots) this flow results in an inlet throat Mach number of 0.79. Performance for the maximum thrust condition is shown in Column 6 of Table 5-II. Approach thrust is assumed to be 65% of the maximum thrust at that flight condition.

Approach engine operating conditions are shown in Columns 7 through 10 using alternate methods to achieve approach power. The conditions shown in Column 7 is for the fan exhaust area (A18) and fan pitch setting set to the takeoff positions. This condition produces the best SFC, but also results in the lowest engine speed, thus, penalizing engine acceleration time.

Shown in Column 8 is an alternative approach setting with the fan exhaust nozzle opened up from 1.657 m^2 (2568 in.^{2}) so that the exit area is set by the flap hinge line area, 21.890 m^2 (2929 in.^{2}). LP spool speed is 84 rpm higher at this condition.

If the fan nozzle is opened further to provide an area larger than that at the hinge line, the nozzle could act as a diffuser. A representative condition is shown in Column 9, where A18 is opened to 2.097 m^2 (3250 in.^{2}). It is expected that the fan exhaust stream would remain attached to the nozzle walls at this small divergent angle. The resulting effect on the cycle is an increase in LP spool speed of 135 rpm over that shown in Column 8.

Another alternative is to hold A18 at the takeoff setting and set the fan rotor pitch angle to produce the objective approach thrust level. This engine operating condition is shown in Column 10.

The effects of these alternative approach settings on component characteristics are shown in Figure 5-5. Inlet throat Mach number shows an increasing trend as A18 is increased. Fan nozzle exit velocity decreases while core exit velocity increases with increasing A18. As noted above, engine speed increases as area increases.

Initial estimates of reverse mode internal cycle parameters and performance are shown in Table 5-IV. The data shown in the table are estimates based on design point calculations and are not based on the component representations which will be incorporated in the cycle deck when it is modified for reverse mode operation.

Reverse mode performance is shown for two alternative engine conditions, reverse through flat pitch and reverse through fan stall. Rotating the rotor blades through flat pitch results in the minimum aeromechanical stress levels to the blading. This mode of operation results in poorer fan aerodynamic

138
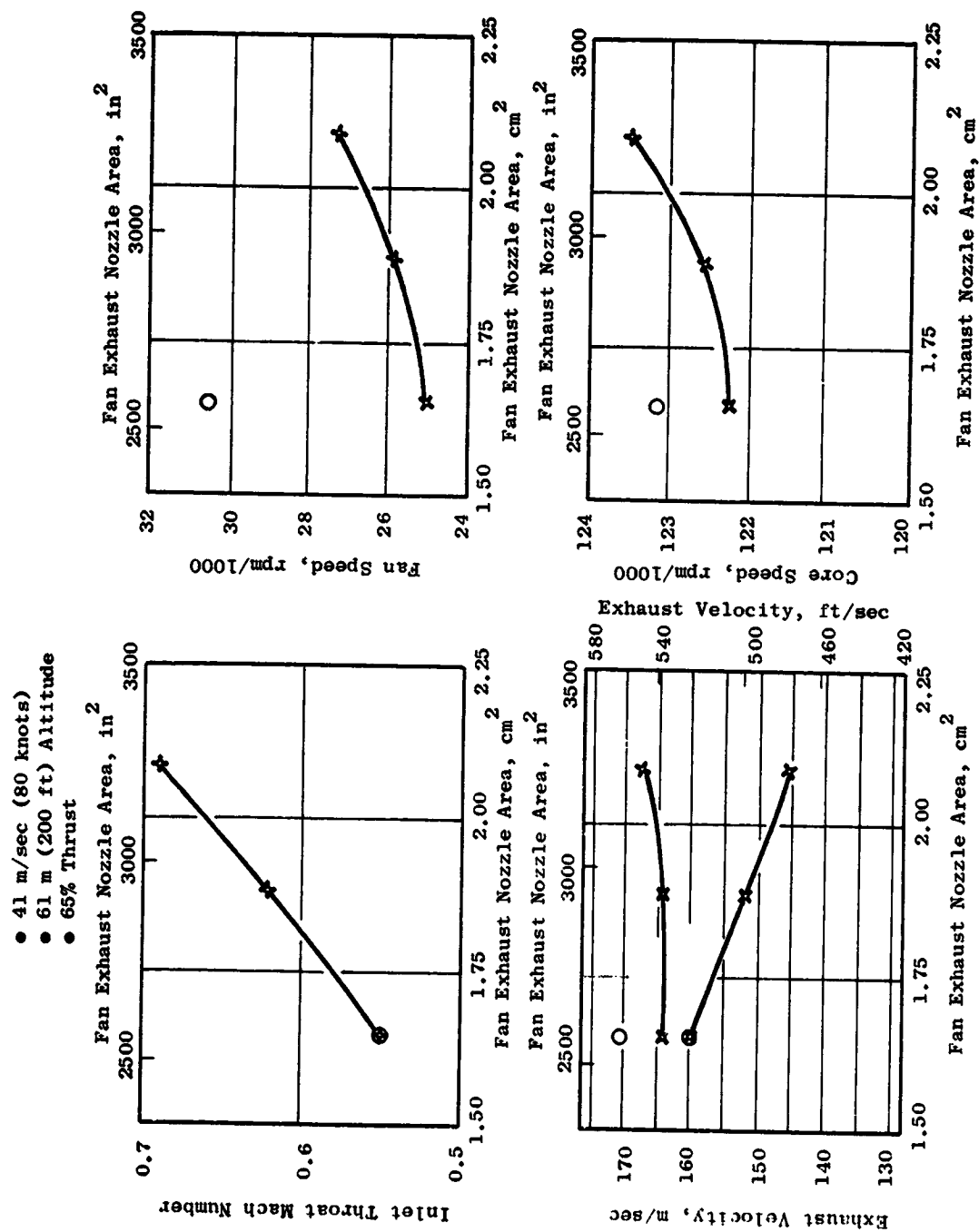
Figure 5-5. UTW Component Operating Characteristics During Approach.

● 41 m/sec (80 knots)
● 61 m (200 ft) Altitude
● 65% Thrust

139

Table 5-IV. UTW Experimental Engine Reverse Mode Performance.

	Through Flat Pitch	Through Stall Pitch
ALT	0	0
XM	0	0
DTAMB	+31	+31
FN	-6405	-6405
SFC	0.678	0.543
W14Q2	8.29	10.36
PAMB	14.696	14.696
ERAM11	0.984	0.980
XM11	-	-
T1	549.67	549.67
P1	14.463	14.408
XNL	3447	2905
PCNLR	106.3	89.5
W2AR	523.8	592.7
W2A	494.8	559.1
P13Q12	1.176	1.136
E12D13	0.476	0.575
ROPDEG	Rev	Rev
W14	441.6	509.9
T14	604	585
P14	17.01	16.36
P18Q14	1.0	1.0
A18	2698	2698
AE18	1704	2279
V19	545	461
FG19	-7446	-7234
T23	549.67	549.67
P23	13.02	12.98
P25Q23	0.90	0.90
T49	2084	1905
P49	41.79	36.51
E49D5	0.905	0.903
P49Q5	2.60	2.32
XNL49	8497	7161
P8Q5	0.978	0.983
W8	54.46	50.18
T8	1678	1568
P8	15.71	15.50
A8	541	541
AE8	528.2	527.8
V9	618	534
FG9	1041	829
FRAM	0	0

Table 5-V. UTW Flight Engine Performance.

	①	②	③
ALT	0	0	30000
XM	0	0	0.8
DTAMB	+31	+31	+18
FN	18300	17400	3856
SFC	0.310	0.324	0.736
W14Q2	12.08	11.98	11.40
PAMB	14.696	14.696	4.364
ERAM11	1.0	0.982	0.993
XM11	-	0.778	0.804
T1	549.67	549.67	484.92
P1	14.696	14.424	6.610
XNL	3157	3157	3319
PCNLR	94.53	94.53	105.81
W2AR	894.0	894.0	894.0
W2A	868.4	852.4	415.9
P13Q12	1.274	1.279	1.394
E12D13	0.882	0.884	0.862
P23Q2	1.209	1.209	1.219
E2D23	0.787	0.788	0.786
ROPDEG	T/O	T/O	Cr
W14	802.1	786.7	382.3
T14	594	595	541
P14	18.72	18.45	9.21
P18Q14	0.986	0.986	0.988
P18	18.46	18.19	9.10
A18	2494	2536	1867
AE18	2417	2458	1836
V19	671	650	1041
FG19	16642	15824	13124
T23	589	589	521
P23	17.77	17.44	8.06
P25Q23	0.983	0.983	0.981
T49	2098	2114	2064
P49	57.25	56.86	28.94
E49D5	0.914	0.914	0.894
P49Q5	3.42	3.42	4.71
XNL49	8208	8208	8629
P8Q5	0.985	0.985	0.958
W8	67.86	67.15	34.31
T8	1593	1606	1473
P8	16.49	16.40	5.89
A8	507.0	515.0	515.0
AE8	484	494	475
V9	789	773	1207
FG9	1659	1610	1284
FRAM	0	0	10514

performance and as a result requires a relatively high engine speed to achieve the required reverse thrust level as shown in Column 1 of Table 5-III. The engine speed level shown exceeds any forward mode engine speed requirement.

Rotation of the rotor blades in the other direction, through fan stall, results in higher aeromechanical stress levels, but when the stalled region is cleared in the reverse position, the blades have better aerodynamic performance. As a result, fan airflow and efficiency are higher and engine speed is significantly less as shown in Column 2, Table 5-III.

5.4 UTW FLIGHT ENGINE AND SYSTEM PERFORMANCE

The UTW flight engine has the same objective thrust levels as the experimental engine. The components are uprated relative to the experimental engine. Fan efficiency levels are approximately 1.5% higher, and MQT level F101 core components are utilized.

Internal cycle parameters and performance for the flight engine are shown in Table 5-V. Parasitic and cooling flows for the flight cycle are included in Figure 5-3, nomenclature is the same as for the experimental engine. Both uninstalled and installed maximum power conditions at sea level static are shown in Table 5-V. Installed performance is shown at the cruise condition, Mach 0.8, 9144 m (30,000 ft). Relative to the experimental engine, the SFC is about 3% better on the flight engine.

5.5 OTW EXPERIMENTAL ENGINE AND SYSTEM PERFORMANCE

The OTW propulsion system incorporates a single-stage, gear-driven fan with the hub stratified to provide a higher pressure rise than the bypass section. The fan stream and core stream exit confluently from a common exhaust nozzle with 17% mixing assumed to occur between the two streams. The cycle provides 93,413 N (21,000 lb) thrust uninstalled at sea level static conditions, flat rated to a 305° K (90° F) day. Installed, with effects of inlet ram recovery allowed for, the thrust level is 90,299 N (20,300 lb). At the cruise condition, Mach 0.8, 9144 m (30,000 ft), the uninstalled engine thrust level is 21,129 N (4750 lb). PFRT level F101 core components are utilized.

Parasitic and cooling flows for both the OTW experimental and flight engines are shown in Figure 5-6.

Internal cycle parameters and performance for the OTW experimental engine are shown in Table 5-VI (see cycle nomenclature Table 5-VII and station designations Figure 5-7). Columns 1 through 4 in Table 5-VI show engine performance corresponding to the objectives presented in Table 5-I. The performance levels shown meet the objective levels with the exception that the turbine rotor inlet temperature is 11° K (19° F) high at sea level static, uninstalled. Since the cooling system capability is significantly greater than that of the base core engine design, these increased temperature levels are not expected to effect experimental engine operation.
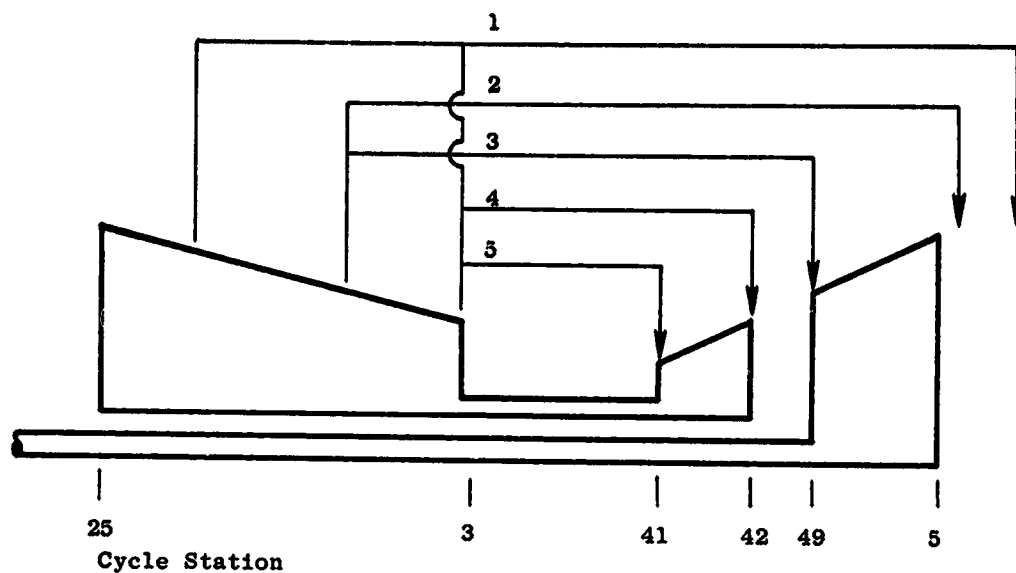
		Source	Sink	Quantity Exper. Engine ($\% W_{25}$)	Flight Engine
1	Balance Piston, LP Shaft & Rear Bearing Cooling	Stg. 3 & CDP	LP Disc	2.01	1.24
2	LP Turbine Rotor Disc & Dovetail Cooling	Stg. 5	LP Disc	1.84	1.00
3	LP Turbine Nozzle Vane & Band Cooling	Stg. 5	LP Rotor Inlet	0	0.50
4	CDP Seal Leakage, HP Turbine Rotor Cooling	CDP	HP Disc	5.46	4.80
5	HP Nozzle Vane & Band Cooling (Nonchargeable)	CDP	HP Rotor Inlet	11.0	9.56

Figure 5-6.   OTW Cooling Flow Schematic.

Table 5-VI. OTW Experimental Engine Performance.

	①	②	③	④	⑤	⑥	⑦
ALT	0	0	0	30000	30000	200	200
XM	0	0	0	0.8	0.8	0.121	0.121
DTAMB	+31	0	+31	+18	+18	0	0
FN	21000	21000	20300	4750	4649	16464	10702
SFC	0.348	0.336	0.363	0.723	0.734	0.408	0.396
W14Q2	10.03	10.08	9.94	9.83	9.83	10.23	10.85
PAMB	14.696	14.696	14.696	4.364	4.364	14.590	14.590
ERAM11	1.0	1.0	0.982	1.0	0.993	0.987	0.994
XM11	-	-	0.778	-	0.804	0.790	0.564
T1	549.67	518.67	549.67	484.92	484.92	519.48	519.48
P1	14.696	14.696	14.424	6.657	6.610	14.554	14.655
XNL	3863	3751	3878	3678	3678	3739	3112
PCNLR	98.93	98.91	99.33	100.3	100.3	98.51	81.98
W2AR	894.0	894.0	894.0	894.0	894.0	894.0	749.5
W2A	868.4	894.0	852.8	418.8	415.9	884.7	746.9
P13Q12	1.347	1.346	1.358	1.383	1.383	1.333	1.217
E12D13	0.867	0.867	0.865	0.857	0.857	0.868	0.877
P23Q2	1.428	1.428	1.428	1.439	1.439	1.425	1.290
E2D23	0.792	0.792	0.792	0.785	0.785	0.792	0.802
W14	789.7	813.3	774.4	380.2	377.5	805.9	683.9
T14	606	512	608	540	540	571	554
P14	19.79	19.78	19.58	9.21	9.14	19.40	17.83
P17Q14	0.978	0.978	0.978	0.979	0.979	0 977	0.982
P17	19.35	19.34	19.16	9.02	8.95	18.96	17.51
T23	624	589	625	553	553	590	569
P23	20.99	20.99	20.64	9.58	9.51	20.74	18.91
P25Q23	0.982	0.982	0.982	0.981	0.981	0.983	0.988
T49	2333	2218	2363	2213	2214	2188	1867
P49	65.51	65.35	65.32	31.50	31.28	63.35	46.60
E49D5	0.902	0.901	0.901	0.897	0.897	0.902	0.893
P49Q5	3.50	3.50	3.53	3.57	3.57	4.35	3.17
XNL49	7963	7734	7996	7583	7583	7709	6416
P57Q5	0.977	0.977	0.982	0.976	0.976	0.977	0.985
P58	19.03	19.02	18.84	8.88	8.81	18.63	17.27
W8	870.4	896.0	854.4	419.8	416.8	886.5	748.0
T8	724	683	729	656	656	678	638
P8	19.03	19.02	18.84	8.88	8.81	18.63	17.27
A8	2790	2790	2853	2319	2319	2853	2853
AE8	2703	2703	2720	2279	2278	2765	2769
V9	787	763	775	1146	1146	741	600
FG9	21000	21000	20300	15339	15164	20177	13836
FRAM	0	0	0	10589	10515	3713	3134

Table 5-VII. Mixed Flow Turbofan Nomenclature.

ALT	Altitude - feet
XM	Flight Mach number
DTAMB	Temperature increment from standard day ambient temperature
FN	Net thrust - lbs
SFC	Specific fuel consumption - lbs/hr/lb
W14Q2	Bypass ratio
PAMB	Ambient pressure - psia
ERAM11	Ram recovery
XM11	Engine inlet throat Mach number
T1	Fan inlet total temperature - deg R
P1	Fan inlet total pressure - psia
XNL	Fan physical speed - rpm
PCNLR	Percent fan corrected speed
W2AR	Engine inlet total corrected flow - lbs/sec
W2A	Engine inlet total flow - lbs/sec
P13Q12	Fan bypass pressure ratio
E12D13	Fan bypass adiabatic efficiency
P23Q2	Fan hub pressure ratio
E2D23	Fan hub adiabatic efficiency
W14	Bypass duct total flow - lbs/sec
T14	Bypass duct total temperature - deg R
P14	Bypass duct inlet total pressure - psia
P17Q14	Bypass duct pressure ratio
P17	Bypass duct discharge total pressure - psia
T23	Fan hub discharge total temperature - deg R
P23	Fan hub discharge total pressure - psia
P25Q23	Intercompressor transition duct pressure ratio
XNH	HP compressor physical speed - rpm
PCNHR	Percent HP compressor corrected speed
W25R	HP compressor corrected inlet air flow - lbs/sec
W25	HP compressor inlet air flow - lbs/sec
P3Q25	HP compressor pressure ratio

144

Table 5-VII. Mixed Flow Turbofan Nomenclature. (Concluded)

E25D3	HP compressor adiabatic efficiency
P3Q2	Overall cycle pressure ratio
T3	HP compressor discharge total temperature - deg R
P3	HP compressor discharge total pressure - psia
P4Q3	Combustor pressure ratio
E36D4	Main combustion efficiency
T4	HP turbine 1st stage nozzle inlet total temperature - deg R
W41	HP turbine rotor inlet gas flow - lbs/sec
T41	HP turbine rotor inlet total temperature - deg R
E41D42	HP turbine adiabatic efficiency
P41Q42	HP turbine pressure ratio
T42	HP turbine discharge total temeprature - deg R
W49	LP turbine rotor inlet total gas flow - lbs/sec
T49	LP turbine rotor inlet total temperature - deg R
P49	LP turbine rotor inlet total pressure - psia
E49D5	LP turbine rotor adiabatic efficiency
P49Q5	LP turbine pressure ratio
XNL49	LP turbine physical speed - rpm
P57Q5	Core duct pressure ratio
P58	Exhaust duct inlet total pressure - psia
W8	Jet nozzle throat total gas flow - lbs/sec
T8	Jet nozzle throat total temperature - deg R
P8	Jet nozzle throat total pressure - psia
A8	Jet nozzle throat actual area - sq in
AE8	Jet nozzle throat effective area - sq in
V9	Jet nozzle exit velocity - ft/sec
FG9	Gross thrust - lbs
FRAM	Ram drag - lbs

Station	Description
0	Free Stream Air Conditions
1	Inlet/Engine Interface
2	Fan Inlet
23	Fan Hub Discharge
25	HP Compressor Inlet
3	HP Compressor Discharge (Stator Exit)
4	Combustor Discharge
41	HP Turbine Rotor Inlet
42	HP Turbine Discharge
49	LP Turbine Rotor Inlet
5	LP Turbine Discharge
57	Core Duct Exit
58	Exhaust Duct Inlet
8	Exhaust Nozzle Throat
9	Exhaust Nozzle Discharge
12	Fan Inlet
13	Fan Tip Discharge
14	Bypass Duct Inlet
17	Bypass Duct Exit

Figure 5-7. Station Designations - Mixed Flow Turbofan Cycle.

A fan corrected flow limit of 406 kg/sec (894 lb/sec) is used to establish maximum power at all flight conditions, as on the UTW engines.

Installed performance at cruise is shown in Column 5. The effect relative to uninstalled thrust is a decrease of 445 N (100 lb). This is due to ram recovery alone, since there are no scrubbing losses as on the UTW.

Installed approach conditions at maximum power (Column 6) and 65% power (Column 7) are also shown in Table 5-VI. Part power operation at approach is accomplished by setting the exhaust nozzle to takeoff area and reducing engine speed to get to the required thrust level.

5.6 OTW FLIGHT ENGINE AND SYSTEM PERFORMANCE

Objective thrust levels for the OTW flight engine are the same as those for the experimental engine. Fan efficiency is uprated 1.5% relative to the experimental engine, and MQT level F101 core engine components are assumed.

Internal cycle parameters and performance for the OTW flight engine are shown in Table 5-VIII. Parasitic and cooling flows are show. in Figure 5-6; nomenclature is the same as for the OTW experimental engine. Maximum power conditions at sea level static are shown in Table 5-VIII for both uninstalled (Column 1) and installed (Column 2) conditions. Installed performance is shown at the cruise condition, Mach 0.8, 9144 m (30,000 ft) (Column 3). The SFC difference relative to the experimentla engine is a little over 2%.

Table 5-VIII. OTW Flight Engine Performance.

	①	②	③
ALT	0	0	30000
XM	0	0	0.8
DTAMB	+31	+31	+18
FN	21000	20300	4647
SFC	0.339	0.355	0.717
W14Q2	10.14	10.03	9.80
PAMB	14.696	14.696	4.364
ERAM11	1.0	0.982	0.993
XM11	-	0.778	0.804
T1	549.67	549.67	484.92
P1	14.696	14.424	6.610
XNL	3870	3885	3692
PCNLR	99.12	99.49	100.7
W2AR	894.0	894.0	894.0
W2A	868.4	852.4	415.9
P13Q12	1.352	1.352	1.392
E12D13	0.881	0.880	0.865
P23Q2	1.430	1.430	1.443
E2D23	0.790	0.790	0.783
W14	790.5	775.1	377.4
T14	606	607	541
P14	19.86	19.65	9.20
P17Q14	0.978	0.979	0.980
P17	19.43	19.23	9.01
T23	625	625	554
P23	21.01	20.66	9.54
P25Q23	0.982	0.982	0.981
T49	2223	2253	2119
P49	68.60	68.52	33.21
E49D5	0.906	0.905	0.893
P49Q5	3.71	3.73	3.81
XNL49	7979	8009	7611
P57Q5	0.985	0.984	0.983
P58	19.11	18.92	8.88
W8	870.3	854.3	416.8
T8	712	717	647
P8	19.11	18.92	8.88
A8	2741	2758	2286
AE8	2655	2673	2247
V9	786	774	1138
FG9	21000	20300	15161
FRAM	0	0	10514

SECTION 6.0

FAN AERODYNAMIC DESIGN

6.1 SUMMARY

The aerodynamic design of both the variable-pitch UTW and fixed-pitch OTW geared fans was completed during the Preliminary Design Phase.

At the major operating conditions of takeoff and maximum cruise a corrected flow of 405.5 kg/sec (894 lbm/sec) was selected for both fans which enables common inlet hardware to yield the desired 0.79 average throat Mach number at the critical takeoff noise measurement condition. The aerodynamic design bypass pressure ratio is 1.34 for the UTW and 1.36 for the OTW which is intermediate between the takeoff and maximum cruise power settings. The takeoff pressure ratios are 1.27 for the UTW and 1.34 for the OTW. The take-off corrected tip speeds are 289 m/sec (950 ft/sec) for the UTW and 354 m/sec (1162 ft/sec) for the OTW. These pressure ratios and speeds were selected on the basis of minimum noise within the constraints of adequate stall margin and core engine supercharging.

The UTW fan was designed to permit rotation of the blades into the reverse thrust mode of operation through both flat pitch (like a propellor) and the stall pitch directions. The vane-frame, which is common to both engines, performs the dual function of an outlet guide vane for the bypass flow and a frame support for the engine components and nacelle. The UTW island configuration was selected specifically for the reverse thrust mode of operation.

6.2 UTW FAN

6.2.1 Operating Requirements

The major operating requirements for the under-the-wing (UTW) fan (Figure 6-1) are takeoff, where noise and thrust are of primary importance, and maximum cruise, where economy and thrust are of primary importance. At take-off a low fan pressure ratio of 1.27 was selected to minimize the velocity of the bypass stream at nozzle exit. A corrected flow of 405.5 kg/sec (894 lbm/sec) at this pressure ratio yields the required engine thrust. The inlet throat is sized at this condition for an average Mach number of 0.79 to minimize the forward propagation of fan noise. This sizing of the inlet throat prohibits higher corrected flow at altitude cruise. The required maximum cruise thrust is obtained by raising the fan pressure ratio to 1.39. The aerodynamic design point was selected at an intermediate condition which is a pressure ratio of 1.34 and a corrected flow of 408 kg/sec (900 lb/sec). Table 6-1 summarizes the key parameters for these three conditions.
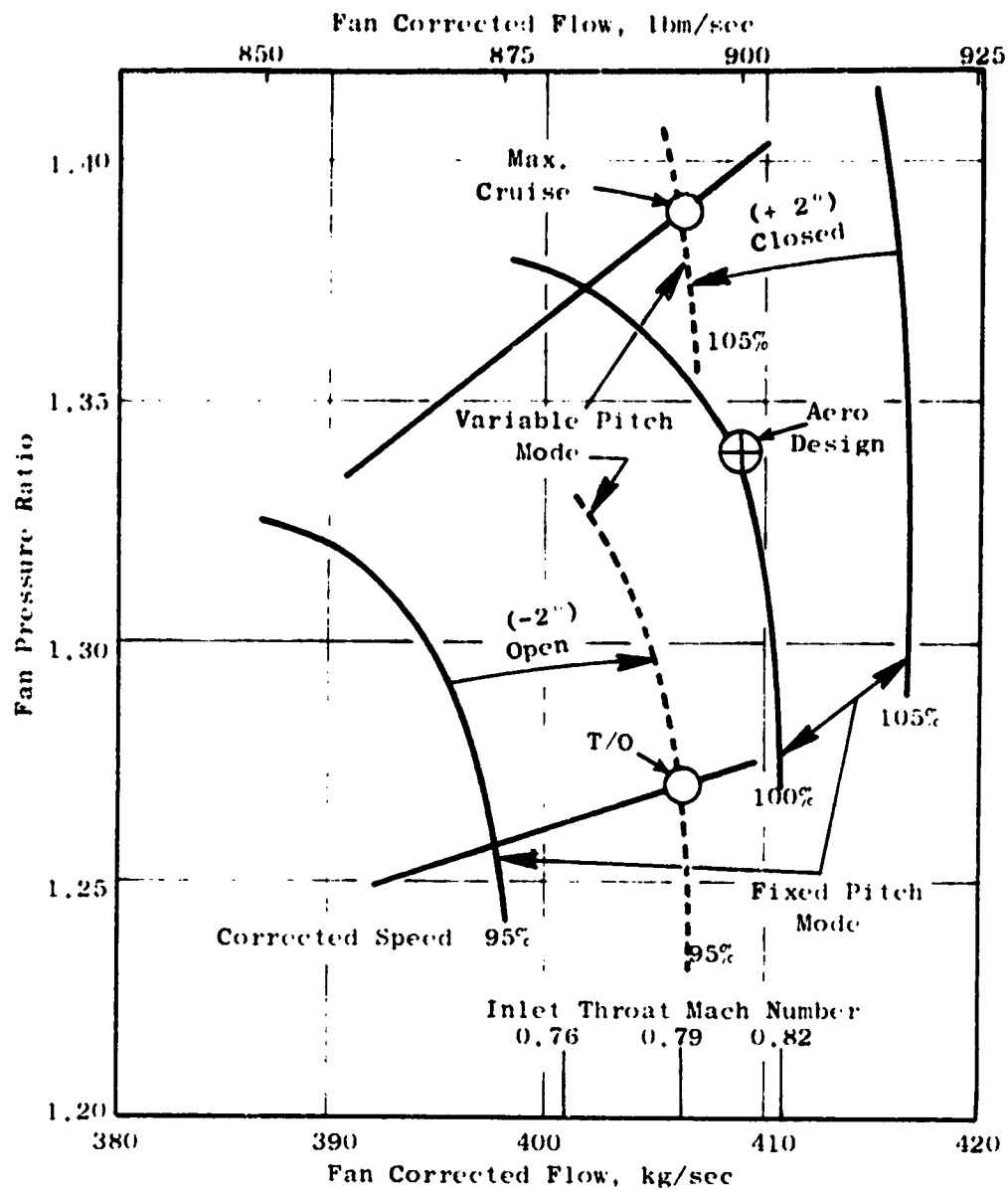
Figure 6-1. UTW Variable Pitch Fan.

Table 6-I. QCSEE UTW Variable-Pitch Fan

Parameter	Design Point	Takeoff	Maximum Cruise
Total fan flow	408 kg/sec (900 lb/sec)	405.5 kg/sec (894 lb/sec)	405.5 kg/sec (894 lb/sec)
Pressure ratio - bypass flow	1.34	1.27	1.39
Pressure ratio - core flow	1.23	1.20	1.21
Bypass ratio	11.3	11.8	11.4
Pitch setting	Nominal	Open 2°	Closed 2°
Corrected tip speed	306 m/sec (1005 ft/sec)	289 m/sec (950 ft/sec)	324 m/sec (1063 ft/sec)

6.2.2 Basic Design Features

A cross section of the selected UTW fan configuration is shown in Figure 6-2. There are 18 variable-pitch composite rotor blades. The solidity of the blades is 0.95 at the OD and 0.98 at the ID. The chord is linear with radius. This permits rotation of the blades into the reverse thrust mode of operation through both the flat pitch (like a propeller) and the stall pitch directions. The spherical casing radius over the rotor tip provides good blade tip clearances throughout the range of blade pitch angle settings. Circumferential grooved casing treatment is incorporated over the rotor tip to improve stall margin. Stall margins are significant because a minimum fan tip speed was selected to minimize noise generation. The circumferential grooved casing treatment type was selected since this type of treatment improves stall margin and has shown negligible adverse impact on overall fan efficiency. An additional benefit of the casing treatment is to reduce the material bulk over the blade tip, for a given clearance, which will reduce the severity of an inadvertent blade rub as might be encountered during a bird strike.

The vane-frame is positioned at an axial distance downstream of the rotor trailing edge equal to 1.5 true rotor tip chords. The vanes are nonaxisymmetric in that five vane geometries, each with a different camber and stagger, are employed around the annulus. This nonaxisymmetric geometry is required to conform the vane-frame downstream flow field to the geometry of the pylon, which protrudes forward into the vane-frame, and simultaneously maintain a condition of minimum circumferential static pressure distortion upstream of the vane-frame. There are 33 vanes in the vane-frame which yields a vane-blade ratio of 1.83. Immediately following the rotor, in the hub region, is an annular ring or island. The 96 OGV's for the fan hub, or core portion flow, are in the annular space between the under side of the island and the hub. A full circumference axial gap separates the island trailing edge from the splitter leading edge. The splitter divides the flow into the bypass portion and core portion. There are six struts in the gooseneck which guide the fan hub flow into the core compressor.

151
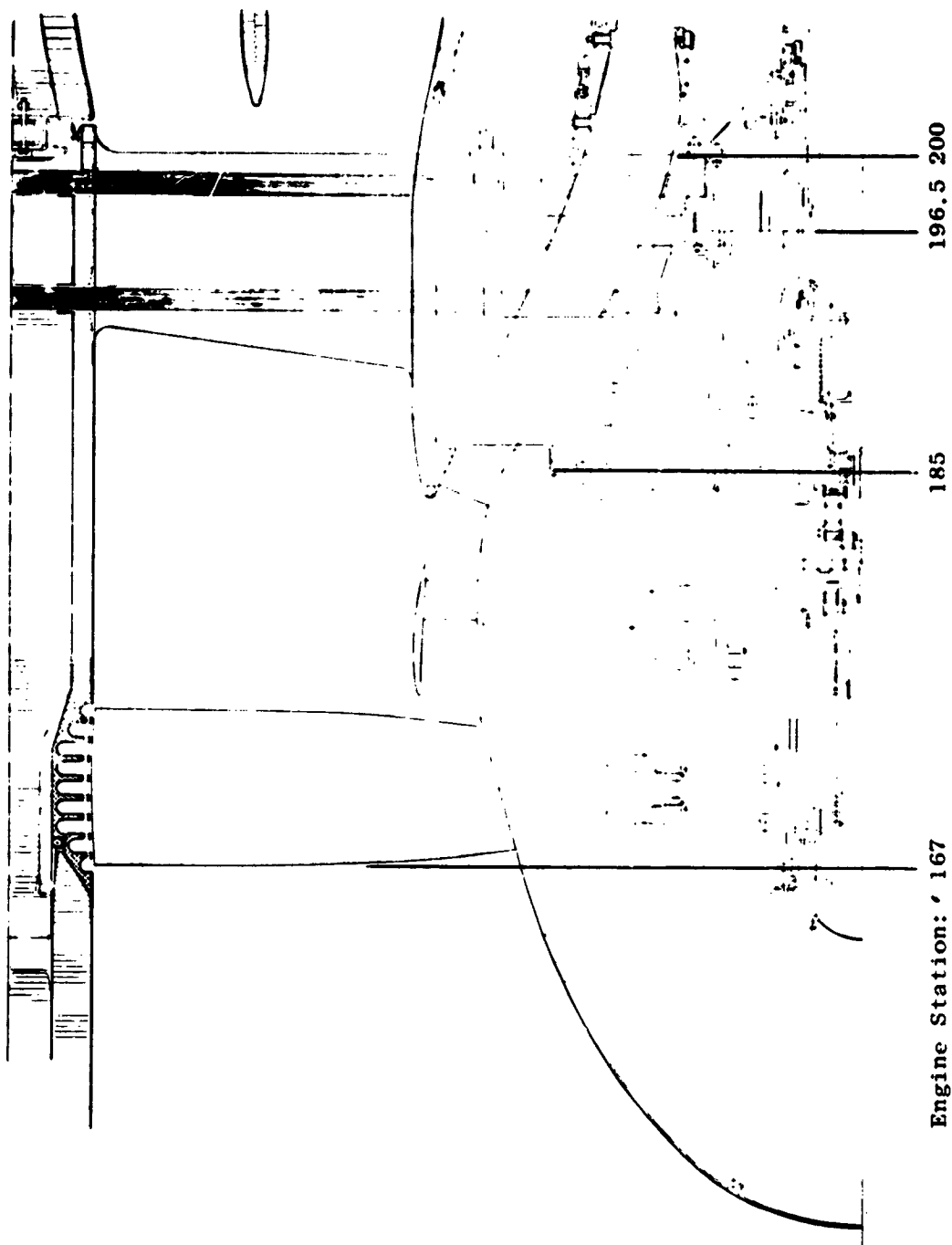
Figure 6-2. Cross Section of UTW Variable Pitch Fan.

Engine Station: 167   185   196.5 200

152

The island configuration was selected specifically to permit the attainment of a high hub supercharging pressure ratio for forward pitch operation without causing a large core flow induction pressure drop during reverse pitch operation, see Section 6.2.3. In the forward mode of operation, a vortex sheet is shed from the trailing edge of the island in the form of a swirl angle discontinuity since most of the swirl in the flow under the island is removed by the OGV. The total pressure on top of the island differs from that under the island only by the losses in the core OGV, hence the Mach numbers of the two streams are nearly the same. The General Electric CF6-6 fan incorporates a similar island configuration, except that the bypass OGV's are on top of the island and there is no swirl in the bypass flow at the island trailing edge. A vortex sheet is shed from the trailing edge of this island configuration also. This vortex sheet is in the form of a velocity magnitude discontinuity. The swirl angle is zero both on top of and under the island but the total pressures differ by the work input in the tip region of the 1/4 stage. Numerically, the strength of the QCSEE UTW island shed vortex is approximately the same as the strength of the CF6-6 island shed vortex. The orientation of the vortex vectors are rotated approximately 70° however.

6.2.3 Reverse Flow

A major feature of the UTW fan is its ability to change the direction of fan thrust by reversing the direction of flow through the fan. This flow reversal affects the pressure level into the core engine (and, hence, the core engine's ability to produce power) in two ways. First, there is the direct loss of the fan hub supercharging pressure; and second, there is the loss associated with inducting the flow into the core engine such as the recoveries of the exlet, vane frame, turn around, splitter leading edge, core OGV's, and gooseneck struts. The first loss is obviously related to the magnitude of the design (forward mode) fan hub pressure ratio, but the second loss is also related to this magnitude. This is so because, when operating in the reverse thrust mode, camber on the core portion OGV's is in the wrong direction and high hub supercharging in forward operation increases the camber of both bypass and core OGV's. Concern over this matter because of relatively high hub pressure ratio of the UTW fan was the primary reason for selecting the island approach. The major advantage to this configuration is that flow can enter the core compressor through the axial gap between the island and splitter and thereby avoid the problem of adversely oriented camber on the core OGV's. The swirling flow must still, of course, pass through the axially oriented struts in the core inlet gooseneck. Relatively, this path for the flow is much less restrictive. A second benefit is that the bluntness of the splitter leading edge, compared to the island leading edge (which would be the splitter leading edge if the axial gap were filled), is conducive to minimizing losses associated with reversing the axial component of the core portion flow from its forward direction in the bypass duct to its aft direction in the core transition duct.

Reverse fan thrust can be achieved by rotating the blades through the flat pitch (like a propeller) or the stall pitch directions. Rotation of the blades into the reverse thrust condition puts a constraint on selection of blade solidity. This depends primarily on the direction in which the blades are

rotated and the blade twist. The constraint is on those blade sections which pass through a tangential orientation, e.g., the leading edge of each blade must be able to pass the trailing edge of the adjacent blade, or physical interference will result. Therefore, those sections must have a solidity less than unity.

Figure 6-3 shows a tip and hub section of two adjacent blades in nominal, reverse through flat, and reverse through stall orientations. The 45° tip stagger for both reverse through flat and reverse through stall was selected based on experimental reverse thrust performance. For blade rotation through the flat pitch direction, the entire blade span is constrained to a solidity less than one. For rotation through the stall pitch direction, the outer portion of the blade is not constrained. However, because of the 40° twist in the blade, the chord of the hub region cannot be increased significantly without interference. The assumed orientation of the tip section would have to be in error on the order of 5° before significant hub region chord increase could be accommodated. Even if a hub region chord increase could be accommodated, a significant increase in supercharging potential is probably not available because the implied increase in blade twist would probably cause a physical interference.

It was therefore concluded that a hub solidity less than unity was a design requirement for reverse through stall pitch rather than a compromise to permit reverse through flat pitch.

6.2.4 Performance Representation with Variable Pitch

The variable pitch feature of the UTW fan adds a third independent variable to the representation of fan performance in that, in addition to normal independent variables of speed and operating line, the blade pitch angle is also required. It has been found, however, that experimental stage characteristics at different rotor pitch angle settings can be collapsed into a nearly universal characteristic applicable for all blade angle settings. The method used to collapse the characteristics was to deduce the rotor incidence and deviation angle from the test data and then calculate the performance of the stage at nominal blade angle with the rotor operating at this incidence and deviation angle and the test efficiency. A separate correlation of aerodynamic loading is used to identify a stall limit, as the collapsing technique breaks down due to the change in aerodynamic loading inherent in the transformation. Figure 6-4 shows the stage characteristics assumed for the UTW fan at 100% corrected speed for a range of pitch angles. In the reverse flow mode of operation a similar, but simplified, form of the universal characteristic approach is used to represent fan performance. The same collapsing technique is incorporated to include the effect of blade angle setting.

154
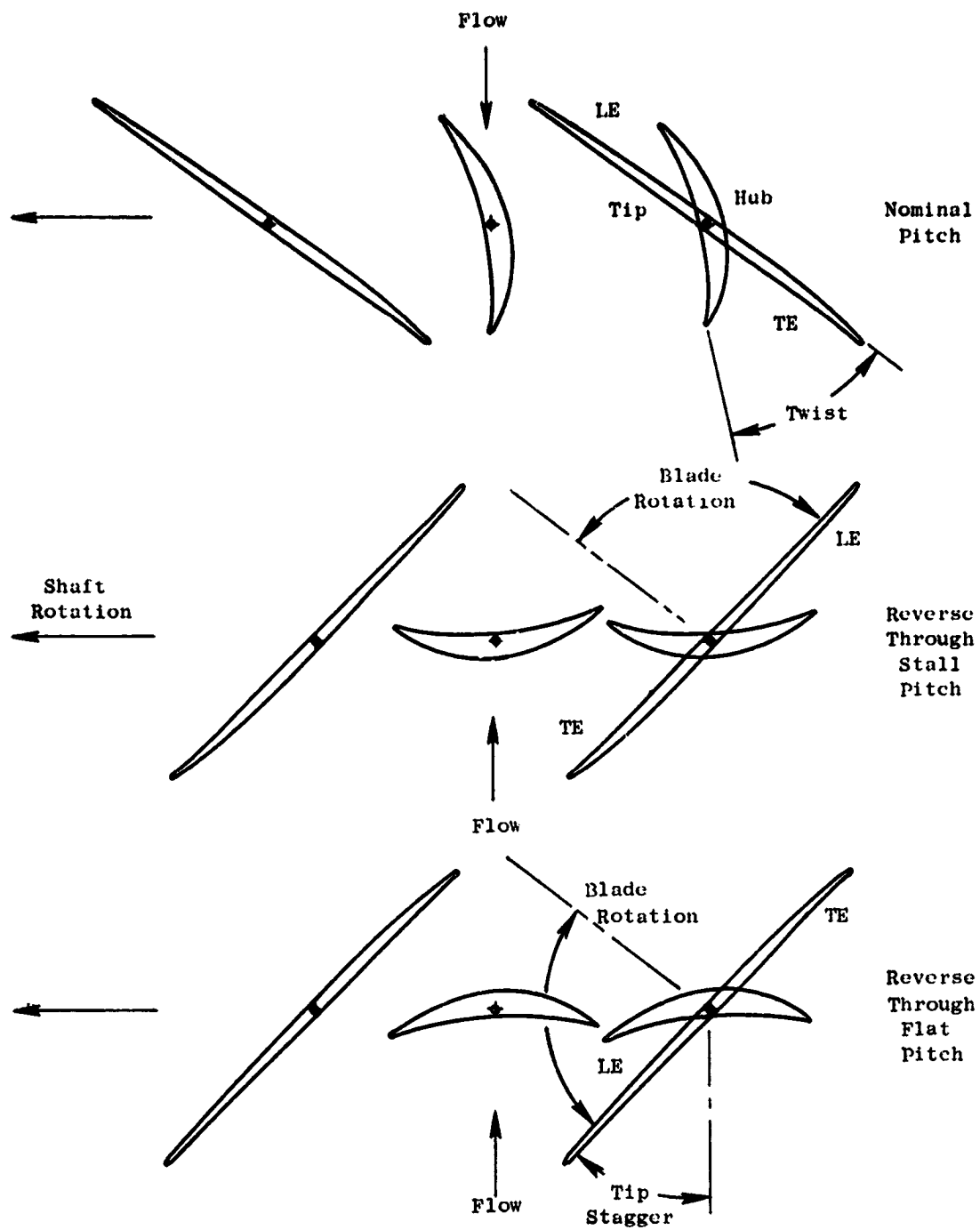
Figure 6-3. UTW Blade Geometry at Different Pitch Angle Settings.
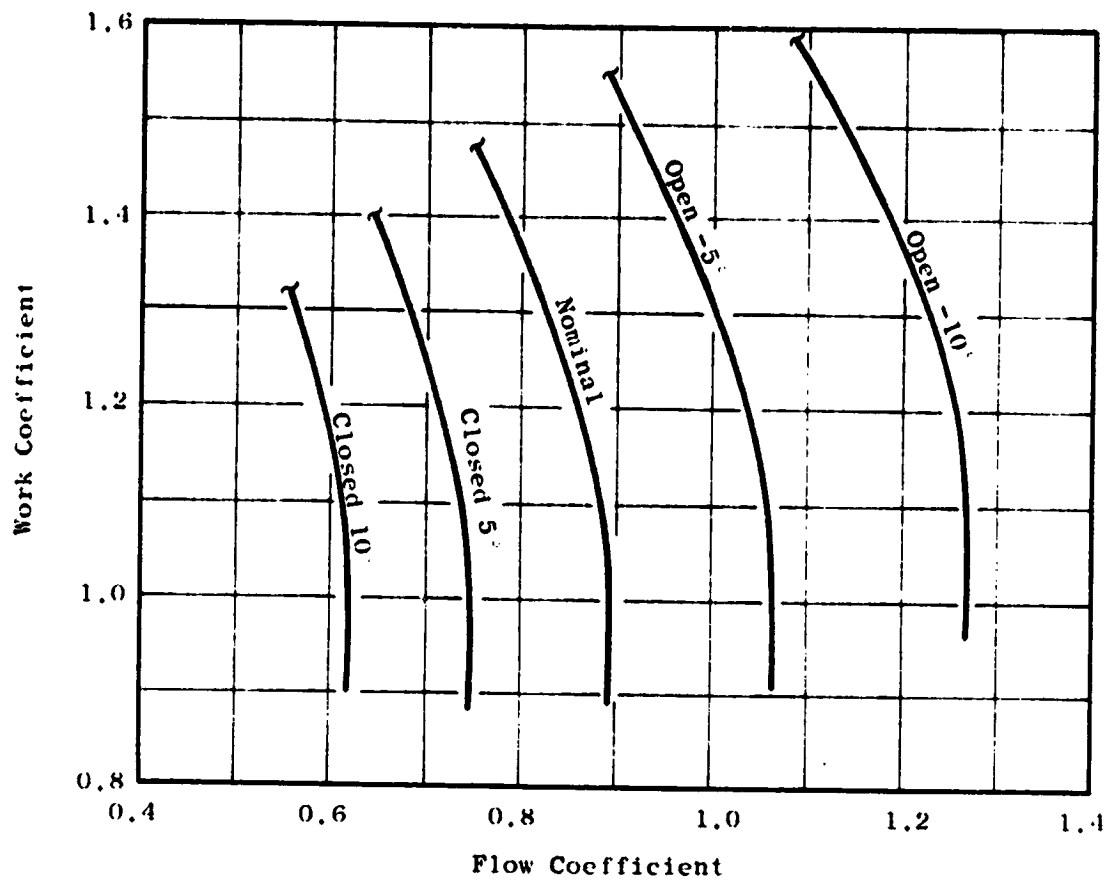
Figure 6-4. UTW Stage Characteristics at 100% Speed for Various Pitch Settings.

6.2.5 Detailed Configuration Design

The corrected tip speed at the aerodynamic design point was selected at 306 m/sec (1005 ft/sec). This selection is a compromise for design purposes between 289 m/sec (950 ft/sec) at takeoff and the 324 m/sec (1063 ft/sec) at maximum cruise. The objective design point adiabatic efficiency is 88% for the bypass portion and 78% for the core portion. A stall margin of 16% is projected at takeoff. This stall margin is provided at minimum tip speed by incorporating circumferential grooved casing treatment over the rotor tip. Minimum tip speed is important because of the favorable impact of low tip speed on fan generated noise, fan efficiency in the transonic region, and the mechanical design of the variable pitch system. An inlet radius ratio of 0.44 balances the desire to minimize fan diameter within the physical constraints of the variable-pitch mechanism and gear box and good fan hub supercharging for the core engine. A fan inlet flow per annulus area of 199 kg/sec-m^2 (40.8 lb/sec-ft^2) at the design point results in a tip diameter of 1.803 m (71.0 in.).

The standard General Electric axisymmetric flow computation procedure was employed in calculating the velocity diagrams. Several calculation stations were included internal to the rotor blade to improve the overall accuracy of the solution in this region. The physical island geometry is represented in the calculations. Forward of the island and in the axial space between the island and the splitter, calculation stations span the radial distance from OD to ID. Within the axial space of the island, calculation stations span the radial distance between the OD and the topside of the island and between the underside of the island and the hub contour. In the bypass and core inlet ducts, calculation stations are also included. At each calculation station effective area coefficients consistent with established design practice were assumed.

A special constraint is necessary in the aerodynamic design of the island geometry in that a smooth flow or Kutta condition must be satisfied at the trailing edge of the island. The technique employed in this design was to specify a calculation station at the axial location of the island trailing edge which spanned the total flowpath height from OD to ID. Using this technique, a continuous radial distribution of static pressure results which was assumed to be consistent with matching the Kutta condition. The radial location of the island stream function at this calculation station was determined and the upstream geometry of the island was then adjusted to provide a smooth continuous contour blending into this point. Iteration was obviously necessary because of the interaction of the assumed geometry with the calculated radial location of the island stream function. Convergence was found to be quite rapid. An artificial radial displacement was incorporated between the island upper surface streamline and the island lower surface streamline in order to avoid problems in calculating the streamline curvatures. This displacement was assumed equal to the island thickness at the trailing edge and was smoothly blended to zero at an axial distance of approximately 10 edge thicknesses downstream.

The design radial distribution of rotor total pressure ratio is shown in Figure 6-5. This distribution is consistent with a stage average pressure ratio of 1.34 in the bypass region. Despite the lower than average pressure ratio in the hub region, it has been maximized to the extent possible subject to the constraint of acceptable rotor diffusion factors so as to provide maximum core engine supercharging. A stage average pressure ratio of 1.23 results at the core OGV exit. The radial distribution of rotor efficiency assumed for the design is shown in Figure 6-6. The assumption of effiency, rather than total pressure loss coefficient, is a General Electric design practice for rotors of this type. This distribution was based on the measured results from similar configurations with adjustments to account for recognized differences. The radial distribution of rotor diffusion factor which results from these assumptions is shown in Figure 6-7. The moderately high diffusion factor in the tip region of the blade, where stall generally initiates, confirm the need for casing treatment to obtain adequate margin. The radial distributions of rotor relative Mach number and air angle are shown in Figures 6-8 and 6-9, respectively.

The assumed radial distribution of total-pressure-loss coefficient for the core portion OGV is shown in Figure 6-10. The relatively high level, particularly in the ID region, is in recognition of the very high bypass ratio of the UTW engine and accordingly the small size of the core OGV compared to the rotor. The annulus height of the core stator is approximately one-half of the rotor staggered spacing, a significant dimension when analyzing secondary flow phenomena. It is anticipated that core OGV will be influenced by the rotor secondary flow over the entire annulus height. The diffusion factor, Mach number and air angle radial distributions which result from the design assumptions are also shown in Figure 6-10. An average swirl of 0.104 radian (6°) is retained in the fluid at exit from the core OGV. This was done to lower its aerodynamic loading and the magnitude of the vortex sheet shed from the island. The transition duct (core inlet) struts are cambered to accept this swirl and remove it prior to entrance into the core engine.

6.2.6 Rotor Blade Design

The detailed layout procedure employed in design of the fan blade generally parallels established design procedures. In the tip region of the blade, where the inlet relative flow is supersonic, the uncovered portion of the suction surface was set to ensure that the maximum flow passing capacity is consistent with the design flow requirement. Incidence angles in the tip region were selected according to transonic blade design practice which has yielded good overall performance for previous designs. In the hub region, where inlet flow is subsonic, incidence angles were selected from NASA cascade data correlations.

The blade trailing edge angle was established by the deviation angle which was obtained from Carter's Rule applied to the camber of an equivalent two-dimensional cascade with an additive empirical adjustment, X. This adjustment is derived from aerodynamic design and performance synthesis for this general

158
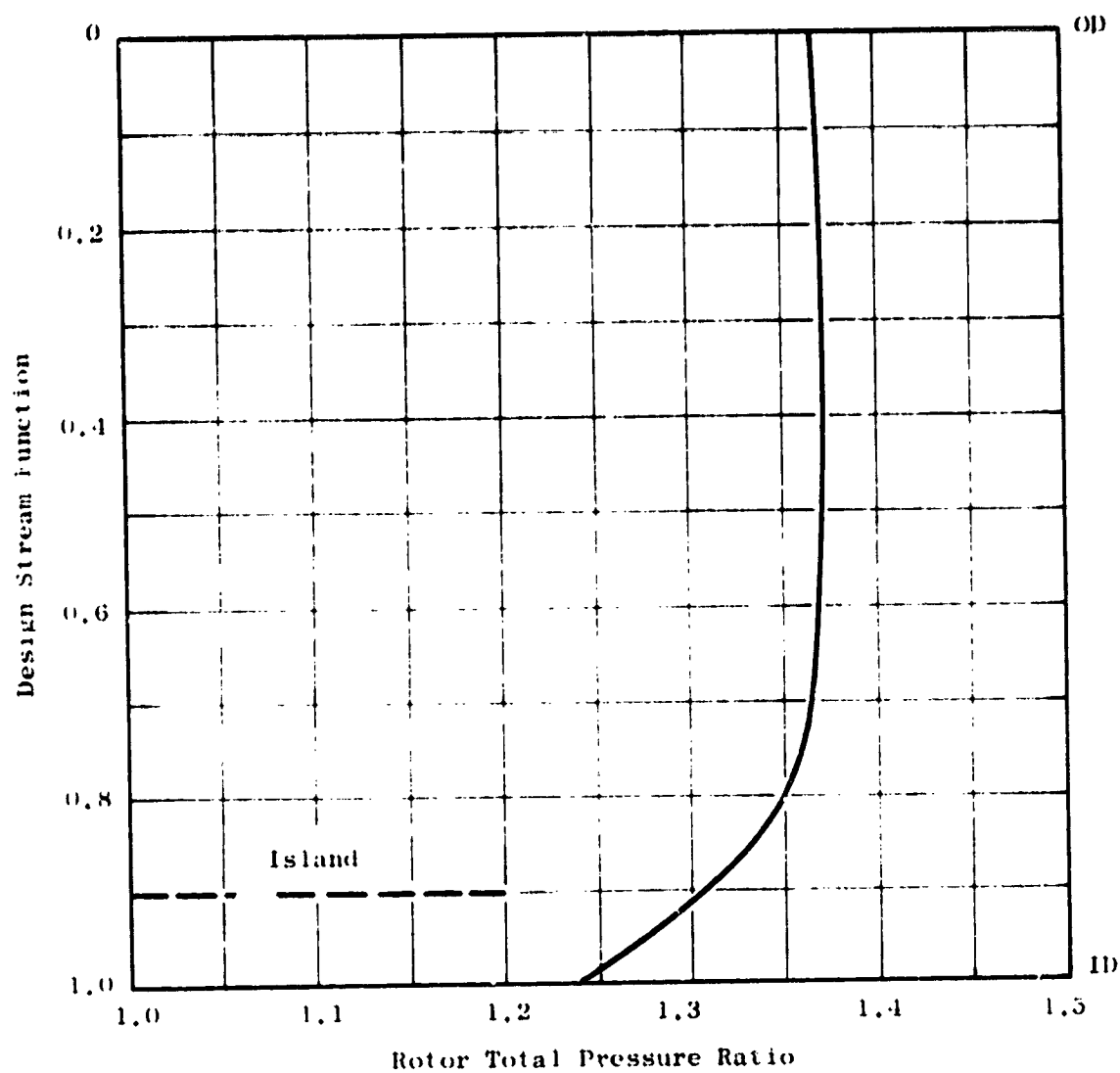
Figure 6-5. UTW Radial Distribution of Rotor Total Pressure Ratio.
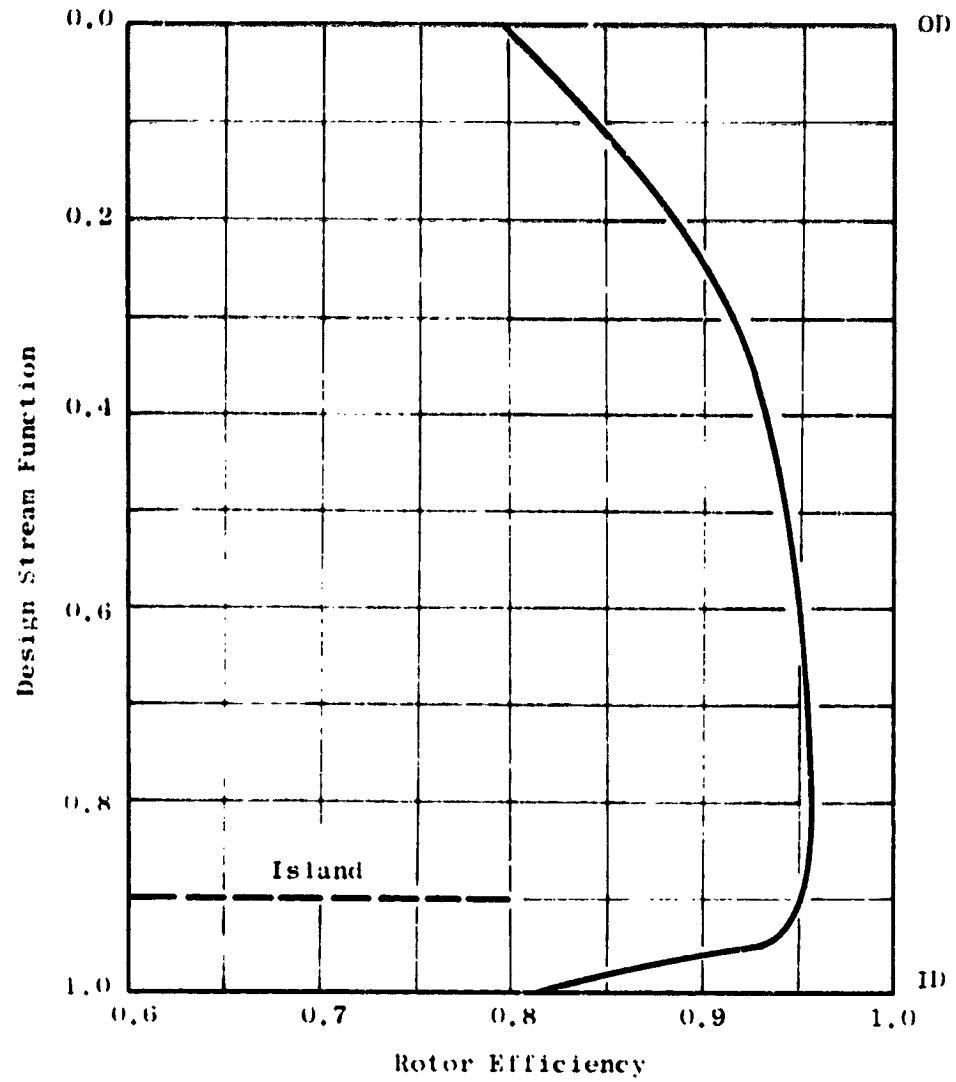
Figure 6-6. UTW Radial Distribution of Rotor
Efficiency.

160
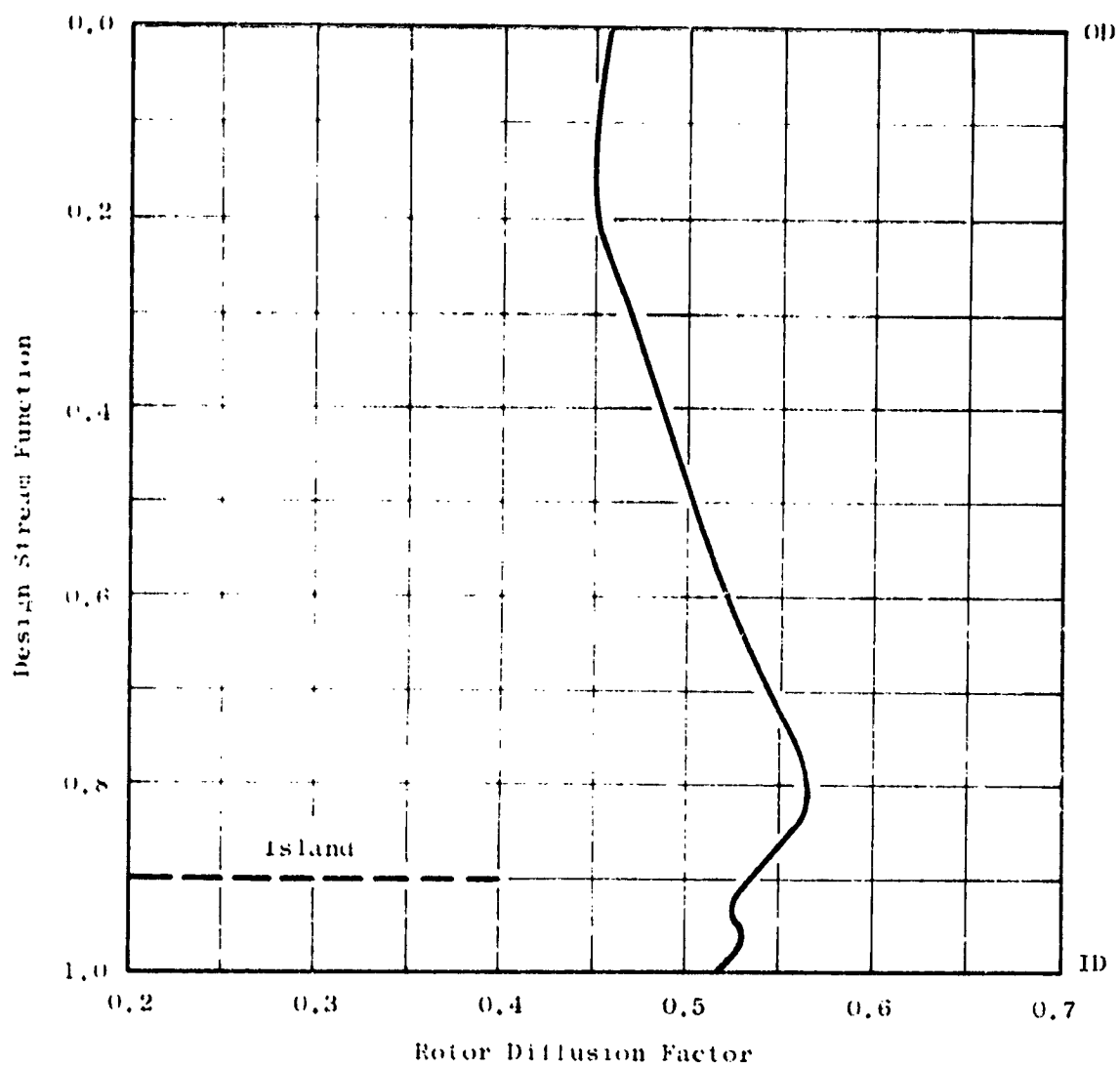
Figure 6-7. UTW Radial Distribution of Rotor Diffusion Factor.
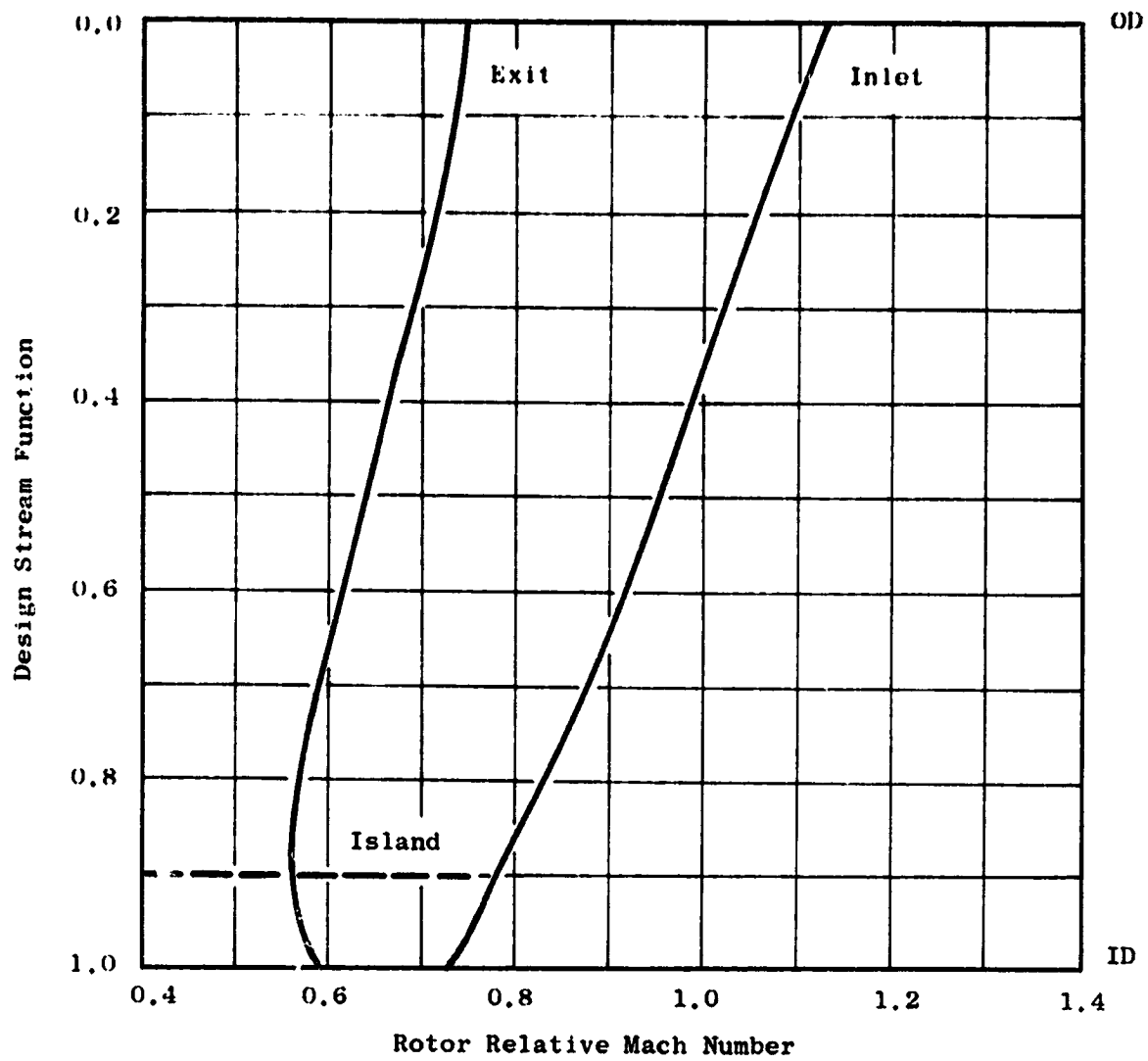
Figure 6-8. UTW Radial Distribution of Rotor Relative Mach Number.
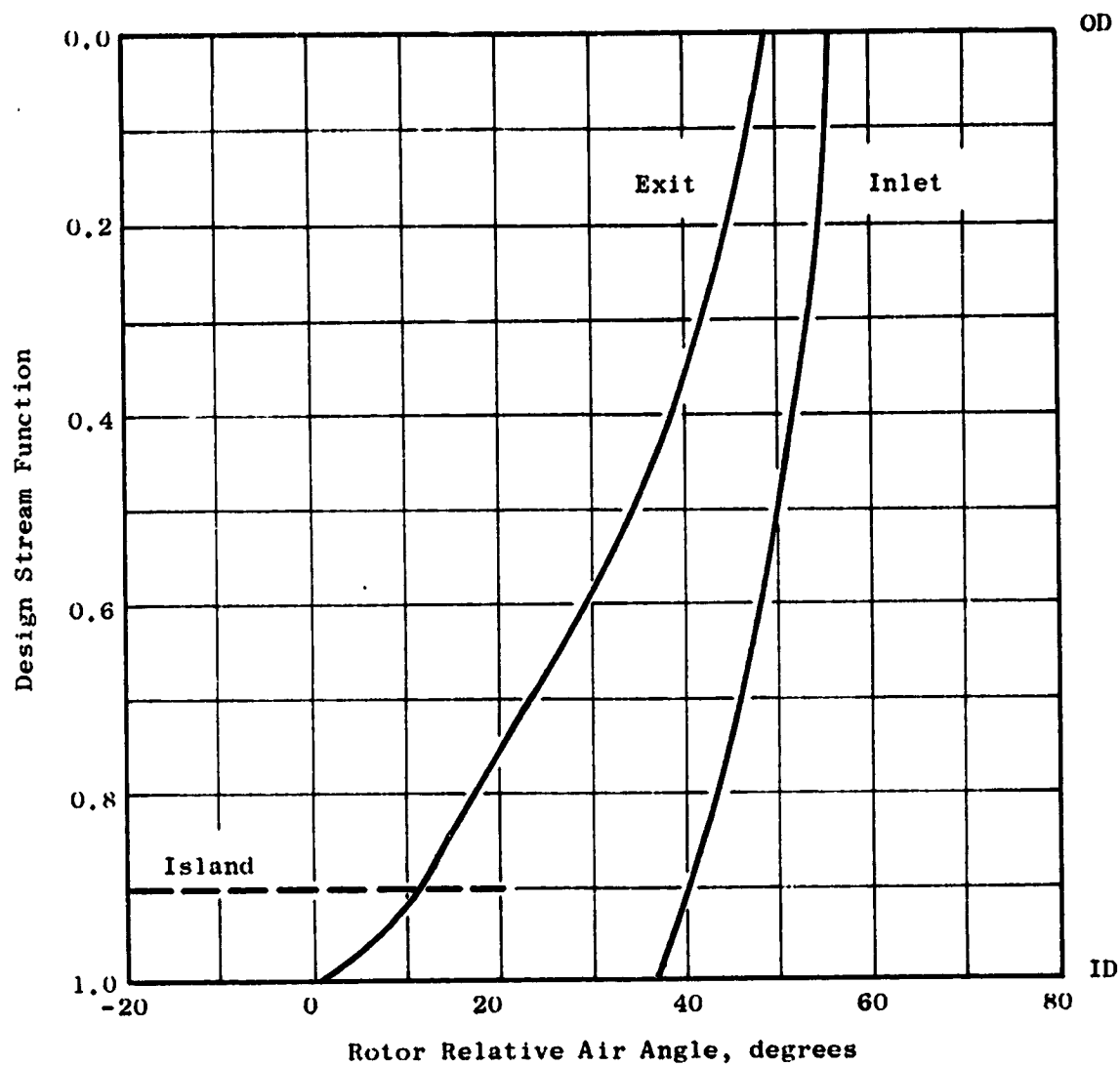
Figure 6-9. UTW Radial Distribution of Rotor Relative Air Angle.

163
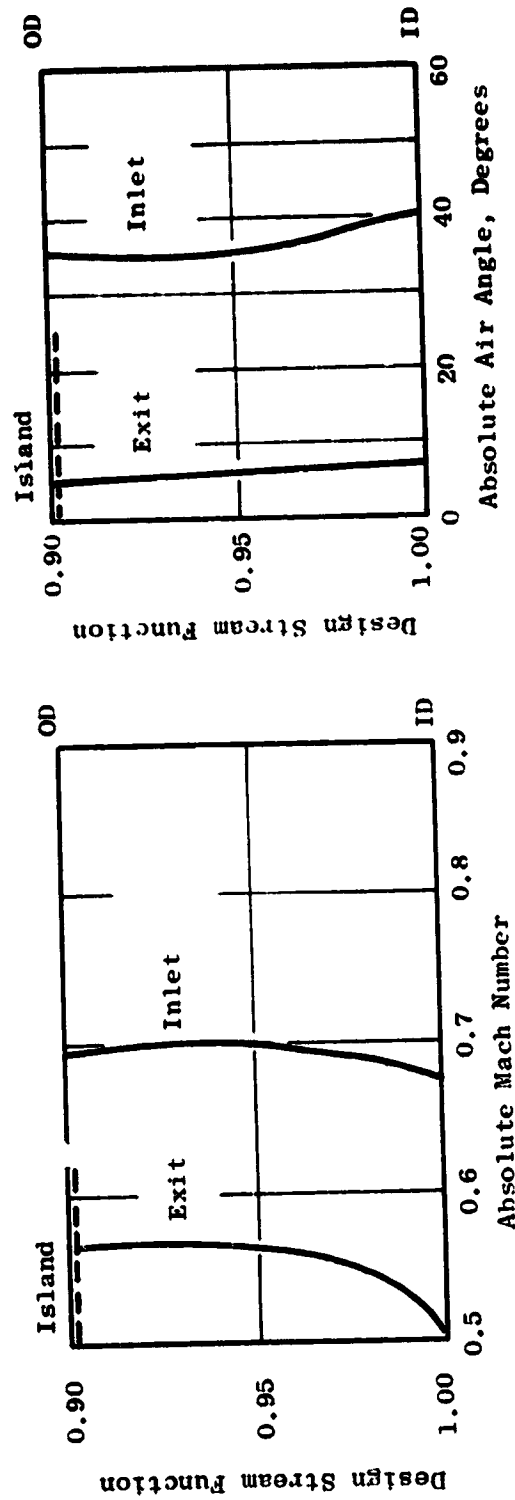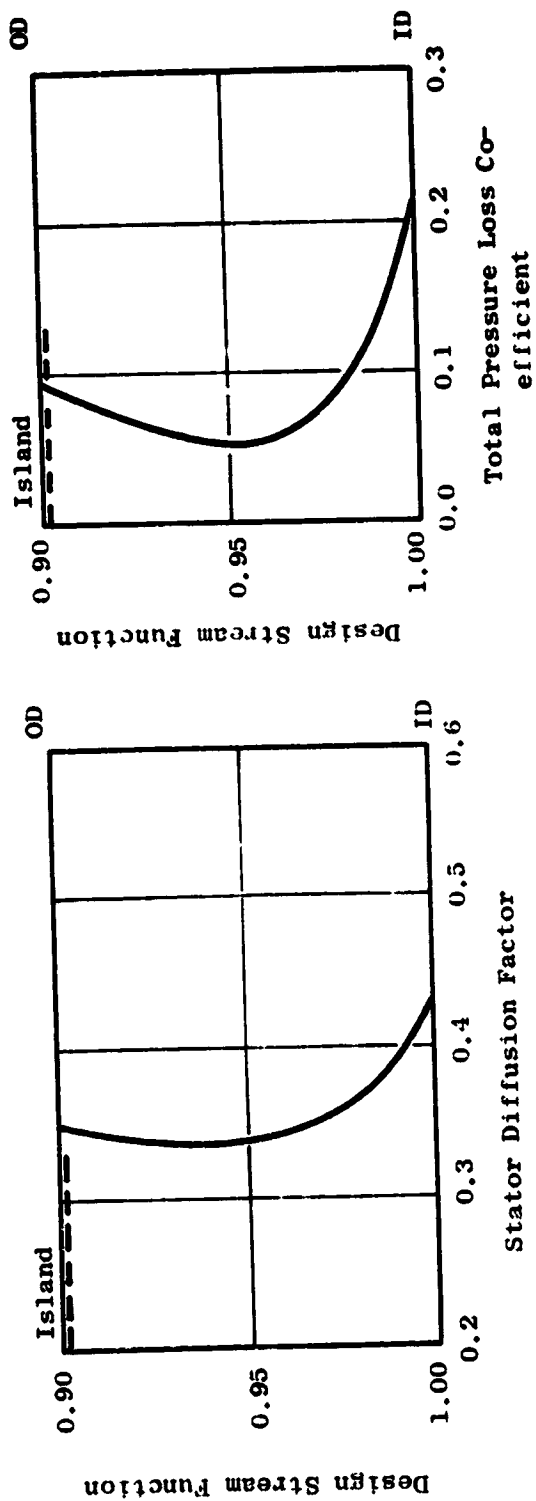
Figure 6-10. UTW Radial Distribution for Core OGV.

164

type of rotor. The incidence and deviation angles and empirical adjustment angle employed in the design are shown in Figure 6-11.

Over the entire blade span, the minimum passage area, or throat, must be sufficient to pass the design flow including allowances for boundary layer, losses, and flow nonuniformities. In the transonic and supersonic region, the smallest throat area, consistent with permitting design flow to pass, is desirable since this minimizes overexpansions on the suction surface. A further consideration was to minimize disturbances to the flow along the forward portion of the suction surface to minimize forward propagating waves that might provide an additional noise source. Design experience guided the degree to which each of these desires was applied to individual section layouts. The percent throat margin, percentage by which the ratio of the effective throat area to the capture area exceeds the critical area ratio, is shown in Figure 6-12. The values employed are generally consistent with past experience. The blade shapes that result are generally similar to multiple circular arc sections in the tip region, with a small percentage of the overall camber occurring in the forward portion. In the hub region, the blade shapes are similar to double circular arc sections.

Figure 6-13 shows plane sections of the blade at several radial locations. Figure 6-14 shows the resulting camber and stagger angle radial distributions. The radial thickness distributions employed, which were dictated primarily by aeromechanical considerations, are shown in Figure 6-15. The 0.13 thickness-to-chord ratio at the hub is larger than conventional practice because of the composite blade requirements and a small performance penalty will result. The additional profile loss created by this thickness, however, is believed smaller than the system penalties associated with altering the configuration (such as reduction in the tip chord or a reduction in blade number) to reduce the hub thickness-to-chord ratio to 0.10, a value more representative of past experience.

6.2.7 Core OGV Design

A moderately low aspect ratio of 1.3 was selected for the core portion OGV to provide a rugged mechanical system. This selection was in recognition of the potentially severe aeromechanical environment (i.e., large rotor wakes) of the core OGV because of its small size in relationship to that of the rotor blade. A solidity at the ID of 1.65 was selected to yield reasonable levels of diffusion factor, Figure 6-10. The number of vanes which result is 96.

The profiles for the core portion OGV are a modified NASA 65-series thickness distribution on a circular-arc meanline. The incidence angle over the outer portion of the span was selected from a correlation of NASA low-speed cascade data. Locally, in the ID region, the incidence angle was reduced 0.07 radian (4°). This local reduction in incidence was in recognition of traverse data results on other high-bypass fan configurations which show core stator inlet air angles several degrees higher than the axisymmetric calculated values. The deviation angle was obtained from Carter's Rule as was described for the rotor blade, but no empirical adjustment was made. The resulting
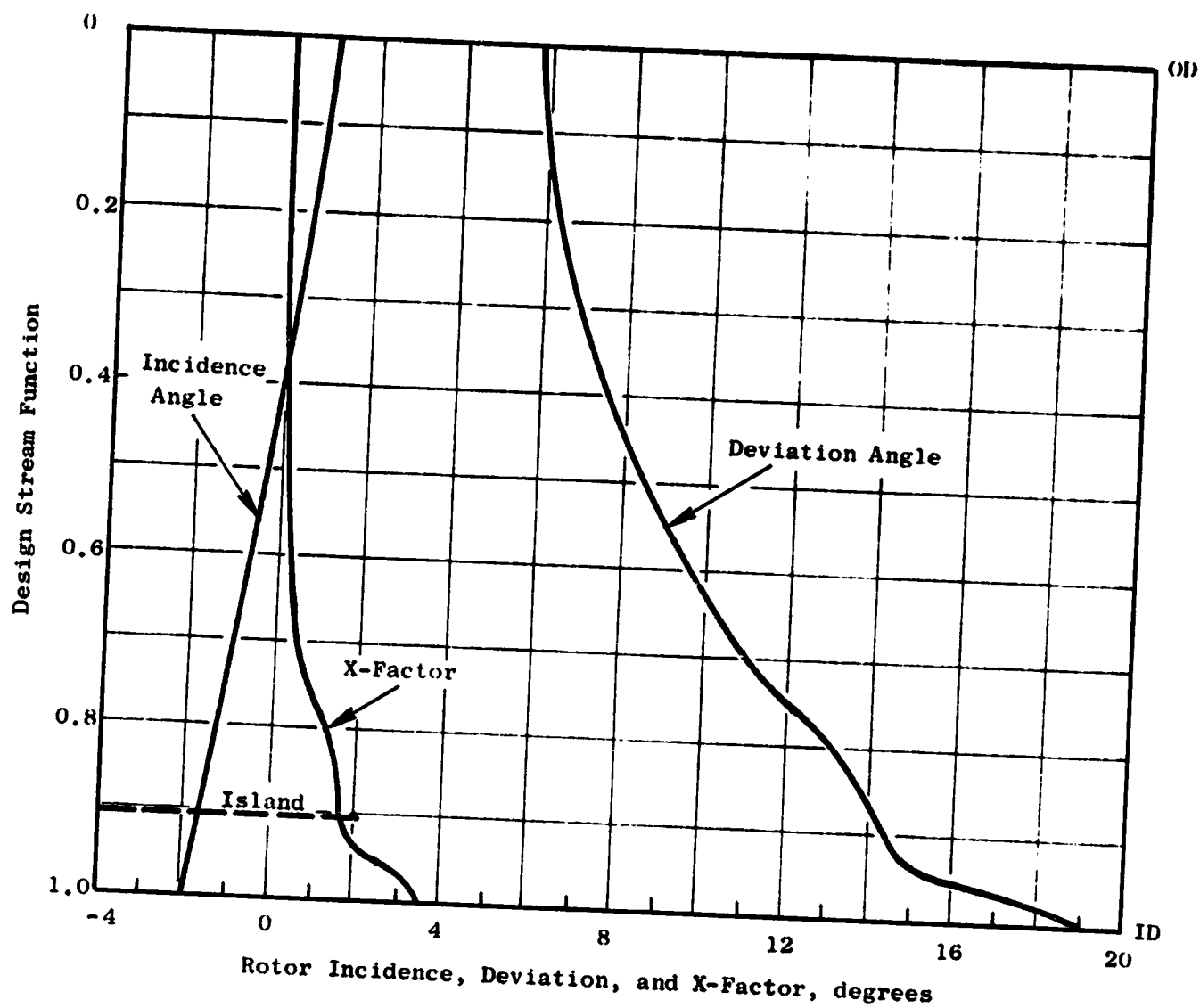
Figure 6-11. UTW Rotor Incidence, Deviation, and Empirical Adjustment Angles.
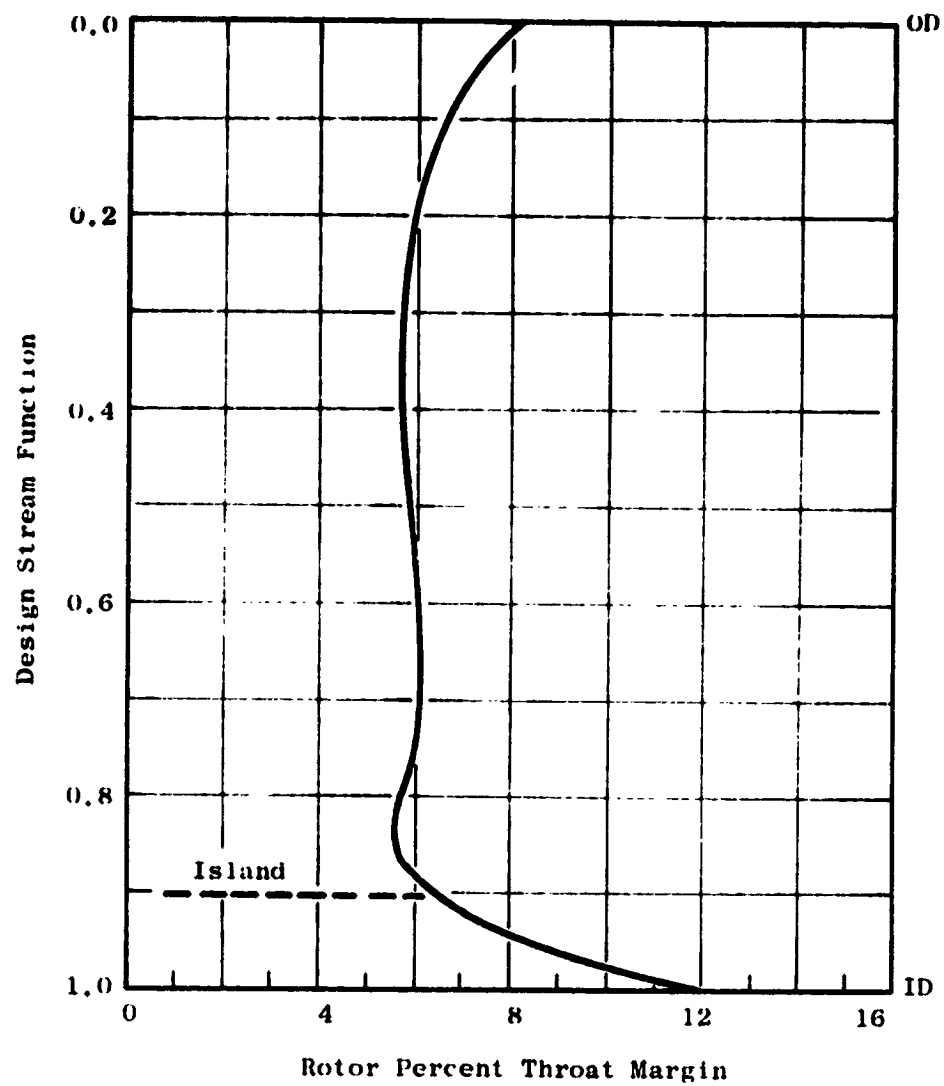
Figure 6-12. UTW Rotor, Percent Throat Margin.

	Radius	
Section	(cm)	(in.)
1	85.8	33.8
2	76.2	30.0
3	66.8	26.3
4	57.2	22.5
5	47.7	18.8

Tip L.E. Radius = 90.2 cm (35.5 in.)
Hub L.E. Radius = 40.1 cm (15.8 in.)

Rotor Rotation ◁
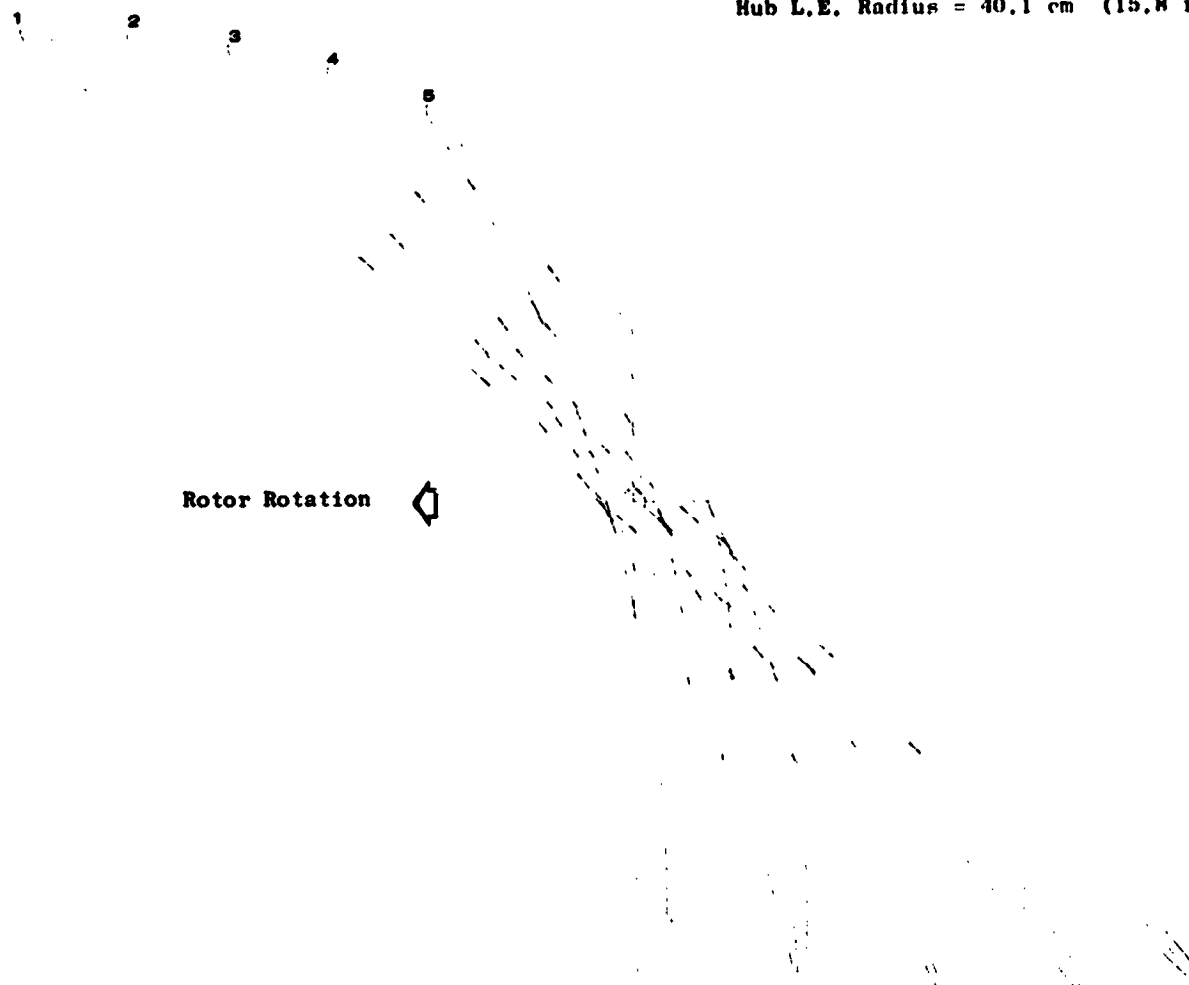
Figure 6-13. UTW Fan Blade Plane Sections.

168
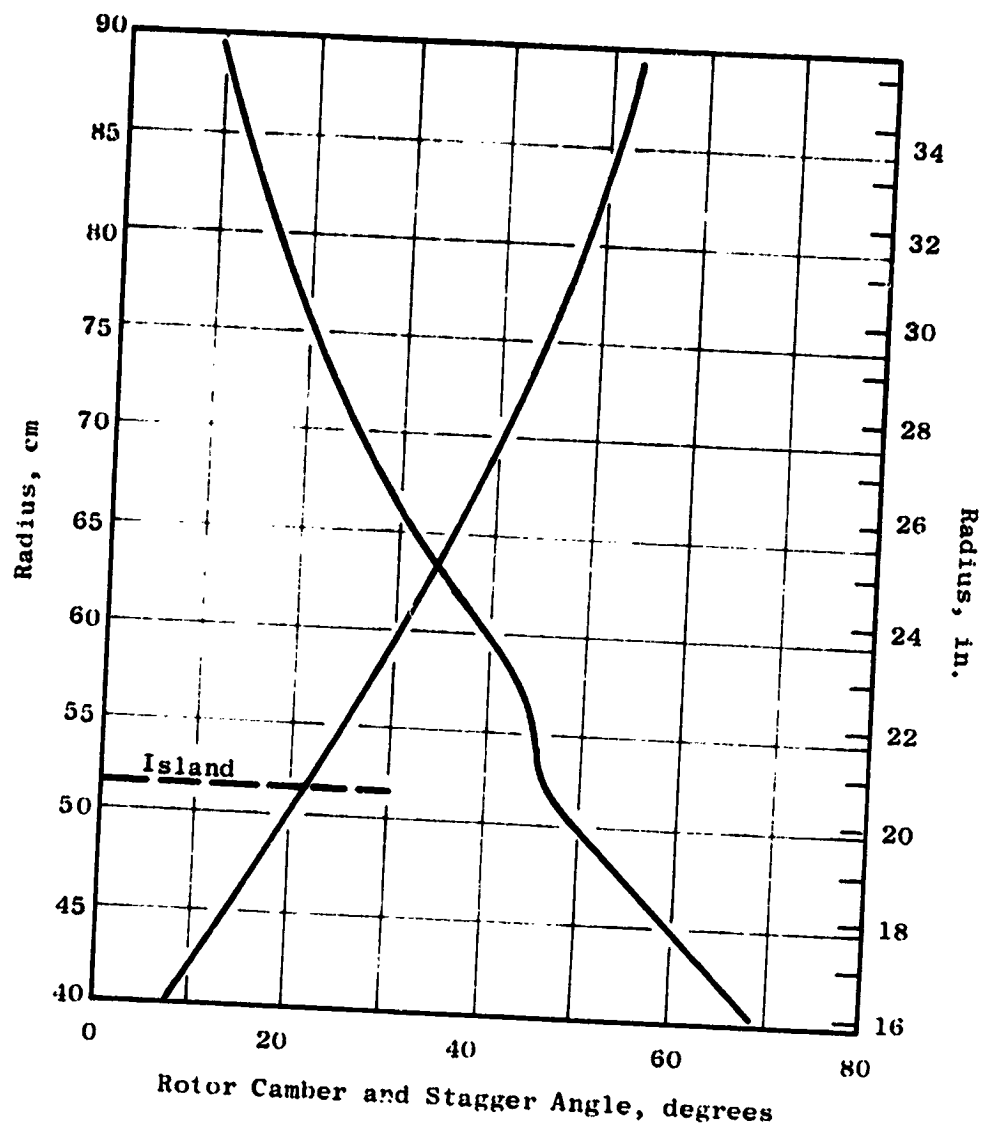
Figure 6-14. UTW Camber and Stagger Angle Radial Distribution.

169
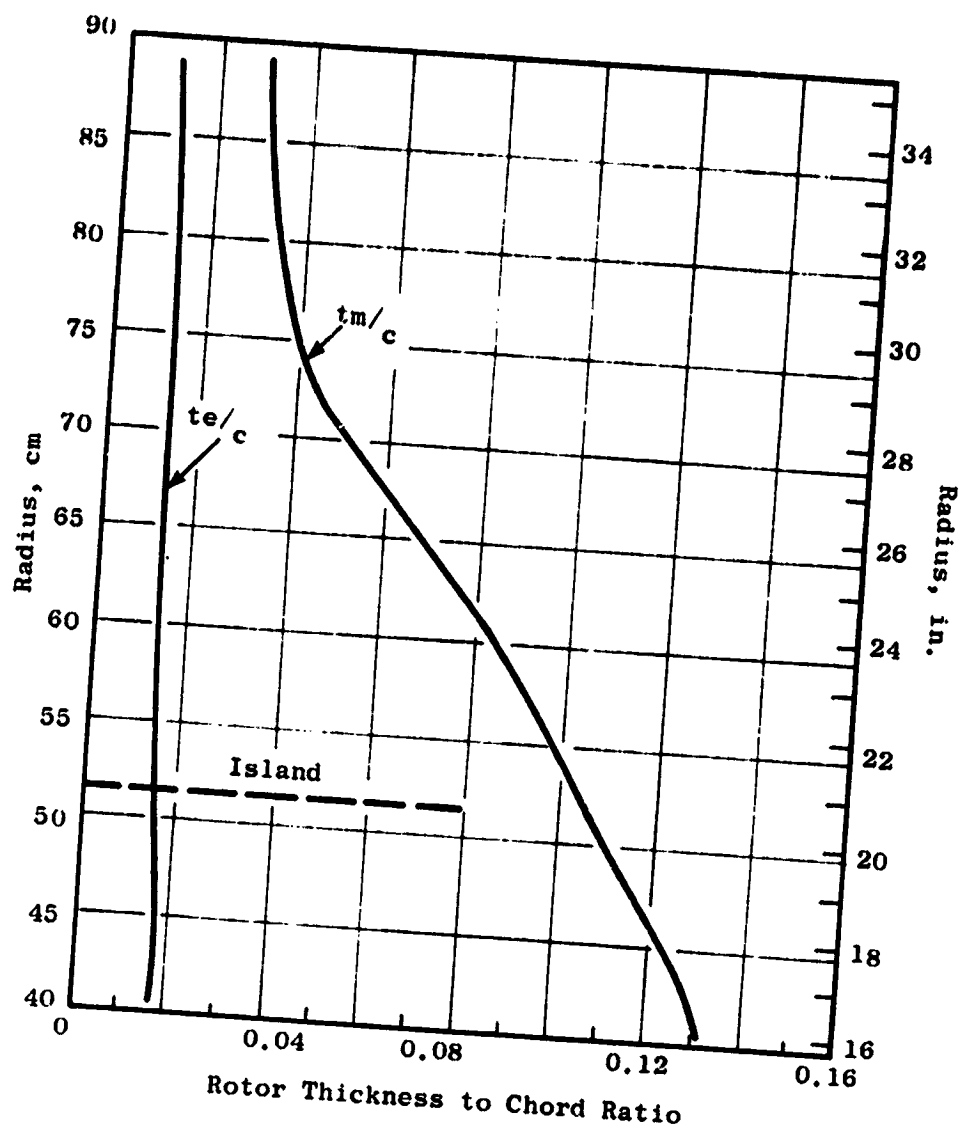
Figure 6-15. UTW Rotor Thickness Distributions.

incidence and deviation angles are shown in Figure 6-16 and the geometry which results is shown in Figure 6-17. The throat area for the selected geometry was checked to ensure sufficient margin to pass the design flow. The results are shown in Figure 6-16. The minimum margin relative to the critical contraction ratio was 6%, which is sufficient to avoid choke. Figure 6-18 is a cylindrical section of the OGV at the pitch line radius.

6.2.8 Transition Duct Strut Design

The transition duct flowpath is shown in Figure 6-19. The ratio of duct exit to duct inlet flow area is 1.02. There are six struts in the transition duct which are aerodynamically configured to remove the 0.105 radian (6°) of swirl left in the air by the core OGV's and to house the structural spokes of the composite wheels (see Figure 6-2). In addition, at engine station 196.5 (Figure 6-2), the 6 and 12 o'clock strut positions must house radial accessory drive shafts. The number of struts and axial position of the strut trailing edge were selected identical with the F101 engine to minimize unknowns in the operation of the core engine system. The axial positions and thickness requirements of the composite wheel spokes were dictated by mechanical considerations. The axial location of the strut leading edge at the OD was determined by its proximity to the splitter leading edge. At the OD flowpath, the strut leading edge is 17.8 mm (0.7 in.) forward of the wheel spoke. A relatively blunt strut leading edge results from the 26.7 mm (1.05 in.) wheel spoke thickness requirement. The wheel spoke is radial. The axial lean of the strut leading edge provides relief from the LE bluntness at lower radii and makes the LE approximately normal to the incoming flow. Since the inlet Mach number in the OD region is less than 0.5 and since the boundary layer along the outer wall initiates at the splitter LE, no significant aerodynamic penalty was assessed because of the bluntness. A NASA 65-series thickness distribution was selected for the basic profile thickness which was modified for the special considerations required in this design. The strut thickness is the same for all radii aft of the forward wheel spoke LE (Figure 6-19) to facilitate fabrication. A cylindrical cut cross section showing the nominal strut geometry at three radii is shown in Figure 6-20. The thickness distribution for the 6 and 12 o'clock struts was further modified for the envelope of the radial drive shaft. Cylindrical cut cross sections of these struts are also shown in Figure 6-20. The leading edge 40% chord of these further modified sections is identical to that of the nominal strut geometry, and aft of forward wheel spoke LE, the strut thickness is the same for all radii. The core engine has demonstrated operation in the presence of a similar thick strut in the F101 application without duress.

6.2.9 Vane-Frame Design

The vane-frame performs the dual function of an outlet guide vane for the bypass flow and a frame support for the engine components and nacelle. It is a common piece of hardware for both the UTW and OTW engine fans. It is integrated with the pylon which houses the radial drive shaft at engine station
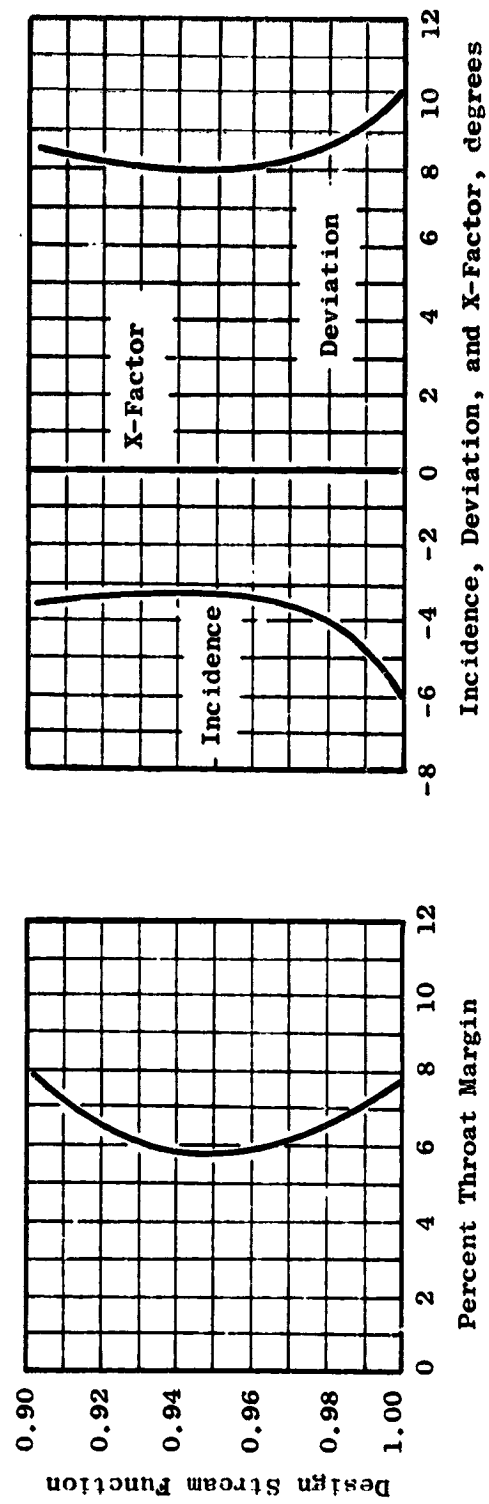
Figure 6-16. UTW Core OGV.
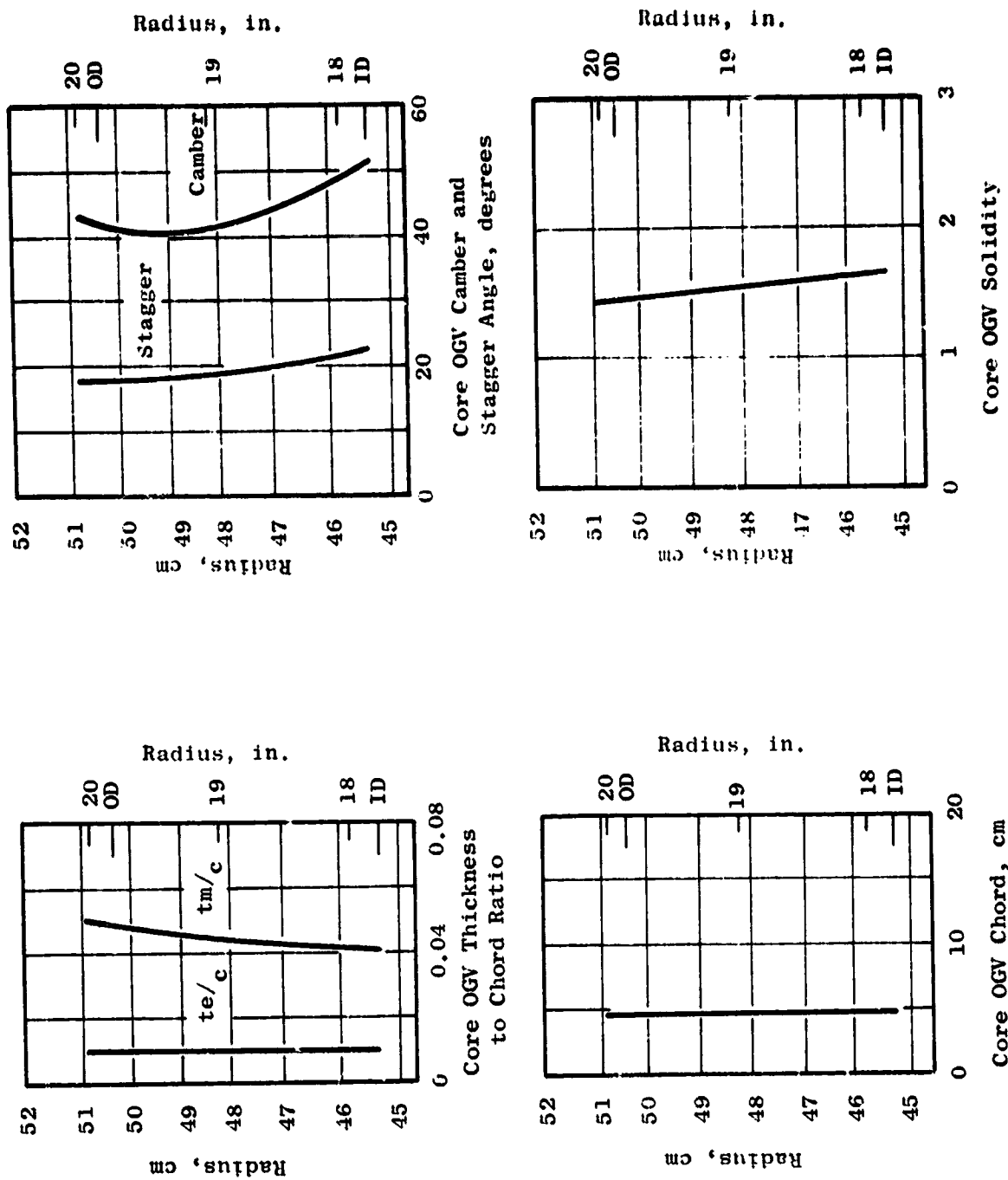
Figure 6-17. QCSEE UTW.
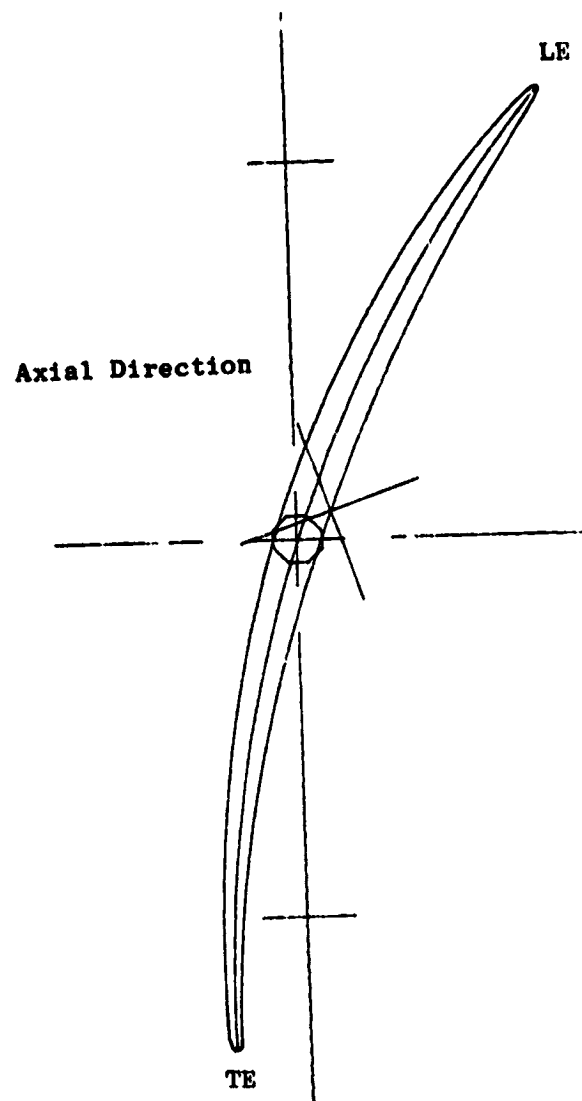
Figure 6-18. Cylindrical Section of UTW OGV
at The Pitch Line Radius.

174
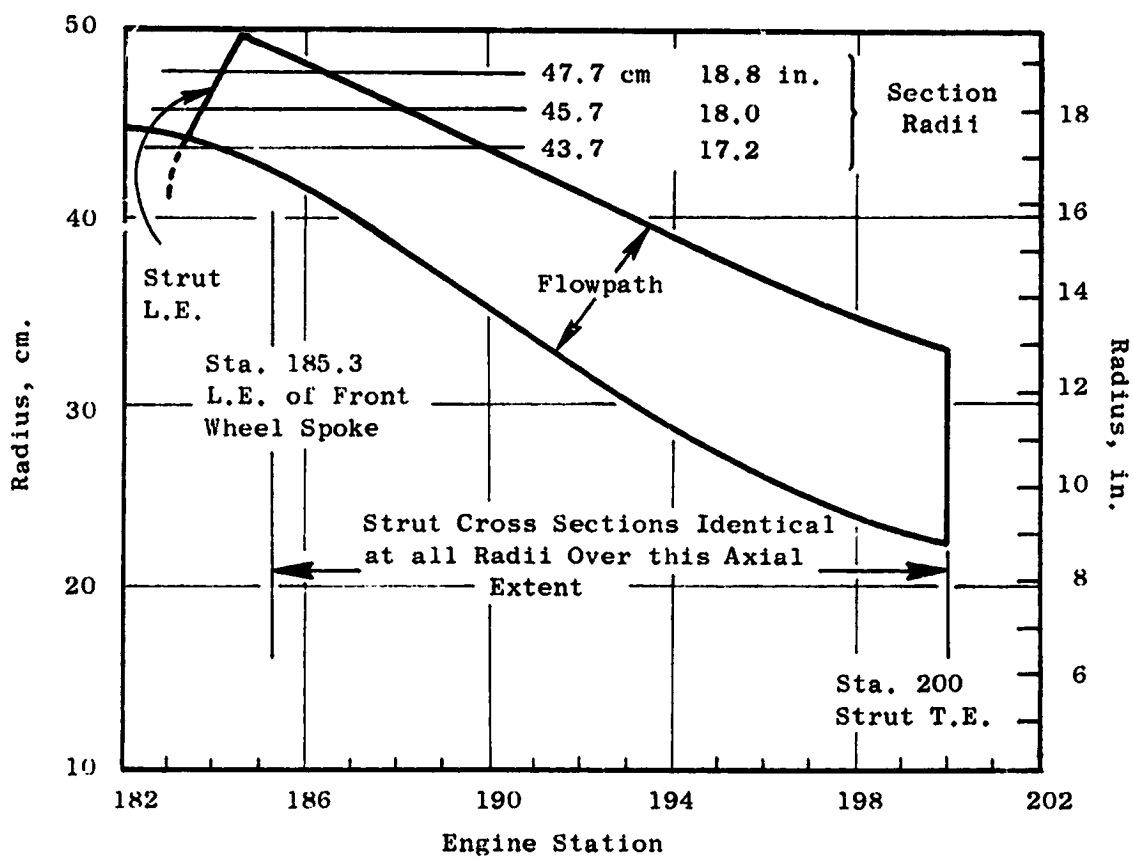
Figure 6-19. Transition Duct Flowpath.
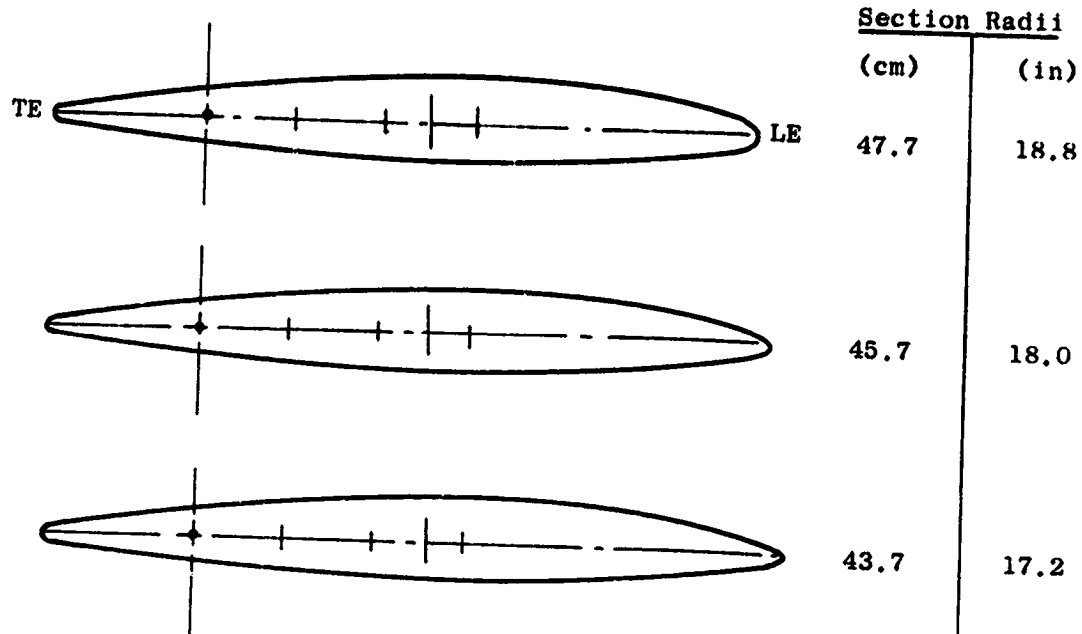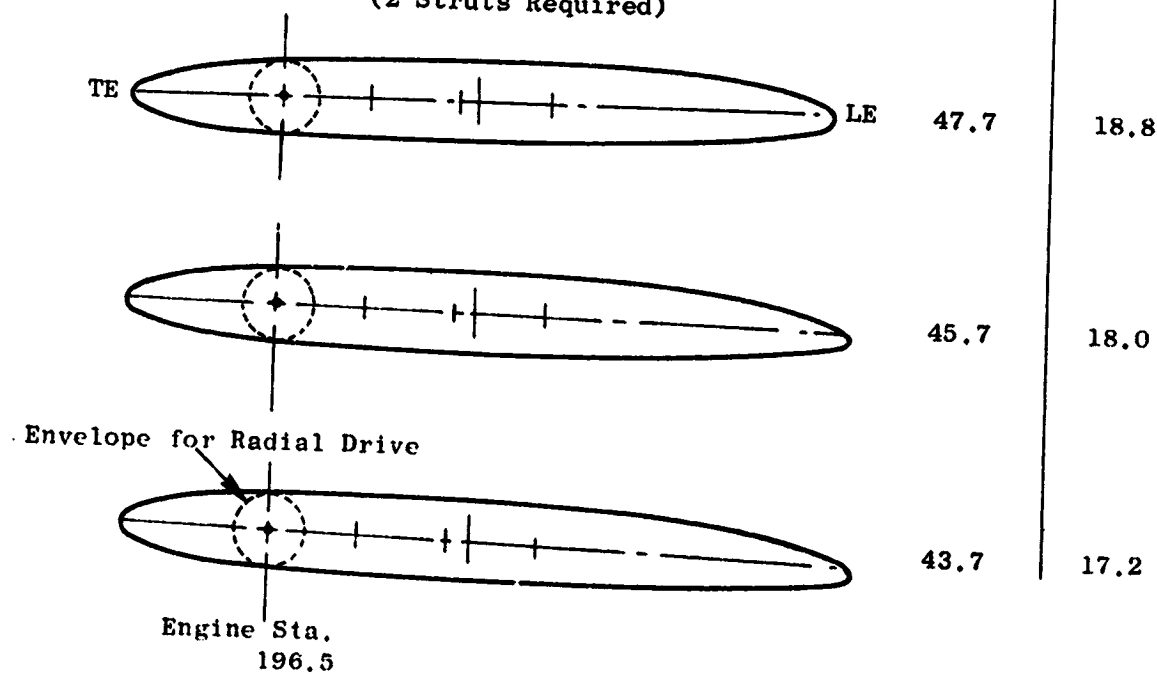
Figure 6-20. Transition Duct Strut.

196.50 (see Figure 6-2), houses the engine mount at approximately engine station 210, provides an interface between the propulsion system with the aircraft system, and houses the forward thrust links. The vane-frame furthermore acts as an inlet guide vane for the UTW fan when in the reverse mode of operation.

A conventional OGV system turns the incoming flow to axial. The housing requirements of the pylon dictate a geometry which requires the OGV's to underturn approximately 0.174 radian (10°) on one side and to overturn approximately 0.174 radian (10°) on the other side. The vanes must be tailored to downstream vector diagrams which conform to the natural flow field around the pylon to avoid creating velocity distortions in the upstream flow. Ideally, each vane would be individually tailored. However, to avoid excessive costs, five vane geometry groups were selected as adequate.

The Mach number and air angle at inlet to the vane-frame are shown in Figure 6-21 for both the UTW and OTW fans. In the outer portion of the bypass duct annulus, the larger air angle in the UTW environment results in a higher incidence angle for it than for the OTW environment. The Mach number in the outer portion of the annulus is also higher in the UTW environment. When selecting incidence angles, a higher Mach number environment naturally leads to the desire to select a higher incidence angle. The amount by which the incidence angle would naturally be increased due to the higher Mach number UTW environment is approximately equal to the increase in the inlet air angle of the UTW environment. In the inner portion of the annulus, the inlet Mach number and air angle are higher for the OTW environment. The natural increase in incidence angle desired because of the higher Mach number is approximately the same as the increase in the inlet air angle. As a result of these considerations, no significant aerodynamic performance penalty is accessed to using common hardware for both the UTW and OTW fans.

Locally, near the bypass duct ID, there is a discontinuity in the aerodynamic environment of the UTW configuration. This discontinuity represents that portion of the flow which passes under the island but bypasses the splitter. The calculation ignored mixing across the vortex sheet. In the design of the vane geometry no special considerations were incorporated because of this discontinuity since it is believed that in a real fluid the mixing process will greatly diminish the vortex strength.

The vane chord at the OD was selected largely by the mechanical requirement of axial spacing between the composite frame spokes. At the ID, the vane leading edge was lengthened primarily to obtain an aerodynamically reasonable leading edge fairing on the pylon compatible with the envelope requirements of the radial drive shaft. The ID region is significantly more restrictive in this regard because of choking considerations, particularly for the OTW environment, with the reduced circumferential spacing between vanes. The solidity resulting fi. a 33 vanes, an acoustic requirement, was acceptable from an aerodynamic loading viewpoint as shown in Figure 6-22. The two diffusion factor curves are a result of the two aerodynamic environments, UTW and OTW, to which the common vane frame geometry is exposed. The thickness is a modfied NASA

177
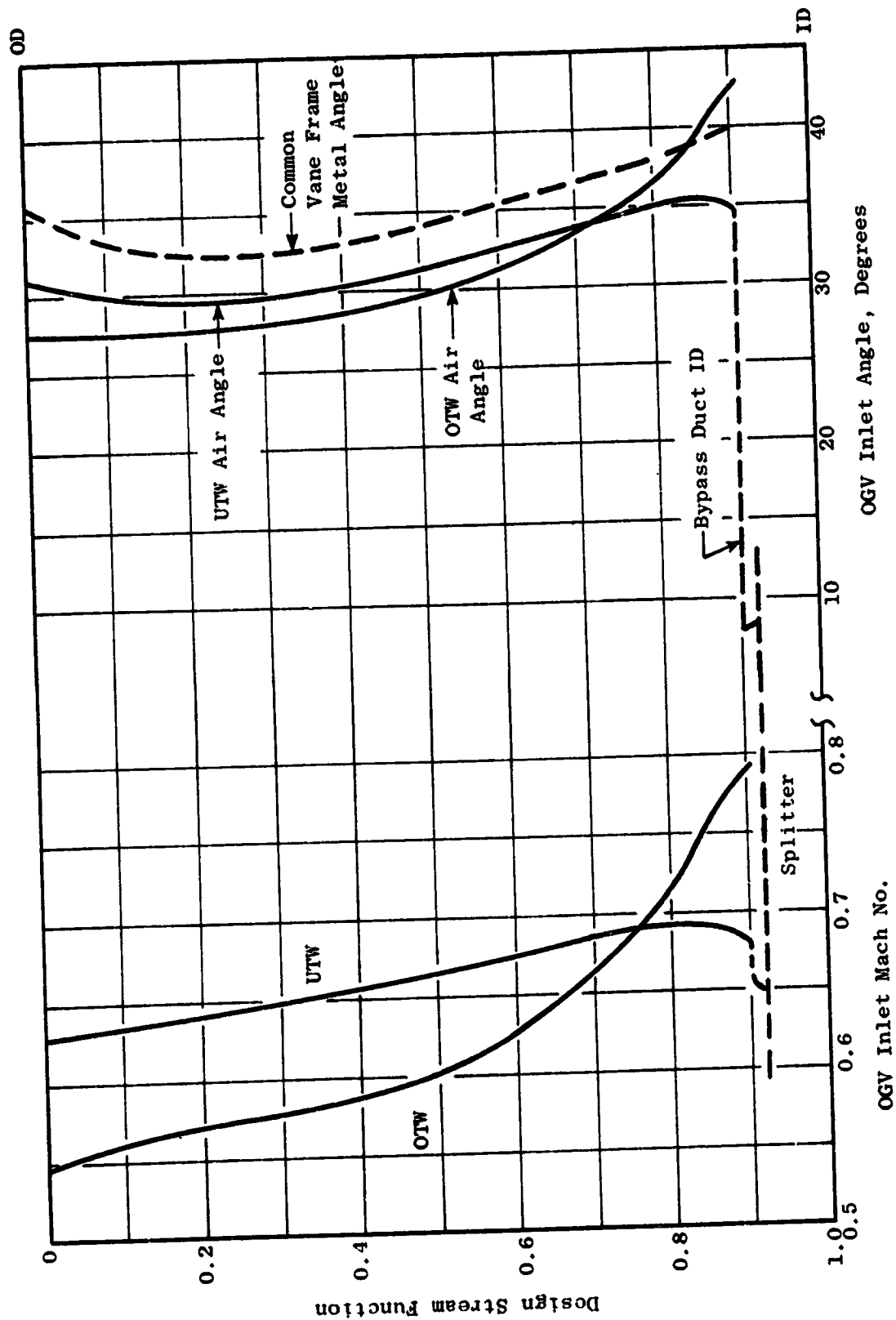
Figure 6-21. Vane Frame Aerodynamic Environment.
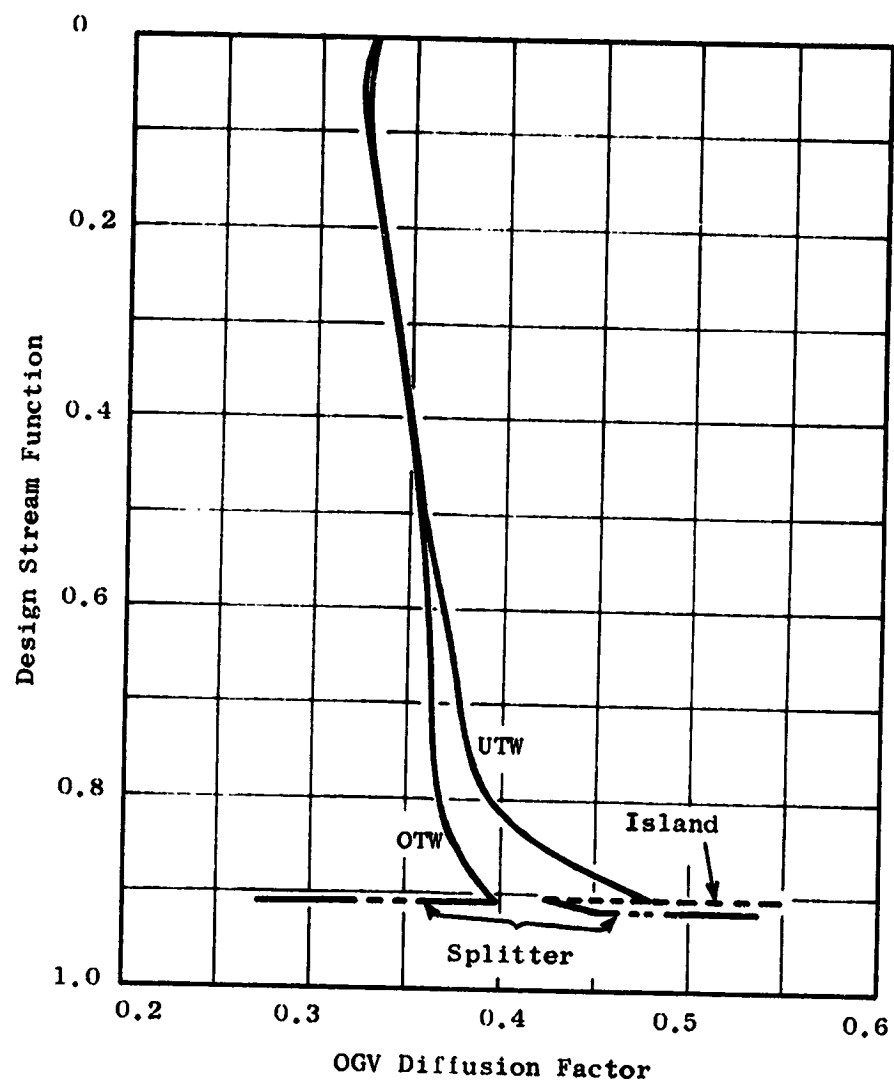
Figure 6-22.   Vane Frame Nominal Vane Config-
uration.

65-series distribution. Maximum-thickness- and trailing-edge-thickness-to-chord ratios of 0.08 and 0.02, respectively, were selected at the OD. The same maximum thickness and trailing edge thickness were used at all other radii which results in maximum-thickness- and trailing-edge-thickness-to-chord ratios of 0.064 and 0.016, respectively, at the ID.

As a guide in the selection of the overall vector diagram requirements of the vane frame, a circumferential analysis of an approximate vane geometry, including the pylon, was performed. This analysis indicated, for uniform flow at vane inlet, that the vane discharge Mach number was approximately constant circumferentially and that the discharge air angle was nearly linear circumferentially between the pylon wall angles. Figure 6-23, an unwrapped cross section at the ID, shows the flowfield calculated by this analysis. The specific design criteria selected for the layout of the five-vane geometry groups was to change the average discharge vector diagram with zero swirl to vector diagrams with ± 5° of swirl and ± 10° of swirl.

The meanline shapes for each of the five-vane groups vary. For the vane group which overturns the flow by +10° the meanline is approximately a circular arc. As a result of passage area distribution and choking consideratons, the meanline shape employed in the forward 25% chord region of this vane group was retained for the other four groups.

The incidence angle for all vane groups was the same and was selected for the group with the highest camber. A correlation of NASA low-speed cascade data was the starting point for the incidence selection. Over the outer portion of the vane, where the inlet Mach number is lower, the incidence angles were slanted to the low side of the correlation. This was done in consideration of the reverse thrust mode of operation for the UTW fan. In this mode, the OGV's impart a swirl counter to the direction of rotor rotation. Additional vane leading edge camber tends to increase the counterswirl and therefore the pumping capacity of the fan. In the inner portion of the vane the incidence angles are higher than suggested by the correlation because of the higher inlet Mach number. Also, in the reverse mode of operation, this reduction in vane leading edge camber in the ID region reduces the swirl for that portion of the fluid which enters the core engine and tends to reduce its pressure drop.

The deviation angle for each of the five vane groups was calculated from Carter's Rule as described for the rotor. The portion of the meanline aft of the 25% chord point approximates a circular arc blending between the front circular arc and the required trailing edge angle. For the vane group which underturns the flow by 10° the aft portion of the blade has little camber. Figure 6-24 shows an unwrapped cross section at the ID of two of the 10° over-cambered vanes and two of the 10° under-cambered vanes adjacent to the pylon. Note that the spacing between the pylon and the first under-cambered vane is 50% larger than average. This increased spacing was required to open the passage internal area, relative to the capture area, to retrieve the area blocked by the radial drive shaft envelope requirements.

180
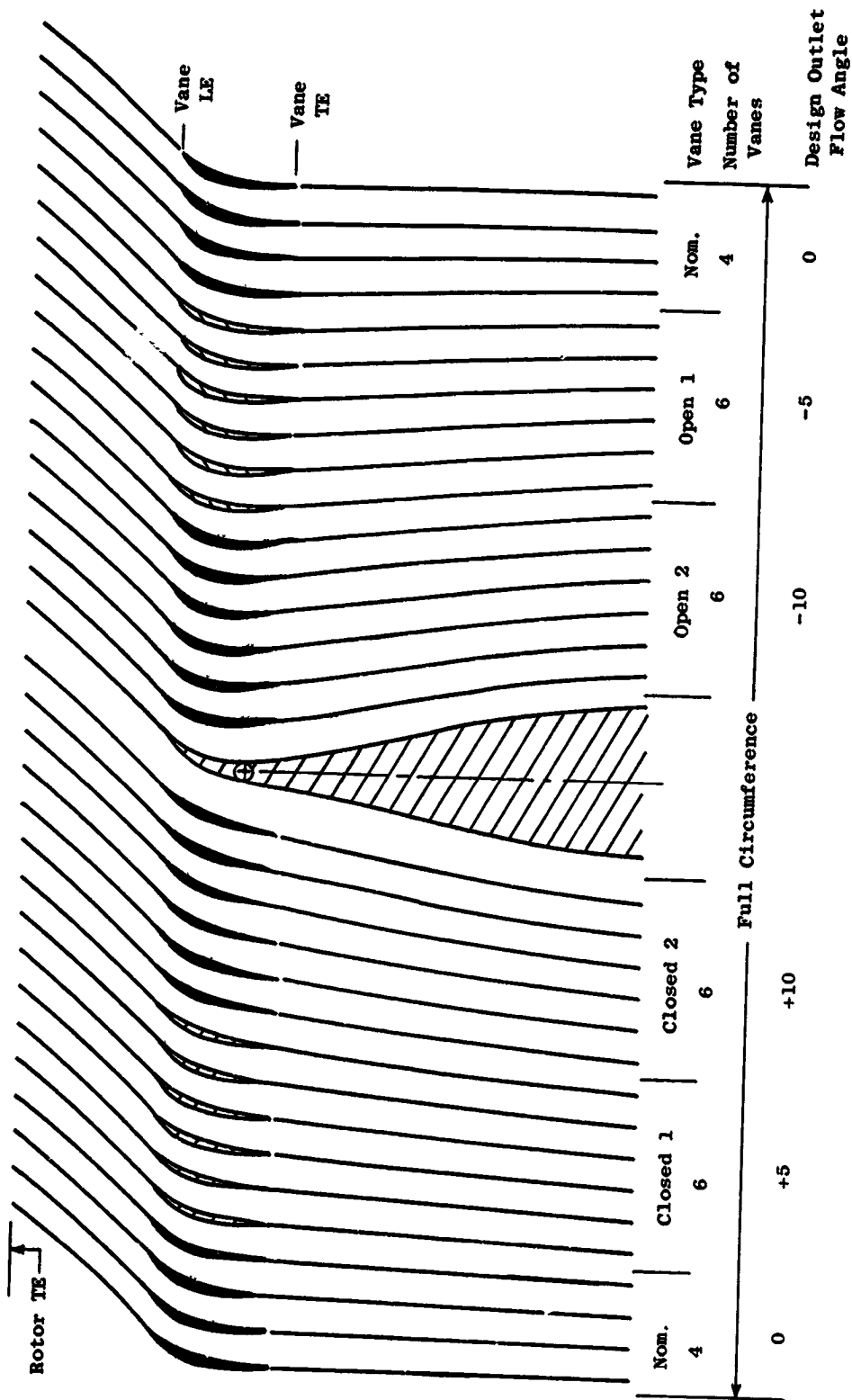
Figure 6-23. Vane Frame Unwrapped Section at I.D.

S

S

1.5S
1 Place

S
Typ 32
Places

0.048 m (1.90 in)
Dia. Envelope
for Radial Drive

Vane Type – Open 2 (– 10°)

Vane Type – Closed 2 (+ 10°)
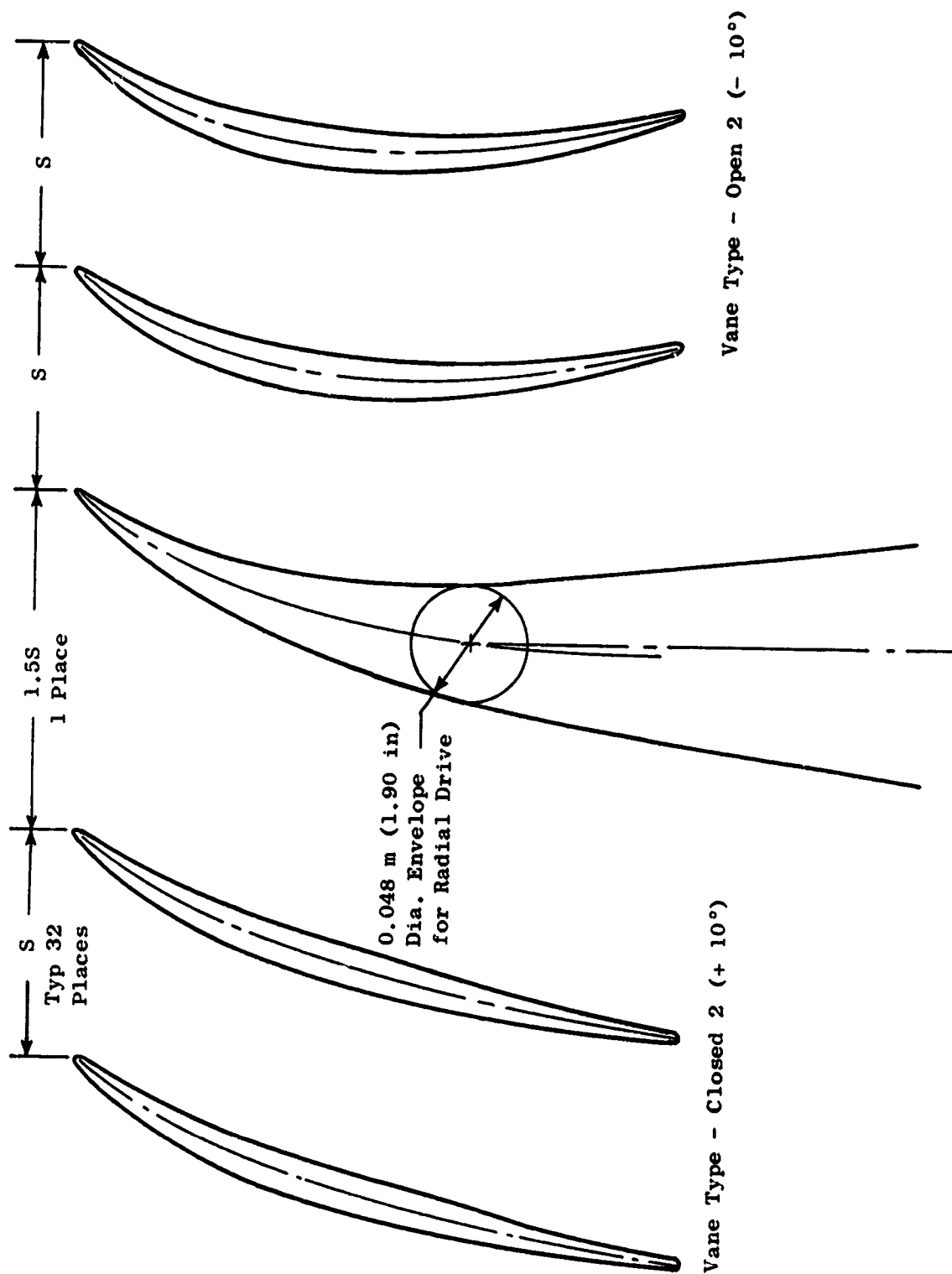
Figure 6–24. Vane Frame Unwrapped Section at I.D., 32 Vanes Plus Pylon L.E. Fairing.

The radial distributions of camber and stagger for the nominal and two extreme vane geometries are shown in Figure 6-25. The radial distributions of chord and solidity for the nominal vane are shown in Figure 6-26. The design held the leading and trailing edge axial projection common for all five groups which results in slightly different chord lengths for the other four vane types.

6.3 OTW FAN

6.3.1 Operating Requirements

The major operating requirements for the over-the-wing (OTW) fan, Figure 6-27, are takeoff, where noise and thrust are of primary importance, and maximum cruise, where economy and thrust are of primary importance. A secondary requirement was to utilize hardware common to the UTW fan when no significant performance penalty was involved. At takeoff, a low fan pressure ratio of 1.34 was selected to minimize the velocity of the bypass stream at nozzle exit. A corrected flow of 405.5 kg/sec (894 lb/sec), the same as for the UTW, at this pressure ratio yeilds the required engine thrust. The inlet throat is sized at this condition for an average Mach number of 0.79 to minimize forward propagation of fan noise. This sizing of the inlet throat prohibits higher corrected flow at altitude cruise. The required maximum cruise thrust is obtained by raising the fan pressure ratio to 1.38. The aerodynamic design point was selected at an intermediate condition, which is a pressure ratio of 1.36 and a corrected flow of 408 kg/sec (900 lb/sec). Table 6-II summarizes the key parameters for these three conditions.

Table 6-II. QCSEE OTW Fan.			
Parameter	Design Point	Takeoff	Maximum Cruise
Total fan flow	408 kg/sec (900 lb/sec)	405.5 kg/sec (894 lb/sec)	405.5 kg/sec (894 lb/sec)
Pressure ratio - bypass flow	1.36	1.34	1.38
Pressure ratio - core flow	1.43	1.43	1.44
Bypass ratio	9.9	10.1	9.8
Corrected tip speed	358 m/sec (1175 ft/sec)	354 m/sec (1162 ft/sec)	359 m/sec (1178 ft/sec)

6.3.2 Basic Design Features

A cross section of the selected OTW fan configuration is shown in Figure 6-28. The fan outer flowpath, vane-frame including outer and inner flowpath and transition duct including the six frame struts are all common to the UTW fan configuration. Thus the integrated nacelle vane-frame assembly is common
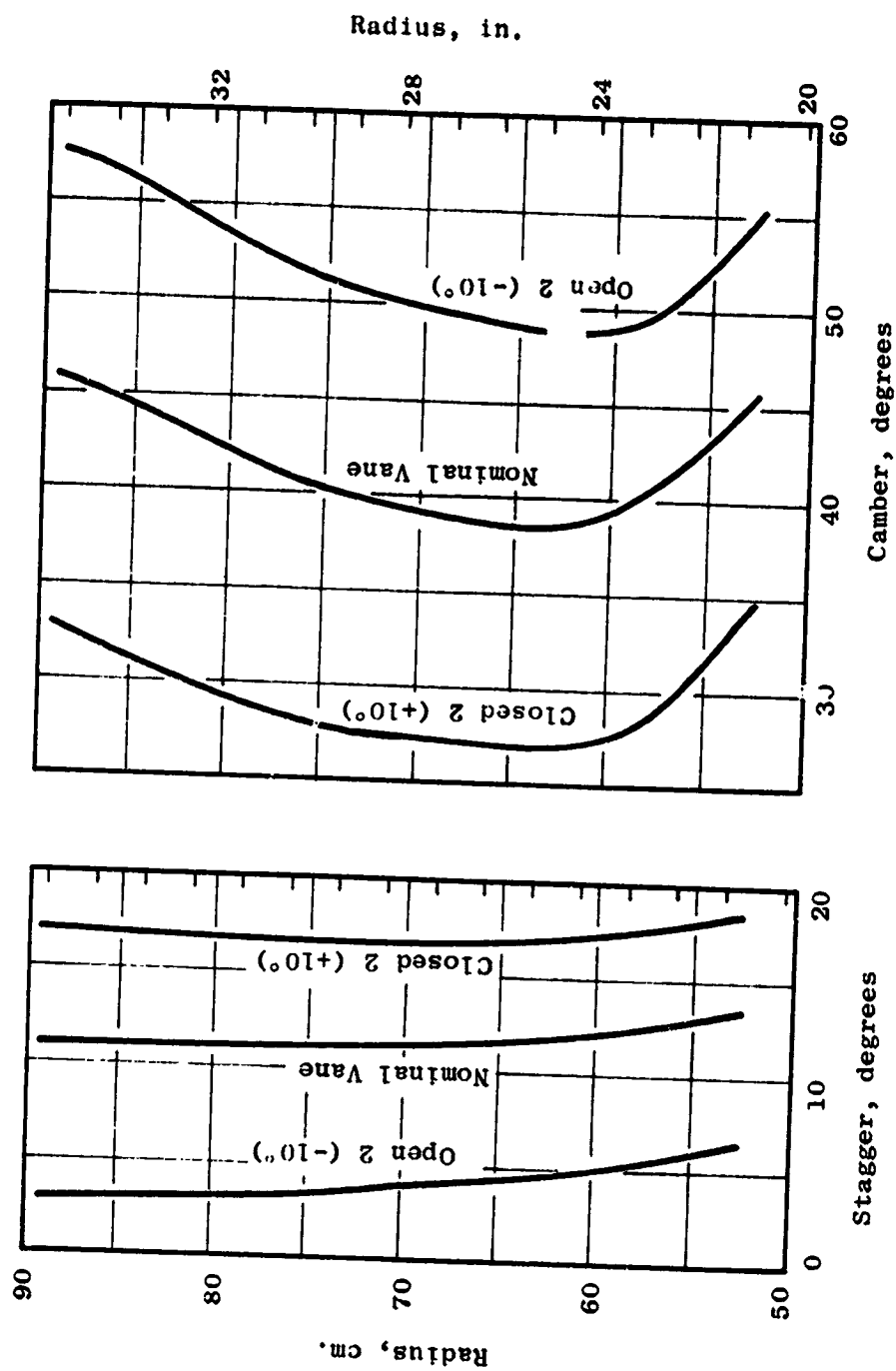
Figure 6-25. QCSEE Vane Frame.
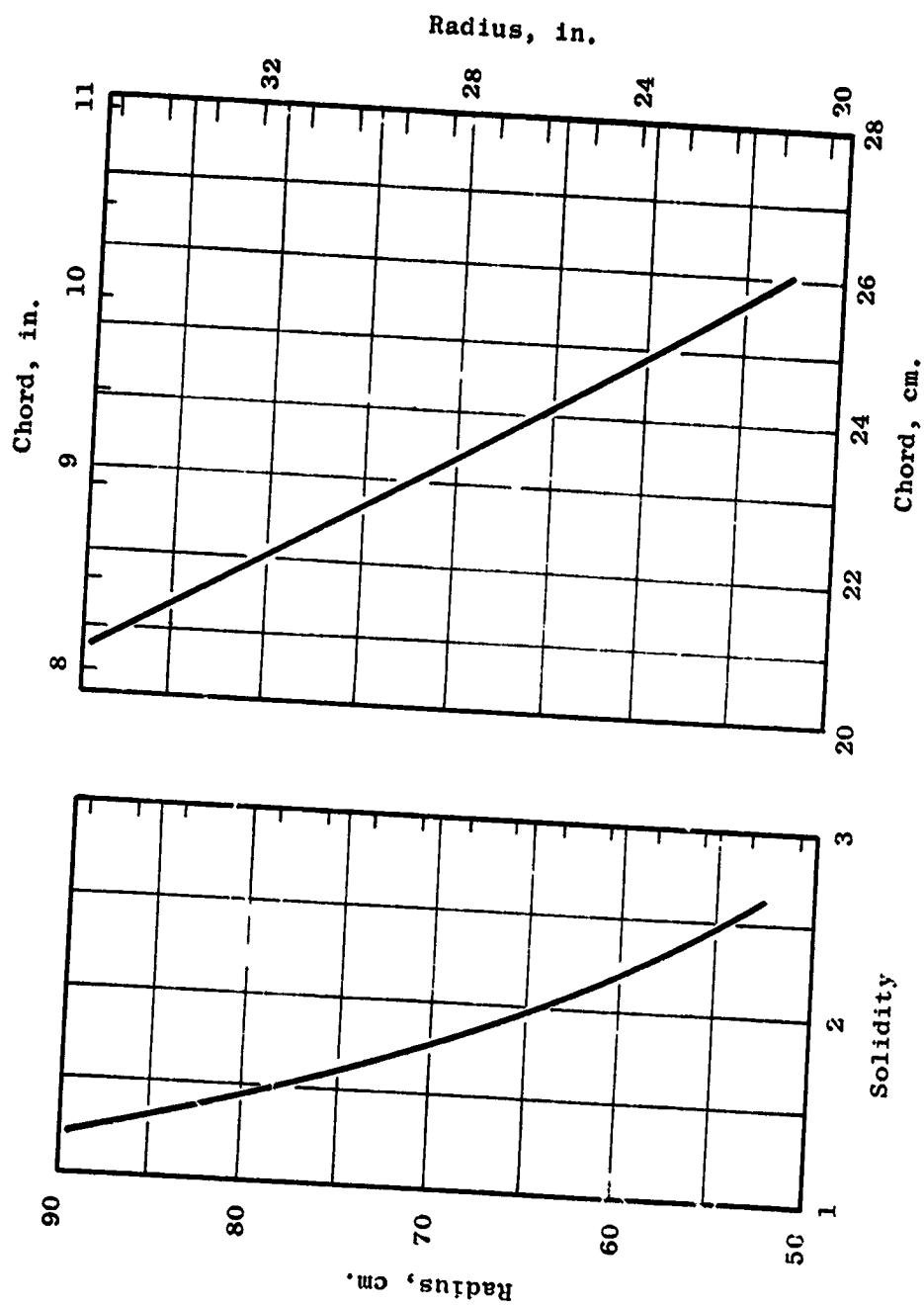
Figure 6-26. QCSEE Vane Frame.
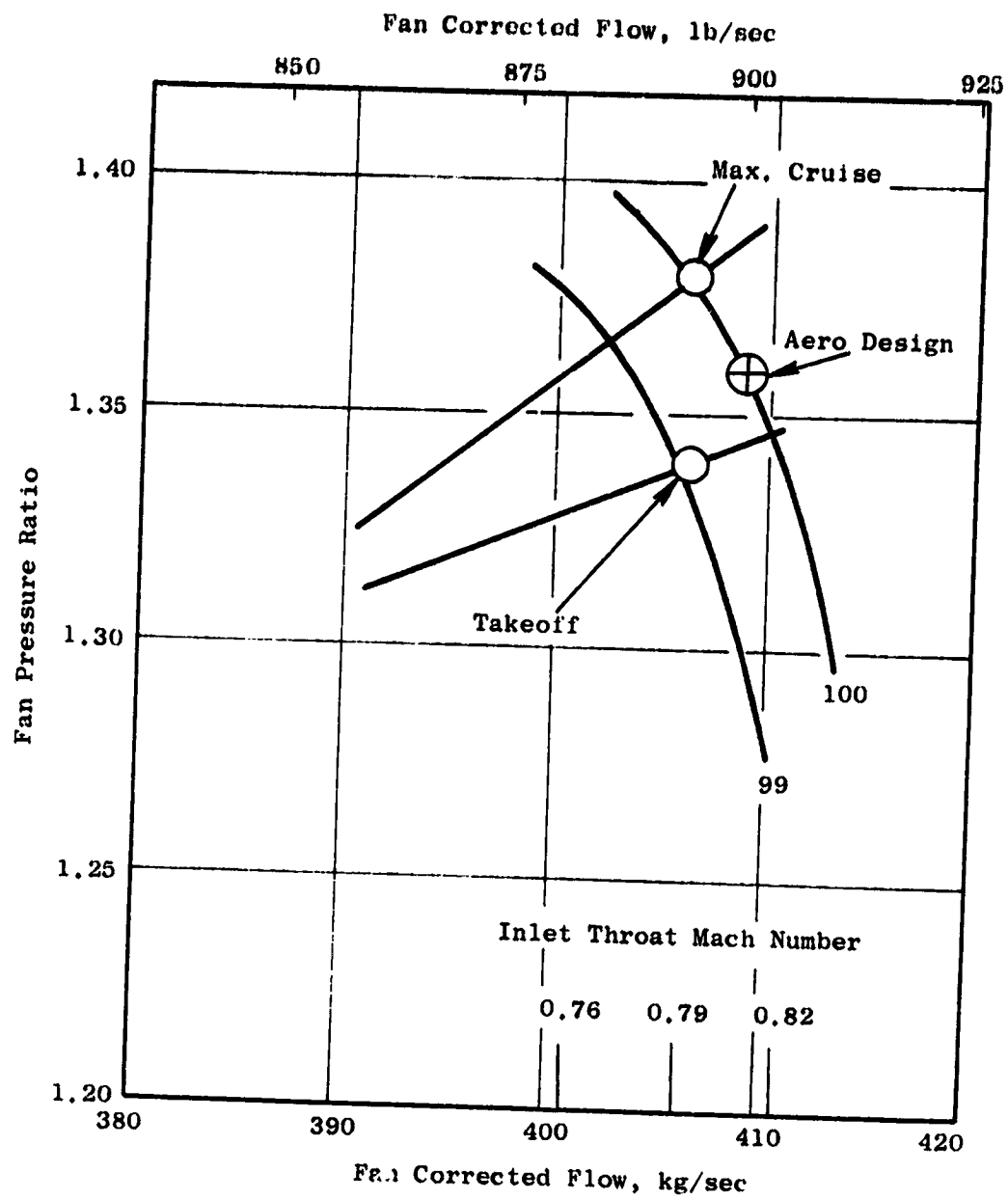
Figure 6-27. Major Operating Requirements for OTW Fan.

Engine Station: 167   185   196.5   200
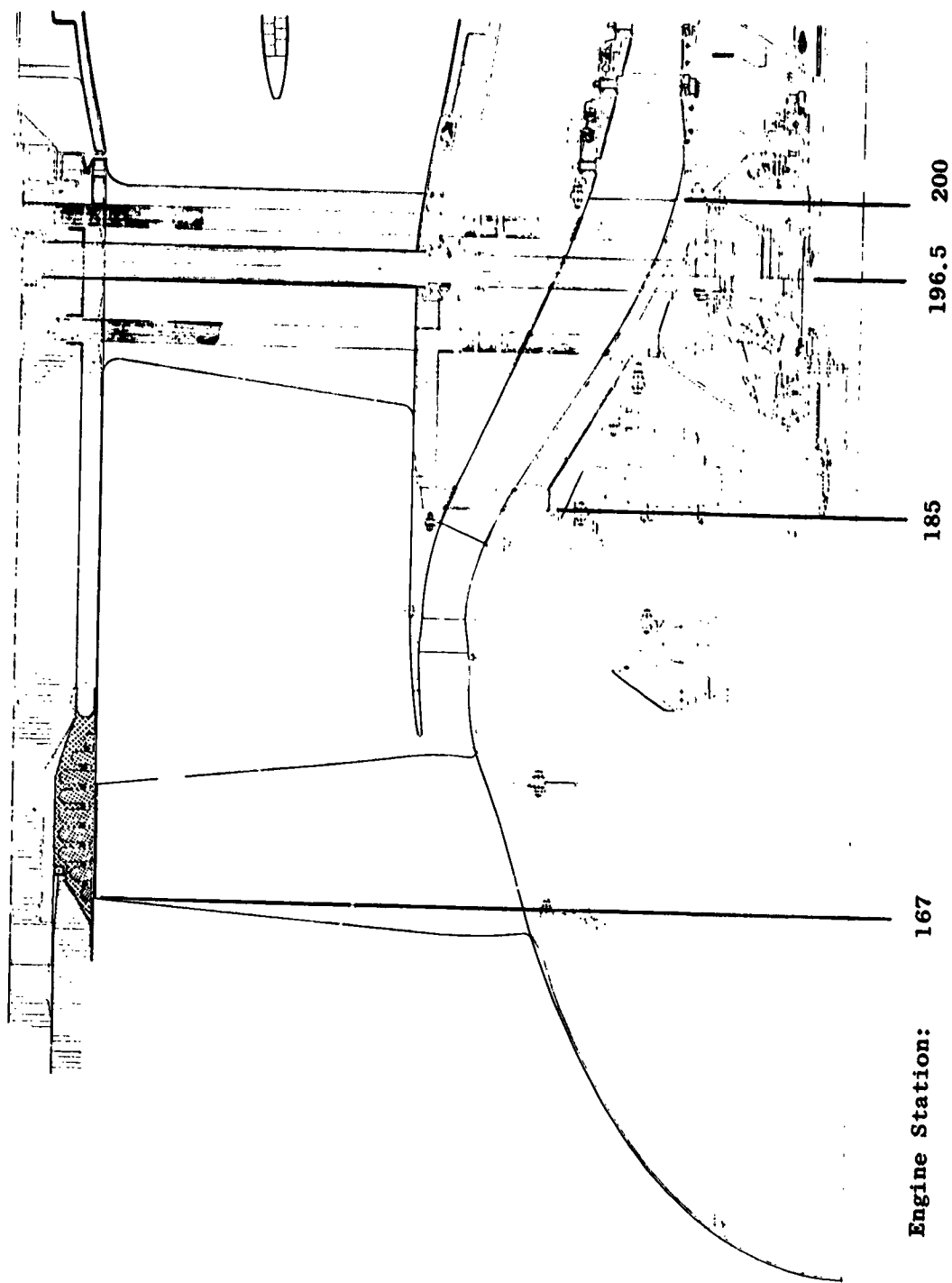
Figure 6-28. Cross Section of OTW Fan.

to both propulsion systems. There are 28 fixed-pitch rotor blades. The overall proportions for the rotor blades, blade number, and radial distributions of thickness and chord were selected to provide a satisfactory aeromechanical flight-type composite configuration. However, to minimize overall program costs, titanium was substituted for the actual blade construction. The stall margin for the OTW fan is projected to be adequate. The circumferential grooved casing treatment, however, can be retained from the UTW fan to provide added protection against stall. The rotor was positioned axially such that the trailing edge hub intersects the hub flowpath at the same axial station as the UTW which puts the aft face of the fan disk at approximately the same engine station. A tip axial spacing between rotor trailing edge and vane-frame leading edge equal to 1.9 true rotor tip chords results. The vane-blade ratio is 1.18. Immediately following the rotor, in the hub region, is a splitter which divides the flow into the bypass portion and core portion. The proximity of the splitter leading edge to the rotor blade is to enable additional design control on the streamlines in the hub region to provide improved surface velocity and loading distributions. The 156 OGV's for the fan hub, or core portion, flow are in the annular space under the splitter.

6.3.3 Detailed Configuration Design

The corrected tip speed at the aerodynamic design point was selected at 358 m/sec (1175 ft/sec). This was selected for design purposes, as a compromise between the takeoff and cruise tip speed requirements. The objective design point adiabatic efficiency is 88% for the bypass portion and 78% for the core portion. Requirements include 16% stall margin at takeoff and high fan hub pressure ratio to provide good core engine supercharging. An inlet radius ratio of 0.42 was selected, compared to 0.44 for the UTW fan, to provide additional annulus area convergence at rotor hub which reduces the hub aerodynamic loading. Discharge radius ratios are approximately the same for the two fans. For the 1.803 m (71.0 in.) tip diameter, a flow per annulus area of 194 kg/sec-m^2 (39.8 lb/sec-ft^2) results.

The standard General Electric axisymmetric flow computation procedure was employed in calculating the velocity diagrams as was outlined in Section 6.2.4.

The design radial distribution of rotor total pressure ratio is shown in Figure 6-29. This distribution is consistent with a stage average pressure ratio of 1.36 in the bypass region. The higher than average pressure ratio in the hub region provides maximum core engine supercharging subject to a balance between the constraints of acceptable rotor diffusion factors, stator inlet absolute Mach numbers, and stator diffusion factors. A stage average pressure ratio of 1.43 results at the core OGV exit. The assumed radial distribution of rotor efficiency for the design is shown in Figure 6-30 which was based on measured results from similar configurations (Quiet Engine, Fan B). The assumption of efficiency rather than total-pressure-loss coefficient is a General Electric design practice for rotors of this type. The radial distribution of rotor diffusion factor which results from these assumptions is shown in Figure 6-31. Figures 6-32 and 6-33 show the radial distributions of rotor relative Mach number and air angle, respectively. At the rotor hub the flow turns 16° past axial which corresponds to a work coefficient of 2.6.

188
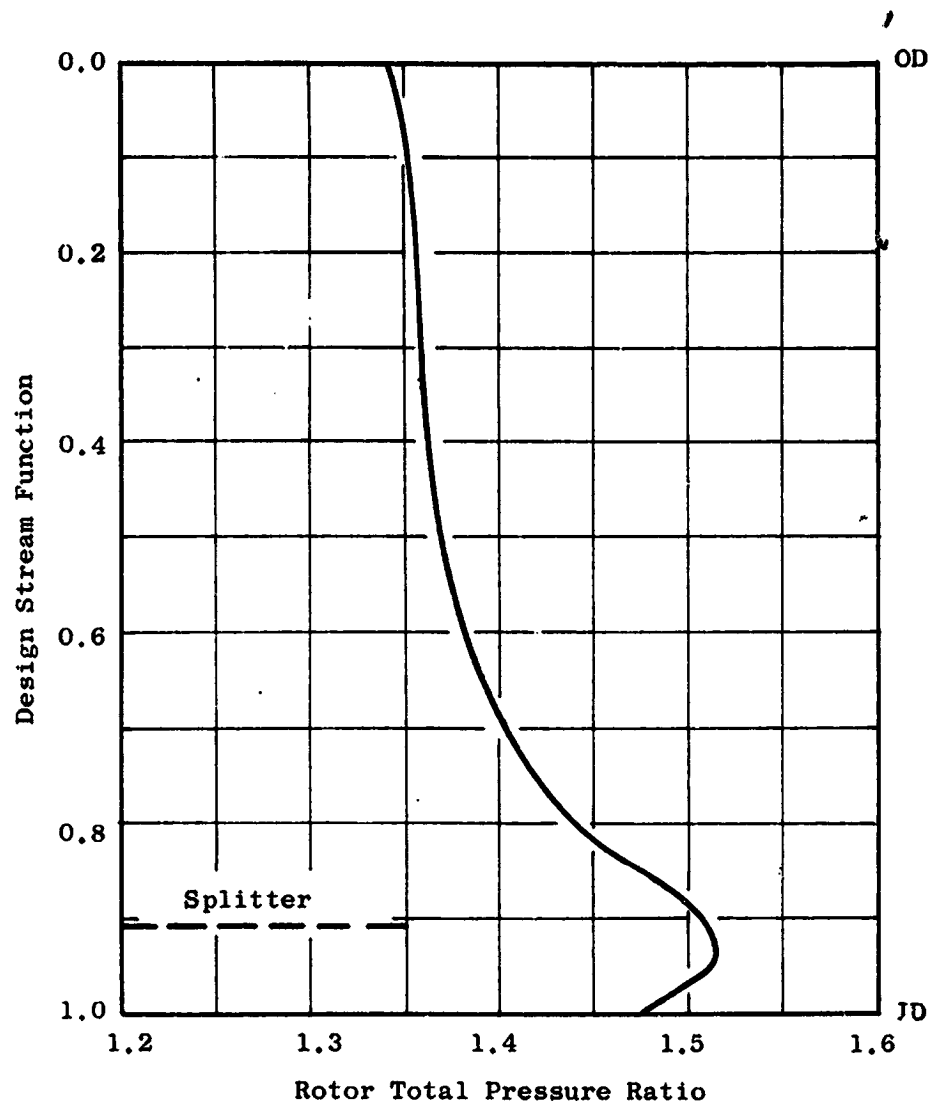
Figure 6-29. OTW Radial Distribution of Rotor Total Pressure Ratio.
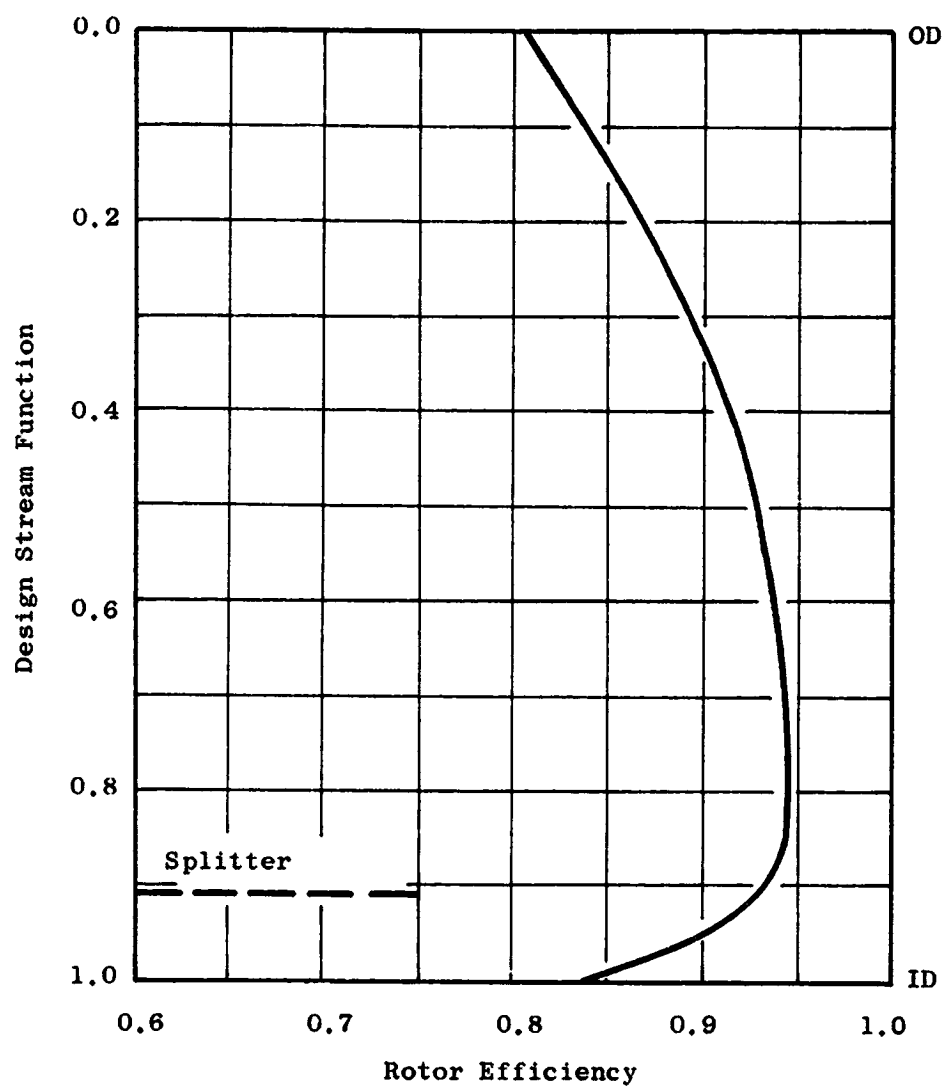
Figure 6-30. OTW Radial Distribution of Rotor Efficiency.
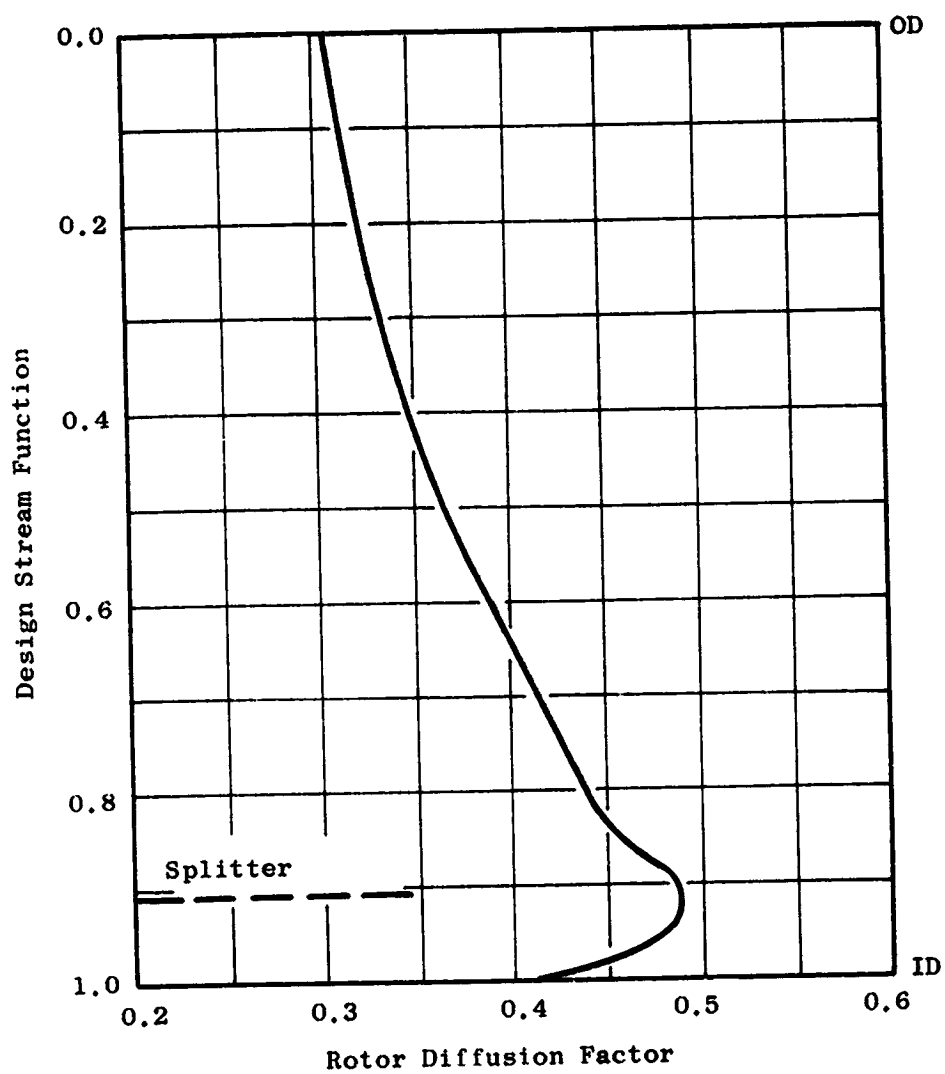
Figure 6-31. OTW Radial Distribution of Rotor Diffusion
Factor.
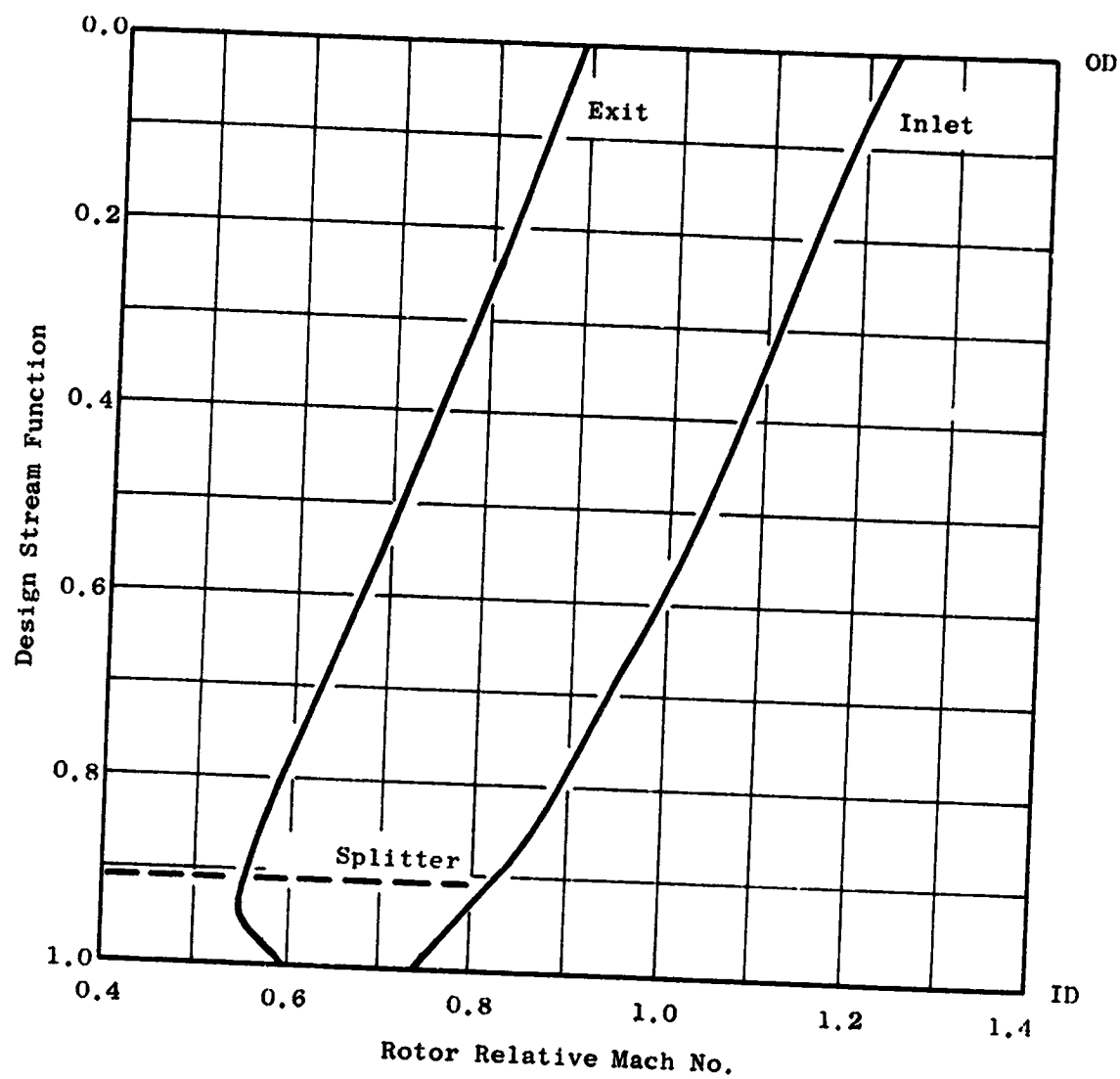
Figure 6-32. OTW Radial Distribution of Rotor Relative Mach Number.
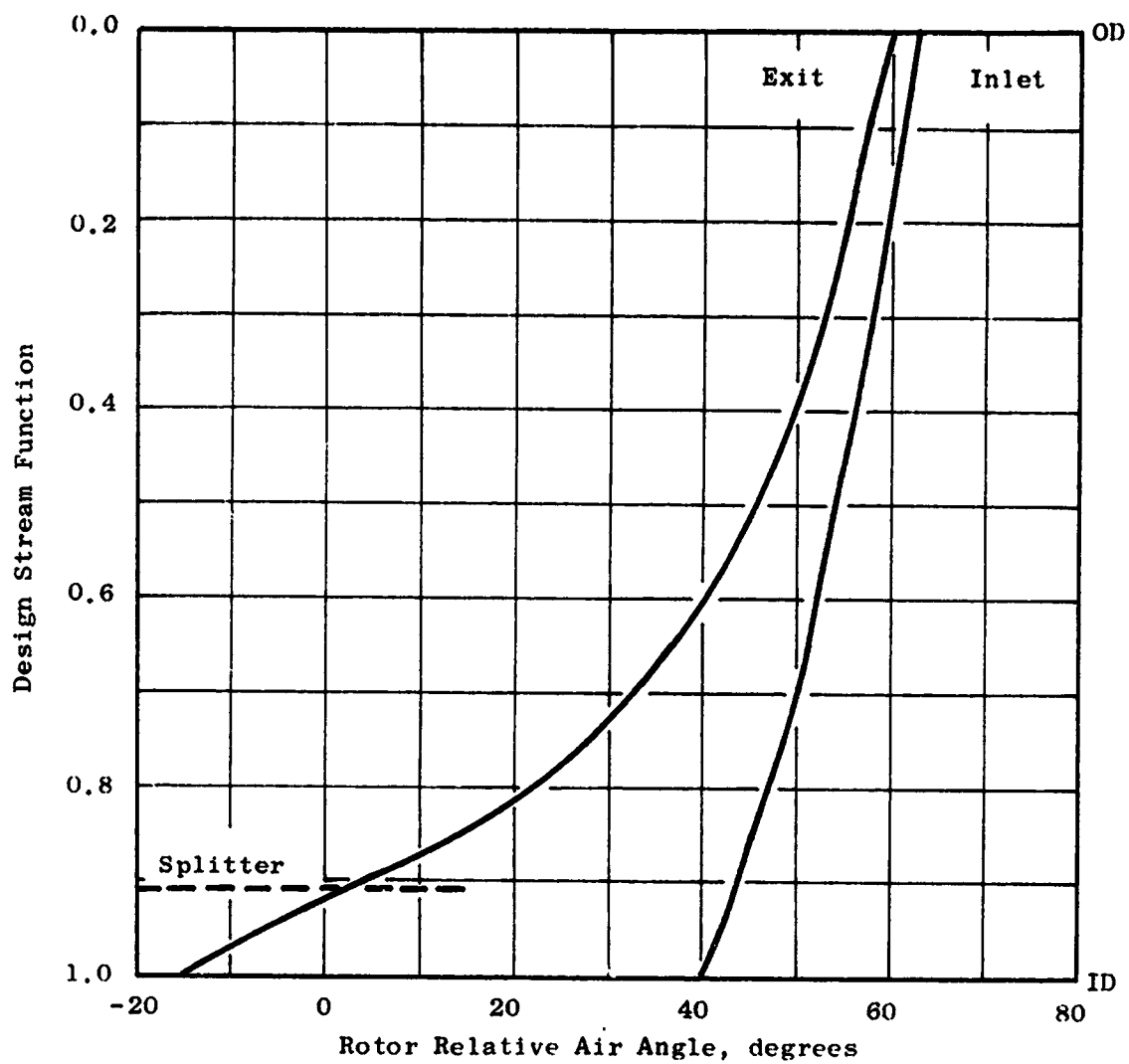
Figure 6-33. OTW Radial Distribution of Rotor Relative Air Angle.

The assumed radial distribution of total-pressure-loss coefficient for the core portion OGV is shown in Figure 6-34. The relatively high level, particularly in the ID region, is in recognition of the very high bypass ratio of the OTW engine and, accordingly, the small relative size of the core OGV compared to the rotor. The annulus height of the core stator is approximately 70% of the rotor staggered spacing, a significant dimension when analyzing secondary flow phenomena. It is anticipated that a significant portion of the core OGV will be influenced by the rotor secondary flows. The moderately high core OGV diffusion factors, turning angles, and inlet Mach numbers, as shown in Figure 6-34, were contributing factors in the total-pressure-loss coefficient assumptions. An average swirl of 6° is retained in the fluid at exit from the core OGV, like the UTW configuration. This was done to lower its aerodynamic loading. The transition duct struts designed for the UTW configuration were cambered to accept this swirl.

6.3.4 Rotor Blade Design

The rotor blade tip solidity was selected as 1.3. With a rotor tip inlet relative Mach number of 1.22, a reduction in tip solidity would lower the overall performance potential of the configuration. The rotor hub solidity was selected as 2.2. The primary factors in this selection were the rotor hub loading and sufficient passage length to do the required 56° turning. The radial chord distribution is linear with radius. Mechanical input was provided to ensure that this chord distribution and the selected thickness distribution, as shown in Figure 6-35 and 6-36, produced a satisfactory aeromechanical configuration.

The detailed layout procedure employed in the design of the fan blade geometry generally parallels established design procedure as outlined in Section 6.2.5. In the tip region of the blade where the inlet relative flow is supersonic, the uncovered portion of the suction surface was set to ensure that the maximum flow passing capacity is consistent with the design flow requirement. The incidence angles in the tip region were selected according to transonic blade design practice which has yielded good overall performance for previous designs. In the hub region, where the inlet flow is subsonic, incidence angles were selected from NASA cascade data correlations with adjustments from past design experience. The blade trailing edge angle was established by the deviation angle which was obtained from Carter's Rule applied to the camber of an equivalent two-dimensional cascade with an additive empirical adjustment, X. This adjustment is derived from aerodynamic design and performance synthesis for this general type of rotor. However, in the rotor hub, the significant turning past axial results in profile shapes that resemble impulse turbine blades. Design practice in turbine blade layout suggested that blade sections using the full empirical adjustment would result in an overturning of the flow. This overturning by the rotor would aggravate a relatively high-Mach-number-high-loading condition on the core OGV. Consequently the empirical adjustment was reduced 2° in this region. The incidence and deviation angles and the empirical adjustment angle employed in the design are shown in Figure 6-37.
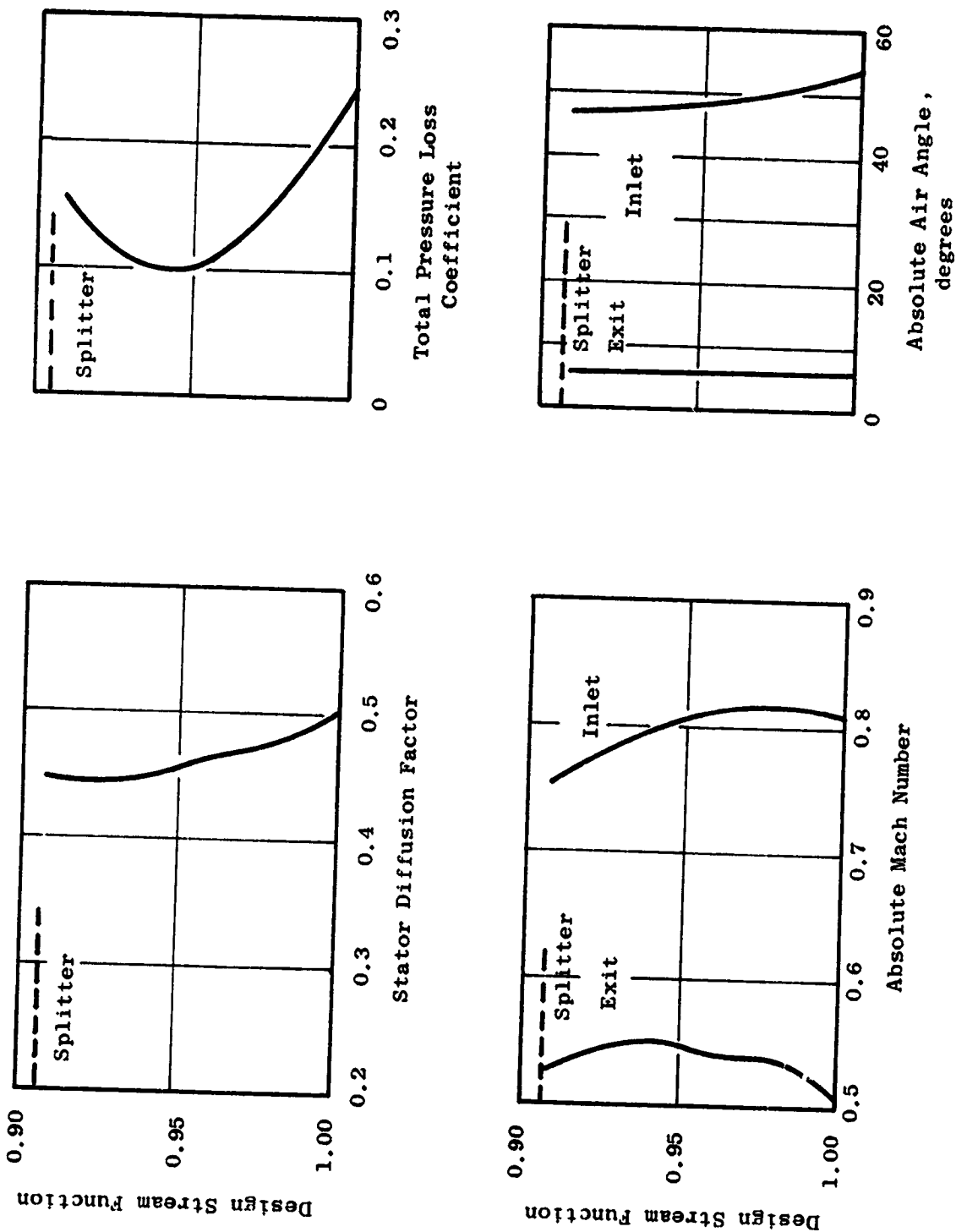
Figure 6-34. OTW Radial Distribution for Core OGV.
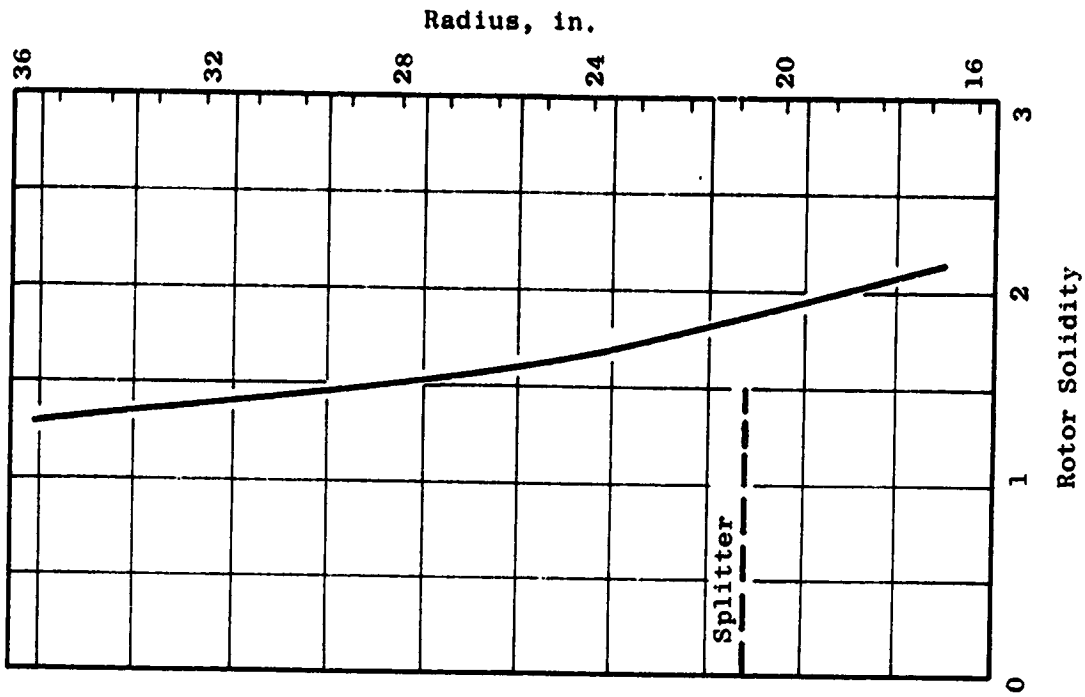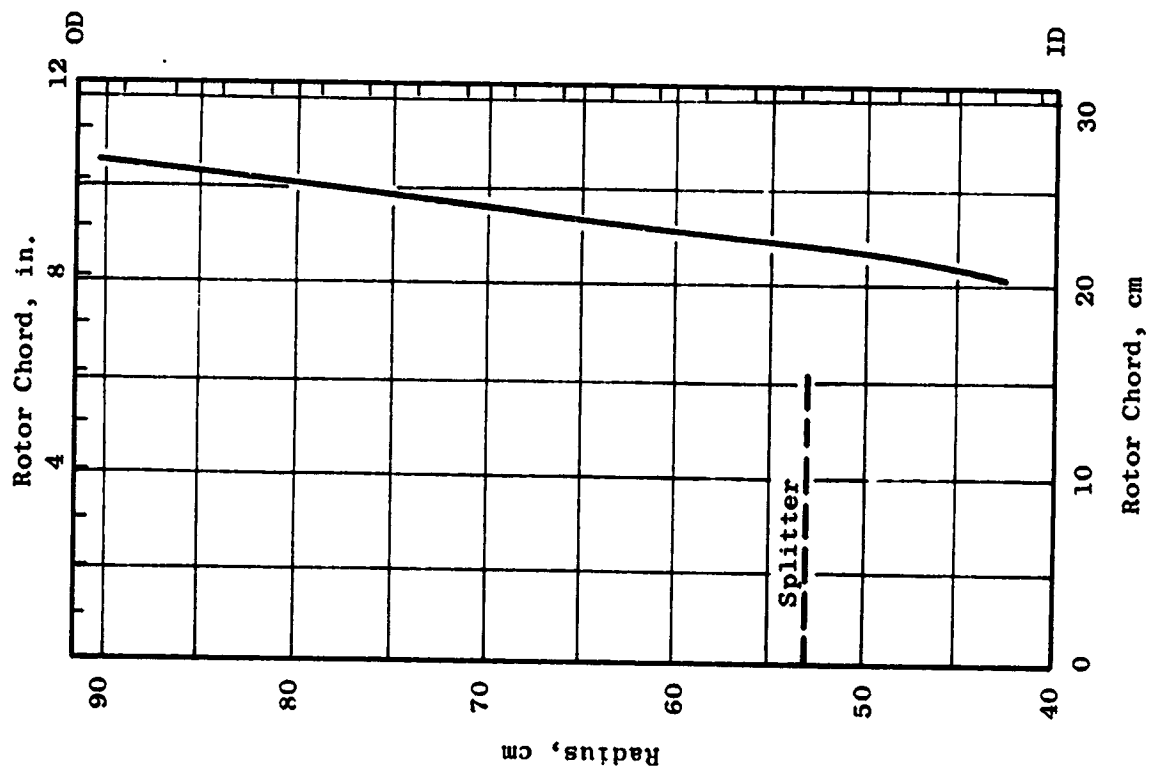
Figure 6-35. OTW Rotor Chord Distribution.
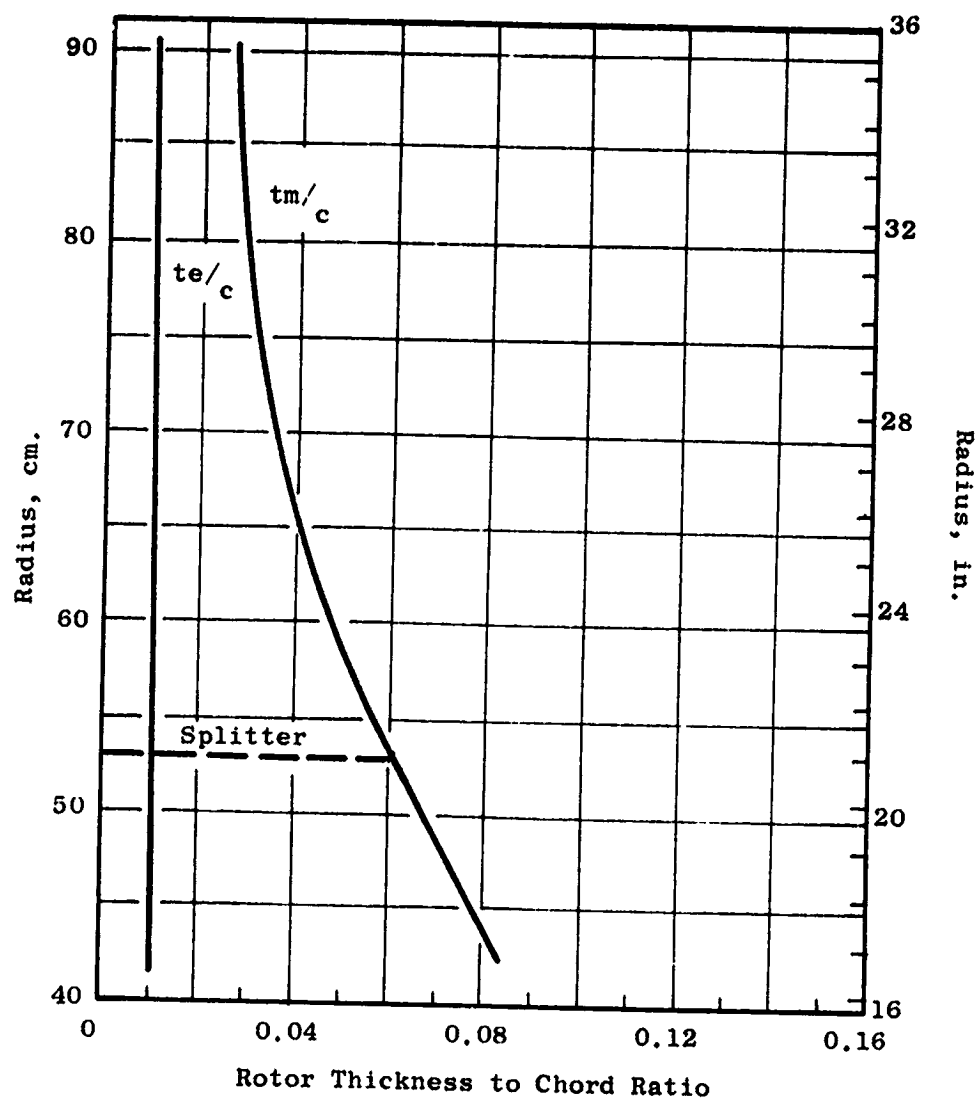
Figure 6-36. OTW Rotor Thickness Distribution.
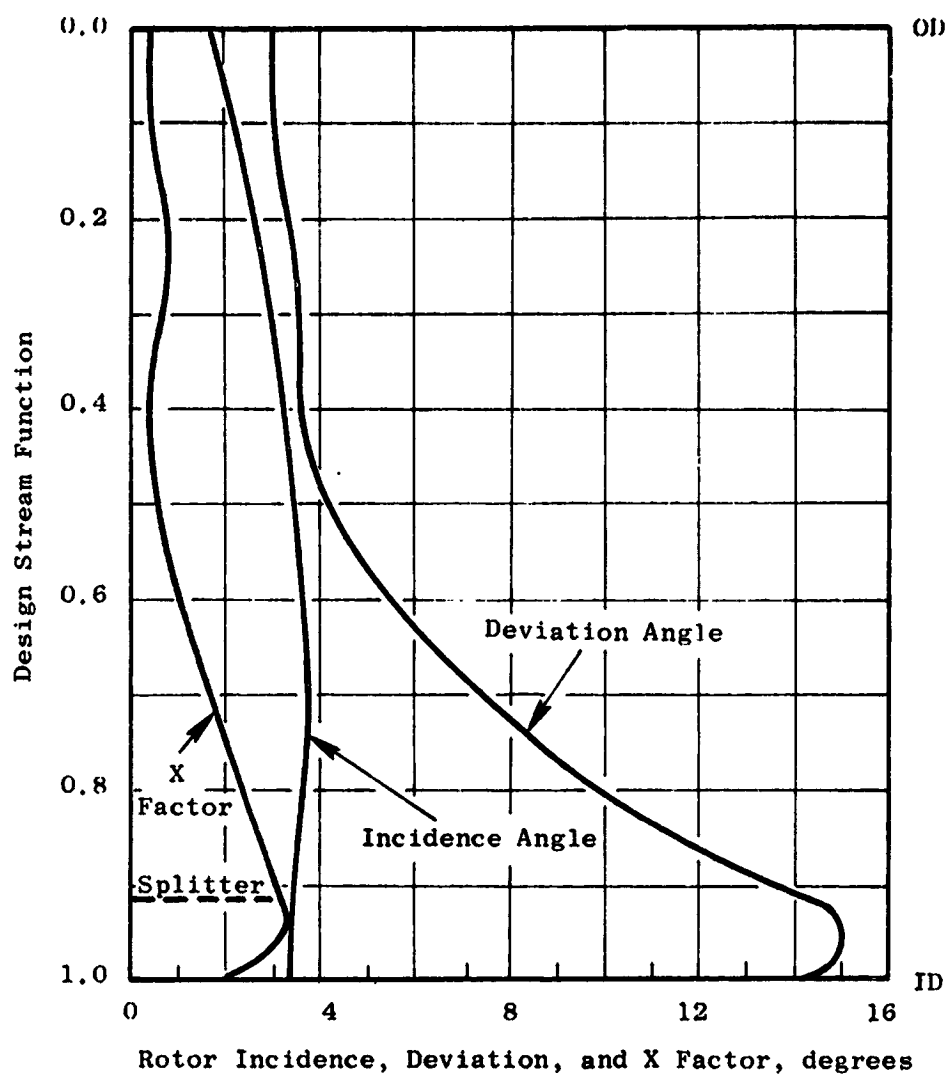
Figure 6-37. OTW Rotor Incidence, Deviation, and Empiri-
cal Adjustment Angles.

Over the entire blade span, the minimum passage area, or throat, must be sufficient to pass the design flow including allowances for boundary layer losses, and flow nonuniformities. In the transonic and supersonic region the smallest throat area, consistent with permitting the design flow to pass, is desirable since this minimizes overexpansions on the suction surface. A further consideration was to minimize disturbances to the flow along the forward portion of the suction surface to minimize forward propagating waves that might provide an additional noise source. Design experience guided the degree to which each of these desires was applied to individual section layouts. The percent throat margin, the percentage by which the ratio of the effective throat area to the capture area exceeds the critical area ratio, is shown in Figure 6-38. The values employed are generally consistent with past experience.

The resulting blade shapes have very little camber in the tip region. In the mid-span region, the shapes generally resemble multiple circular arc sections with the majority of the camber occurring in the aft portion. In the inner region, the shapes are similar to a double circular arc. Figure 6-39 shows plane sections through the blade at several radial locations. The resulting camber and stagger radial distributions are shown in Figure 6-40.

6.3.5 Core OGV Design

A moderately low aspect ratio of 1.3 was selected for the core portion OGV to provide a rugged mechanical system. This selection was in recognition of the potentially severe aeromechanical environment of the core OGV, i.e., large rotor blade wakes, because of its small size in relationship to that of the rotor blade. A solidity at the ID of 2.24 was selected to yield reasonable levels of diffusion factor, Figure 6-34. The number of OGV's which result is 156.

Profiles for the core OGV are multiple circular arcs. The incidence angle over the outer portion of the span was selected from a correlation of the NASA low-speed cascade data. Locally, in the ID region, the incidence angle was reduced 4°. This local reduction in incidence was in recognition of traverse data results on other high bypass fan configurations which show core stator inlet air angles several degrees higher than the axisymmetric calculated values. The deviation ·gle was obtained from Carter's Rule as was described for the rotor blade, but no empirical adjustment was made. The resulting incidence and deviation angles are shown in Figure 6-41. An average throat area 5% greater than the critical contraction ratio was employed in the design. The throat area margin is shown in Figure 6-41. Locally, in the ID region, the margin is zero for the axisymmetric vector diagrams. However, as noted above, the anticipated inlet air angle in this region will be several degrees higher, and therefore the capture area will be several percent lower than the axismmetric calculation. The effective throat-to-capture area ratio will therefore increase to provide adequate margin.

The multiple circular arc mean line consisted of a maximum radius arc forward of the throat, which occurs at the passage leading edge. This arc was determined by the incidence and throat area selection. A small blend region transitioned into a second arc prescribed by the overall camber requirement. The resulting radial distributions of camber, stagger, solidity, chord, and thickness-to-chord ratio are given in Figure 6-42. Figure 6-43 is a cylindrical section of the OGV at the pitch line radius.
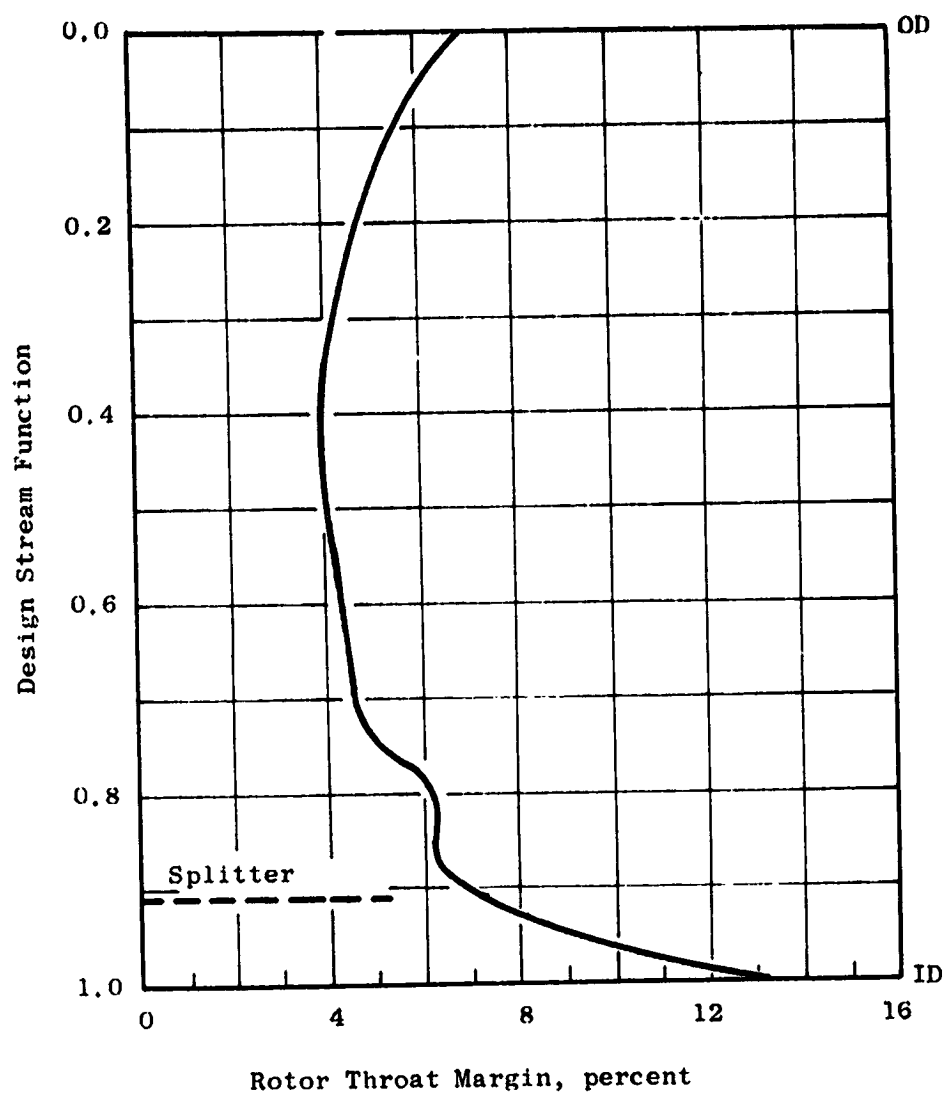
Figure 6-38.   OTW Rotor, Percent Throat Margin.

Section	Radius (cm)	(in)
1	85.4	33.6
2	76.0	29.9
3	67.6	26.6
4	56.9	22.4
5	47.2	18.6

Tip L.E. Radius = 90.2 cm (35.5 in.)
Hub L.E. Radius = 38.1 cm (15.0 in.)

Rotor Rotation
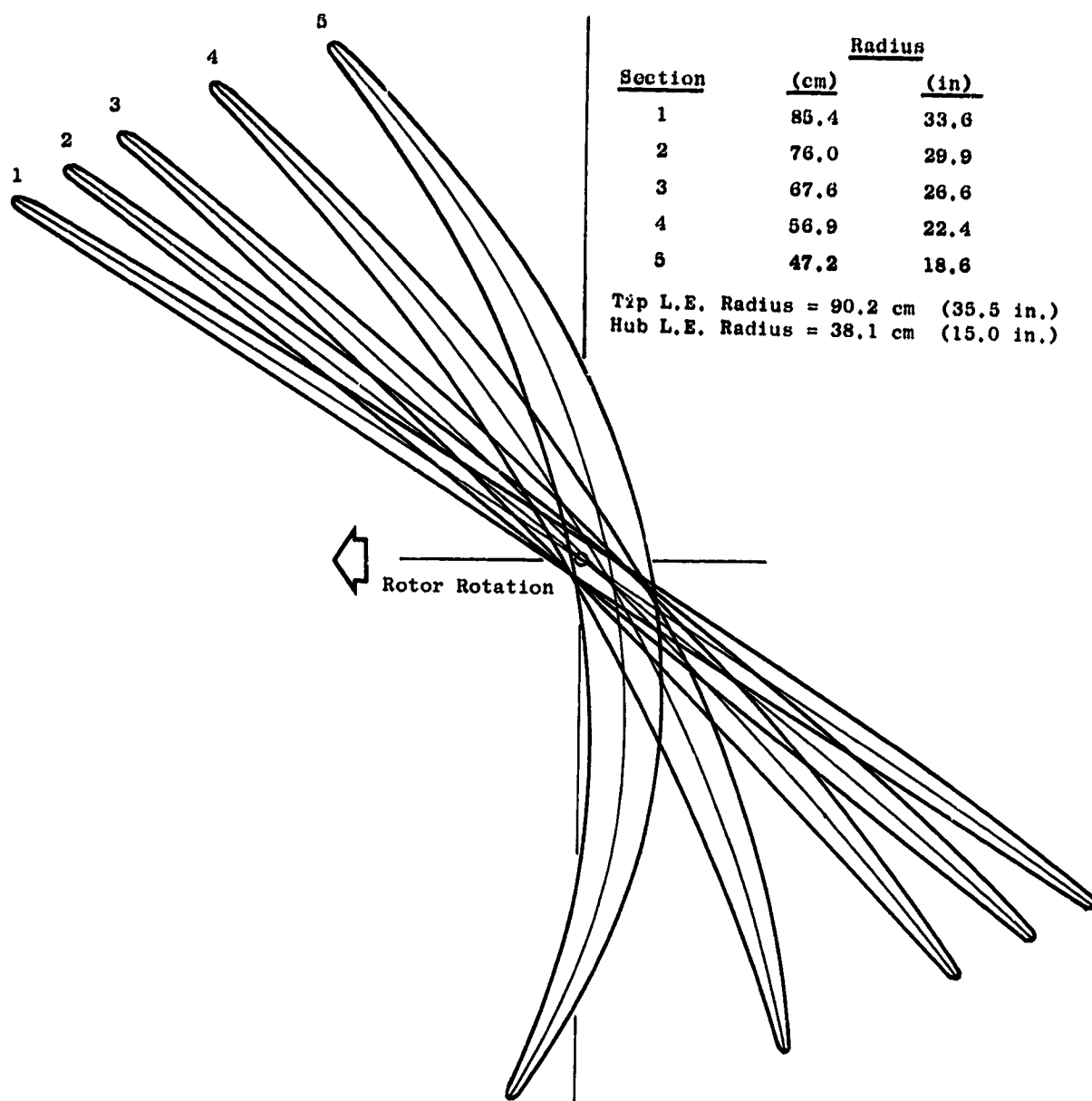
Figure 6-39. OTW Fan Blade Plane Sections.
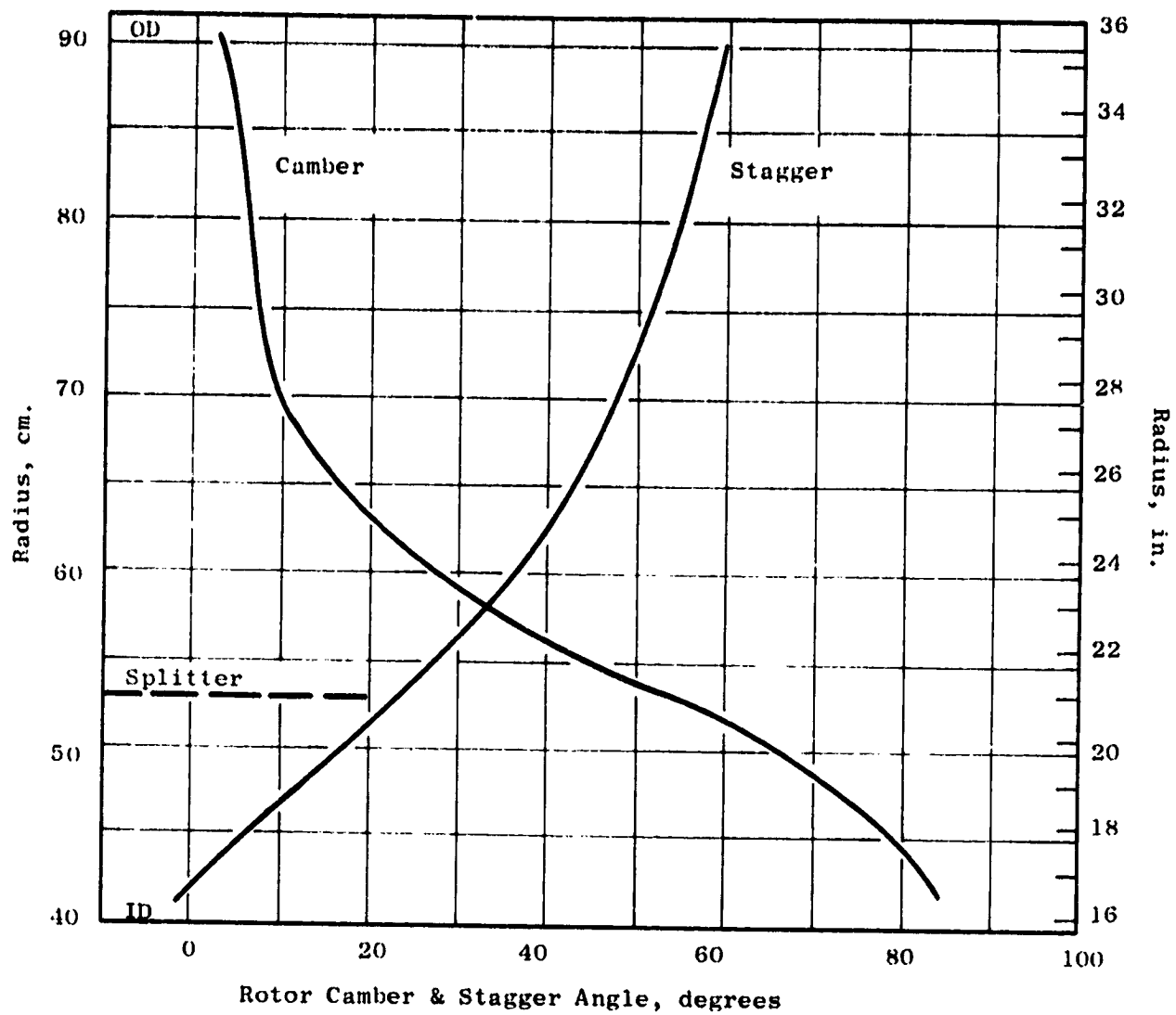
Figure 6-40. OTW Camber and Stagger Radial Distribution.
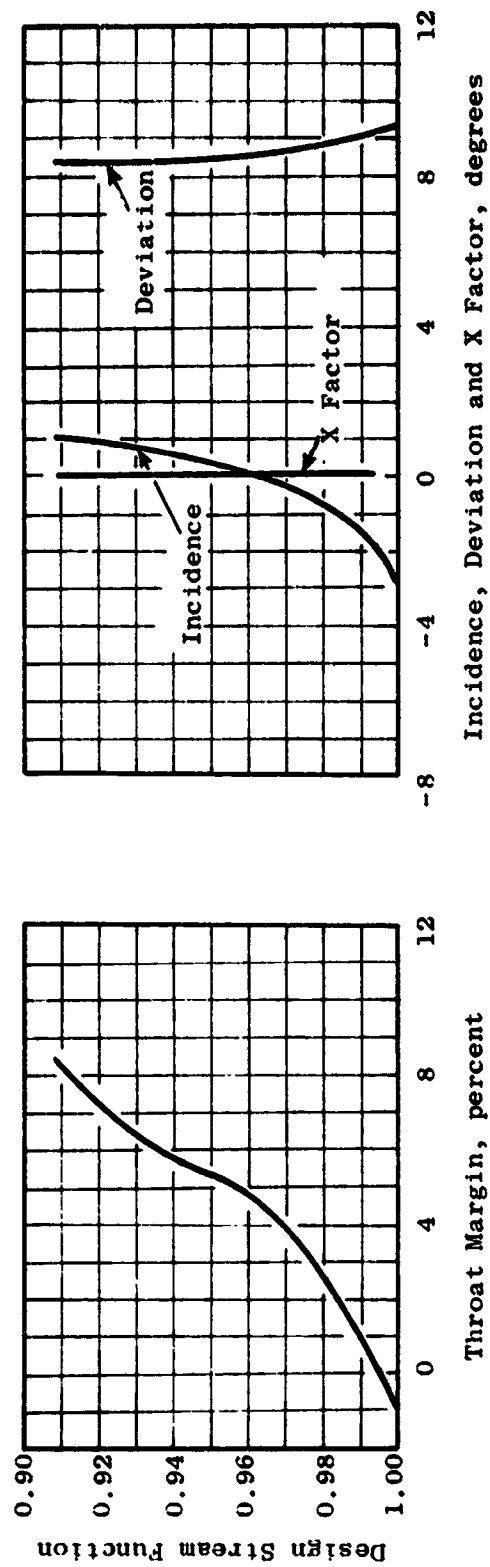
Figure 6-41. OTW Core OGV.
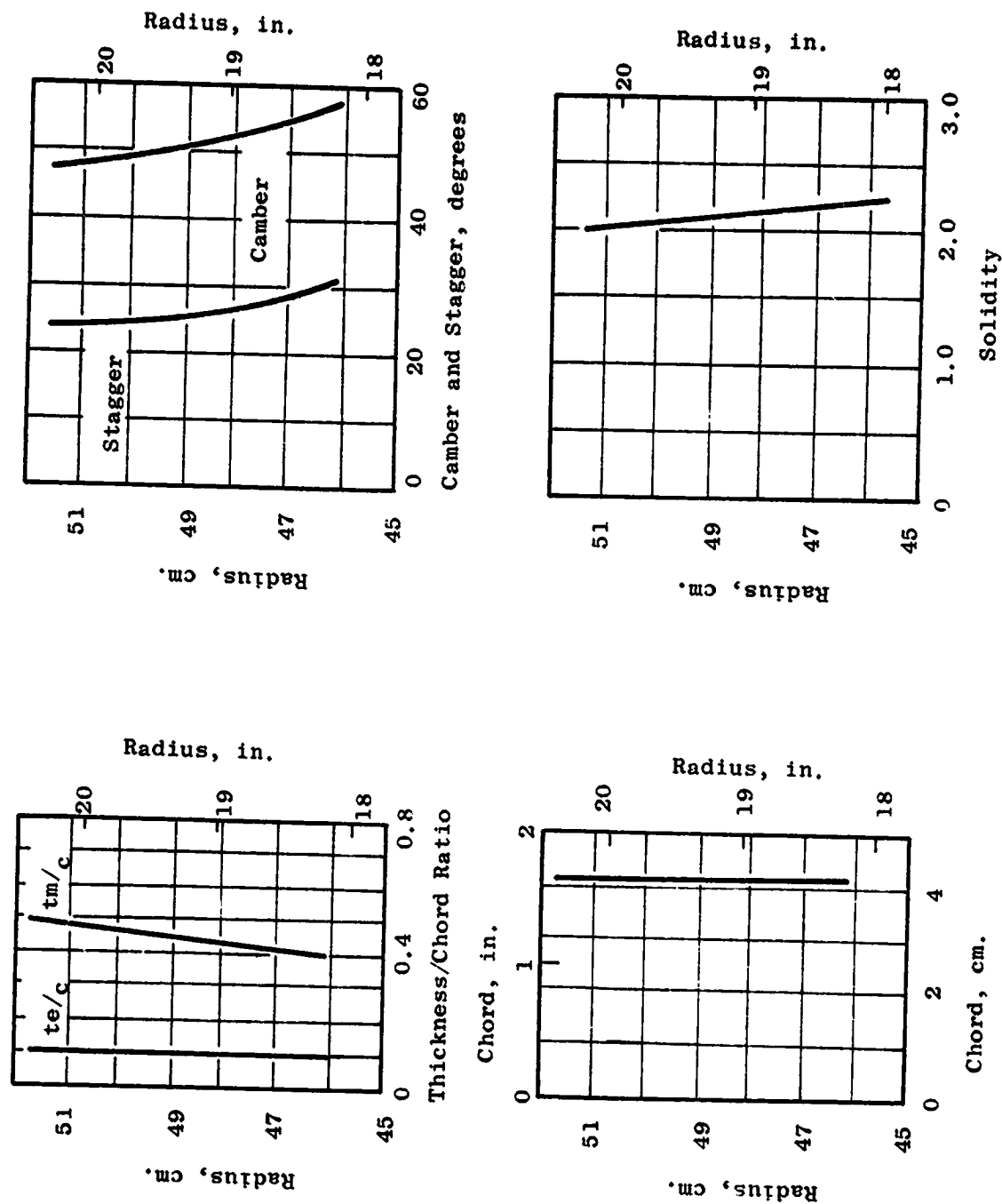
Figure 6-42. OTW Core OGV.
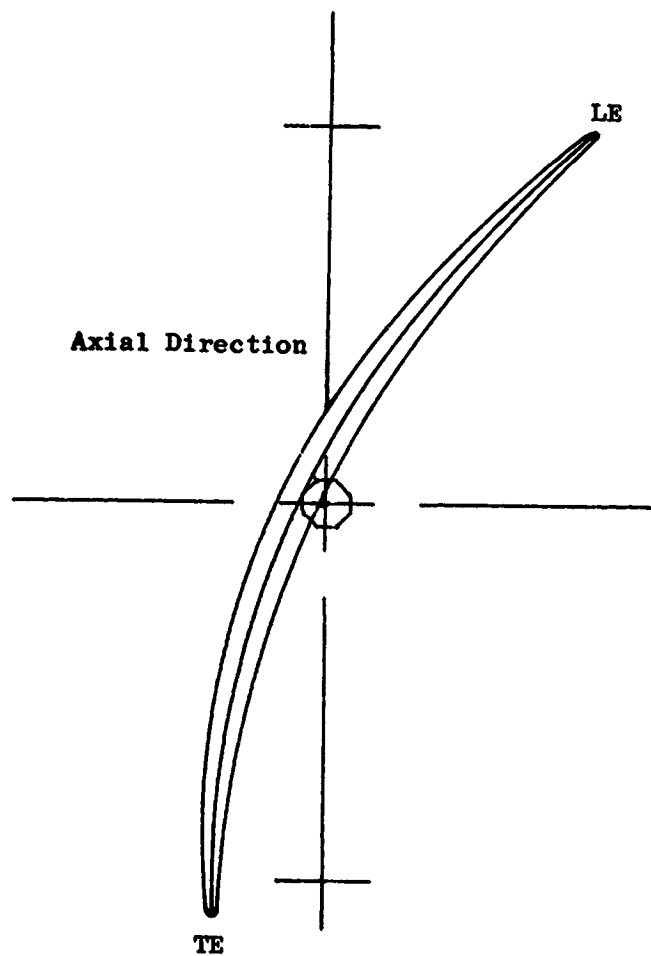
Figure 6-43. Cylindrical Section of OTW OGV
at the Pitch Line Radius.

SECTION 7.0

QCSEE VARIABLE-PITCH ACTUATION SYSTEMS

During the preliminary design phase of the QCSEE Program, a number of variable-pitch dynamic blade actuation concepts were studied. The three most promising concepts were the General Electric recirculating ball screw system, the Hamilton-Standard harmonic drive system, and the Curtiss-Wright power hinge system. A competition, with formal proposals, was held between these three designs.

The proposed designs included the fan blade retention system, fan rotor disk, variable-pitch actuation system, and power drive and control system for the variable-pitch actuator. The evaluation resulted in the selection of the General Electric fan blade retention system and fan rotor disk. The Hamilton Standard actuation system was judged to offer the greatest future potential in terms of lower system weight, improved maintainability, and better overall suitability for airline service. The proposed General Electric actuator was judged to have greater background experience and lower development risk. The Hamilton Standard power drive and control systems were rated best of those proposed. In order to achieve significant advancement in state of the art for future aircraft systems, while limiting the amount of the variable-pitch system on the overall QCSEE program risk to an acceptable level, it was recommended by General Electric that, funds permitting, both the Hamilton Standard and General Electric actuation systems be developed and engine tested.

This section of the report covers only the General Electric and Hamilton-Standard variable-pitch systems.

7.1 DESIGN REQUIREMENTS AND CRITERIA

The preliminary designs of all proposed variable-pitch fan systems were conducted in accordance with requirements defined in GE Specification M50TF1623-S1. A life requirement of 36,000 hours (48,000 mission cycles) was specified for all component parts, with the exception of bearings and standard nonreusable parts, when the actuation system was operated in accordance with the conditions specified in the Mission Duty Cycle presented in Figure 7-1. The mechanisms were to be designed for no replacement of parts (including bearings and nonreusable parts) at intervals of less than 9,000 hours.

The variable pitch systems, including retention bearings, were also to be designed to be capable of meeting the life cycle requirements of the experimental engines, defined as follows:
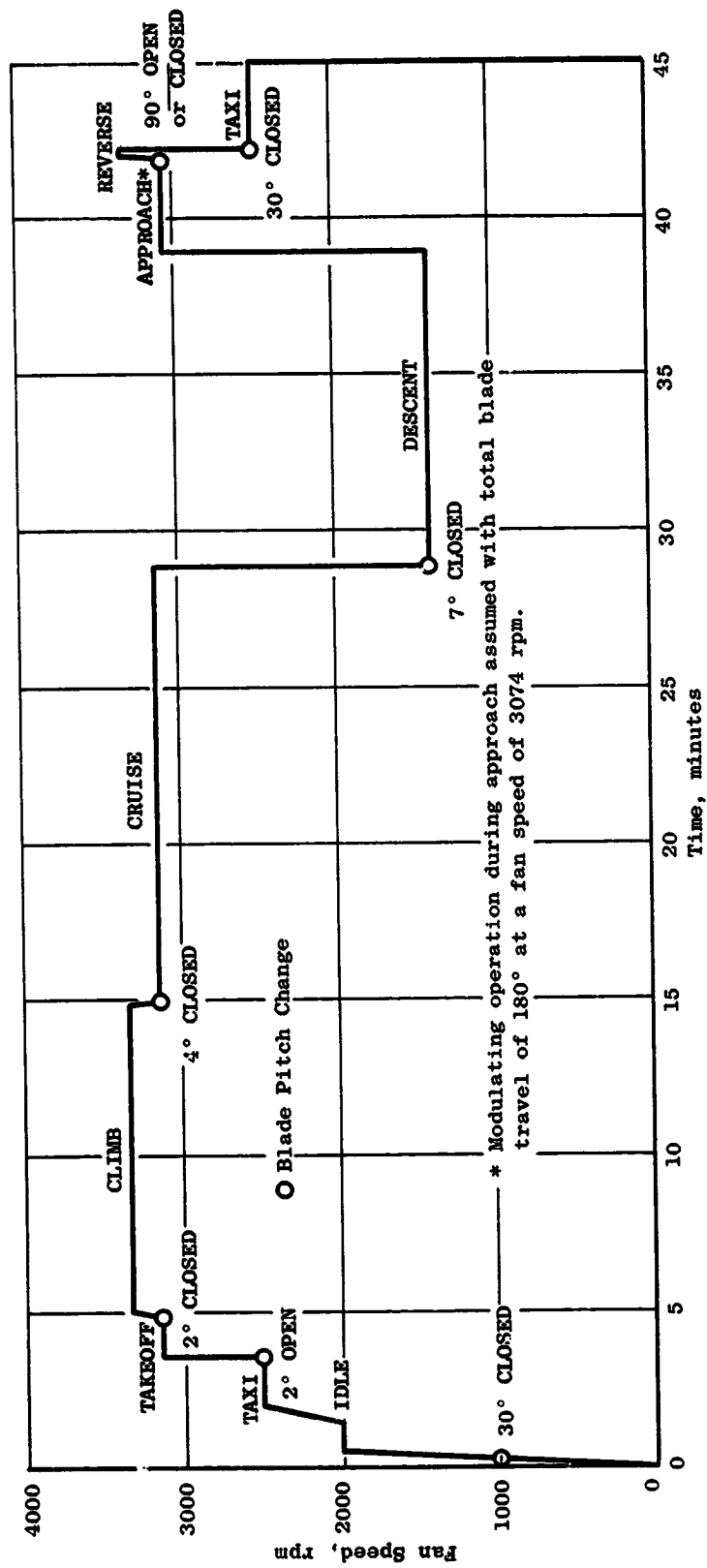
Figure 7-1. UTW Mission Duty Cycle.

207

	Fan Speed (rpm)	Input Fan Power		Time (hours)
		Mega-watt	Horsepower	
1	3300	9.8	13116	1
2	3143	13.7	18362	1
3	3143	12.7	17050	.5
4	3143	10.8	14428	15
5	3143	9.8	13116	150
6	2829	7.8	10493	500
7	2357	4.9	6558	1000
8	707	1.0	1312	1000

In addition, for the experimental engines, the system operational capability was to be consistent with the following:

- 500 total reversals through flat pitch or sta' it maximum fan speed

- Items 1 through 4
  360 actuations at 5 minute intervals in the range of operation from 5° open to 5° closed

- Items 5 through 8
  10,000 actuations in 5° increments from 5° open to 20° closed

Additional design requirements imposed during the preliminary design studies are shown in Table 7-I and Figure 7-2.

The preliminary designs were also to be based on consideration of the following requirements:

- Following foreign object ingestion the dynamic pitch change mechanism must be capable of 10 additional cycles at maximum torque and actuation rate.

- The system must be capable of withstanding 20 g vibratory and should not impose over 5 g vibratory on the engine.

- The system must be capable of operation after exposure to fluids conventionally used by Airlines such as "Skydrol Type" hydraulic fluids, methylene chloride, and butyl cellasolve.

The target weight established for the complete variable pitch fan system, including the fan blade retention system and fan rotor disk was 109 kg (240 lb).

7.2 GENERAL ELECTRIC ACTUATION SYSTEM

A geared variable-pitch fan (VPF) has been selected for the NASA/GE QCSEE Program and will be demonstrated on the UTW engine. This VPF concept, which includes full reverse thrust capability, is expected to offer significant advantages to a high-bypass fan system, including:

208

Table 7-I. Variable Pitch System Design Requirements.

	Normal Range	Extreme Range
RPM of Fan	0 - 3326	3450 without Actuation
Blade Twisting Torque[1]	See Figure 7-2	1695 Nm (15,000 lb-in.)[2]
Blade Overturning Moments		22,600 Nm (200,000 lb/in.)[2]
Centrifugal Load for Blade and Dovetail Only	15,196 kg (33,500 lb) (at 3200 rpm)	Must not burst at 4432 rpm (141% of T/O rpm)
Actuation Rate	135°/sec max	
Actuation Jogging at Blades	0.5° Steps Minimum	
Feedback Signal Accuracy	$\pm$0.25° Blade Position	
Flight Maneuver Forces[3]	Per MIL-E-5007C (12/30/65) Par 3.14 except Precession Rate shall be one Radian per Sec Max	

---

[1] Friction must be included over and above this data.

[2] FAA Advisory Circular AC 33-1B, 4-22-70.

[3] Polar moment of inertia of blades = 305 MN/m^2 (44,376 psi)
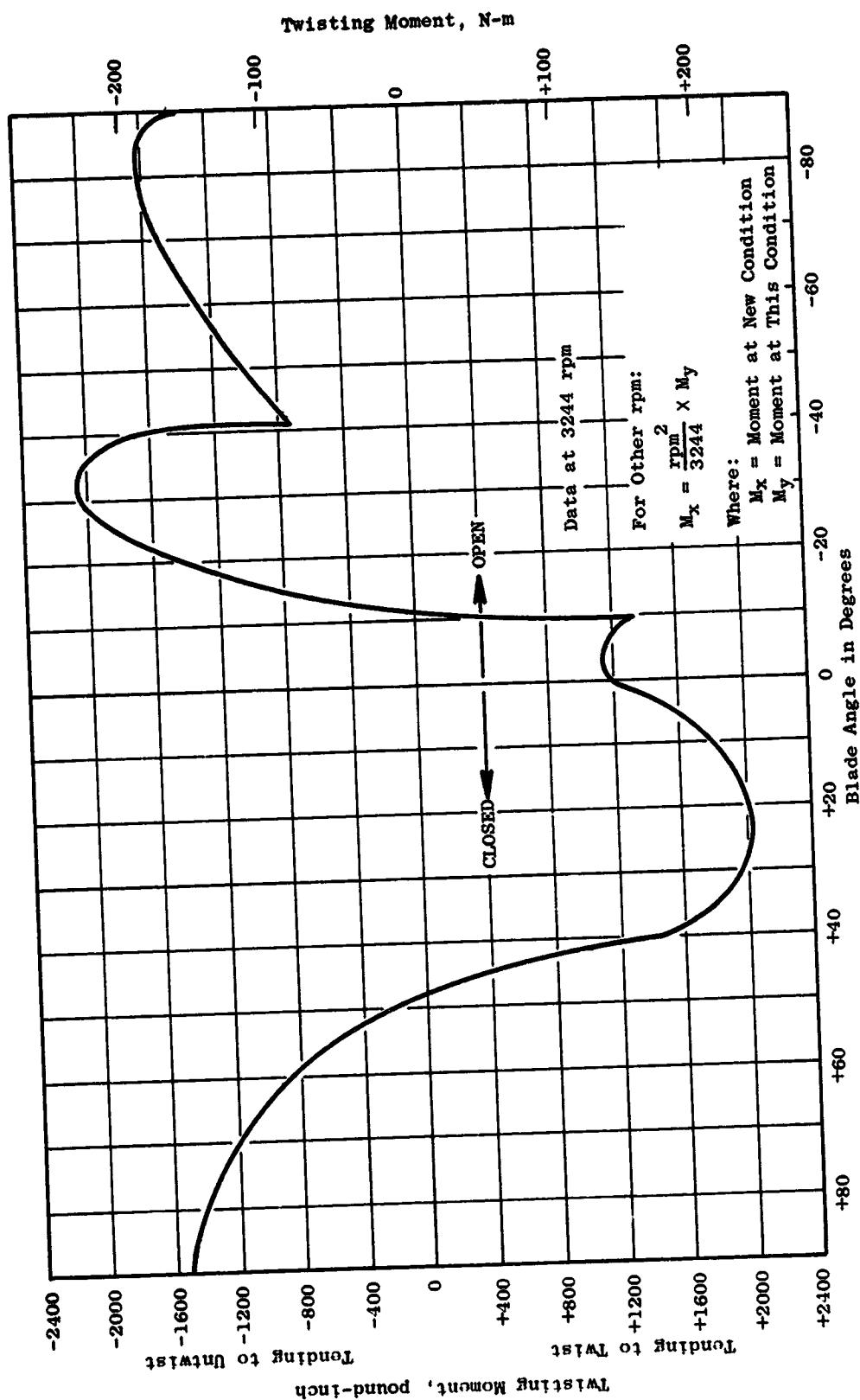
Figure 7-2. UTW Fan Maximum Net Twisting Moment.

- Lighter weight, due to elimination of the heavy, large diameter thrust reverser

- Faster thrust response

- Improved off-design SFC

- Reduced off-design noise generation.

General Electric has already demonstrated the capability to successfully design and develop variable-pitch fan rotor systems. The variable-pitch fan program included a demonstration of on-line blade pitch variation on a high speed fan rotor. This fan completed over 60 hours of fault-free operation in December 1972. This system was disassembled, inspected, and rebuilt into the reverse pitch fan (RPF) configuration, shown in Figure 7-3. The reverse pitch fan completed a comprehensive test program spanning an additional 100 hours. The RPF Program was also completely free of mechanical problems and provided successful demonstration of on-line modulation between forward and reverse thrust.

7.2.1 Design Studies

Design studies on the QCSEE UTW variable-pitch fan blade actuation mechanism have been completed by General Electric as part of the total effort to define a viable variable-pitch fan system concept for possible commercial application. Major considerations in these studies included structural integrity, bird strike resistance, life and reliability, weight, development risk and cost, maintainability, production unit cost, and suitability for eventual usage by the airlines.

The proposed GE ball spline actuation system, shown in Figure 7-4, functions in the following manner. Pinion bevel gears attached to each of 18 fan blades are rotated by the motion of two counteracting master bevel gears. These master bevel gears are rotated by a double-acting helical ball spline driven by a rigid translating sleeve. A ball screw drives the translating sleeve through a stroke of 10.2 cm (4 in.) to achieve a blade rotation of 2.36 radians (135°). All thrust loads developed are close looped within the actuator mechanism.

As shown in Figure 7-4, power to drive the ball screw is provided by the fan shaft, acting through a gear differential which is controlled by a system of hydraulically actuated disk brakes. A ball/ramp-type no-back is included between the differential gear and the ball screw to allow torque to be transmitted only in one direction.

Torsional stops at each end of the ball screw limit the actuator travel. Mechanical stops in the ball spline, although normally not engaged, are a backup system to limit stroke. In this particular design the large master gears are easily reindexed to permit demonstrator testing through both flat pitch and stall.

At maximum fan speed stop-to-stop actuation time is one second. A linear variable displacement transformer (LVDT) is used to provide the intelligence to the position feedback system.

SPHERICAL
BLADE TIP

BLADE OPEN

THRUST WASHER
(TEFLON COATED)

16 TOOTH
PINION

PITCH
LOCK

HYDRAULIC OIL
TRANSFER TUBE

POSITION
TRANSDUCER

THRUST BRG
(SEALED &
GREASE PACKED)

GEAR ROTATION
TO OPEN BLADES

STROKE TO
OPEN BLADES
(CI)

PISTON

HELICAL BALL SPLINE

LINEAR BALL SPLINE

FACILITY DRIVE
SHAFTING
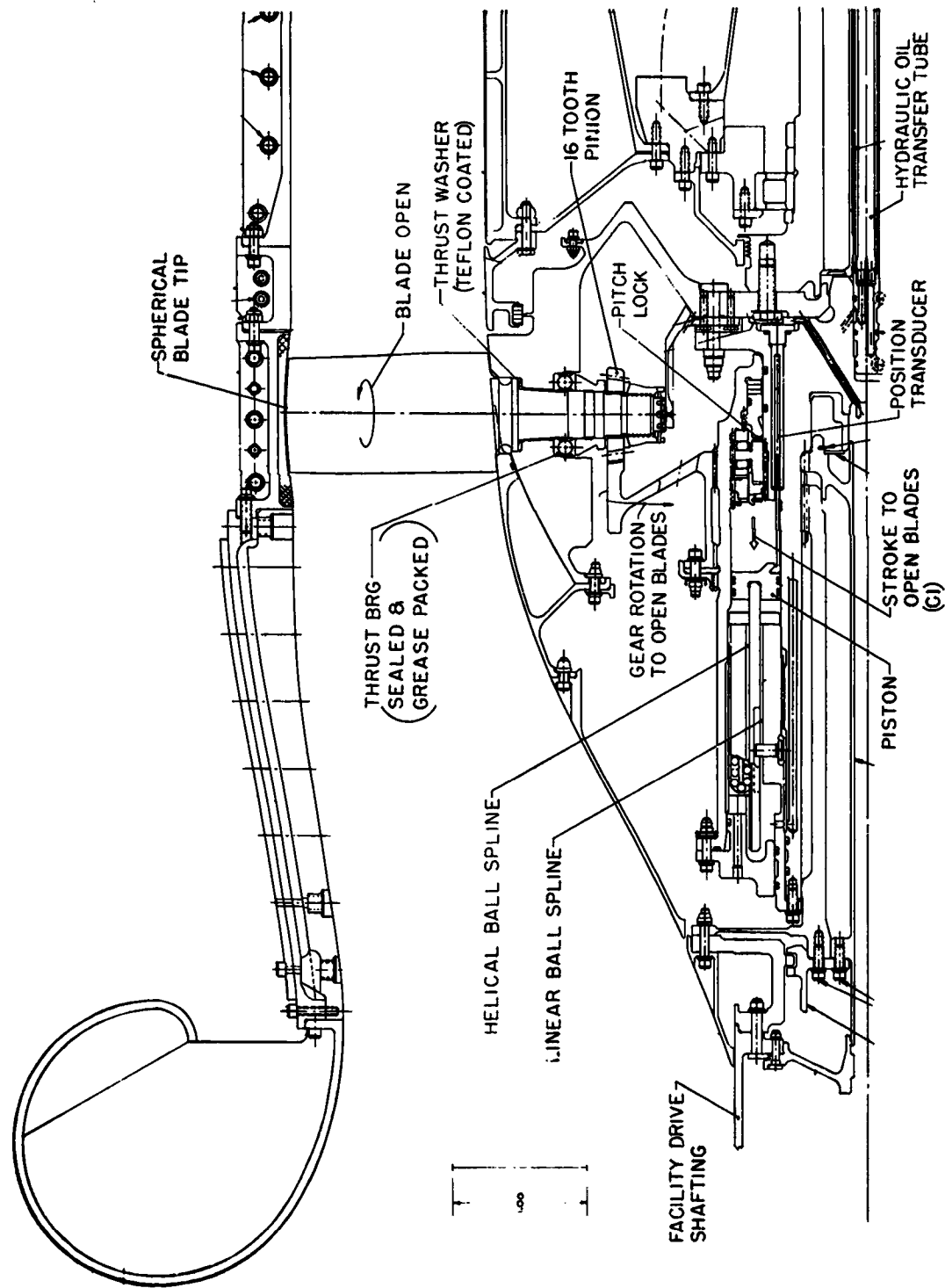
Figure 7-3.   Reverse Pitch Fan Cross Section.

212
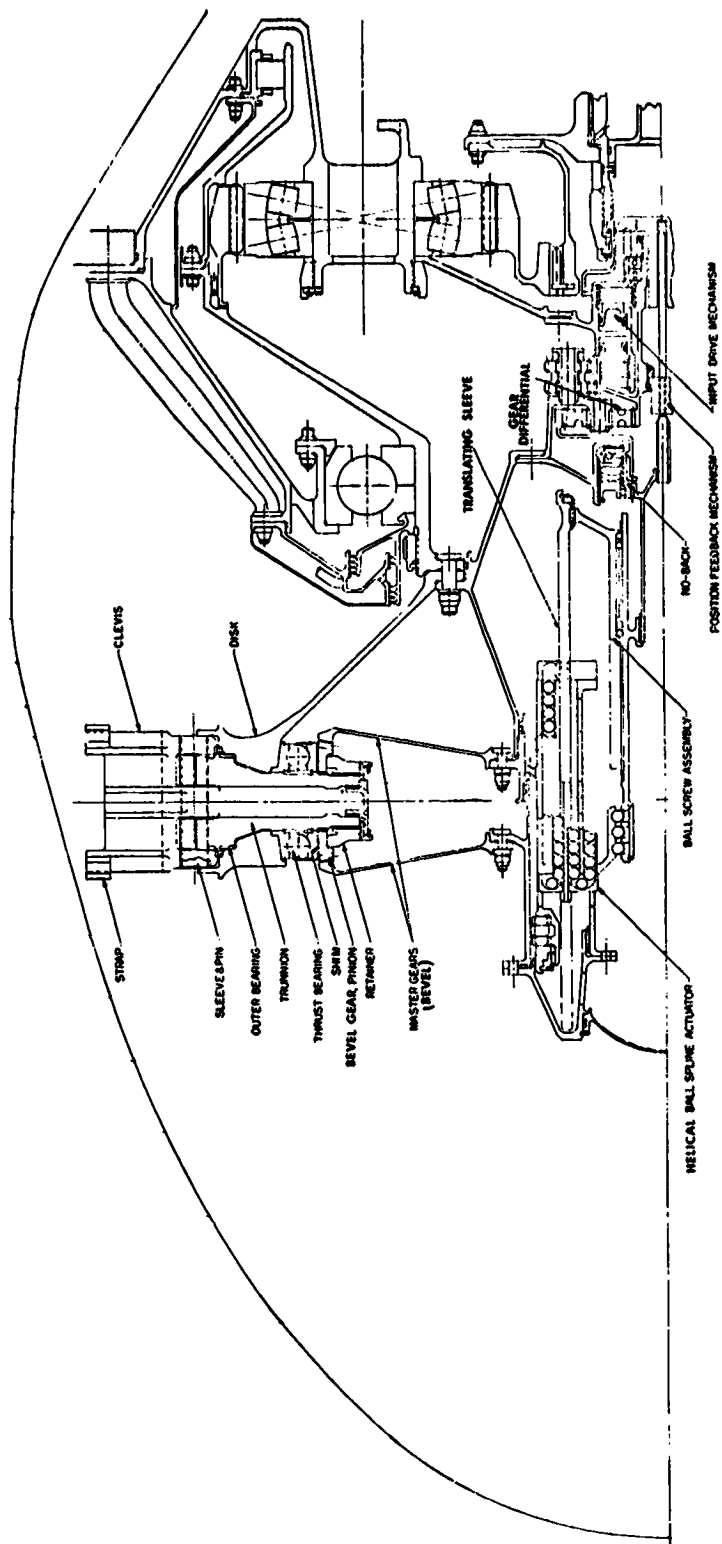
Figure 7-4. GE Ball Spline Actuator System.

213

Significant improvements of this second generation actuator over the VPF/RPF design are:

1. Two counter-rotating master gears are provided for redundancy by connecting the the inner spline member to a second master gear instead of the f‹ disk.

2. A ball screw has replaced the hydraulic piston and transfer seal assembly. The ball screw is lighter, more reliable, and permits the ball spline to be packaged in a smaller diameter.

3. The pitch lock has been replaced by a "no-back". This device transmits input torque through the system, but prevents the net blade twisting torque from back-driving the actuator ball screw.

4. The VPF/RPF hydraulic actuator required a large high pressure pump, drive system, heavy piping, and a hydraulic transfer package. The QCSEE actuator input torque is supplied by the engine fan shaft. Two lightweight methods of extracting torque from the fan drive shaft have been studied and encompass the use of a differential gear controlled by either a system of disk brakes or a combination differential/lube pump.

The advantages of the proposed GE ball spline actuation system are:

1. Design is based on a demonstrated system which has proven to be trouble free.

2. High reliability based on simple rugged design.

3. Elements subject to wear are balls which are easy and inexpensive to replace.

4. The rolling action of the ball spline and screw offers a very high efficiency system which does not require additional gearing to reduce torque levels to the "no-back" and differential gearing.

5. The actuator design lends itself to modular assembly and disassembly and allows easy access to differential gearing.

6. Recirculating engine oil rather than grease packing is used for lubrication.

7. Overload torques associated with bird impact requirements are satisfied.

214

7.2.2 Ball Spline Mechanical Design

The 18 individual pinion bevel gears are splined to the blade posts by a fine pitch spline which allows indexing of the pinions for proper synchronizing with the two master bevel gears. As shown in Figure 7-5, the two master gears allow load sharing and add redundancy to the system. The overall gear ratio of this mesh is designed to achieve the maximum gear capacity within the space available between two adjacent blades. A shim is provided to ensure proper tooth meshing. The shim is located to visually ascertain proper assembly. Gear stresses are low for normal actuation torques since the gear is designed to allow torques up to 1694.8 Nm (15,000 lb/in.), which could occur due to a bird strike.

Consideration will be given in the design phase to match the master gear deflections with respect to the pinion gears to ensure a proper contact pattern during operation. These methods proved very successful for the VPF/RPF actuator.

The forward master bevel gear is driven by the inner portion of the ball spline and the aft master gear by the outer portion of the ball spline. Both master gears are easily removed at their bolted flange joints for modular assembly and disassembly.

The forward torque member also forms the outer wall of the actuator housing, thus eliminating the need for an extra wall to retain the lubricating oil.

The ball spline is scaled from the proven design used in the VPF/RPF test vehicles and does not deviate from the successful design approach used at that time. By using a ball screw rather than a hydraulic piston to translate the ball spline middle member, the overall diameter of the ball spline can be reduced. This is compensated for by not only increasing the number of ball tracks from six to eight but also increasing the ball diameter in the ball spline.

In the ball spline, the balls ride in helical tracks whose leads are approximately 1694 mm (66.3 in.) and the overall travel of the translating sleeve is 101.6 mm (4.00 in.). This stroke was selected over a shorter one to keep the resulting ball screw thrust load to an acceptable level for the thrust bearing design.

The balls ride in a continuous path made up of a loaded track and a return guide. The return guides are tubes located out of the load zone. The loaded tracks and return guides are connected by end return caps very similar to those used in the VPF/RPF design. These individual end caps allow for easy replacement of the balls during servicing.

The maximum actuator design thrust load is approximately 117.9 kN (26,500 lb) and is carried by two thrust bearings. The larger bearing is a face roller bearing which is representative of a design used in the VPF/RPF. For the smaller bearing, a multiple row angular contact bearing will be used.

The ball spline translating member is integrated with a ball screw very similar to designs successfully used in engine thrust reverser actuators. Torsional stop concepts used in thrust reverser ball screws will be used, along with a backup set of hard stops on the translating sleeve.

215
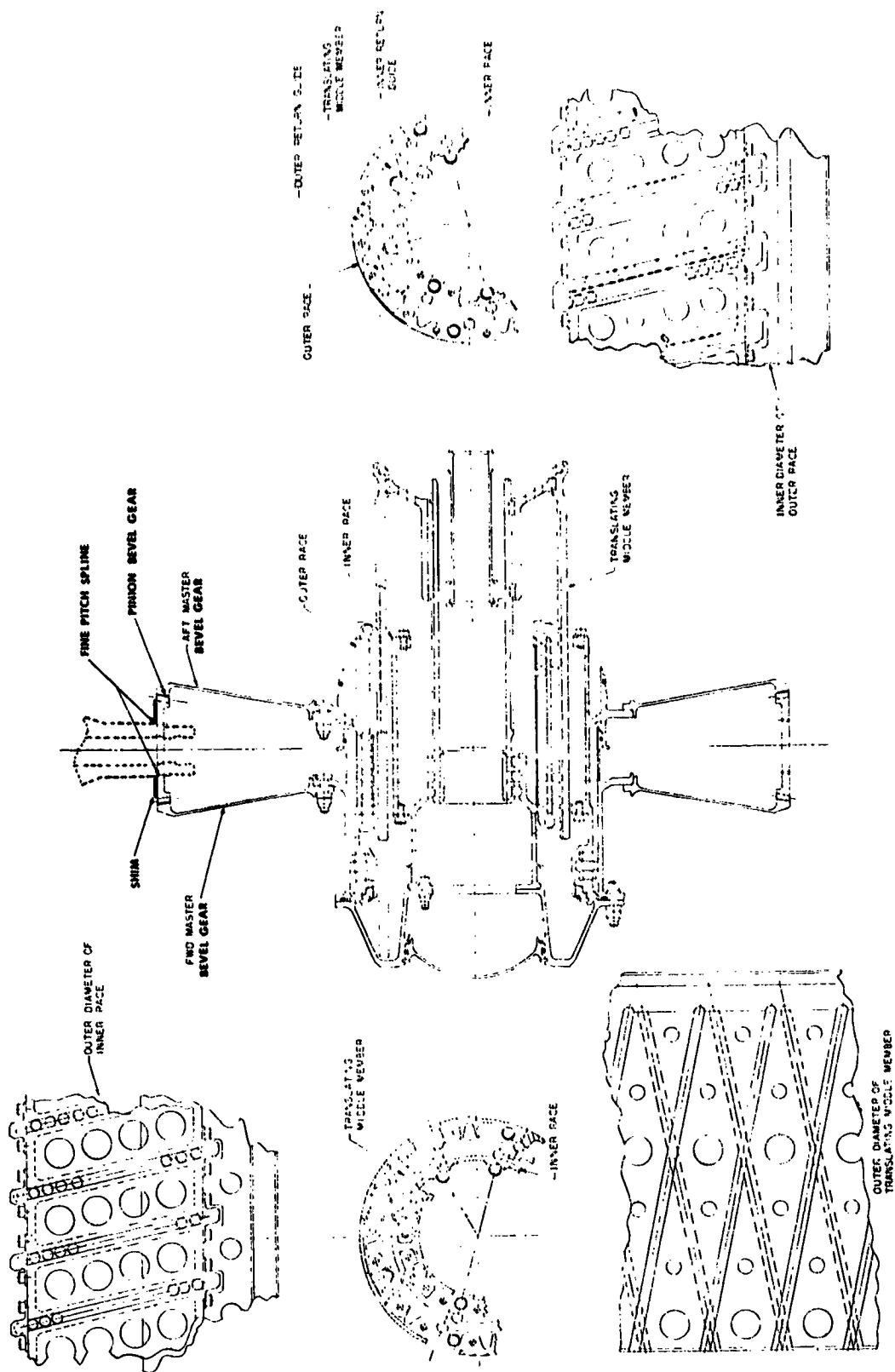
Figure 7-5. UTW Ball Spline Actuator.

216

Actuator design loads are:

- Maximum Input Torque   28,472 Nm (252,000 lb-in.)

- Maximum Allowable Stall Torque   53,667 Nm (475,000 lb-in.)

- Calculated Life (travel) 24.01×10^4 m (9.8×10^6 in.)

- Required Life for 48,000 Missions 1.67×10^4 m (0.656×10^6 in.)
  (travel)

Assuming an efficiency of the ball spline and screw of 81%, the input torque requirement to the "no-back" and differential mechanism is approximately 154.8 Nm (1370 lb-in.). This includes the frictional torque requirement of the thrust reacting bearings.

Lubrication is provided from the engine lube system and will be supplied at the engine centerline from the stationary housing of the brake drive assembly. Although this detail is not shown on the included cross sections, no problems are anticipated in providing a system of sleeves and dams to centrifugally direct the oil to the critical areas in the actuator. Oil will be centrifuged outward and drain back to the sump along the outer housing wall. All seals will be designed so no dynamic head of oil is present at the seal interface.

7.2.3 Brake Drive and Differential Gearing

A gear differential controlled by a system of disk brakes is shown in Figure 7-6. Although the actuation system also lends itself to the possibility of being actuated by a combination differential/main engine lube pump which is being studied for the QCSEE engine, it is proposed to actuate the brakes hydraulically by the same source as the fan nozzle actuation system. The disk brake system included in this design is basically the same as clutch designs used successfully on Curtis-Wright turboprops.

A planetary differential gear concept, shown in Figure 7-6, overdrives or underdrives the actuator with reference to the fan shaft speed by selectively activating the proper brake. When one brake is activated, the speed reducing sun gear is stopped and the planetary motion is imparted to the ring gear of the speed reducer gearing causing it to overdrive the fan shaft speed. Activating the other brake allows the differential motion gear to increase the speed of the sun gear in the speed reducer gearing so that the ring gear underdrives the fan shaft speed.

The differential motion gear is composed of two sun gears to which three double-planet gears, and three single-planet gears mesh. The forward sun gear is designed to prevent clashing with the double-planet gear and meshes with the single planet. The speed reducer gear ratio has been selected to provide 2.36 radians (135°)/second blade rotation at 100% fan speed.
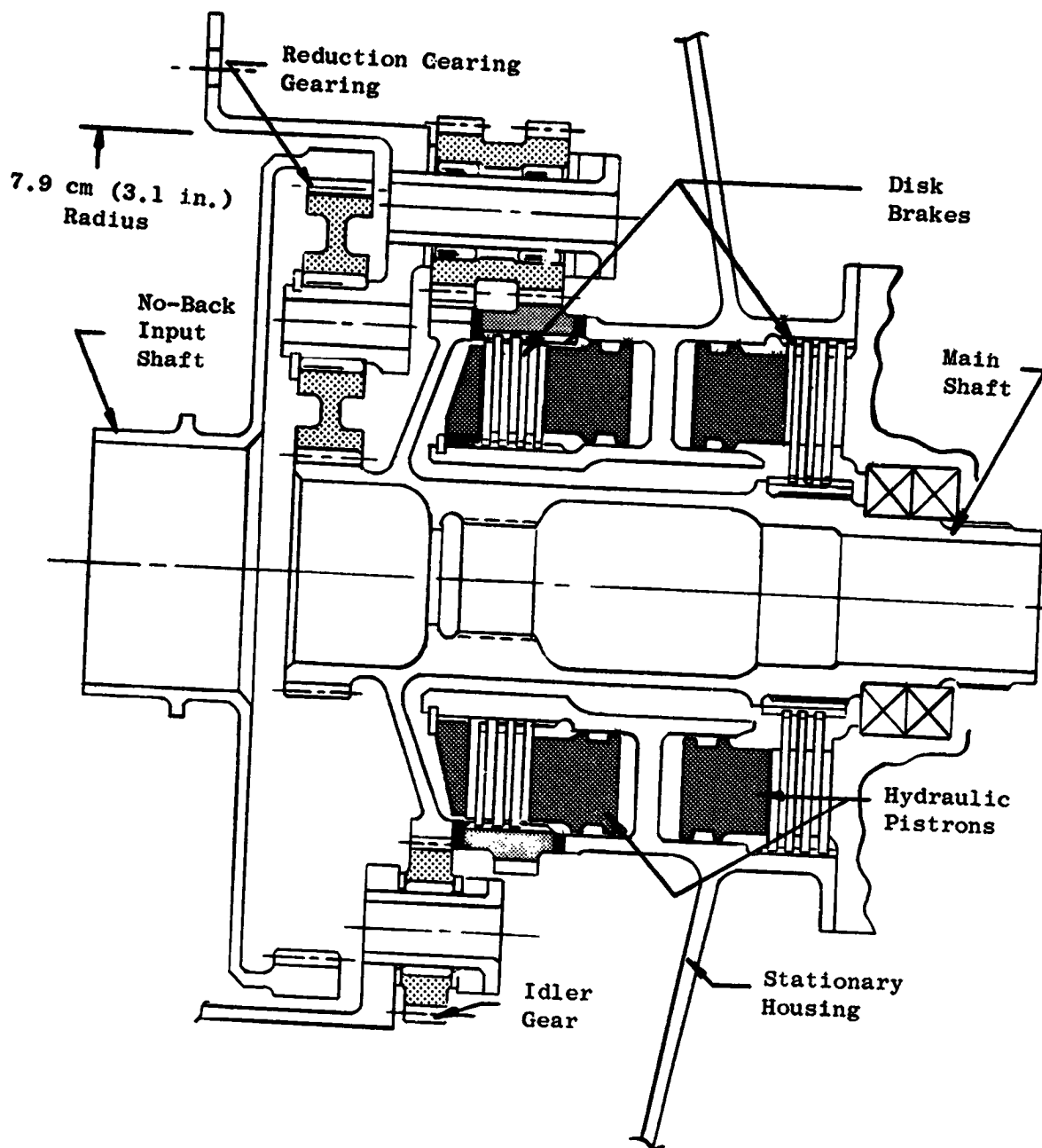
Figure 7-6. Brake Drive and Differential Gearing.

218

A "no-back" is provided just forward of the planetary differential gear. The concept shown in Figure 7-4 features a disk brake acted upon by ramp riding balls which allow torque to be transmitted only in one direction. The design shown is commercially available.

7.2.4 Feedback Mechanism

The feedback mechanism shown in Figure 7-4 is a linear variable differential transformer (LVDT). LVDT's are presently preferred for sensing position on jet control systems; their reliability and performance are proven. The inherently rugged construction is needed for the severe aircraft engine environment. The LVDT is accurate to within +0.25% of full scale. When this accuracy is combined with backlash and signal conditioning, blade position would be measured within ±0.5° over the environmental temperature range.

A LVDT translates the displacement of the magnetic core into an ac output voltage which is proportional to the displacement. These transducers are constructed of one primary coil and two secondary coils. An alternating current is fed through a primary winding. The magnetic core couples the primary and secondary coils by conducting the alternating field inside the coils. When the core is in the center position, an equal portion of the core extends into each of the secondary coils and affects an equal coupling between the primary coil and each secondary coil. An alternating voltage of equal magnitude is induced in the secondary coils. With the secondary coils connected in series opposed, the output is close to zero. As the core is moved to either side, the coupling between the primary and one secondary coil is increased while the coupling between the primary and the other secondary is decreased. A larger alternating voltage is then induced in one secondary coil and the output voltage will be the difference between the two voltages.

Movement of the core is accomplished by a small dependable ball screw which is mounted to the differential sun gear. The screw is coupled to the actuator ball screw assembly through a sliding spline. Relative rotation between the differential and the actuator ball screw translates the core.

7.2.5 Weight

A summary of the major component weights for the proposed variable-pitch fan system is presented in Table 7-II.

Table 7-II. Weight Summary - General Electric Variable-Pitch Fan System.

	Weight	
	kg	lb
Fan Disk	23.9	52.7
Blade Retention System	43.6	96.2
Thrust Bearing	10.4	23.0
Pinion Gear and Shims	3.7	8.2
Actuator Assembly	29.4	64.8
No-Back and Differential Gear	2.7	5.9
Brake Assembly/Feedback/Control Value	3.9	8.7
Actuator Support Housing	2.2	4.9
Total	119.8	264.4

7.3 HAMILTON STANDARD ACTUATION SYSTEM

The proposed Hamilton Standard variable-pitch fan actuation system is presented in Figure 7-7. Major components included in the system are the Beta Regulator Module (electro-hydraulic servovalve, hydraulic motor, and two linear variable differential transformers), flexible drive shaft, differential gear train, spring-type no-back, harmonic drive, cam, integral spindle and trunnions (blade actuation arms), and the fan rotor disk and drive core.

A schematic of the overall system is shown in Figure 7-8. An analog input command is given from the engine digital control to an electro-hydraulic servovalve. The servovalve motion directs high pressure oil to the hydraulic motor which drives a rotating flexible cable sending a pitch change command through the differential gear set to the no back; motion of the no back is sent through the harmonic and cam track to the blades. There is a fixed relationship between the turns of the hydraulic motor and the blade angle (beta) postion; thus the LVDT is driven by the hydraulic motor output providing a beta feedback to the digital control which closes the loop. The design description is separated into the following components.

1. Cam Drive Harmonic Actuator

    • Cam and Trunnion

    • Harmonic Drive

    • Spring Clutch (No-Back)

    • Diffential Gears

220
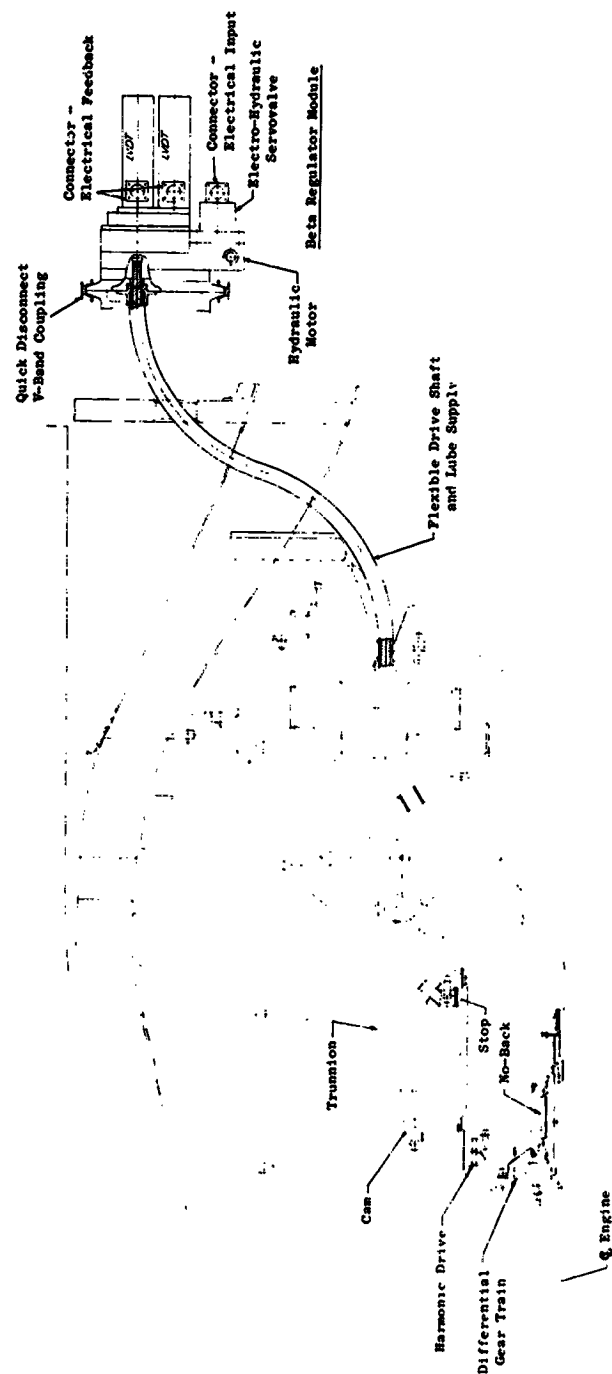
Figure 7-7. QCSEE Variable Pitch Actuation System.

Connector – Electrical Feedback

Connector – Electrical Input

Electro-Hydraulic Servovalve

Beta Regulator Module

Quick Disconnect V-Band Coupling

Hydraulic Motor

Flexible Drive Shaft and Lube Supply

Trunnion

Stop

No-Back

Cam

Harmonic Drive

Differential Gear Train

₵ Engine
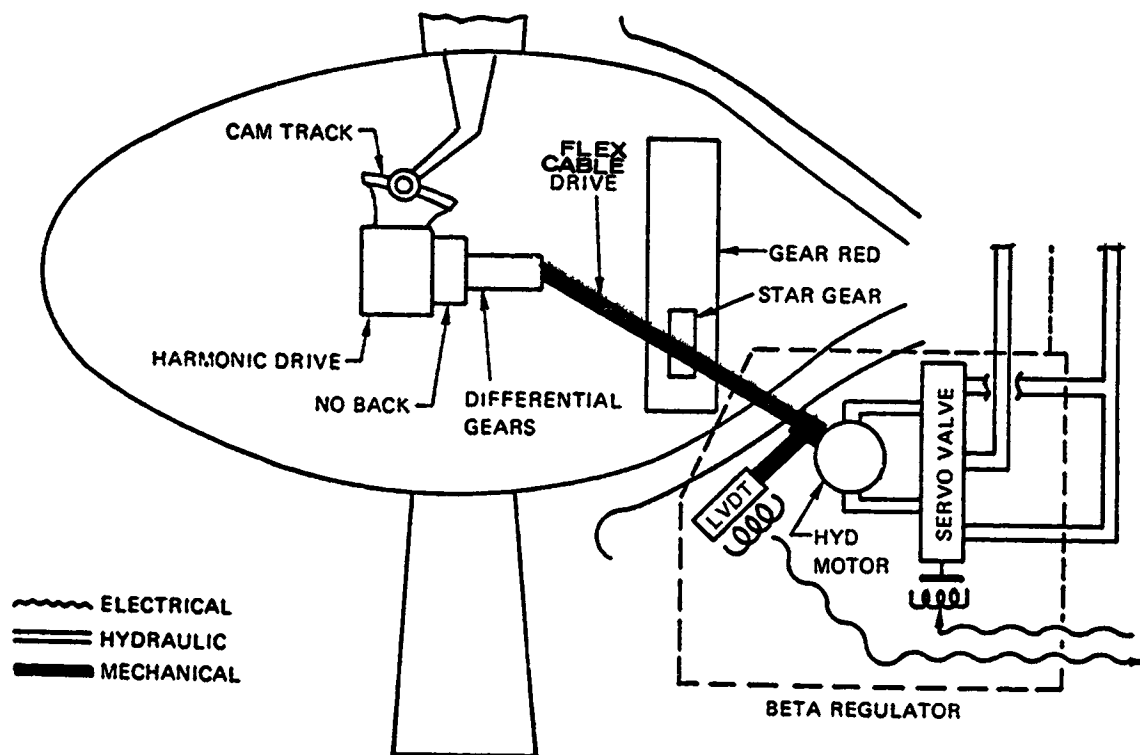
Figure 7-8. Hamilton Standard Actuation System Schematic.

2. Input Power

- Flex Cable Drive

- Beta Regulator (EHV, Hydraulic Motor, and Two LVDT's

7.3.1 Blade Trunnion and Roller

As illustrated in Figure 7-9, the blade torque is transmitted to the cam by a titanium trunnion. The trunnions collect blade torque for summation at the cam and reach from the large peripheral diameter of the disk to the smaller diameter of the cam. The ratio of trunnion-length-to-cam-radius has been optimized close to the point of minimum system weight. Based on the trade study, a ratio of 0.775 was chosen for the QCSEE application. Except in the area of the roller retention, the trunnion is stiffness designed in bending and balanced to minimize torsional deflection from the roller load in order to maximize blade angle accuracy. The roller retention area is stress limited for the bird strike condition at 1694.8 Nm (15,000 lb-in.). The trunnion and roller centrifugal twisting moment provides torque compensation for the blade mass twisting moment resulting in a lower harmonic output requirement.

The cam roller is through-hardened AISI 52100 steel chrome plated with a Purebon Molalloy (PBM-3) bushing and is crowned to eliminate end loading. Dry film lubrication of the roller and track has been selected in order to avoid dynamic oil seal at each blade trunnion. Molalloy is a compaction of refractory materials with molybdenum disulfide (MoS_2) and, based on testing at Sikorsky Aircraft, can meet the life requirement for this application. Wear life also appears to be further enhanced by break-in lubrication with grease.

The roller pin will be AMS 4340 steel with hard chrome plate for corrosion protection and wear resistance. The pin is press fit to the trunnion and is cross pinned. Rollers of similar proportions have been used extensively on Hamilton Standard propellers such as the 54H60 and the 33LF. The significant difference is in the use of dry film lube for the QCSEE application.

7.3.2 Cam Drive Harmonic Actuator

The pitch change actuator proposed consists of two assemblies; the harmonic drive actuator and blade drive cam, as described below.

Blade torsional loads are reacted by a trunnion and roller assembly which engages a spherical cam track. The cam track is mounted integrally with the output of a high ratio harmonic drive. This assembly is supported by an extension attached to the disk mounting bolt pattern. The harmonic is driven by the output of a planetary-type differential gear train which transmits the rotary input signal across the rotating boundary of the fan assembly. Pitch change power is provided by the pitch regulator module located in the fan cowl and is transmitted to the differential by a rotary flexible cable.
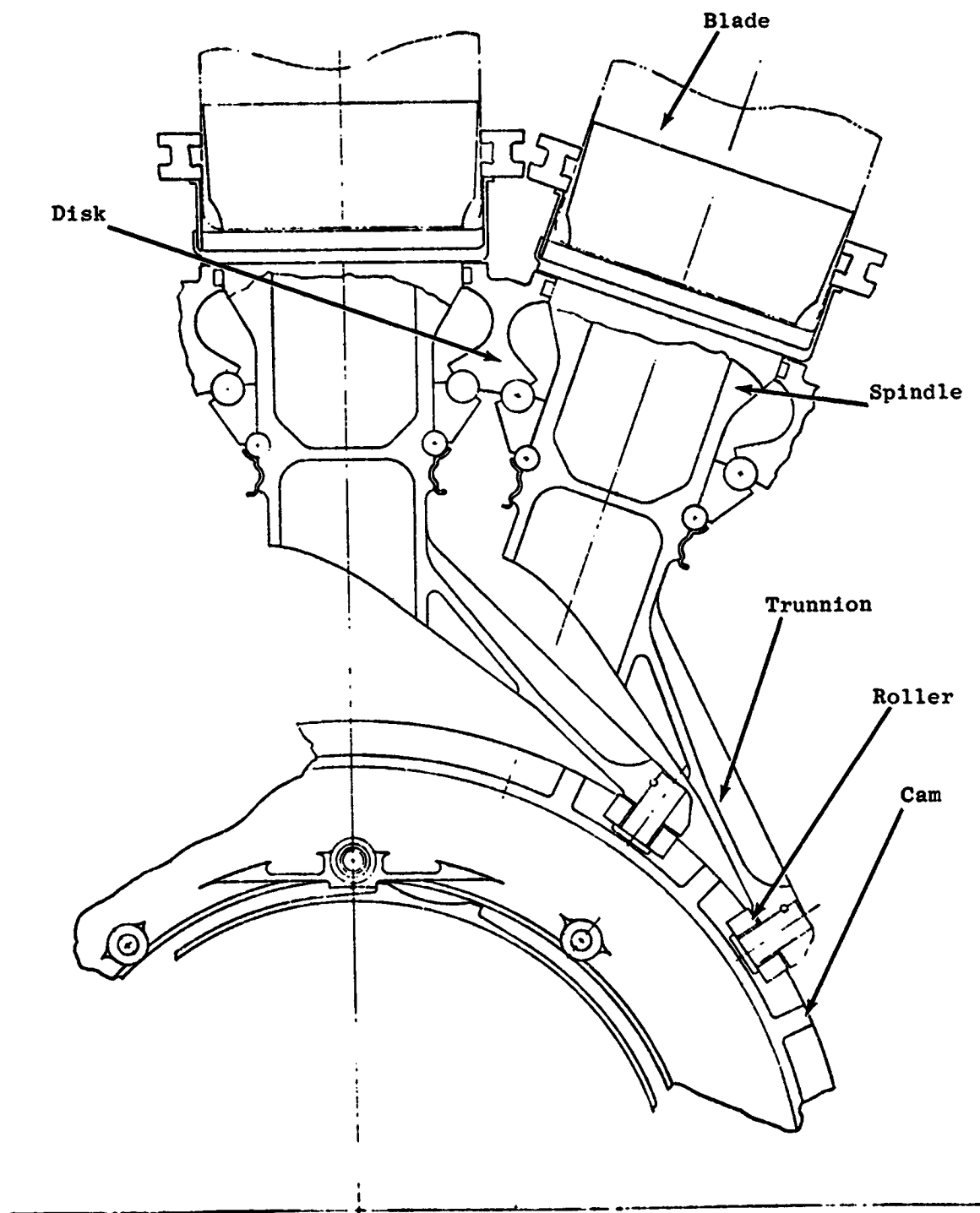
Figure 7-9. Blade Retention and Actuation System.

Blade aerodynamic and mass distribution moments defined by GE specification M50TF1623-S1 have been combined with Hamilton Standard's estimate of blade friction twisting moment (FTM) and the resulting total twisting moments have been plotted versus blade angle as shown on Figures 7-10 and 7-11. The FTM was calculated by a Hamilton Standard computer program using a centrifugal load of 284.7 kN (64,000 lb) and a ball bearing sliding coefficient of friction of 0.075. In addition, the blade twisting moments have been reduced by the counter-weighting effect of the blade trunnion. The maximum counterweight moment is 113 Nm (1000 lb-in.) toward open at a blade angle of -22 degrees when reversing through flat pitch and 84.75 Nm (750 lb/in.) toward close at an angle of -35 degrees when reversing through feather.

7.3.3 Cam

The cam provides a means for summing individual blade loads and, in addition, permits contouring to reduce the maximum torque required at the harmonic output. The cam roller tracks a spherical surface with the roller centerline always normal to the spherical surface. Thus, the roller remains parallel to the cam track similar to a bevel gear mesh. The cam material is 300M through hardened to 51 R_c minimum for surface durability and for high yield strength for the bird strike load. It is coated all over with Dow Corning 3400A per MIL-46010 (MoS$_2$ + epoxy binder) for lubrication and corrosion protection.

7.3.4 Harmonic Drive

Hamilton Standard has worked very closely with United Shoe Machinery (USM) Corporation on several aircraft applications of high-ratio rotary actuator harmonic drives. The latest of these was a development program to determine the maximum operating, maximum holding, and life characteristics as related to circular spline stiffness for the SST leading edge flap system. In addition, USM has done extensive development testing and analytical modeling to determine the critical design requirement for harmonic drives. USM has built and developed a three-lobed harmonic drive for the Bell X-22A Duct rotation system which is of similar size, load, and critical application to the proposed design for the QCSEE pitch-change actuator. Another critical aerospace application is the wheel drive for the Lunar Rover Vehicle.

The harmonic drive consists of three basic elements: the wave generator, the flexspline, and the circular spline. The three-lobed wave generator is ellipsoidal in shape and is surrounded by a ball bearing. A flexing element, called the flexspline, is in the form of a thin-walled cylinder with a set of external gear teeth. The flexspline is deflected into the ellipsoidal shape by the wave generator. The circular spline is a rigid circular ring with internal gear teeth which are in intimate contact with the ellipsoidal-shaped external gear teeth of the flexspline. The number of gear teeth on the flexspline differs from the number of teeth on the circular spline. Rotation of the wave generator causes the circular spline to clock relative to the flexspline producing the desired differential movement. In the proposed variable-pitch system (Figure 7-7), the opposite end of the flexspline cylinder (shown
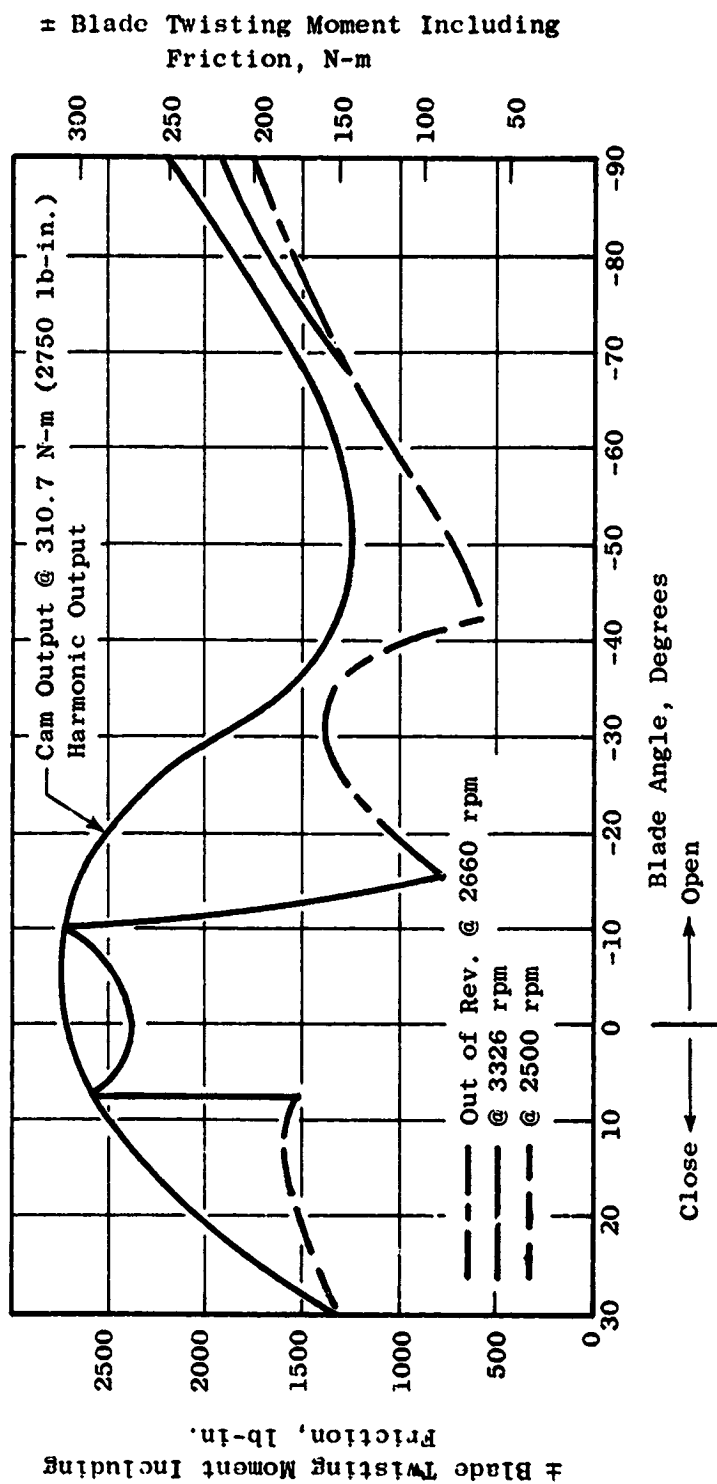
Figure 7-10. Cam Output Characteristics Reverse Through Feather.

226

± Blade Twisting Moment, N-m
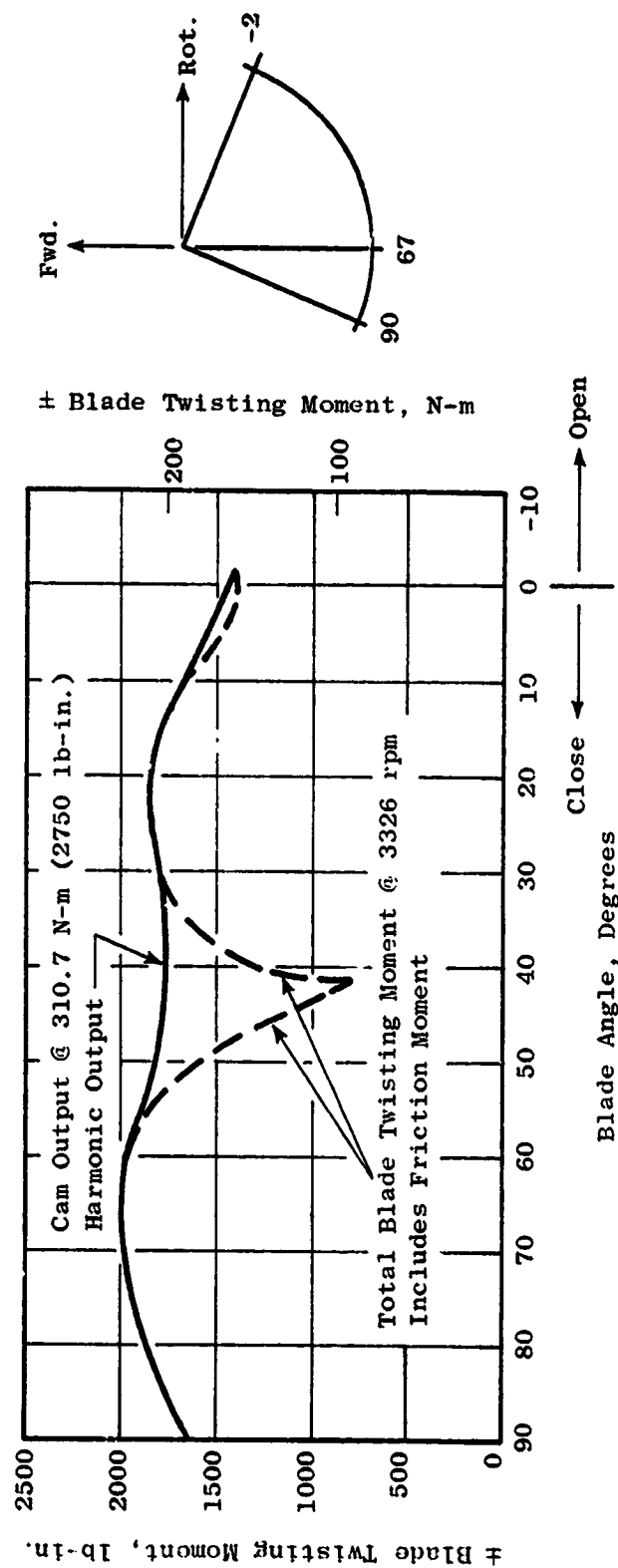
Figure 7-11. Cam Output Characteristics Reverse Through Flat Pitch.

Cam Output @ 310.7 N-m (2750 lb-in.)
Harmonic Output

Total Blade Twisting Moment @ 3326 rpm
Includes Friction Moment

Blade Angle, Degrees

Close ← → Open

± Blade Twisting Moment, lb-in.
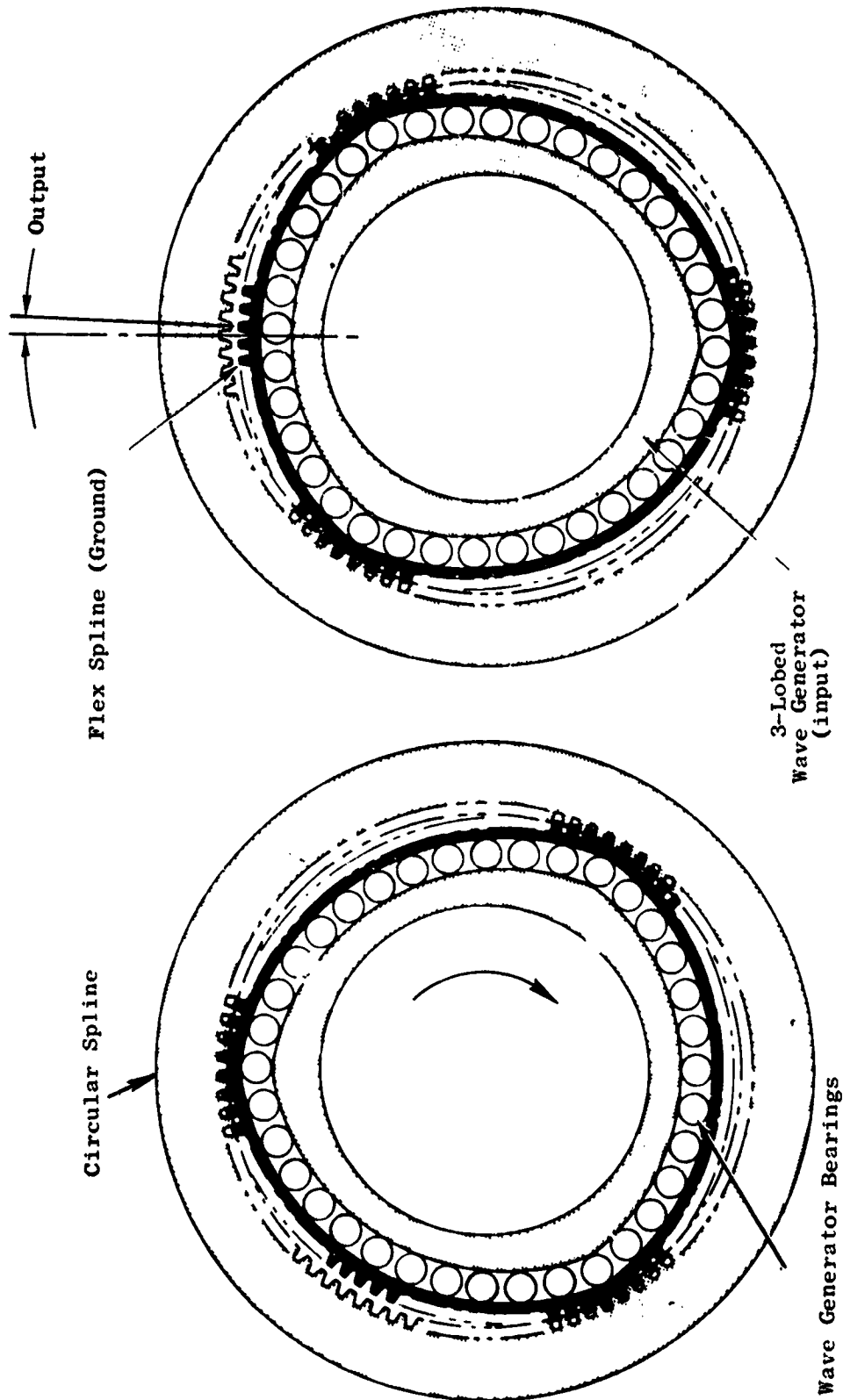
Figure 7-12. Harmonic Drive Schematic.

Output

Flex Spline (Ground)

3-Lobed
Wave Generator
(input)

Circular Spline

Wave Generator Bearings

228

below and to the right of the trunnion roller) is splined to the fan rotor. Movement of the harmonic drive wave generator therefore causes the cam to clock relative to the fan rotor.

In the proposed design, the flexspline and circular spline are vacuum melted AMS 4340 alloy steel at 35-39 R_c. The wave generator is AMS 4150 steel.

In the basic harmonic drive configuration, the wave generator is the input element and the output is the flexspline. The reduction ratio for this drive is determined by the following formula:

$$\text{Ratio} = \frac{N_C}{N_F - N_C}$$

where N_F is the number of teeth on the flexspline and N_C is the number of teeth on the circular spline, three more than N_F (as applied to the proposed design this would represent a ratio of 230:1).

It is convenient from a comparative standpoint to say that the output capacity of the harmonic drive follows the relationship: $T = KD^3$, where

T = Torque capacity, Nm (lb-in.)
D = Pitch diameter of the output member, cm (in.)
K = Torque constant, I/D^3

Using this relationship it is possible to compare designs of similar characteristics for overall capacity. These data are shown in Table 7-III.

In the proposed QCSEE design, as in the Bell X22A duct rotation system, a three-lobed wave generator is used which results in a lighter design than a two-lobed unit since the load is reacted at three points rather than two. The resultant lower separating forces, stiffer rings, and improved tooth meshing combine to minimize weight. The principal concern in harmonic drive reliability is fatigue failure of the flexspline and/or the wave generator bearings. Thus, designs for high reliability are based on configurations which minimize these stress levels.

Table 7-III. Harmonic Drive Application - Design Characteristics.						
Unit	No. of Lobes	Design Condition	Gear Ratio	Diameter		K
				(mm)	(in.)	
Bell X-22A Duct Rotation	3	Max. Operating	300:1	318.5	12.54	92
Saturn Ground Transporter	2	Infinite Life	-	362.0	14.25	104
SST Leading Edge Flap	3	Max. Operating	176:1	101.6	4.0	93
HSD VC-82S	3	Finite Life	260:1	164.1	6.46	164
HSD Test Unit	3	Norm Operating	226:1	254	10.00	57
HSD Test Unit	3	Max. Operating	226:1	254	10.00	108
GE QCSEE	3	Max. Operating	230:1	208.3	8.20	90
GE QCSEE	3	Limit Operating	230:1	208.3	8.20	135

Infinite flexspline fatigue life is based upon stress levels which fall below the limiting line on a modified Goodman diagram for the material used. These stresses are the result of the combined effects of deflection associated stress (which is related to the change of curvature of the flexspline) plus those arising from the output torque and those due to the "g" field. The deflection stresses are directly proportional to the bed thickness under the spline while the torque stress is inversely proportional to the bed thickness. The bed thickness is optimized by combining these stresses, with the proper stress concentration factor, and minimizing their values on the Goodman diagram. The stress due to the centrifugal field is primarily a hoop stress. This "g" field stress is added as a mean and also as an increment to the cyclic stress of the flexspline due to the slight increase in the flexspline deflection.

Experience has shown that when the above method is used no failures of the flexspline have resulted.

In addition to the flexspline load stress and life considerations, it is desirable that a particular physical relationship of the spline teeth be main-tained at the major axis or point of tooth engagement to minimize tooth wear. This relationship consists of maintaining a coincident pitch line contact of the teeth within $\pm$ 5% of the theoretical flexspline defleciton when the system is under normal load conditions. Under these conditions, the sliding of engaging or disengaging teeth approaches zero and the wear rate is negligible. This pitch line concept is accomplished by anticipating the extent of the tooth separation due to deflection and centrifugal load of the parts by analysis. The tooth mesh design is then over engaged (by providing a small amount of backlash) to the extent of this deflection. Accordingly, under load and "g" field the resultant forces provide tooth contact at the correct pitch line. This is a proven technique which is employed in varying degrees with all harmonic drive transmissions.

Hamilton Standard has been testing a large harmonic drive unit designed for a fan pitch change actuator for over a year. A comparison of this test unit with the proposed design is presented in Table 7-IV.

Table 7-IV. Comparison of Harmonic Drives.		
	HS Test Unit	Proposed Unit
Pitch Diameter	254 mm (10 inch)	208.3 mm (8.2 inch)
Ratio	226:1	230:1
Pressure Angle	30°	20°
Design Loads		
Max. Operating	12,202 Nm (108,000 in.-lb)	5592.7 Nm (49,500 in.-lb)
Design K Values (1)		
Cubic Mean	57	70
Max. Operating	108	90
(1) Load Capacity = K (Pitch Dia.)^3		

Extensive testing and field experience has demonstrated several important points regarding the wave generator ball bearing.

1. The normal mode of bearing failure in harmonic drives is identical to that in any normally applied ball bearing; it consists of a fatigue spall on the inner raceway.

2. The load capacity and resultant life at any load are in agreement with that of conventional round ball bearings provided that the resultant loads due to deflecting both the flexspline and the bearing outer race are considered as well as those loads imposed from transmitting torque and due to centrifugal effects on balls. Rotational bearing loads are based on relating the per ball load to an equivalent radial load as recommended by Dr. Palmgren in Ball and Roller Bearing Engineering.

7.3.5 Spring Clutch

A bidirectional spring clutch or "no back" is provided between the differential gearing and the harmonic drive. This is to hold blade angle at the last called for position whenever input torque is removed. This device consists of a self-energizing, silver-plated AMS 6350 steel spring which is in contact with the inner surface of the AMS 6419 steel housing, the input and output shafts, and the necessary couplings and bearings.

Figure 7-13 schematically illustrates the working of the clutch. View A illustrates the device holding a fixed blade angle. The blade loads are transmitted to ground (housing) via the spring. View B shows the input raising the load. Under this condition the input shaft contacts the spring sufficiently for the load to drive against the spring and produce a blade angle reduction.

When changing blade angle in the same direction as the load (lowering the load), all of the energy of the change is dissipated in the clutch. The clutch then holds the blades until the blades are moved in a raising load direction. Due to the short duty cyle, the total heat rise is low and contained in the mass of the clutch. Principals of operation, including control of surface temperature, have been successfully demonstrated by Hamilton Standard in the production no-back design for the F14 wing sweep actuator. In addition, a no-back design of similar size and loads was successfully developed for the SST Leading Edge Flap system.

7.3.6 Differential Gearing

A planetary differential gear mesh is utilized to cross the rotating boundary of the fan. This unit is similar to those designed and developed by Hamilton Standard for the 54H60 prop (C120), AH56A, and NC400.

The differential has a ratio of 4.25 and is composed of a grounded sun gear, an input sun gear, three pairs of planet gears on a bearing support carrier, a reference speed ring gear, and a second ring gear connected to the no-back. The speed of the carrier is determined by the reference speed ring gear and the grounded sun gear. With no pitch change input the output ring gear must rotate

Maintaining Blade Angle

Input Drive

Housing
(Ground)

Spring

A

Increasing Blade Angle

Input Drive

Load

Spring

Housing
(Ground)

B

Decreasing Blade Angle

Input Drive

Load

Spring

C
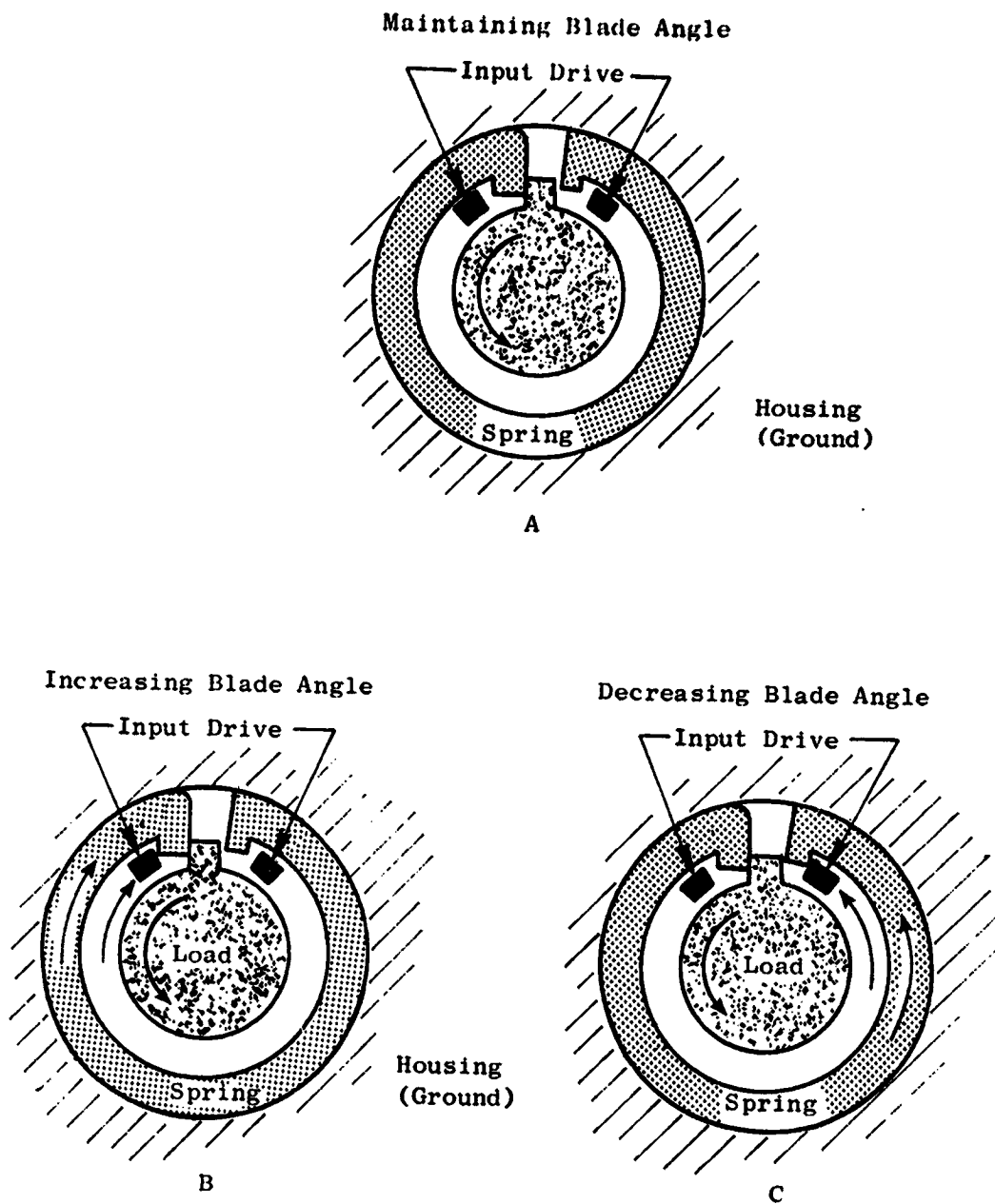
Figure 7-13. Spring Clutch (No-Back) Schematic.

at fan speed. Rotation of the input sun gear will cause the output ring to either advance or recede with respect to fan speed. This change in output is the input to the no-back.

The differential gears, which are made of vacuum melted AMS 6265 with carburized and hardened teeth to 60 R_c, are capable of running at limit load for infinite life with a dynamic factor of 2.5. The gears are mounted on needle bearings and are spray lubricated.

7.3.7 Blade Pitch Stops

Fixed limit stops are located between the cam and the support housing. Three lugs on the cam contact three mating lugs grounded to the disk.

7.3.8 Input Shafting

The interconnection between the powering system and the pitch change actuator is a rotary flexible cable. An operating speed of 17,000 rpm was selected to minimize the cable torque and to improve blade angle accuracy. The core has a diameter of 8.74 mm (0.344 in.) and is supported by a Teflon-lined casing. It is designed for stiffness and has a balanced winding for control of wind-up in both directions. The flexible core and casing is mounted within a rigid conduit which is routed through the engine planetary gears and connected through a sealed joint with the hydraulic motor housing. Motor leakage oil supplemented by engine lubrication oil is directed through the casing for lubrication of the core and casing. The core and casing can be removed and replaced as a unit by removing the regulator assembly.

The shaft sizing is a balance of bend radius 190.5 mm (7.5 in. min.) based on path configuration, maximum core diameter for stiffness and accuracy, and dynamic inertia loading from misrigging and contacting the fixed stops in the actuator. This balance provides a 9.53 mm (0.375 in.) diameter core which will have a maximum wind-up in either direction of 65.6°/m (20°/ft) at maximum operating torque of 9.2 Nm (82 lb-in.) and can withstand a dynamic impact inlet torque of 24.86 Nm (220 lb-in.) without permanent deformation.

7.3.9 Beta Regulator

The pitch change command and blade angle feedback is a compact unit referred to as the beta regulator and is located in a readily accessible area in the engine core cowling. A simple schematic is shown on Figure 7-14. A blade angle change request is sent from the control to the EHV. Movement of the servovalve directs supply pressure either into the increase or decrease pitch line to the hydraulic motor which provides an input to the pitch change actuator. Since there is a known relationship between the hydraulic motor angular position and blade angle, the rotation of the motor is sensed by the dual LVDT which provides a blade angle position feedback to the control.
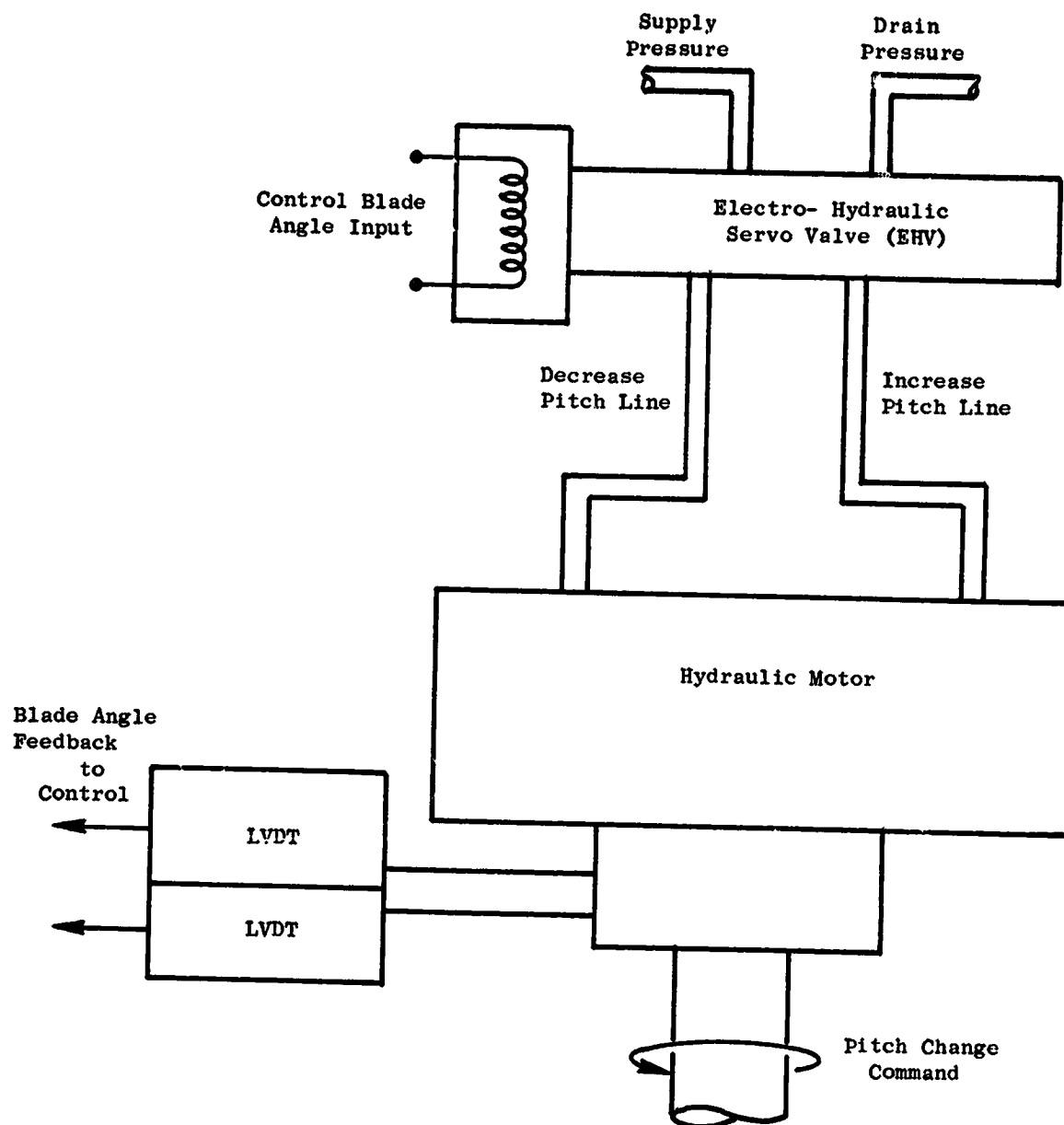
Figure 7-14. Blade Angle or Beta Regulator.

7.3.10 Hydraulic Motor

The hydraulic motor is a gear-type motor similar in design to one used by Hamilton Standard in its VC82S propeller control. It is of sandwich construction with steel gears and centerbody and either steel or aluminum end housings. The gears are floating for end face alignment and control of end clearance. The gear shafts are mounted on needle bearings for high running efficiency and low breakout torque. The motor is designed for 82.73 N/m^2 (1200 psi) across the motor at 75 deg/sec pitch change rate. Stall pressure is 117.20 N/m^2 (1700 psi), and the no-load speed is equivalent to 135 deg/sec pitch change rate.

7.3.11 LVDT and EHV

The EHV is a two-stage unit mounted integral with the hydraulic motor housing.

The LVDT drive mechanism is a screw thread device which is driven by the hydraulic motor shafts. The proposed design would contain redundant LVDT's (two units) which would be mechanically linked to the shaft which is indicative of β angle. The mechanical stroke input to the LVDT would be designed to be 50.8 mm (2 in.). For this stroke, the LVDT case length would be about 1106 mm (6.6 in.) and is required to obtain the specified ± 0.25% of full-scale linearity. In the demonstration program, the particular positioning tolerances for the LVDT's could be eliminated by proper calibration techniques as well as minimizing any large thermal shaft errors. For a production application the unit-to-unit scale shift and thermal shifts can be removed by incorporating individual scale trim and thermal trim resistors within the LVDT case.

7.3.12 Lubrication

The differential gearing, no-back, and harmonic drive are lubricated continuously by the gearbox lubrication system. Oil from the EHV return pressure (lube pressure) is routed through the flexible cable casing to the input drive quills and to the differential and to the harmonic wave generator plug where it is directed between the duplex bearings. Oil flow from one bearing flows through the harmonic fixed spline. The dynamic seal between the harmonic and the support tube is a graphite-filled Omni seal similar in design to that used in the SST leading edge flap system. The oil then flows centrifugally back to the gearbox.

7.3.13 Accuracy

The components which have a significant stiffness effect on the blade angle accuracy in going from no load to full load are summarized as follows:

Trunnion	± 0.15 deg. blade angle
Harmonic Drive	± 0.10
Flexible shaft	± 0.10
	± 0.35

Note that the high gear ratio provides a micrometer relationship between input and actual blade angle since the input turns 755° for every degree of blade angle.

As mentioned earlier, the trunnion is designed for minimum deflection, and the flexible shaft is a balanced design with low deflection. Careful attention will be given to the design of the harmonic to ensure proper preloading of the bearings for stiffness. In addition, close control of tolerances and fits will be required as well as optimizing the stiffness of the wave generator and the circular spline. Improved effective accuracy can be obtained by adding compensation to the electronic control equal to the mean load for each operating condition. By this method it is felt that the desired accuracy of ± 0.25 degrees can be met.

7.3.14 Test Hardware Consideration

To provide capability to reverse through flat pitch and feather during the development program, two options are available. The first concept has a blade spindle and cam follower trunnion with a constant-torque cam design for reversing through feather. For reversing through flat pitch, a mirror image of this cam would then be used in conjunction with rotating the blade 180 degress at the spindle trunnion interface.

The second approach is to use one cam for both directions and provide a splined joint between the trunnion and the blade spindle which permits re-indexing between the blade and the pitch change mechanism.

7.3.15 Weight

A summary of the major component weights for the proposed variable pitch fan system is presented in Table 7-V.

The weight breakdown in Table 7-V is for a reverse through flat pitch actuator; the reverse through feather has a longer stroke or increase blade angle travel and therefore weighs 2.3 kg (5 lb) more.

The bird strike capacity of the pitch change mechanism is 11,000 in-lbs twisting moment and it is estimated that a 1.7 kg (2.4 lb) increase in weight would be required to increase this to 1695 Nm (15,000 lb-in.). The disk and retention have a bird strike impact moment capacity of 9040 Nm (80,000 lb-in.).

The engine weight to adapt to the system arrangement selected involves slight increases in weight to the power shaft, lube pump, hydraulic lines and the addition of an off-load solenoid. This penalty is estimated at 1.4 kg (3.0 lb.).

236

Table 7-V. Weight Summary - Hamilton Standard Variable Pitch Fan System.

	kg	(lb)	kg	(lb)
Disk and Drive Cone	50.3	(111.0)		
Retention Spindle and Blade Locks	43.8	(96.5)		
Total Disk and Retention			94.1	(207.5)
Trunnions and Rollers	7.3	(16.1)		
Cam, Stops, Support, Brg	9.6	(21.2)		
Harmonic Drive	6.2	(13.6)		
Spring Clutch - No Back	1.2	(2.6)		
Differential Gear	1.4	(3.0)		
Total Actuator			25.7	(56.5)
Flexible Drive Shaft			2.0	(4.5)
Hydraulic Motor	1.8	(4.0)		
LVDT (2) + drive	0.7	(1.6)		
EHSV	0.9	(2.1)		
Manifold	0.3	(0.6)		
Mounting Flanges Clamp	0.5	(1.2)		
	4.2	(9.5)	4.2	(9.5)
			126.0	(278.0)

SECTION 8.0

FAN ROTOR MECHANICAL DESIGN

8.1 SUMMARY

An under-the-wing (UTW) and an over-the-wing (OTW) fan rotor will be built and tested as part of the NASA QCSEE program. The UTW fan is a variable-pitch design with 18 composite fan blades. This concept, which includes full reverse thrust capability, is expected to offer significant advantages to a high-bypass fan system including:

- Lighter weight through the use of composite fan blades and by eliminating the heavy, large diameter thrust reverser

- Faster thrust response

- Improved off-design SFC

- Reduced off-design noise generation.

Blade solidity has been established at less than unity to permit a detailed investigation of the reverse pitch mode through both flat pitch and stall. The flowpath has been contoured to maintain tight blade tip and hub clearances throughout the blade actuation range. All rotor components for the UTW fan rotor will be of a flight-weight design.

The OTW fan employs 28 fixed-pitch fan blades. A flight version of the design would use composite fan blades, but titanium fan blades will be used in the experimental fan as a cost saving measure. The conceptual design with composite blades was used to establish the number of fan blades, and in conjunction with the aerodynamic design, the blade airfoil shape. The metal blades require a larger fan disk rim than would be required for composite blades. The fan disk support cone and the remaining fan components on the experimental engine will be of flight design.

Design practices and rotor material selections will be consistent with flight designed fan rotors for both the UTW and the OTW. This includes consideration for fan LCF life and for such FAA flight requirements as burst speed margin and bird strike capability.

8.2 UTW FAN ROTOR

The UTW fan rotor has 18 composite blades mounted on a disk in a manner permitting changes in the pitch of the blades. This rotor is shown in Figure 8-1. The blades will be fabricated from a hybrid combination of PRD-49, graphite, boron, and S-Glass fibers in order to provide the desired combination of bird impact resistance and blade stiffness. The blades incorporate a metal foil leading edge to provide additional FOD and erosion protection. The solidity of the blades is slightly less than unity along the entire blade span to allow

238
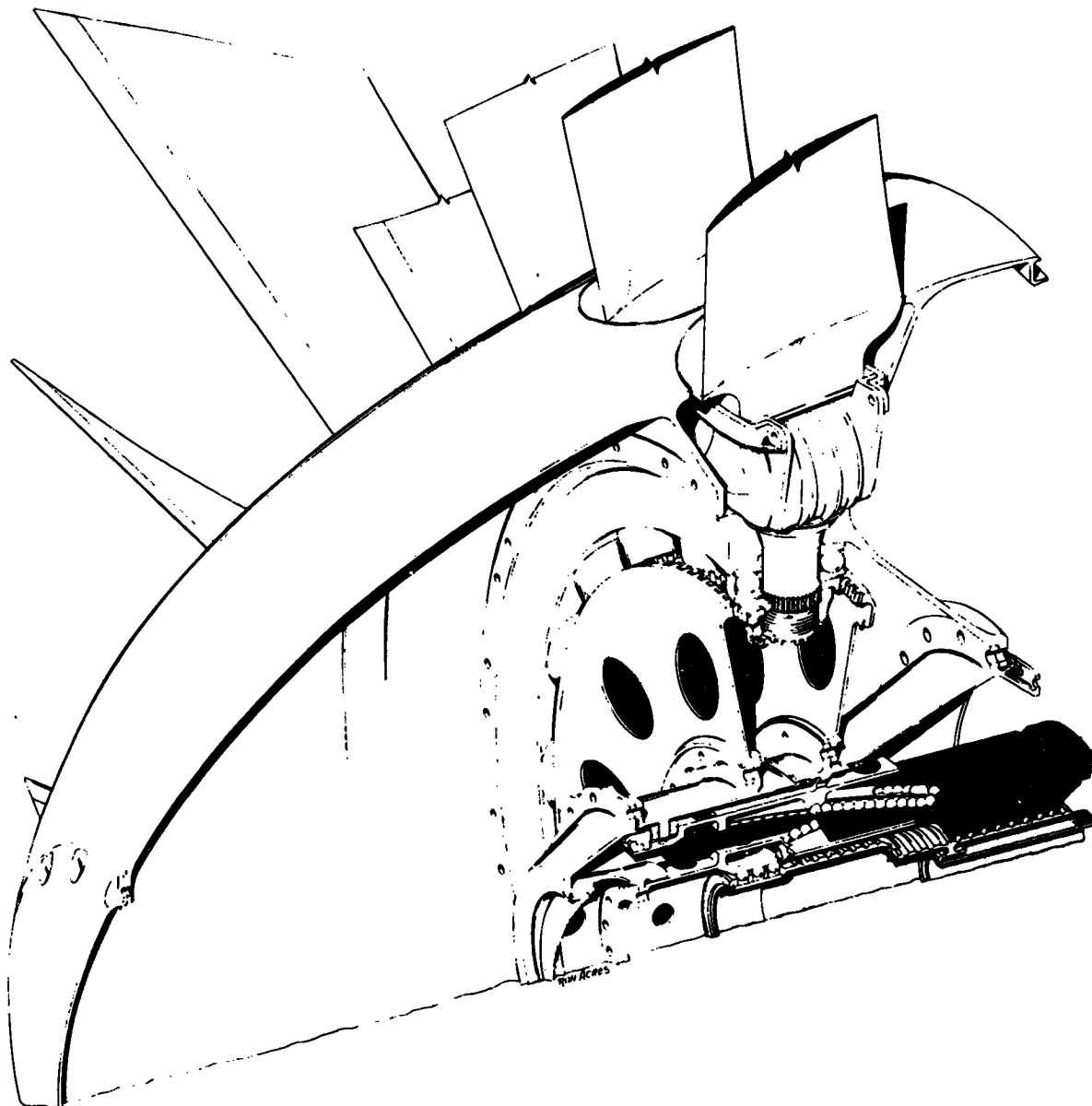
Figure 8-1. UTW Variable Pitch Fan.

the blades to clear during actuation to reverse pitch through flat pitch. There are no mechanical restrictions on being able to reverse pitch the blades through either flat pitch or stall.

In a concept similar to that used on the CF6-50 fan, balance weights are accessible in the fan spinner, and field balance of the fan is possible without removing the spinner. Ease of maintenance has also been considered in the design of the other rotor components.

After removal of the spinner, the blades can be individually removed and replaced without disassembly of the blade trunnion. Access holes in the flange of the aft rotating flowpath permit removal of the fan rotor, blade actuator, and the reduction gear as a complete subassembly.

The centrifugal force for each blade and trunnion is carried by a single-row ball thrust bearing. This bearing has a full complement of balls to reduce the per-ball loading. The race has a much higher conformance than is standard for thrust bearings because of its highly loaded, intermittently actuated environment. The bearing is grease lubricated, with a cup shield completely covering the upper race and most of the lower race, thus preventing the grease from leaking out under high radial "g" loads. This concept was successfully demonstrated on General Electric's reverse pitch fan. Grease tests have been completed that identified a grease for the QCSEE bearing which will not permit separation of the oil from the thickening base or extreme pressure additives after extended running in a centrifugal field higher than those planned for the UTW fan rotor. Fail-safe lubrication is accomplished by a tungsten disulfide coating applied to the balls and races. With this coating and under the loading planned, this bearing is capable of operating 9000 engine hours after loss of lubricant with only a slight increase in coefficient of friction and negligible wear.

Secondary and vibratory loads from the trunnion are resisted by dry thrust and journal bearings located in the OD of the fan disk.

8.2.1 Composite Fan Blades

Design Considerations

Aerodynamic design of the UTW fan blade is presented in Section 6.2.6. Mechanical design considerations for the UTW fan blade were primarily a result of the requirement for variable pitch operation through both the stall and flat pitch direction. The need for a composite blade was established early in the preliminary design phase for the following reasons.

- A practical metallic blade meeting aeromechanical requirements would require solidities of greater than 1.0 in the root which would restrict the variable-pitch operation of the blade to reverse pitch in only one direction.

- Even with a higher root solidity the metallic blade design and resulting disk and actuation system were extremely heavy and would

240

have resulted in a low reliability, high bearing loads, and high actuation loads.

The preliminary design of the composite blade was based primarily on the aero-mechanical and bird impact requirements. Consideration was given to several hybrid materials and layup configurations which would provide the required blade stiffness and still maintain the capability to absorb the impact of a 1.8 kg (4 lb) bird without root failure. To reinforce the impact capability of the hybrid blade several dovetail designs were evaluated aimed at providing more root flexibility during impact.

Mechanical Design Requirements

The design requirements for the UTW composite fan blade were established to provide realistic long life operation of a flight engine based on the typical mission shown in Table 2-I. These preliminary design requirements are listed as follows.

- Design Mechanical Speeds

  - 100% mechanical design - 3244 rpm

  - 100% SLS hot day takeoff - 3143 rpm

  - Maximum steady-state speed - 3326 rpm

  - Maximum design overspeed - 3614 rpm

  - Maximum burst speed - 141%

- Design Life & Cycles

  - 36,000 hours

  - 48,000 cycles

  - 1000 ground checkout cycles, full power

- Mechanical Requirements

  - Blades must operate through flat pitch and stall pitch without aeromechanical problems.

  - Blades must satisfy FAA bird impact requirements as follows:

Bird	Size	Number
Starling	0.08-0.11 kg (3-4 oz)	54
Pigeon	0.67 kg (1-1/2 lb)	9
Duck	1.8 kg (4 lb)	1

- Blades shall be individually replaceable without major teardown

- Blade untwist will be factored into airfoil configuration.

- Stresses shall be within Goodman Diagram with sufficient vibratory margin.

- First flex frequency shall cross 2/rev in low speed range and have 15% margin over 1/rev at 115% speed.

- Blade leading edge protection will be kept within aero airfoil limits.

Of these requirements, the first two are of prime importance. Successful operation of the experimental engine hinges to a great degree on having a rugged blade which can withstand reverse pitch operation and other inlet disturbances including crosswind testing. The bird impact requirements are important in that the successful application of composite blades to short-haul aircraft necessitates adequate resistance to foreign objects found in the short-haul environment.

Aerodynamic Blade Parameters

A summary of the aero blade parameters is presented in Table 8-I. The low root solidity of 0.98 is required for reverse pitch operation. Except for the large tip chord (high blade flare) the blade length, thickness, and twist dimensions are similar to previous composite blades which have undergone extensive development and proof testing.

Blade Configuration

The blade molded configuration consists of a solid composite airfoil and a straight bell-shaped composite dovetail. The dovetail is undercut at the leading edge and trailing edge to reduce local stresses and to permit better transitioning of the cambered airfoil section into the straight dovetail.

The airfoil definition is described by 15 radially spaced airfoil cross sections which are stacked on a common axis. The dovetail axial centerline is offset from the stacking axis by 0.254 cm (0.1 in.) to provide a smooth airfoil-to-dovetail transition. The molded blade drawing, as shown in Figure 8-2 provides a reduced leading edge thickness to allow a final coating of wire mesh/nickel plate for leading edge protection. The blade leading edge protection is shown on the finished blade drawing (see Figure 8-3).

Blade Layup/Material Selection

The material selection and ply arrangement for the UTW hybrid composite blade is based on previous development efforts conducted by General Electric and sponsored by NASA under contract NAS 3-16777. This work led to the
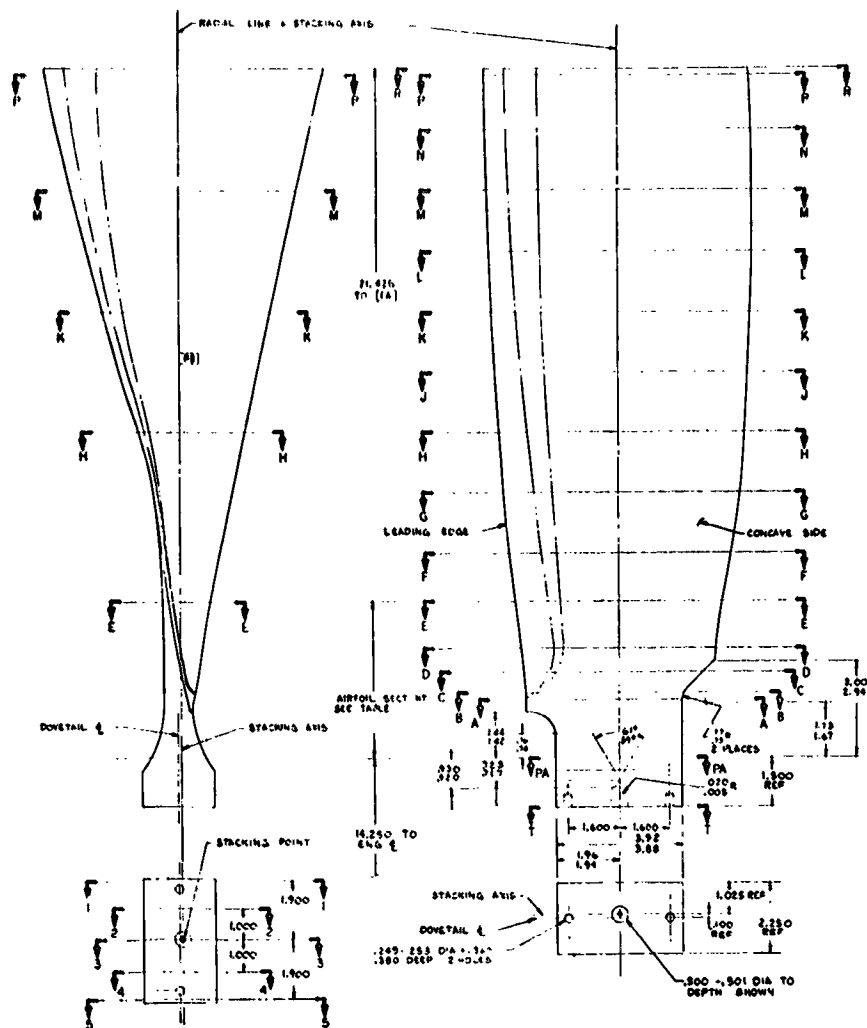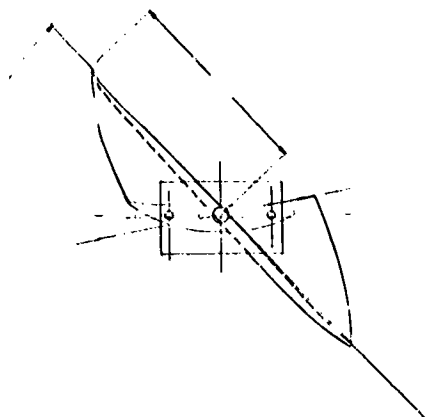
242

TYPICAL SECT THRU DOVETAIL
BASIC DIMENSIONS

CONTOUR LIMITS TYPICAL

SECT D-D thru L-L

SECT M-M, N-N, P-P & R-R
DEFINITION OF TANGENT LINE OTHERWISE
SAME AS SECTS D-D thru L-L

Figure 8-2. QCSEE Stage I Molded Fan

⋮E Stage I Molded Fan Blade.

Figure 8-3. QCSEE Fa

244

FOLDOUT FRAME
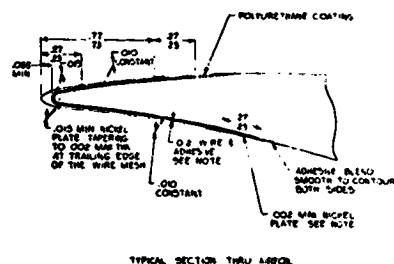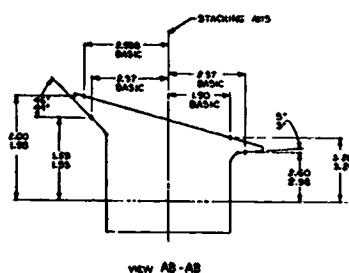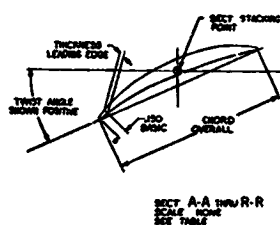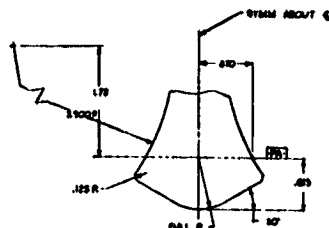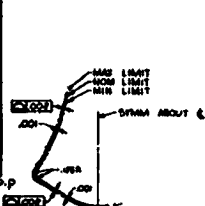
Figure 8-3. QCSEE Fan Blade.

Table 8-I. QCSEE UTW Composite Blade Preliminary
Design Summary.

Aero Definition

Tip Speed	298 m/sec (978 ft/sec)
Tip Diameter	180 cm (71 in.)
Radius Ratio	0.452
Number of Blades	18
Bypass Pressure Ratio	1.27 Takeoff
Aspect Ratio	2.11
Tip Chord	30.3 cm (11.91 in.)
Root Chord	14.8 cm (5.82 in.)
T_M Root	1.92 cm (0.076 in.)
T_M Tip	0.91 cm (0.036 in.)
Root Camber	66.2°
Total Twist	45°
Solidity	
Tip	0.95
Root	0.98
Angle Change from Forward to Reverse	
Through Flat Pitch	85°
Through Stall	90°

selection of a combination of fibers in a single blade to provide the proper frequency response and bird impact characteristics to satisfy STOL engine conditions. Figure 8-4 shows the general arrangement of the plies in the QCSEE UTW composite blade. The flex root surface plies in the lower region of the blade contain S-glass fibers. These plies being near the surface and having relatively low bending stiffness and high tensile strength provide higher strain-to-failure characteristics thereby allowing the blade to absorb large bird impact loading without the classic root failure that usually accompanies brittle composite materials. Torsional stiffening plies in the airfoil region of the blade are oriented at $\pm 45°$ to provide the shear modulus required for a high first torsion frequency. These plies will contain fibers of graphite and/or boron depending on the measured frequency characteristics and experimental FOD resistance to be obtained in the several preliminary blades. Plies of Kevlar 49 will be interspersed throughout the rest of the blade with the majority of them being in the longitudinal direction of the blade. Several of the Kevlar plies in the tip region of the blade will be oriented at 90° to the longitudinal axis to provide chordwise strength and stiffness to the blade for local impact improvement.

The resin system being used in this program is a product of the 3M Company and is designated as PR288. This is a resin system that has proven satisfactory for the needs of advanced composite blading. Some of its unique characteristics in the prepreg form are:

- Has consistent processing characteristics

- Can be prepregged with many different fibers including hybrids

- Uniform prepreg thickness and resin content.

Typical properties of the PR288/AU prepreg are shown in Table 8-II. Material properties for several fiber composite prepregs are shown in Table 8-III. The basic ply layup arrangement and fiber orientation for the OCSEE preliminary blade is shown in Figure 8-5. The graphite/Kevlar system is preferred from the standpoint of bird impact and cost; however, it may be necessary to use some boron plies to achieve the desired first torsion frequency.

Blade Vibration Analysis

Blade "instability" or "limit cycle vibration" can be a problem on fans. It is characterized by a high amplitude vibration in a single mode (normally the first flexural or torsional mode) at a nonintegral per-rev frequency. It is not one of the classical airfoil flutter cases and is apparently confined to cascades. Because of the nonlinearity in the aerodynamics involved, it has resisted practical solutions by solely theoretical means. Accordingly, General Electric has adopted a semiempirical "reduced velocity" approach for limit cycle avoidance. Reduced velocity, V_R, gives a measure of a blade's stability against self excited vibration. This parameter is defined as

$$V_R = \frac{W}{bf_t}$$

246
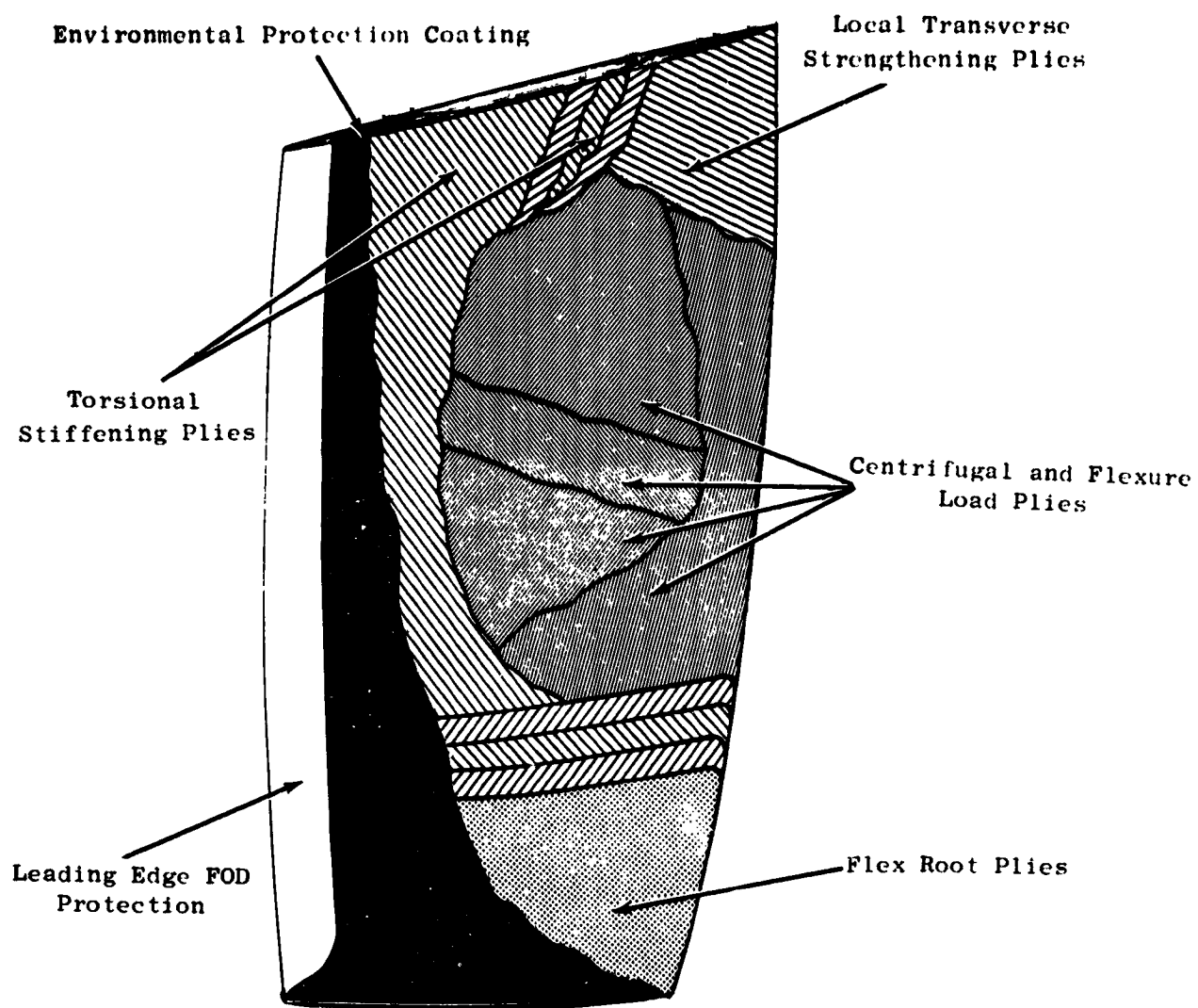
Figure 8-4. QCSEE Composite Blade.

Table 8-II. PR288/AU Prepreg Properties.

Property	PR288/AU
Supplier	3M
Process	Film – Cont. Tape
Cure Schedule	2.5 hrs at 129° C (265° F)
Postcure Schedule	4 hrs at 135° C (275° F)
Flex. Strength/Elast. Mod./Short Beam Shear	
Room Temp	193/11.9/8.0 kN/cm^2(280/17.2/ 11.6 ksi)
121° C(250° F)	138 /11.6/5.2 kN/cm^2(200/16.8/ 7.5 ksi)
Charpy Impact	21.2 J (15.0 ft-lb)
Fiber Volume, %	59.8
Sp. Gr., g/cc	1.58
Void Content, %	0.0
Cost per kg (lb)	$232 ($105)

248

Table 8-III. Composite Material Properties.

	PR288 AU	PR288 Boron	PR288 S-Glass	PR288 Kevlar 49	Hybrids PR288 AU 20% S-Glass	Hybrids PR288 AU 20% Kevlar 49	Kevlar 29 Epoxy
Fiber Volume, Percent	60	55	60	60	60	60	60
Elastic Modulus, 10^6 N/cm^2 (10^6 psi) (0° Orientation)	11.9 (17.2)	20.0 (29.0)	5.9 (8.5)	7.6 (11.0)	10.6 (15.4)	11.0 (15.9)	3.7 (5.4)
Elastic Modulus, 10^6 N/cm^2 (10^6 psi) (90° Orientation)	1.1 (1.6)	1.2 (1.8)	0.8 (1.1)	0.6 (0.8)	1.0 (1.5	1.0 (1.4)	0.6 (0.8)
Elastic Modulus, 10^6 N/cm^2 (10^6 psi) (0/22/0/-22 Orientation)	9.5 (13.8)	11.7 (17.0)	4.7 (6.8)	5.9 (8.6)	8.6 (12.5)	8.9 (12.9)	3.2 (4.6)
Shear Modulus, 10^6 N/cm^2 (10^6 psi) (0/22/0/-22)	1.1 (1.6)	1.9 (2.7)	0.6 (0.9)	0.6 (0.93)	1.0 (1.46)	1.0 (1.47)	0.6 (0.85)
Poisson's Ratio (0/22/0/-22)	0.65	0.97	0.39	0.90	0.60	0.70	---
Density, G/cm^3 (lb/in^3)	1.5 (0.056)	1.9 (0.070)	2.0 (0.072)	1.4 (0.050)	1.6 (0.059)	1.5 (0.055)	1.4 (0.050)
Tensile Strength, kN/cm^2 (ksi) (0°)	138 (200)	138 (200)	138+ (200+)	138 (200)	130 (189)	121 (176)	138 (200)
Tensile Strength, kN/cm^2 (ksi) (0/22/0/-22)	95 (138)	95 (138)	95+ (138+)	95 (138)	89 (129)	83 (121)	95 (138)
Flex Strength, kN/cm^2 (ksi) (0°)	193 (280)	---	---	62 (90)	---	---	62 (90)
Flex Strength, kN/cm^2 (ksi) (0/22/0/-22)	168 (244)	---	172 (250)	59 (85)	---	---	59 (85)
Shear Strength, kN/cm^2 (ksi) (0°)	8.0 (11.6)	7.6 (11.0)	8.1 (11.8)	3.4-7(5-10)	7.2 (10.5)	6.8 (9.8)	3.4-7(5-10)
Charpy Impact, m-N (ft-lb) (±10°)	20 (15)	10 (7.5)	47 (35)	23 (17)	26 (19.4)	19 (14.0)	---

Figure 8-5. QCSEE Orientation (Design Number 1).

Basic Orientation [0.0254 cm (0.010 in) Plies]

+45° Graphite
0° Kevlar 49
-45° Graphite
0° Kevlar 49

3 Plies Kevlar 49
90° Tip and 0° Root

Graphite Insert Plies (Typ.)
+45°/0°/-45°/0°
[0.0504 cm (0.020 in) Stack]

Total Airfoil Plies   154
Total Dovetail Plies   450

4 Plies [0.0127 cm (0.005 in) each]
±10° S-Glass

4 Plies [0.0127 cm (0.005 in) each]
+45° Graphite
0° Kevlar 49
-45° Graphite
0° Kevlar 49

Surface

4 Machining Plies [0.0127 cm (0.005 in) each]
±45° Graphite

Center

where:

   b = 1/2 chord at 5/6 span-m

   W = average air velocity relative to the blade over the outer third of the span-m/sec

   f_t = first torsional frequency at design rpm-rad/sec.

The basic criterion used for setting the design of the UTW composite blade was the requirement of having a reduced velocity parameter in the range of 1.3 to 1.4. This allowable range is based on previous testing of a variety of fan configurations in combinaton with the specific aerodynamic design of the UTW blade. Figure 8-6 shows the results of a 20- and 18-blade analysis for several fiber material candidates. The 18-blade design using the 50% graphite/50% Kevlar material was selected as providing the desired aeromechanical requirements and bird impact characteristics. The operating and stall characteristics of this blade are presented in Figure 8-7 in terms of reduced velocity versus incidence angle. This shows an acceptable blade design as compared with the anticipated QCSEE blade stability limit.

The Campbell diagram for the UTW blade is shown in Figure 8-8. The expected range of first flexural frequencies in the 2/rev crossover is shown to be between 54 and 67% speed. The margin over 1/rev at 100% speed is approximately 60%.

Airfoil Stress Analysis

A preliminary stress analysis of the UTW composite blade was performed using a homogeneous twisted blade computer program. This program is limited to accepting only effective longitudinal properties of the composite blade. It has been used successfully for preliminary design work in the past and offers an approximate state of stress for steady-state operating conditions. Correlation with detailed finite element analysis shows it to be a reasonable preliminary design tool. The resultant radial stresses for the steady-state operating condition including gas loads are shown in Figure 8-9. This shows the maximum stresses to be in the root leading edge and trailing edge areas having values of 1.38 and 1.66 kN/cm^2 (20 and 24 ksi), respectively. The average centrifugal stress at the root is 0.551 kN/cm^2 (8 ksi). The estimated room temperature stress range diagram for the radial direction of the proposed hybrid composite blade is shown in Figure 8-10. For the UTW composite blades, the anticipated maximum vibratory stress is 1.38 kN/cm^2 (20 ksi) single amplitude. For the steady-state condition shown, that of a hot day takeoff and maximum cruise, the combination of steady-state mean stress and expected maximum vibratory stress results in an acceptable blade life.

In addition to the airfoil stresses, the displacement and twist characteristics of the blade are presented in Figure 8-11. The maximum untwist is 2° without leading edge protection.

The steady-state airfoil loads resulting from the twisted blade analysis are:
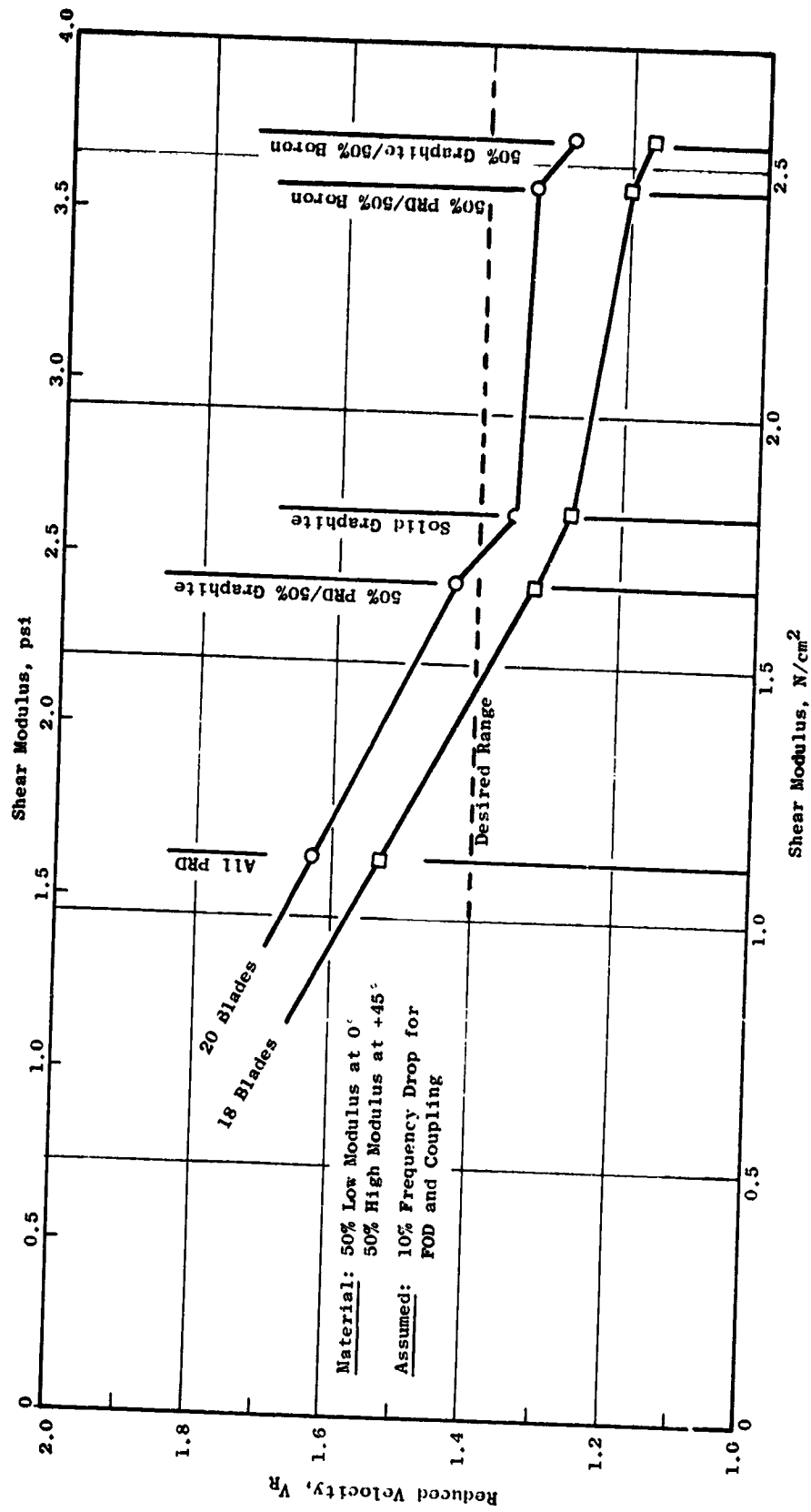
Figure 8-6. QCSEE UTW Composite Blade.
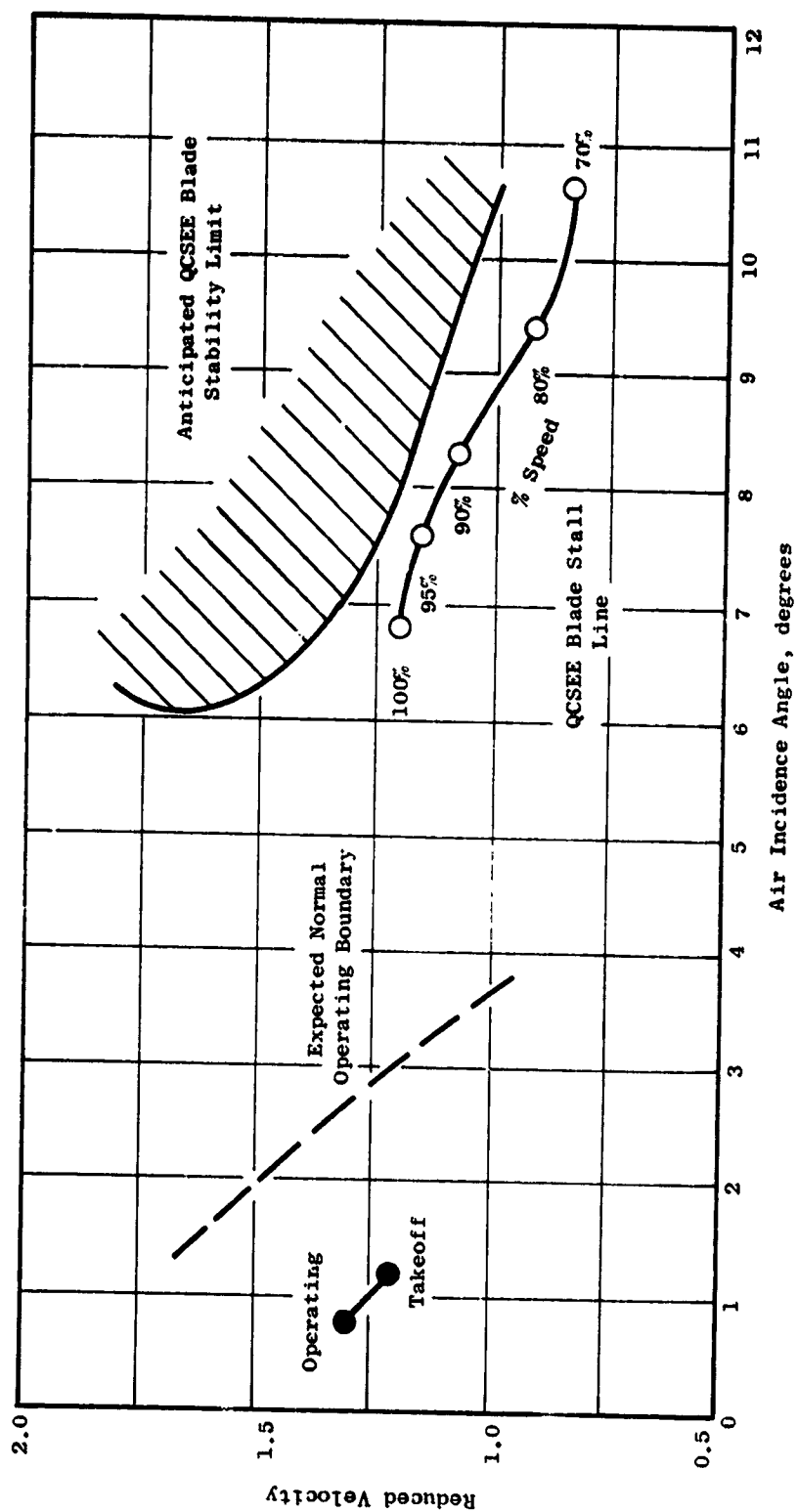
Figure 8-7. Limit Cycle Boundaries.
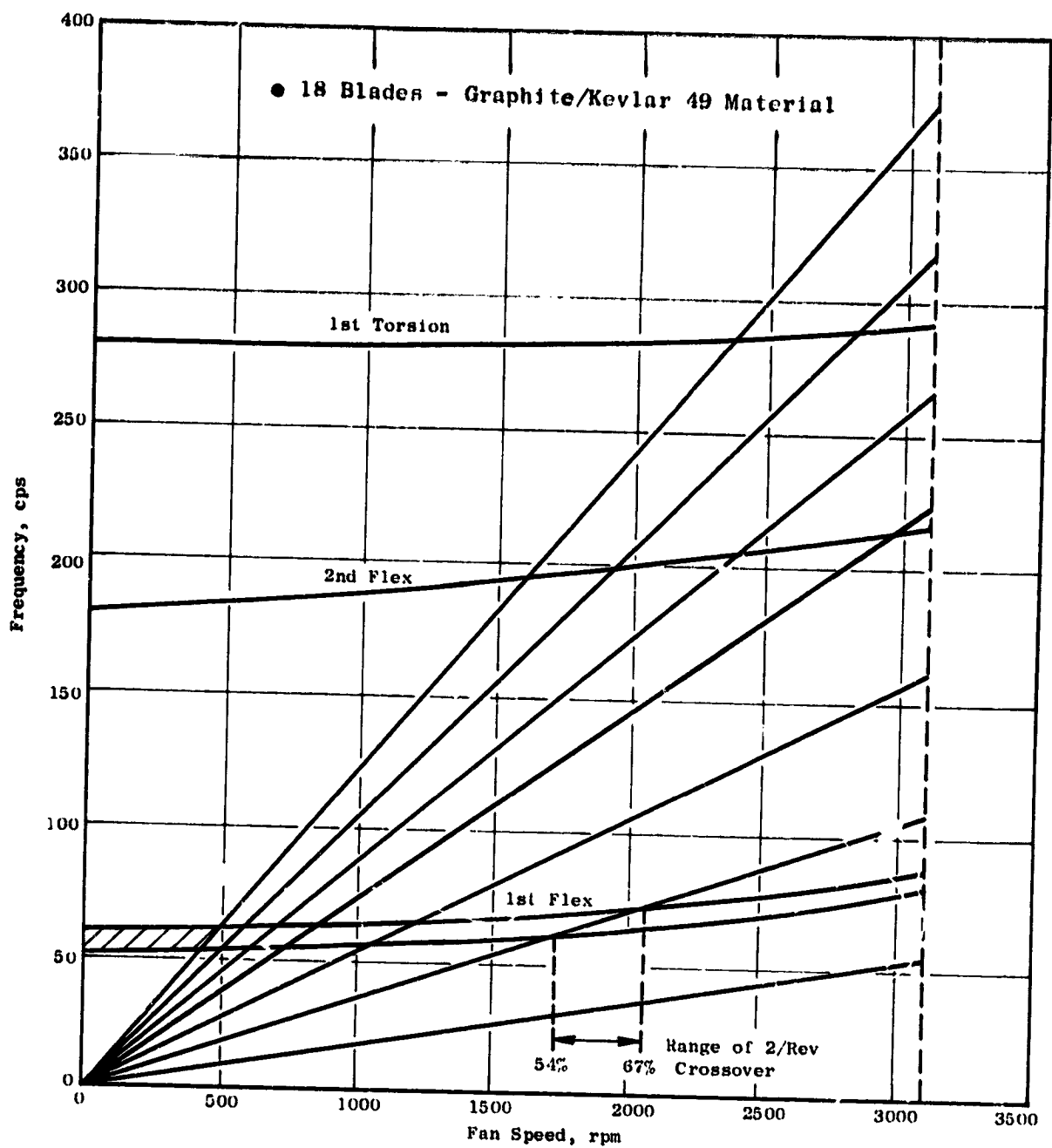
Figure 8-8.   QCSEE UTW Composite Blade.

254
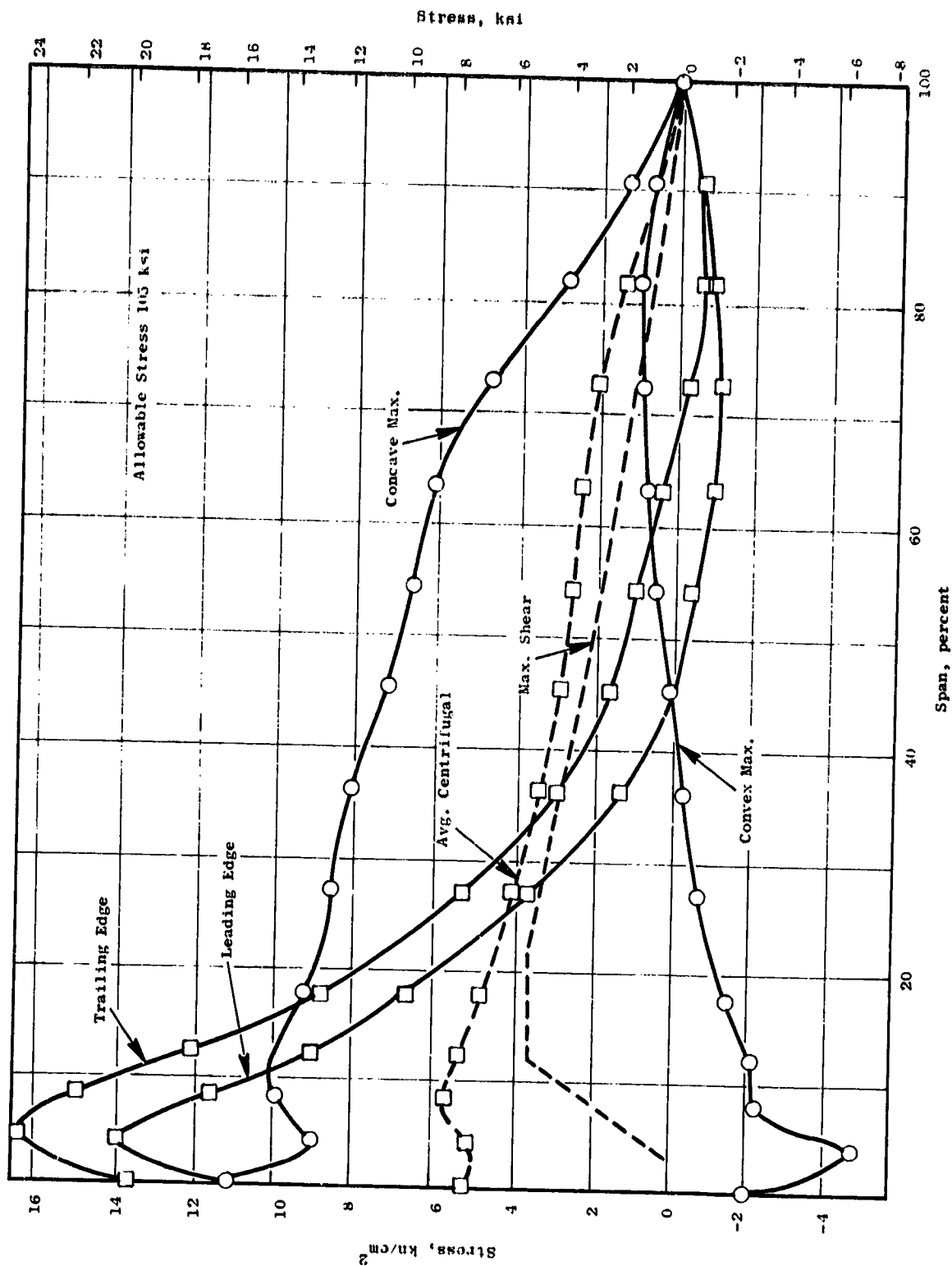
Figure 8-9. UTW Blade Resultant Radial Stress – 3157 RPM.
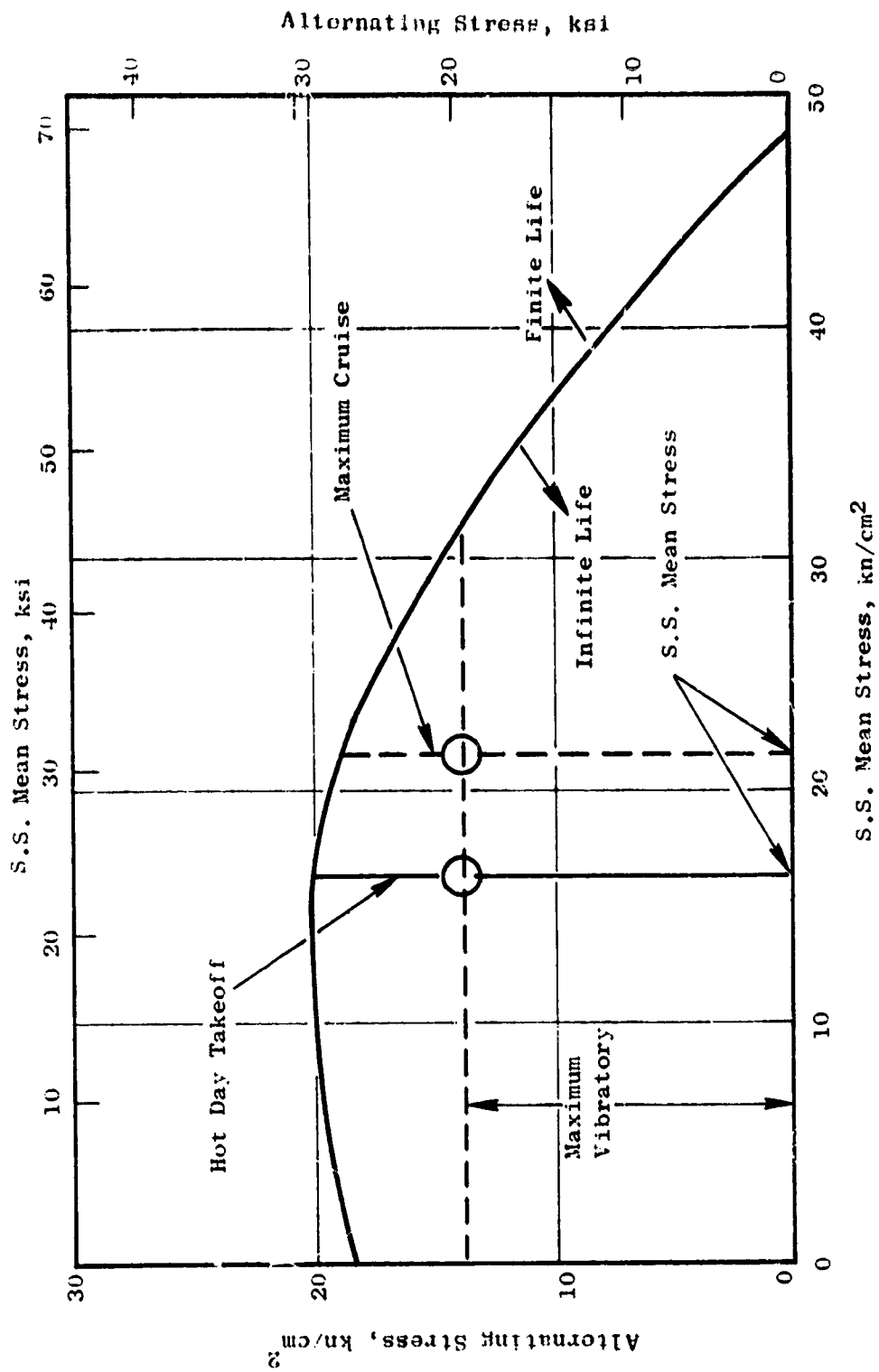
Figure 8-10. Blade Life (Goodman Diagram).
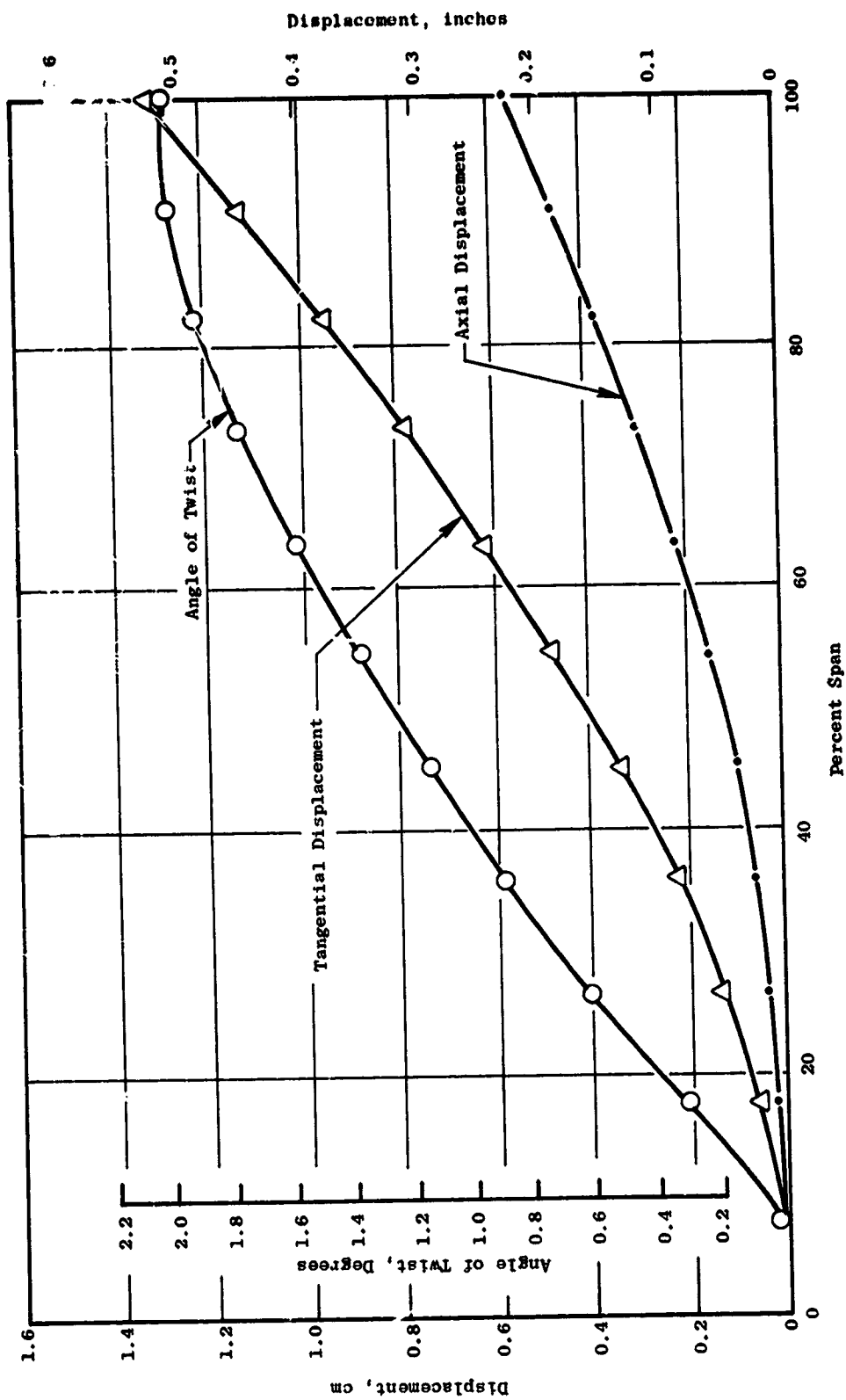
Figure 8-11. UTW Blade Displacements and Twist - 3157 RPM.

- 100% rpm centrifugal force: 118,000 N (26,500 lb)

- maximum centrifugal force: 155,000 N (35,000 lb)

- $M_{tang} = 50,900$ cm-N (4500 in-lb), $M_{axial} = 61,000$ cm-N (5400 in-lb) $M_{twist} = 7900$ cm-N (700 in-lb)

More detailed stress analysis using three-dimensional finite element techniques are planned during the final design phase.

Dovetail Design

The dovetail design for the UTW composite blade consists of a straight bell-shaped dovetail with a 7.6 cm (3 in.) radius. The bell-shaped dovetail design reflects many years of development efforts to achieve an efficient dovetail configuration having both high static pull strength and good fatigue strength. The dovetail crush normal and shear stresses were calculated and are shown on their respective stress range diagrams in Figures 8-12 and 8-13. The combination of mean stress and vibratory stress indicate there is considerable margin for infinite life under steady-state operating conditions.

Impact Analysis

In addition to the primary aeromechanical consideration of satisfying flutter requirements, designing for bird impact resistance is also of prime importance. The QCSEE blade is required to absorb the impact of 54 starlings, 9 pigeons, and a 1.8 kg (4 lb) duck in order to satisfy FAA specifications. The objectives are to sustain little or no damage during starling ingestion have only moderate local damage during pigeon ingestion with the loss of small segments of the blade tip being acceptable and to limit the gross damage during 1.8 kg (4 lb) bird impact to the loss of airfoil tips with no root failures.

The projected elimination of root failures during large bird impact in the QCSEE blade has been achieved by a combination of judicious airfoil and dovetail design. More flexibility and strain-to-failure capability has been built into the blade root through the use of hybrid materials. The dovetail design provides for energy dissipation through centrifugal recovery and increase in friction energy. Figure 8-14 illustrates the magnitude of energy that has to be absorbed by the blade at the root, tip, and pitch for the spectrum of relative bird velocities for a 1.8 kg (4 lb) bird. This shows that the most vulnerable condition and blade impact location is during climb approximatly 91.4 m/sec (300 ft/sec) and at the blade pitch, respectively. The gross impact capability of the QCSEE blade is shown in Figure 8-15. This shows the advantages of the QCSEE dovetail attachment and the use of hybrid materials over the previous fixed-root solid graphite-type blade.

258
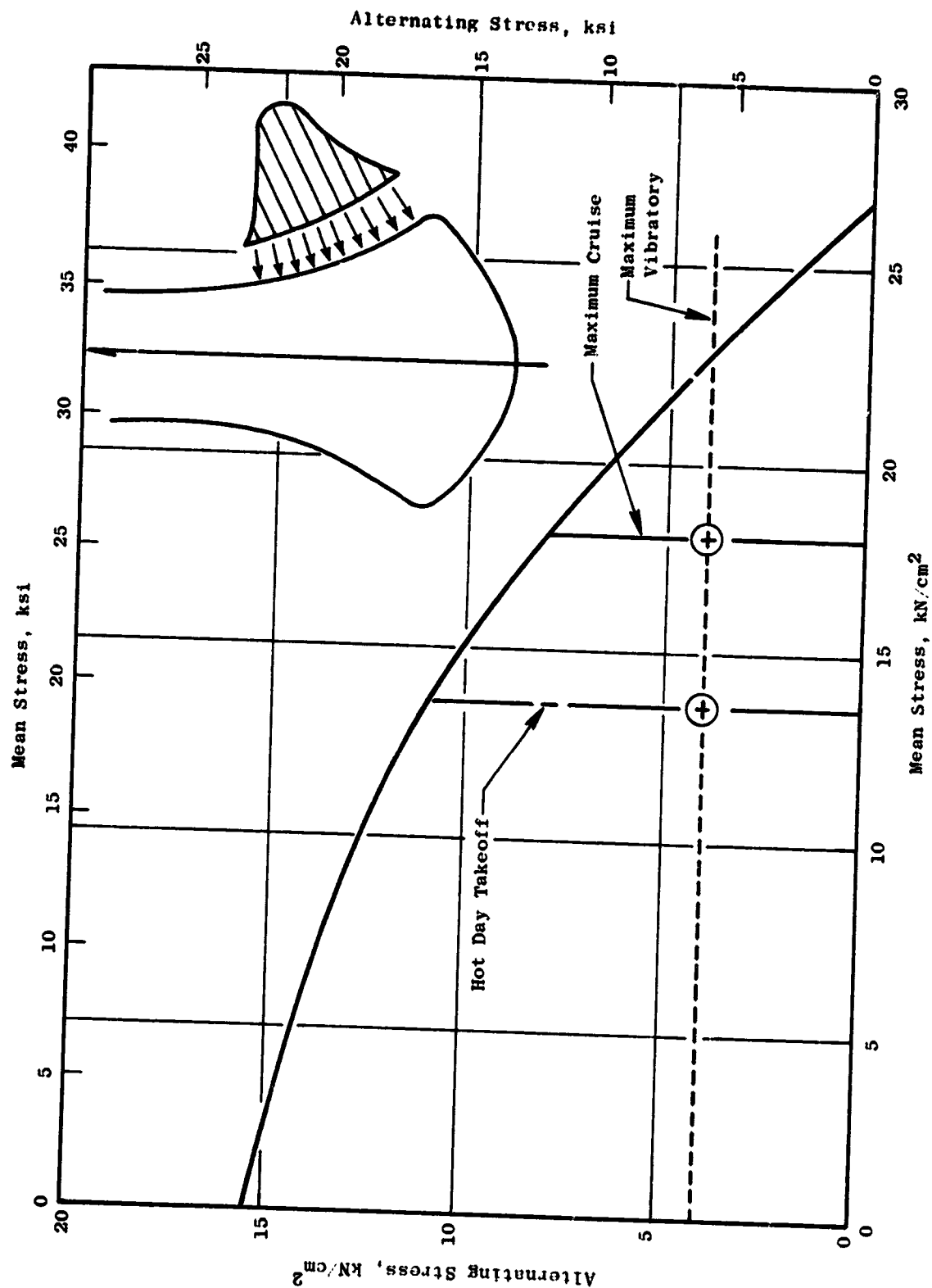
Figure 8-12. Allowable Stress Range Diagram – Dovetail Normal Stress.
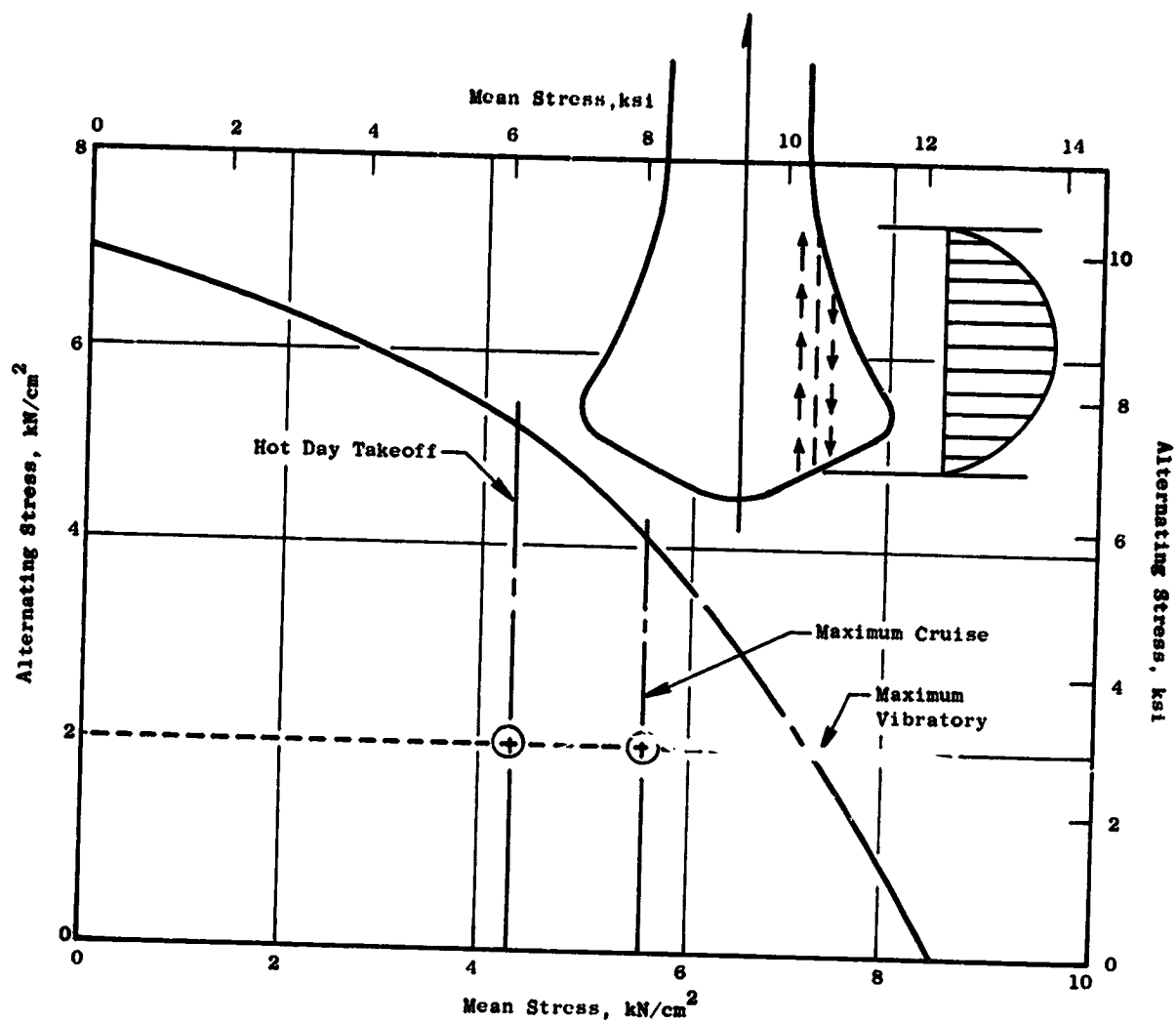
Figure 8-13.   Allowable Stress Range Diagram - Dovetail Shear
(PRD/Glass/Graphite Epoxy).
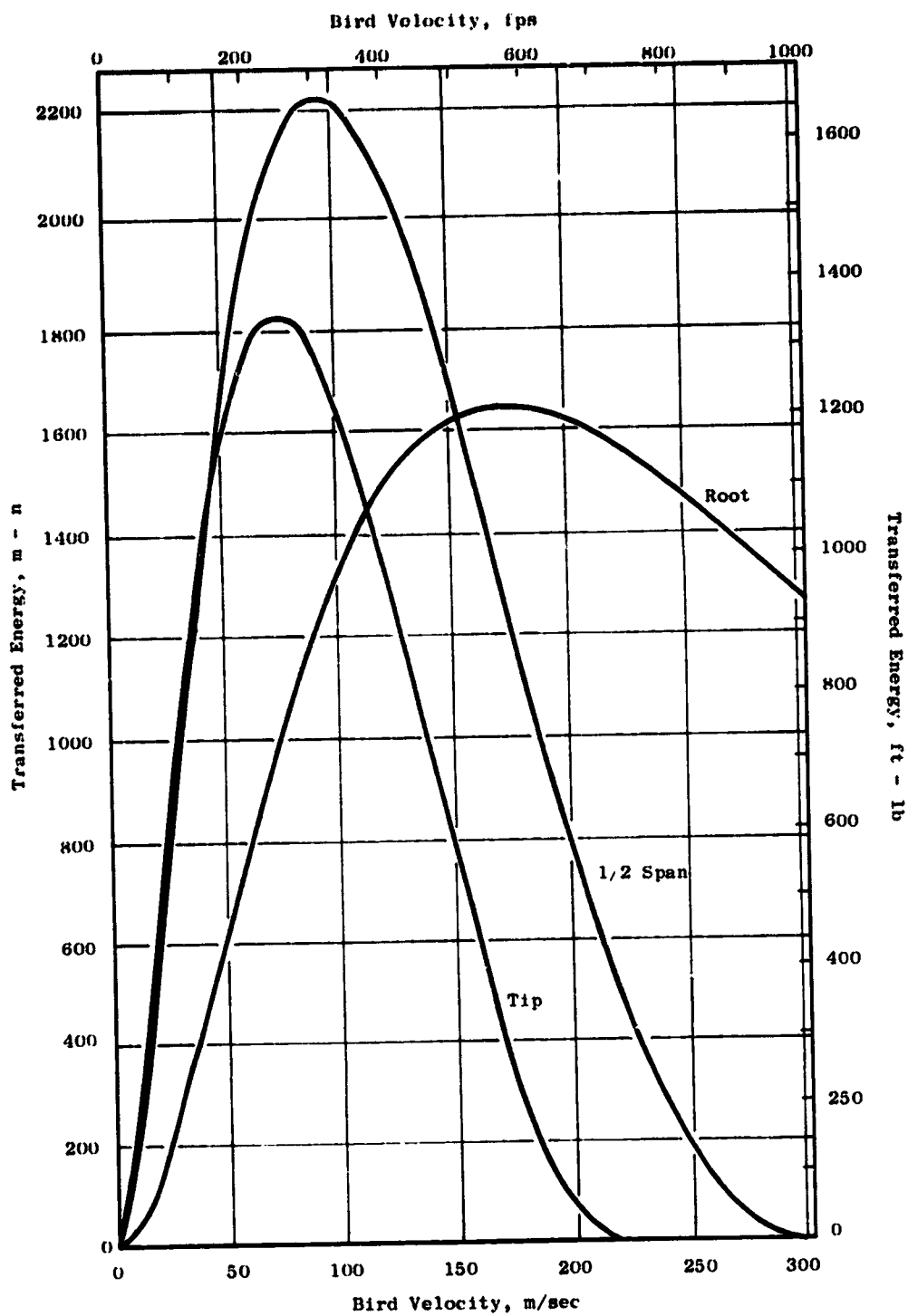
Figure 8-14. Eighteen Blade QCSEE Impacted by a 1.81 kg (4 lb) Bird.
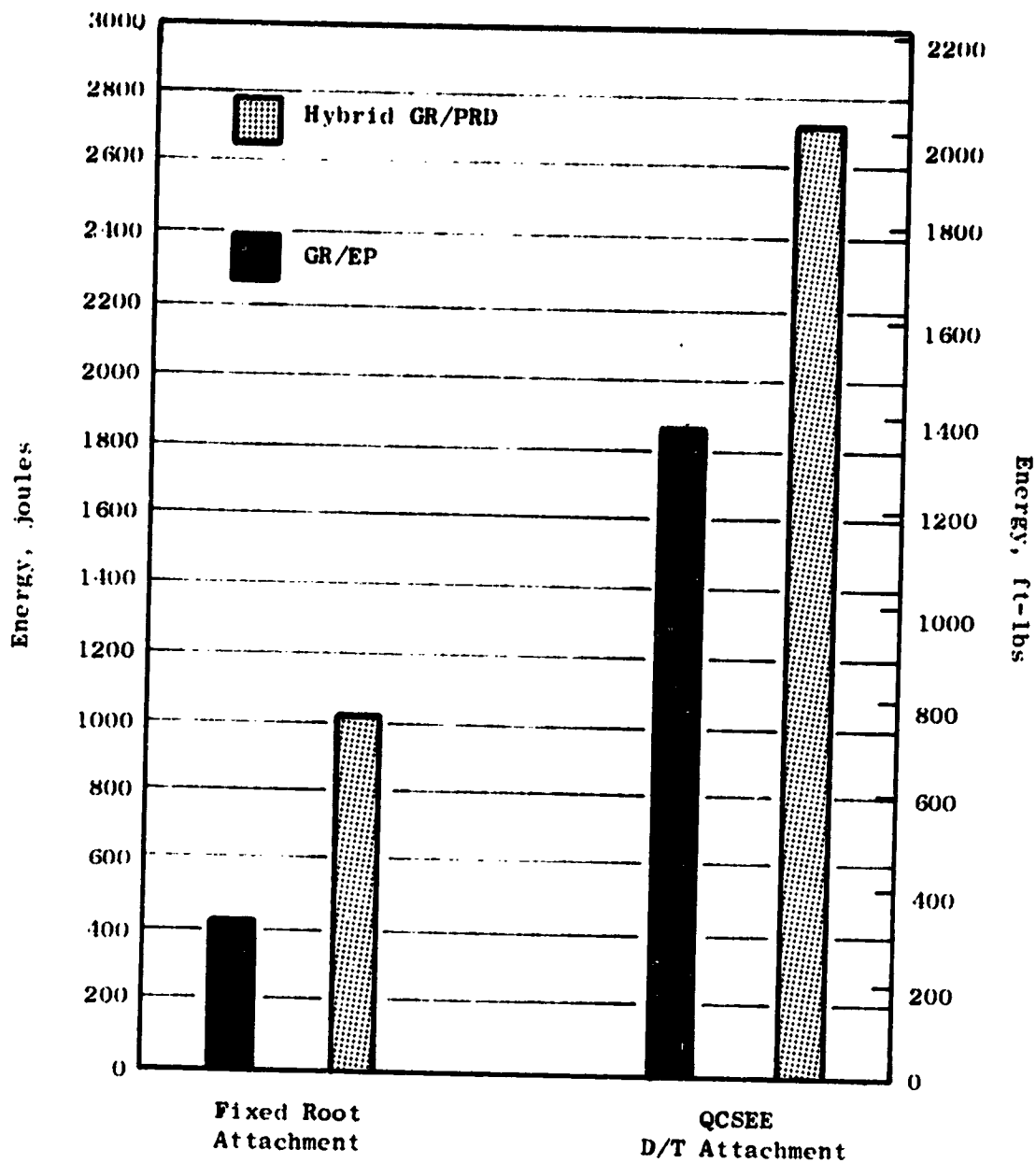
Figure 8-15. QCSEE Composite Blade Predicted Gross Impact Capability.

8.2.2 Fan Disk

The fan disk is a single-piece-machined 6Al-4V titanium ring forging designed for a commercial life in excess of 36,000 hours. This disk is shown in Figure 8-16. Eighteen holes pierce the disk ring to provide for the blade support trunnion while retaining the blades. The excess disk material between the holes is removed where possible to reduce the dead disk weight and lower the stress concentration around these holes. An integral cone on the aft side of the disk connects the disk to the main bearing shaft through a bolted flange. The disk cone is contoured to alleviate LCF problems generated by the forward and aft cycles of thrust generated during engine operation. Flanges on the outside of the disk rim provide attachment planes for the spinner and aft flow-path adapter.

The inside of the disk rim is a turned modified spherical blade bearing seating surface for the blade retention bearing (Figure 8-17). This results in a low-cost, lightweight disk design with a uniformly stressed rim. The blade thrust bearings have mating spherical seats and are mounted as shown in Figure 8-17. The bearing seating surface is not machined perfectly spherical but is designed to become spherical under operating loads. An antifretting coating will be applied between the disk and the bearing, although at the pressure loadings expected beneath the bearing, fretting is not expected to be a problem.

The UTW fan disk design data are shown in Table 8-IV.

8.2.3 Blade Support Bearing

The blade support bearing has a full complement of balls to reduce the per-ball loading. Bearing race conformance is a relatively high 51% to extend the bearing fatigue life in its highly loaded environment. All surfaces on this bearing will be coated with a tungsten disulfide film. Tests on previous General Electric variable-pitch fan bearings have shown this coating provides enough lubrication to enable the bearing to safetly operate for 9000 flight hours in the event as a loss-of-grease situation.

The QCSEE support bearing is show in Figure 8-18. Shields attached to the outer race create a centrifugal "c" which prevents the grease from leaking out in the high centrifugal field w. a the engine is running. Grease will not leak from the clearance gaps at the bottom of the shields when the engine is not operating due to the high viscosity of the grease, provided oil separation from the grease soaping agent does not occur. General Electric has conducted centrifuge tests on various greases and has identified one which has little tendency to separate even under prolonged periods of higher "g" loads than planned for the QCSEE bearing. The bearing test rig is shown in Figure 8-19.

Design criteria peculiar to variable-pitch blade support bearings had to be developed and applied to the design of this bearing. The unique design criteria used in designing the QCSEE UTW bearing are as follows:

- Low Cycle Fatigue Life
- Life with 0.025 cm x 0.076 cm
  (0.01 inch x 0.03 inch) Defect
- Precession Loads
- Blade Out
- 141% Speed Without Bursting
- Bearing Seat Tailored for Disk
  Centrifugal Growth

Figure 8-16. UTW Fan Rotor Disk.

Spherical
Surface
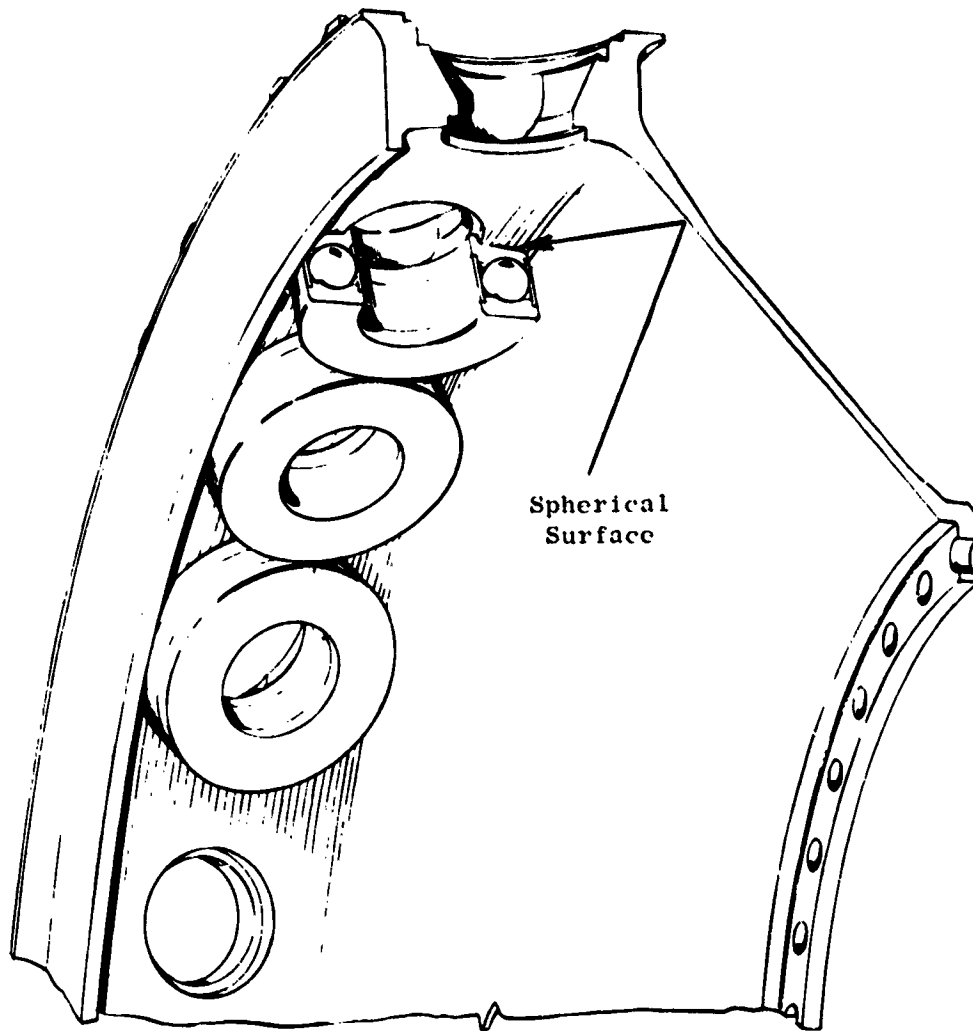
Figure 8-17. UTW Bearing and Disk Seat.

Table H-IV. UTW Fan Disk Design Data.

Total Blade and Blade Attachment Load at 100% Mechanical Design Speed (3,244 rpm)	270,000 N/blade (60,777 lb/blade)
Total Live Rim Load at 100% Speed	5,043,691 N (1,133,867 lb)
Average Disk Rim Stress at Max. Duty Cycle Speed (3,326 rpm)	38.7×10^7 N/m^2 (56,085 psi)
Max. Disk Stress at Peak Location at Max. Duty Cycle Speed	42.1×10^7 N/m^2 (61,078 psi)
Overspeed Capability	4,865 rpm
LCF Life with 3σ Material Properties	> 48,000 Cycles
LCF Life with 0.025 x 0.076 cm (0.01 in. x 0.03 in.) Initial Defect	> 16,000 Cycles

266
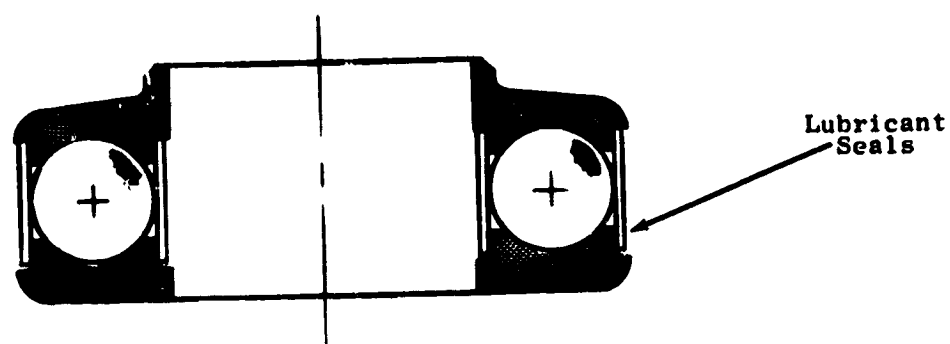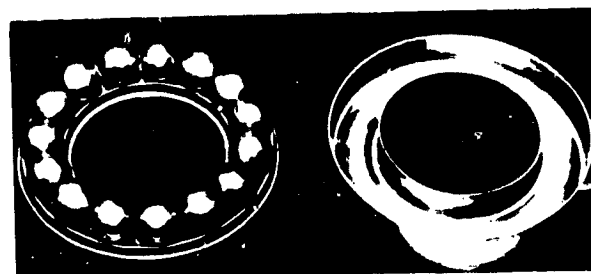
- Single Row Ball Thrust Bearing
- Full Complement of Balls (12)
- High Conformance (51%)
- Separable Races
- Lubricant Seals

Figure 8-18. Blade Thrust Bearing.
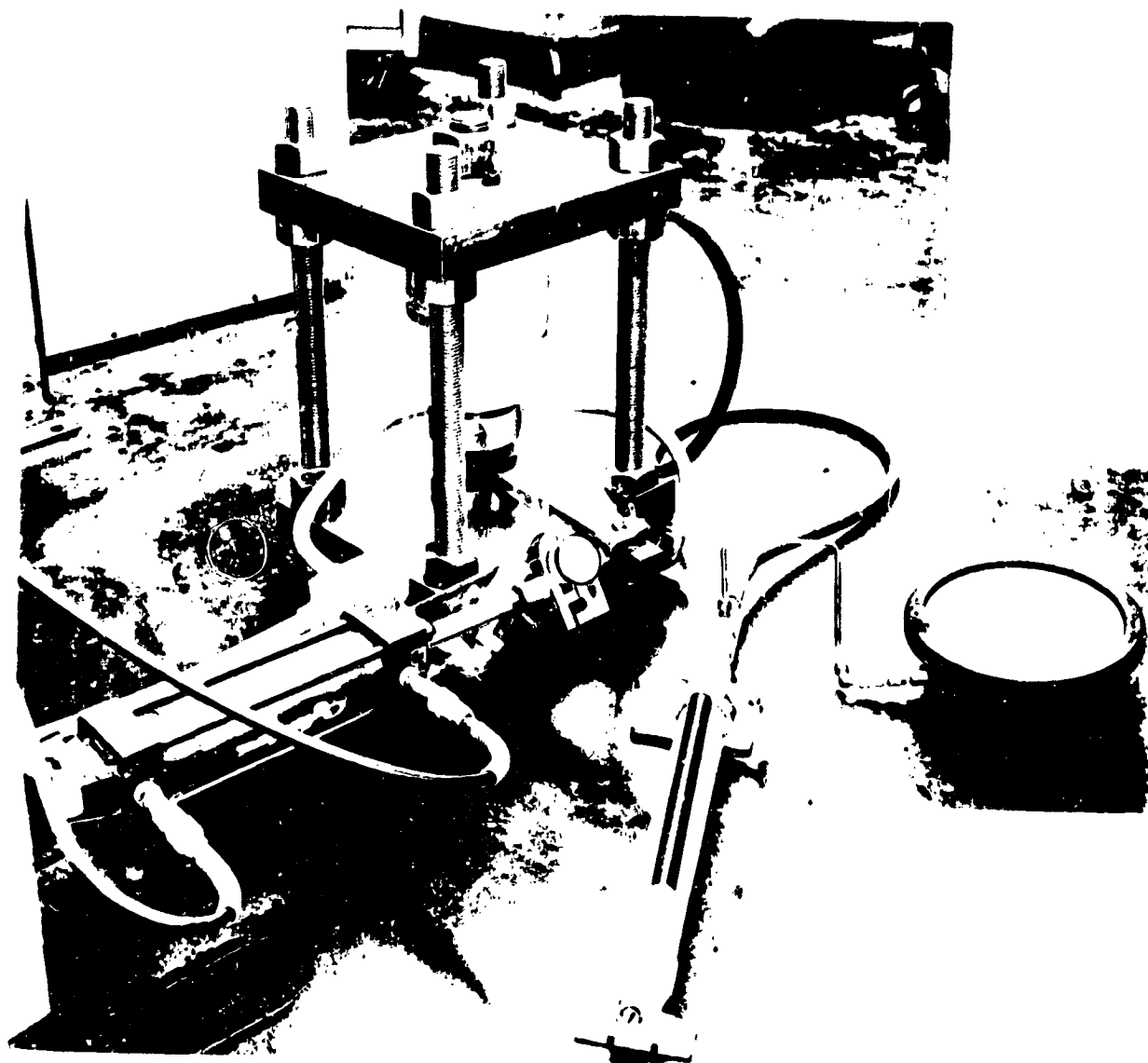
Figure 8-19.   Bearing Test Rig.

1. The blade support bearing system B10 life should be 9000 flight hours. This requires an individual bearing B10 life of over 13 times the system B10 life. The need for this stringent requirement is based on the statistical problem of a multibearing system in a multiengine aircraft.

2. Blade bearings will not be dependent upon the grease lubricant to obtain 9000 hours between overhauls. This restriction ensures that failure will not occur due to loss of bearing grease. In addition to normal bearing design criteria, the following requirements must also be met, or by definition, failure i. said to occur:

    a. An apparent coefficient of friction at the pitch diameter less than 0.01. This allows the blade actuator to be designed to a maximum capacity with assurance that it will not be overloaded because of worn bearings.

    b. Bearing wear less than the bearing preload [approximately 0.00508 cm (0.002 inch) total wear]. This definition provides a simple method for condition monitoring without rotor disassembly.

3. Ball or race fracture must not occur under the maximum possible bird impact loads. The actuation system of an 18-bladed fan is sufficiently powerful to cause secondary damage upon seizure any one of the individual bearings. Ball fracture, a potential cause of such seizure, must be eliminated as a potential problem.

4. Bearing life calculations are based on the mission/duty cycle as shown in Figure 7-1.

The top bearing race is a spherical surface which is designed in conjunction with the disk bearing seat to minimize transmission of warping stress to the race under operating condition. This spherical mating surface will be coated with an antifretting coating to ensure that loss of LCF life of the fan disk will not occur. Bearing loads and life predictions are given in Table 8-V.

8.2.4 Blade Retention Trunnion

The blade retention trunnions mechanically tie the composite blades to the fan disk through the blade support bearing. They also provide an attachment point through which torque might be applied by the blade actuator to change the pitch of the blades. The QCSEE UTW blade retention trunnion is shown in Figure 8-20 (Appendix B).

Table 8-V. Bearing Load and Life Summary.

Average Bearing Load - Balls at 100% Mechanical Design Speed (3244 rmp)	262,392 N (58,988 lb)
Bearing Static Load Capacity	297,812 N (66,951 lb)
Bearing Elastic Deflection at 3244 rpm	0.0124 cm (0.0049 in.)
Individual Bearing B10 Life	128,190 Flight Hours

The entire blade support system is designed to withstand the maximum possible loads which can be transmitted into it by the blades without blade failure. This includes not only the trunnion but all of its mating components. This ensures that in the event of extensive foreign object damage only the small composite blade pieces will be broken off and secondary engine damage will be minimized.

The fan blades slide into the dovetail slots on top of the trunnion and are retained by shouldered strips. A relatively new material, MP159, is being considered for the strips because of its natural corrosion resistance and very high strength.

Restraint of the blade about the dovetail axis is provided by ester-based urethane rubber bumpers under the blade mount. This material has exceptional load absorption capabilities and is not affected by commonly used jet engine oils, fuels, or solvents.

The dovetail slot will be protected by an antifretting coating applied to the blade dovetails. Tests will be conducted to determine the best antifretting system. Two plasma sprayed coatings, one plated coating, and a chemical conversion coating are presently being considered for this wear coating.

The trunnion will be machined from single forgings of 6Al-4V titanium. This material was selected based on its natural corrosion resistance, low density, and high strength. This material also allows relatively large diameter threads to be rolled out on the trunnion end (Per Mil-S-8879) for retention purposes by more conventional capacity thread rolling equipment. This rolling procedure has been used on the titanium trunnions of previous General Electric variable-pitch fans and produces above average properties in this critical region.

Each trunnion is held in the hole of the disk by a threaded steel retainer. This retainer can be torqued to preload the blade support bearing, and is locked by a redundant locking system. Either a pinion gear for the GE actuation system or a lever arm for the Hamilton Standard System is captured on the trunnion between the retainer and the blade support bearing [see Figures 8-21 (GE) and 8-22 (H.S.)].

Composite Blade

18 Blade Retention
Assemblies

Fan Disk

18 Bearings

Trunion

18 Pinions

Retainer

Master
Gears

Ball Spline
Actuator

Differential
Gearing

Brakes

No-Back

Ball Nut

LVDT Feedback
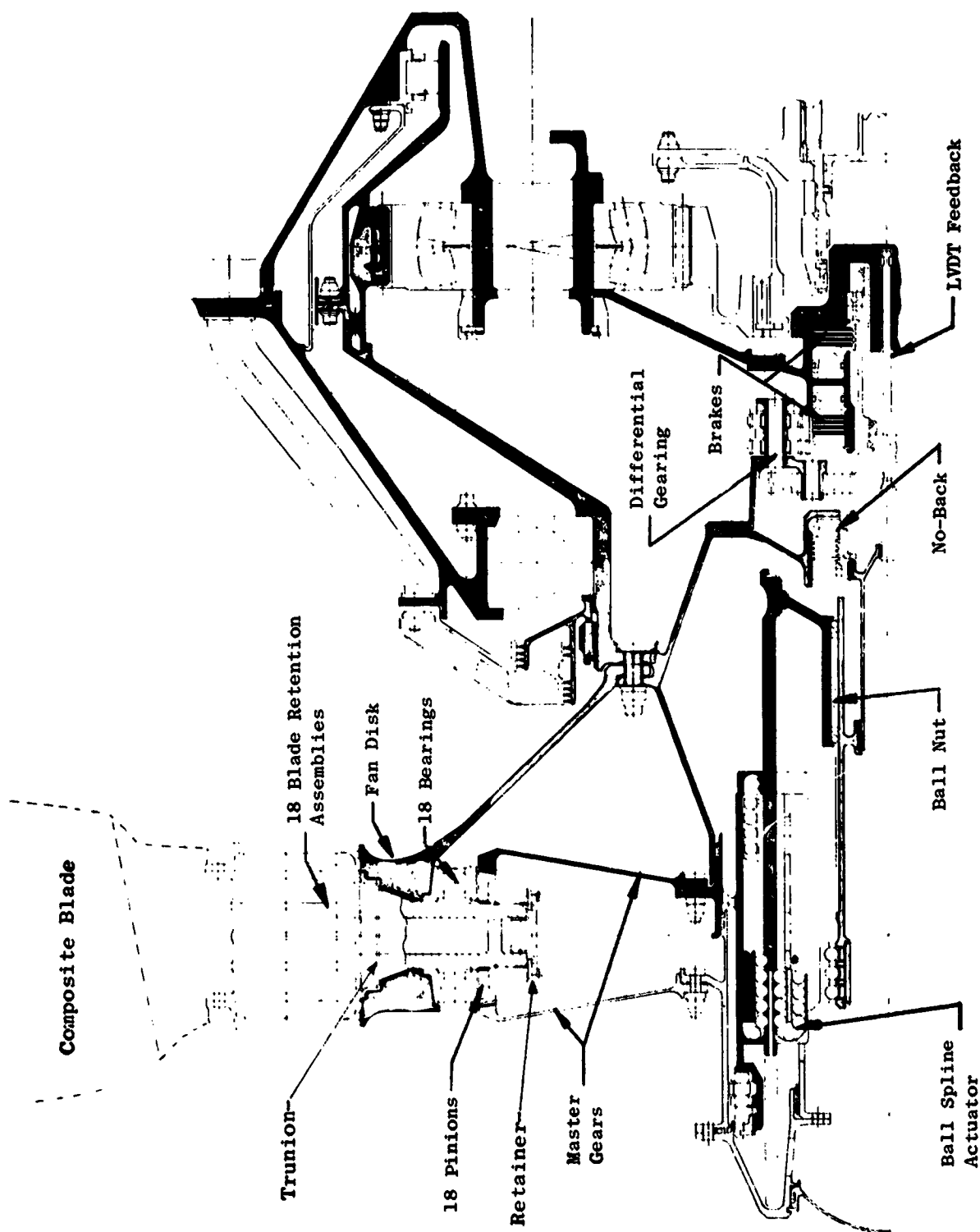
Figure 8-21. UTW Variable Pitch Fan with GE Actuation System.
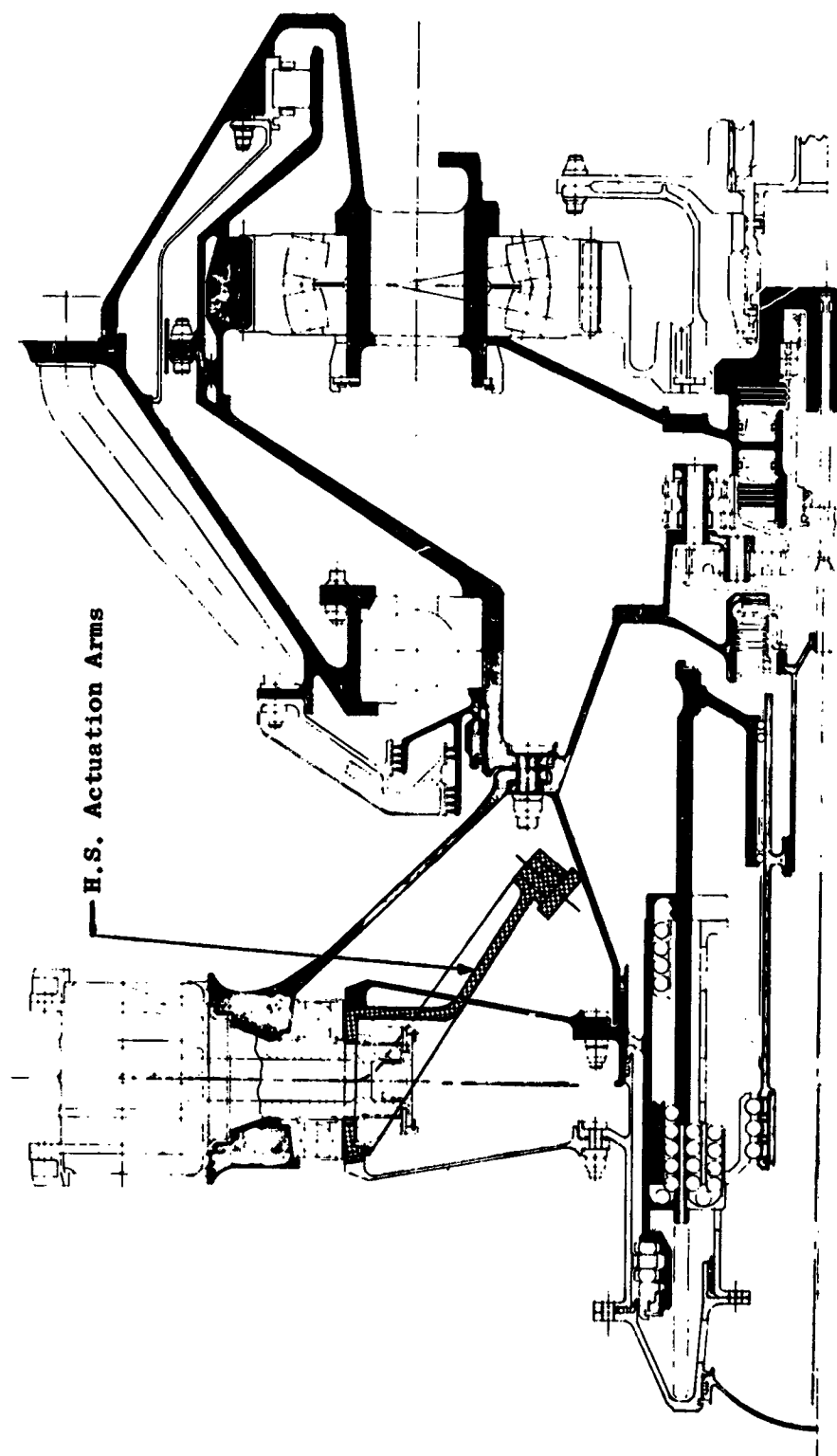
H.S. Actuation Arms

Figure 8-22. UTW Variable Pitch Fan with Hamilton Standard Actuation Arms.

Torque to change the blade pitch is carried through this device into mating splines just above the trunnion threads.

Outer sliding bearings support the top of the trunnion. The axial thrust washer is made of commercially available refractory matrix material containing molybdenum disulfide. Wear and load carrying characteristics of this material are excellent, and no measurable creep is expected under preload. This bearing serves as a weather seal under static conditions, but runs 0.0076 cm (0.003 in.) loose under normal engine speeds due to the elastic properties of the blade support bearing. The outer sleeve sliding bearing is a very high capacity bearing of Nomex and Teflon fibers. This bearing seats inside the disk and can easily tolerate the circumferential strain of the disk. The high capacity of this bearing, compared to conventional ball bearings, enables it to easily withstand anticipated vibratory and bird impact loads. Both outer bearings have resistance to all oils, fuels, and solvents which might normally come in contact with engine parts.

8.2.5 Fan Spinner

The UTW fan has both a rotating forward spinner and flowpath adapter as shown in Figure 8-1. These parts attach to flanges on the fan disk. Both are scalloped where they meet to provide round holes for the blade platforms. Together they provide the inner flowpath for the fan. The spinners will be fabricated from 6061 Aluminum. This material has good section stiffness-to-weight and has the good welded properties needed for fabricating development hardware.

The forward spinner will also have a spinner cap for inspection and access to the interior of the fan assembly. After removal of the fan spinner, all of the rotating hardware and sump regions forward of the fan frame are easily accessible. Blades may be individually replaced and the blade actuator or the actuator and disk assembly may be removed as a package. This permits removal of the fan disk assembly, blade actuator, and main reduction gear as a complete module.

Radial fan balance screw bosses will be provided in the spinner. This will permit field balance of the engine without removal of the spinner. The concept has been developed and used successfully on General Electric's CF6-50 engine.

The aft flowpath adapter continues the inner flowpath back to the fan core OGV's. A flow discourager seal inhibits air recirculation at this point. There are access holes in the flange of the aft spinner which, with the forward spinner removed, permit access to the fan frame flange which retains the main reduction gear.

8.3 OTW FAN ROTOR

The OTW experimental fan has 28 fixed-pitch metal blades with a 180 cm (71 in.) fan tip diameter similar to that of the UTW fan. This rotor is shown in Figure 8-23. The conceptual design of this fan is based on using composite

273
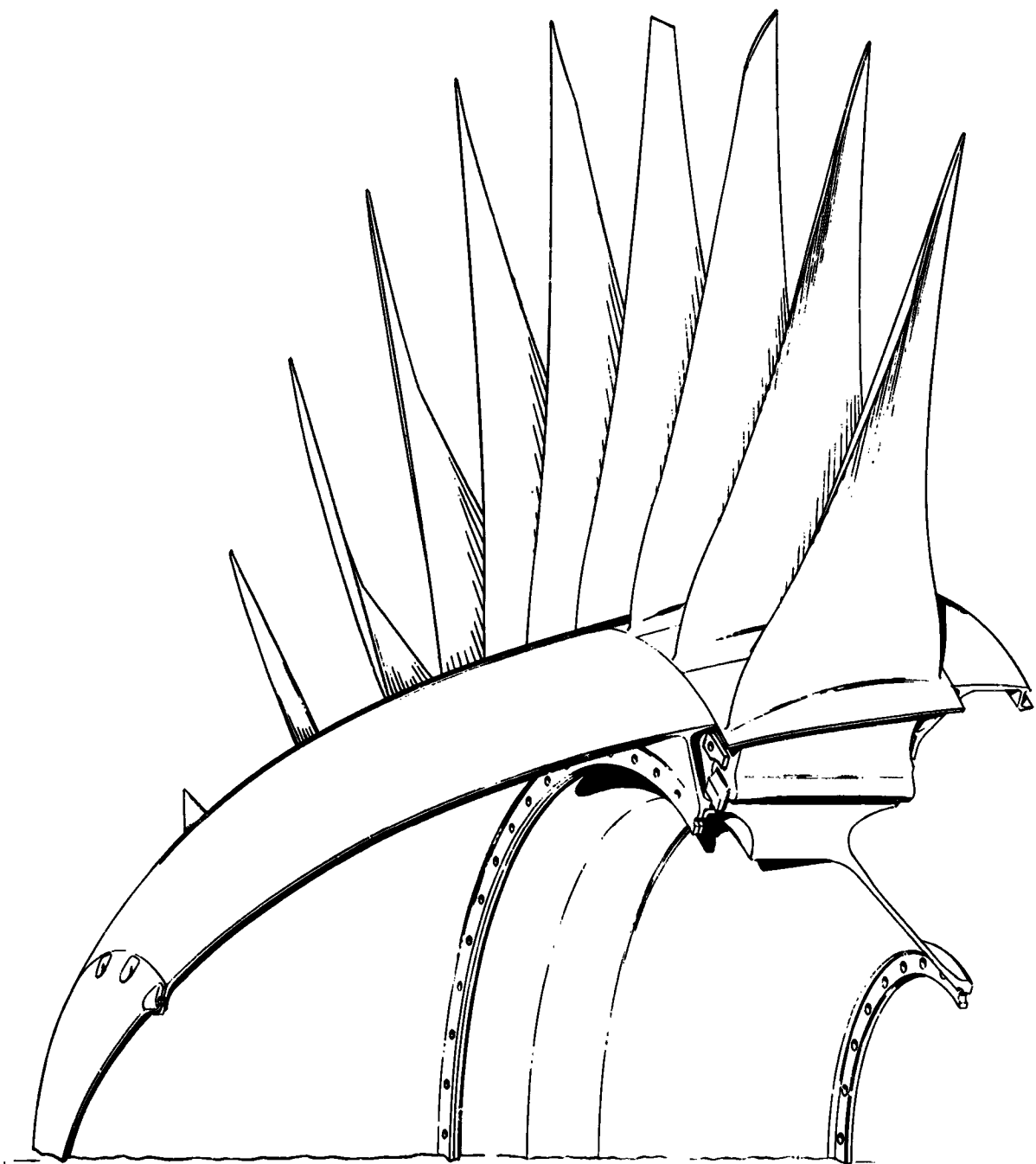
Figure 8-23.   QCSEE OTW Fan Rotor.

fan blades, but metal blades will be used for reasons of economy and low risk. The conceptual composite bladed design dictates the absence of blade shrouds, determines the number of fan blades, and affects the sizing of such parameters as the blade solidity, reduced velocity, and leading edge thickness. In the flight engine, composite blades would be substituted for the metal blades without aerodynamic change or compromise in the composite blade mechanical design. While the demonstrator fan disk is heavier than the composite bladed flight weight disk, it reflects a flight configuration in both design criteria and material selection. A comparison between the experimental and flight OTW fan design criteria is given in Table 8-VI.

The OTW fan has both a forward rotating spinner and aft flowpath adapter. The inner flowpath formed by these two parts and the blade platform is identical to the inner flowpath of the UTW fan from a point near the blade trailing edge aft. The tip speed of the OTW fan is about 14% higher than for the UTW Fan. The OTW fan, reduction gear, and fan frame assembly are shown in Figure 8-24.

8.3.1 OTW Fan Blade

The OTW fan blades will be machined 6A1-4V titanium forgings. The steady-state operating stresses in the blade are relatively low, reflecting the relatively low tip speed of this fan. The mechanical design of these blades avoids resonance and fan blade instability in the operating range.

The fan blades are a "low-flexed" design, i.e., the first flexural frequency of the blades is less than two times the per-rev frequency of the fan in its operating speed range. Without a thicker blade root, which would have been aerodynamically unsatisfactory, low-flexing was necessary because of the lack of blade shrouds. This approach, though not common, is used successfully on General Electric's TF34 fan and J79 stage 1 compressor blade and was successful on NASA's Quiet Engine C fan. The first flexural blade frequency Campbell diagram is shown in Figure 8-25. The frequency of the disk-blade assembly will be somewhat lower than the individual blade frequency (solid curve, Figure 8-25) due to the flexibility of the supporting fan disk. This allows for some adjustment of the 2 per-rev resonant point during final disk design as shown by the two dashed lines. This resonance crossover will occur below approach fan speed but above flight idle in a region of the performance map not used for steady-state operation. The Campbell diagram for the first three modes is shown in Figure 8-26. In the absence of frame struts or inlet guide vanes ahead of the fan, higher order resonances have not been a problem on similar configuration engines such as TF34 and CF6.

As described in Section 8.2.1, reduced velocity is used as a basis for comparing instability margins of blading as a function of the air incidence angle on the blade. The design practice is to have the blade stall before instability occurs. Blade instability apparently does not occur once the blades are stalled. The blades are designed so that when the fan is throttled, stall is expected to occur before the emperically predicted blade instability is encountered. The blade stability is affected by varying the blade chord and thickness distribution which changes the reduced velocity parameter. The operating and stall characteristics of this blade are presented in Figure 8-27 in terms of reduced velocity versus incidence angle. This shows an acceptable blade design in

275

Table 8-VI. QCSEE OTW Fan Design Criteria.

	Demonstrator	Flight
Materials		
Disk	Titanium	Titanium
Blades	Titanium	Composite
Number of Blades	28	28
Per Blade Centrifugal Load, N (lb)	558,696 (125,600)	184,156 (41,400)
Design Point Speed, rpm	3792	3792
Design Burst Speed, rpm	5729	5729
Disk Low-Cycle Fatigue Life (Min)	> 48,000 Flight Cycles	> 48,000 Flight Cycles
Disk Low-Cycle Fatigue Life with Initial 0.025 x 0.076 cm (0.01 x 0.03 in.) Defect	> 16,000 Flight Cycles	> 16,000 Flight Cycles

276
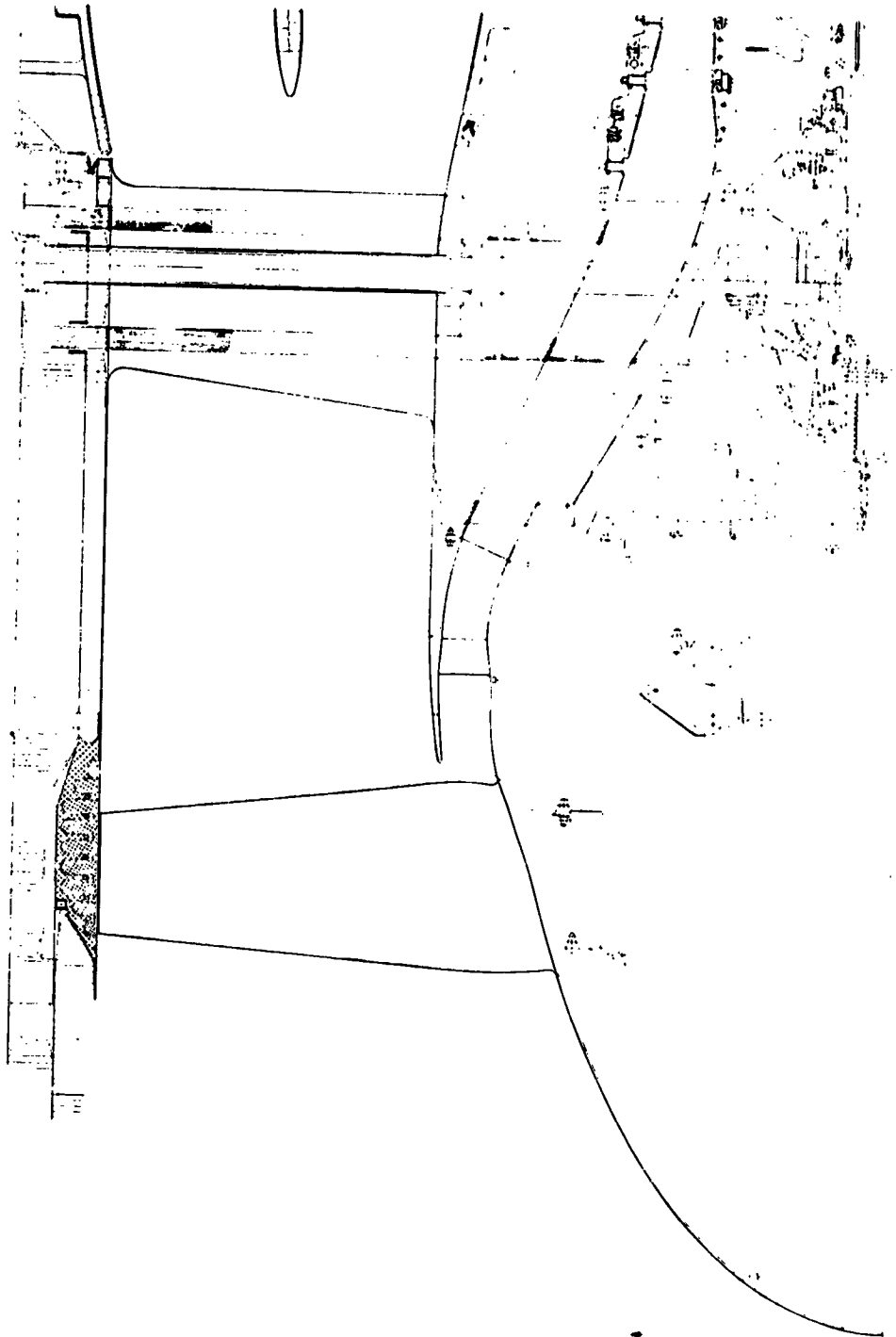
Figure 8-24. QCSEE OTW Fan.

277
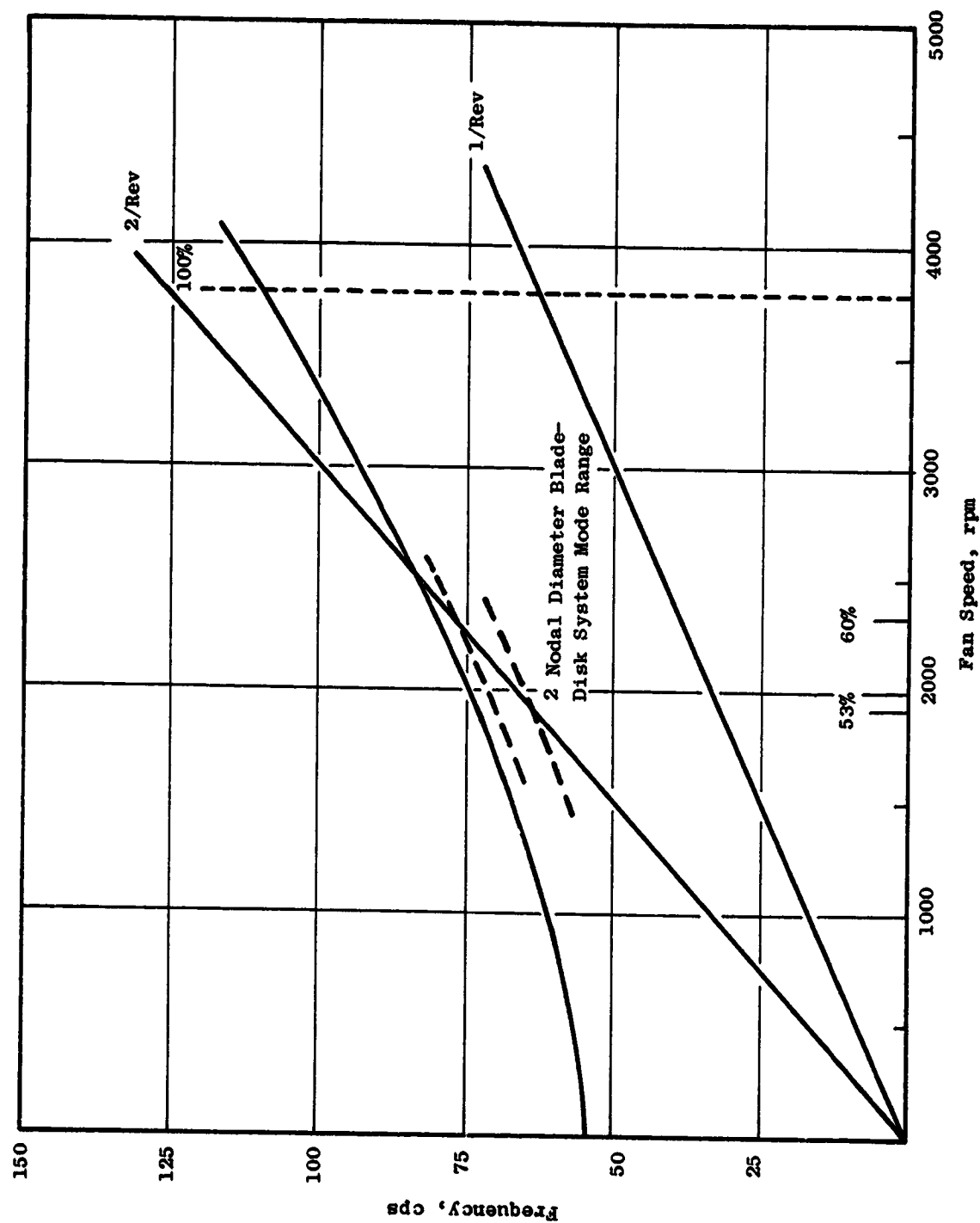
Figure 8-25. QCSEE OTW Fan Campbell Diagram – First Flexural Frequency.
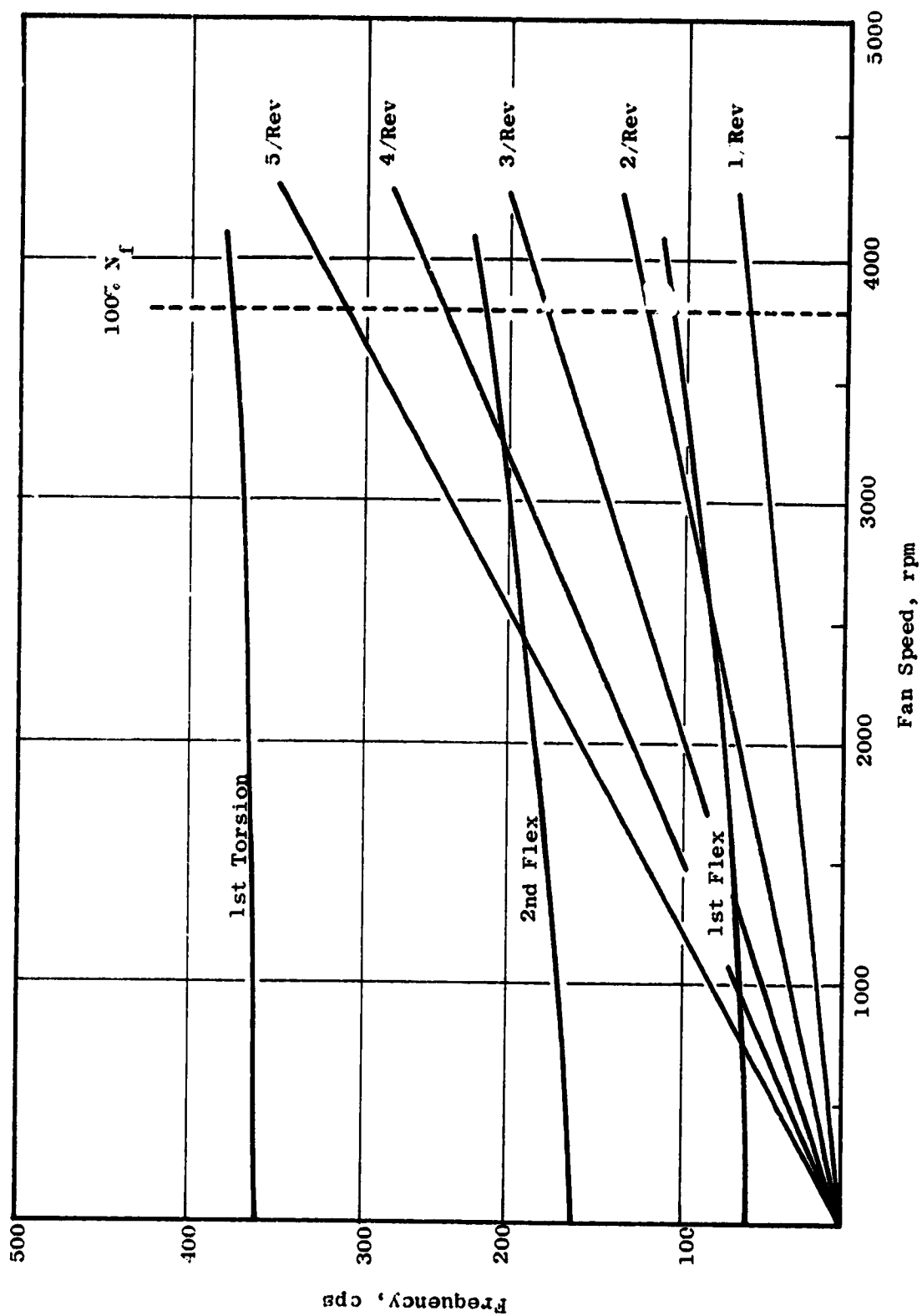
Figure 8-26. QCSEE OTW Fan Blade Campbell Diagram.

279
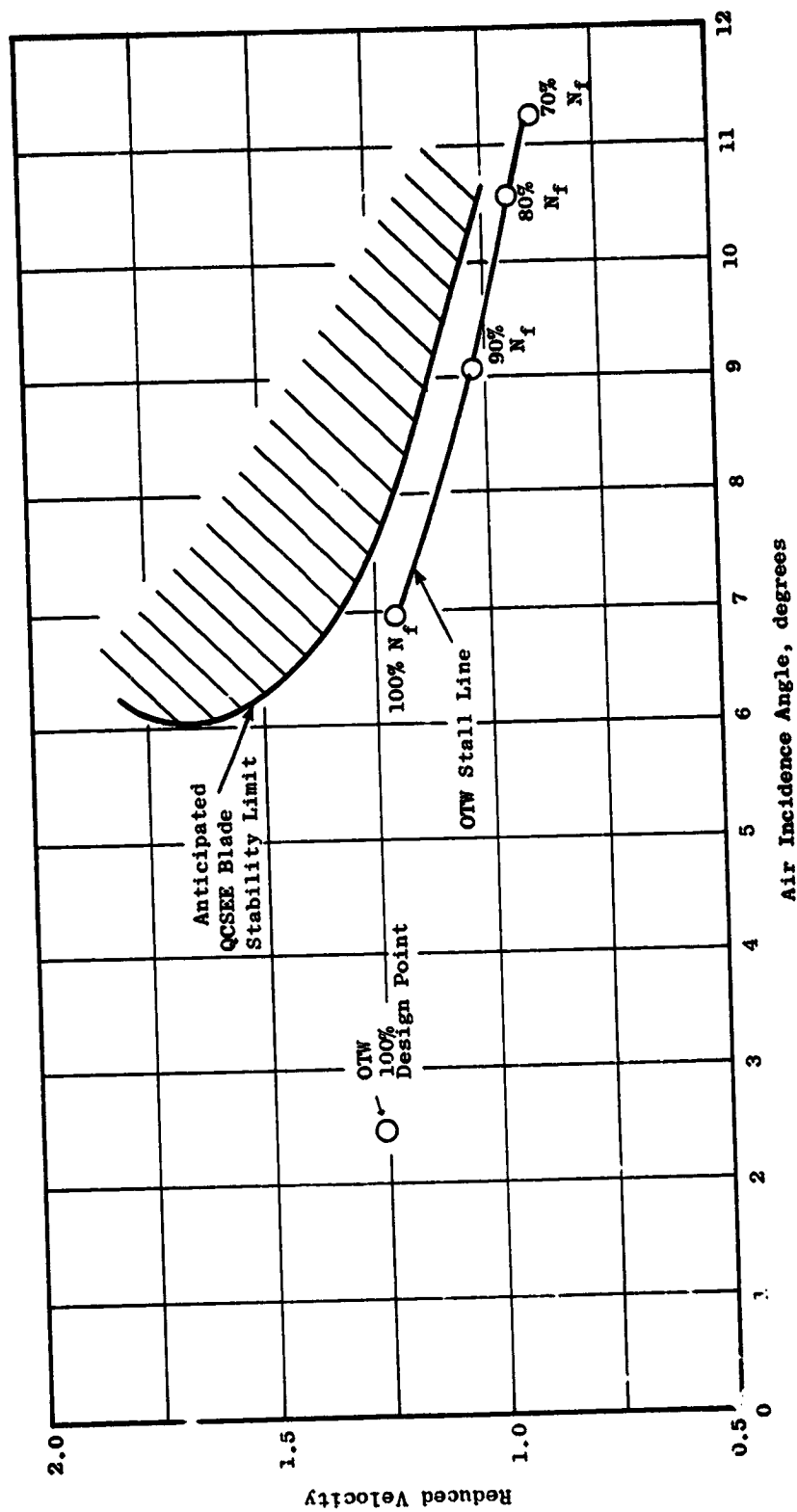
Figure 8-27. Limit Cycle Boundaries.

which the throttle fan will stall before encountering the anticipated blade stability limit.

The OTW composite flight blade would have additional stability margin due to the higher stiffness-to-weight ratio possible in composite designs.

The blade will be attached to the disk by a conventional dovetail. The outer flowpath contour will permit individual blade removal in the engine without the necessity of "drop down" dovetail slots. This dovetail will be plasma sprayed with a copper-nickel-indium coating for dovetail fretting protection.

Figure 8-28 shows a OCSEE OTW fan blade model. The design description of the blade is provided in Table 8-VII and in Figures 8-29 and 8-30.

8.3.2 OTW Fan Disk Design

The OTW fan disk will be machined from a single-piece 6A1-4V titanium forging. An integral cone attaches the ring disk to the main reduction gear shafting. The blades will be retained in the disk dovetail slots by individual steel straps and tangs on the blades. The spinner and aft flowpath adapter attach to flanges on the OD of the disk rim as shown in Figure 8-31.

The fan disk is designed for a burst margin of 141% of the maximum cycle speed and for a low-cycle fatigue life in excess of 36,000 flight hours.

8.3.3 OTW Fan Spinner

The OTW spinner and aft flowpath adapter will be fabricated from the same 6061 aluminim forgings used for corresponding parts on the UTW fan. Fan balance can be performed without removing the spinner by means of radial spinner balance weights, and the blades can be individually removed and replaced in the field by removing the forward spinner only. Access holes in the aft adapter permit unbolting the number one bearing support cone and pulling the disk and main reduction gear as a complete package. Since the OTW fan does not have a pitch change mechanism, the forward spinner cap also provides access for a visual inspection of the main reduction gear.

Figure 8-28. OTV Fan Blade.

282

Table 8-VII. QCSEE OTW Fan Blade.

Number of Blades   28

Fan Tip Diameter, cm   180.3
              (in.)   (71)

Airfoil Length, cm   52.1
              (in.)   20.5

Aspect Ratio   2.1

Average Root Centrifugal
    Stress, N/cm^2 15,291
              (psi)   (22,177)

	Blade Tip	Blade Root
Chord, cm	26.31	20.68
(in.)	(10.36)	(8.14)
Max. Thickness/Chord, %	2.65	8.6
Solidity	1.3	2.34
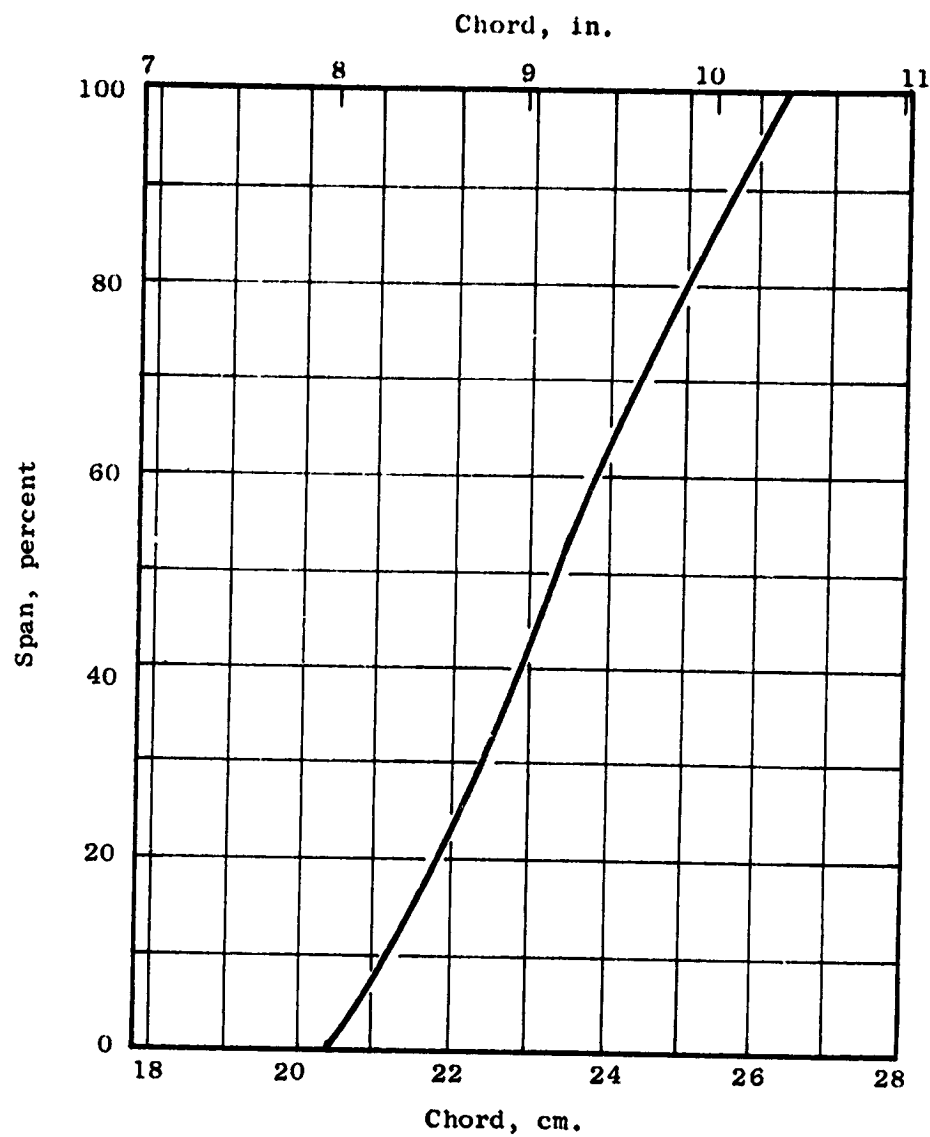
Figure 8-29. QCSEE OTW Fan Blade Chord Vs Span.
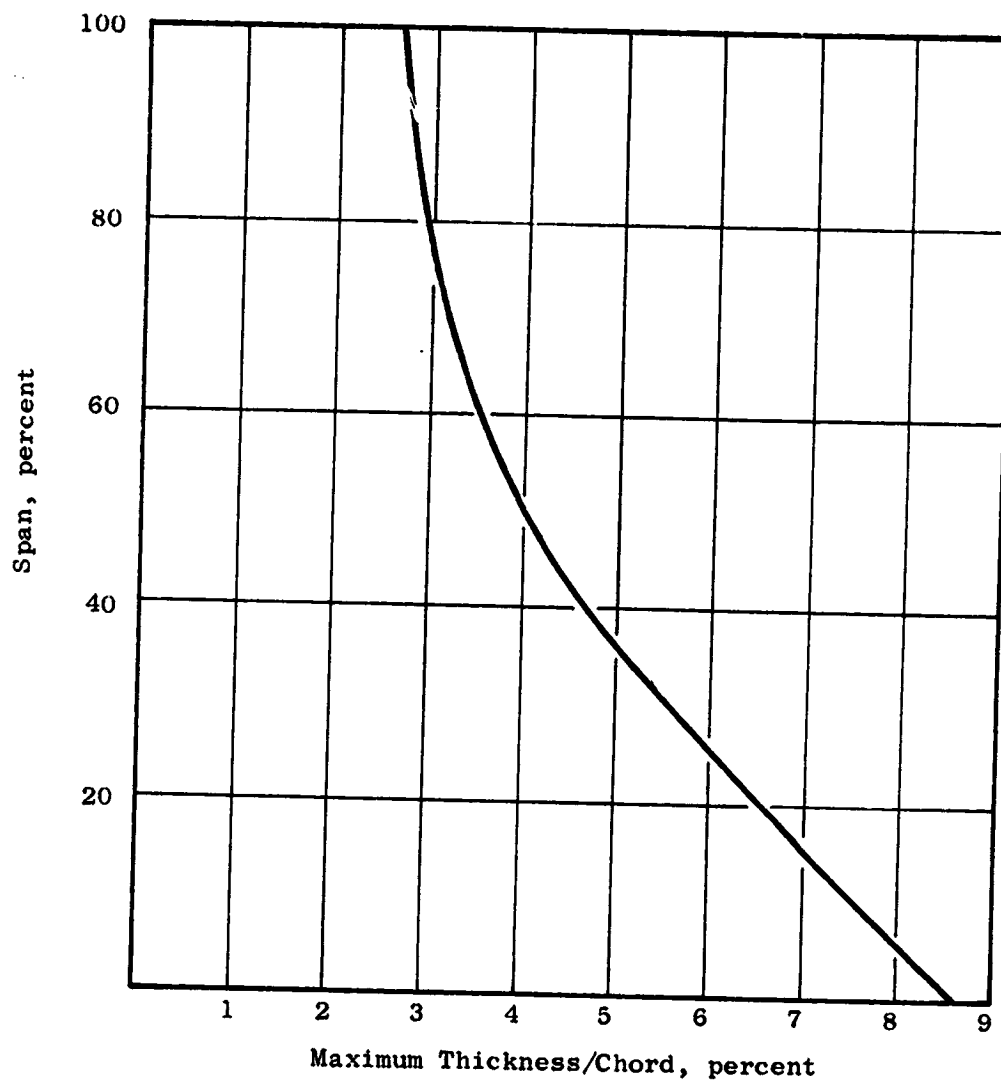
Figure 8-30. OTW Fan Blade Maximum Thickness/Chord Vs Span.
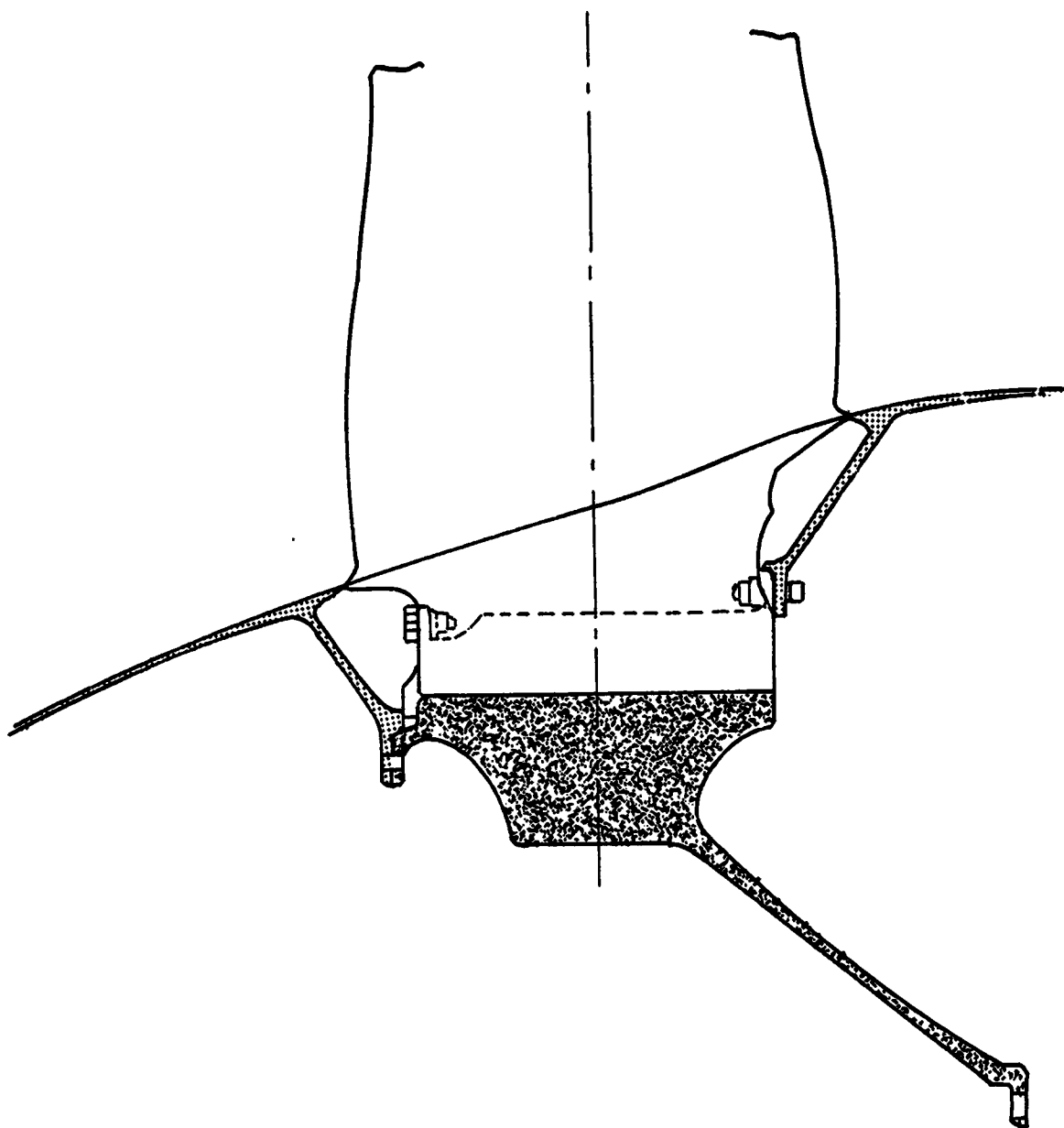
Figure 8-31. OTW Fan Rotor.

286

SECTION 9.0

FAN FRAME MECHANICAL DESIGN

9.1 SUMMARY

The QCSEE fan frame, for both the UTW and OTW engines, is an integrated design constructed of advanced composite materials. Integration of design is achieved by combining the functions of the fan stator vanes, fan outer casing, and fan frame into one unitized structure as shown in Figure 9-1. This approach saves considerable duplication of structure, resulting in a significantly lighter weight design. This unitized approach is particularly suited to use of composite materials since these materials are more efficient when employed in large bonded structures rather than smaller structures which must be bolted together.

The composite design concept used for the frame is essentially that which was developed for and demonstrated by the F101 simulated composite front frame shown in Figure 9-2. The concept basically consists of "wheels" in which the inner, mid, and outer rings and the spokes are fabricated as a one piece integral structure. Two or more of the wheels are then joined together by flowpath panels to form the basic frame. This concept, as applied to the QCSEE fan frame, is shown in Figure 9-3. Its major advantage is that the major radial load carrying structure, the spokes of the wheels, and the major circumferential load carrying structure, the ring or hubs of the wheels, are integrally bonded structures rather than separate structures which must transfer load by means of bolted joints.

The composite material system selected as the basic material for the frame is Type AS fiber in Hercule's 3501 epoxy resin matrix. This material was selected based on the rather extensive data base for the material, its good mechanical properties, and its ready availability.

A mathematical model of the frame was constructed to represent the structure shown in Figure 9.3. Externally applied loads were determined and applied to the model. Several iterations were made using thicknesses and material ply orientations until a design of adequate strength and stiffness was determined. This sizing then formed the basis for the preliminary design and the weight calculation.

To verify the structural integrity of the critical joint areas, a subcomponent test plan was outlined and will be finalized as detail design progresses. In addition, an element test program was initiated to verify predicted mechanical properties for specific orientations required for the frame.

The frame was designed primarily for the UTW engine and there is no difference between the flight and experimental engine design as far as the frame is concerned. There are two minor differences between the UTW frame and OTW experimental engine frame: there is a slightly different flowpath configuration over the fan blade and the fan core OGV structure is different. These changes are simple to incorporate in the basic frame. The flowpath
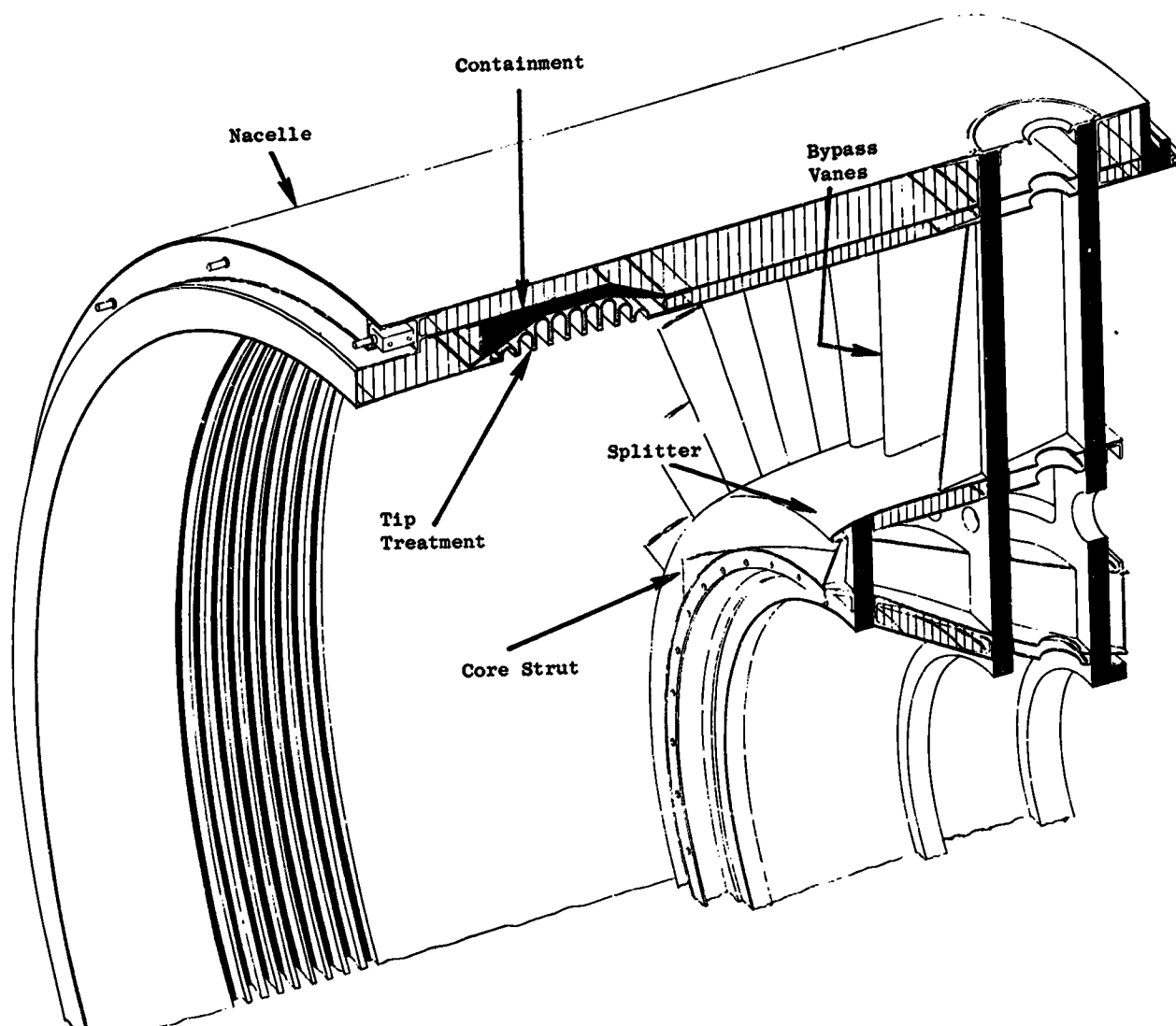
Figure 9-1. QCSEE Fan Frame.
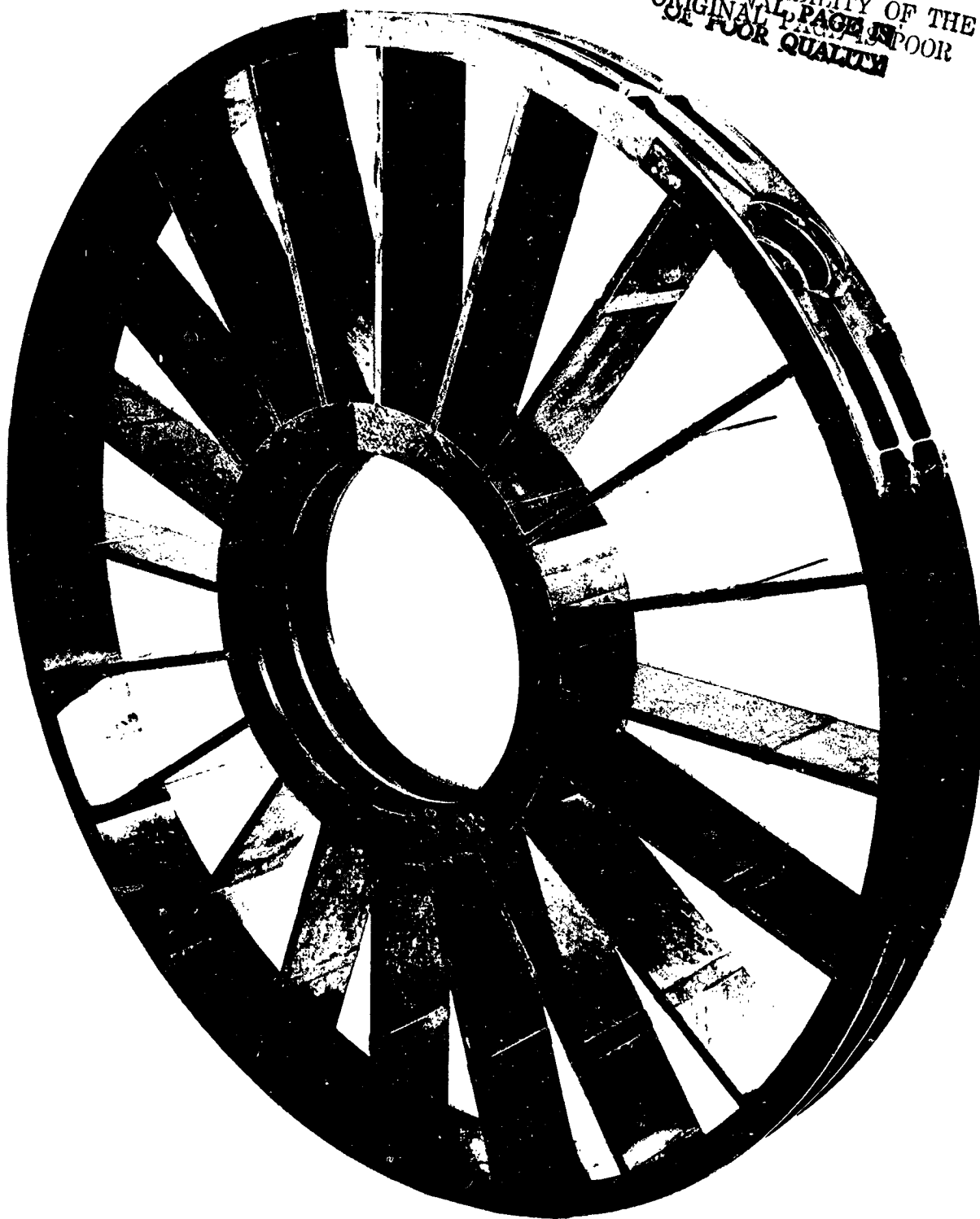
Figure 9-2. Simulated Composite Frame.
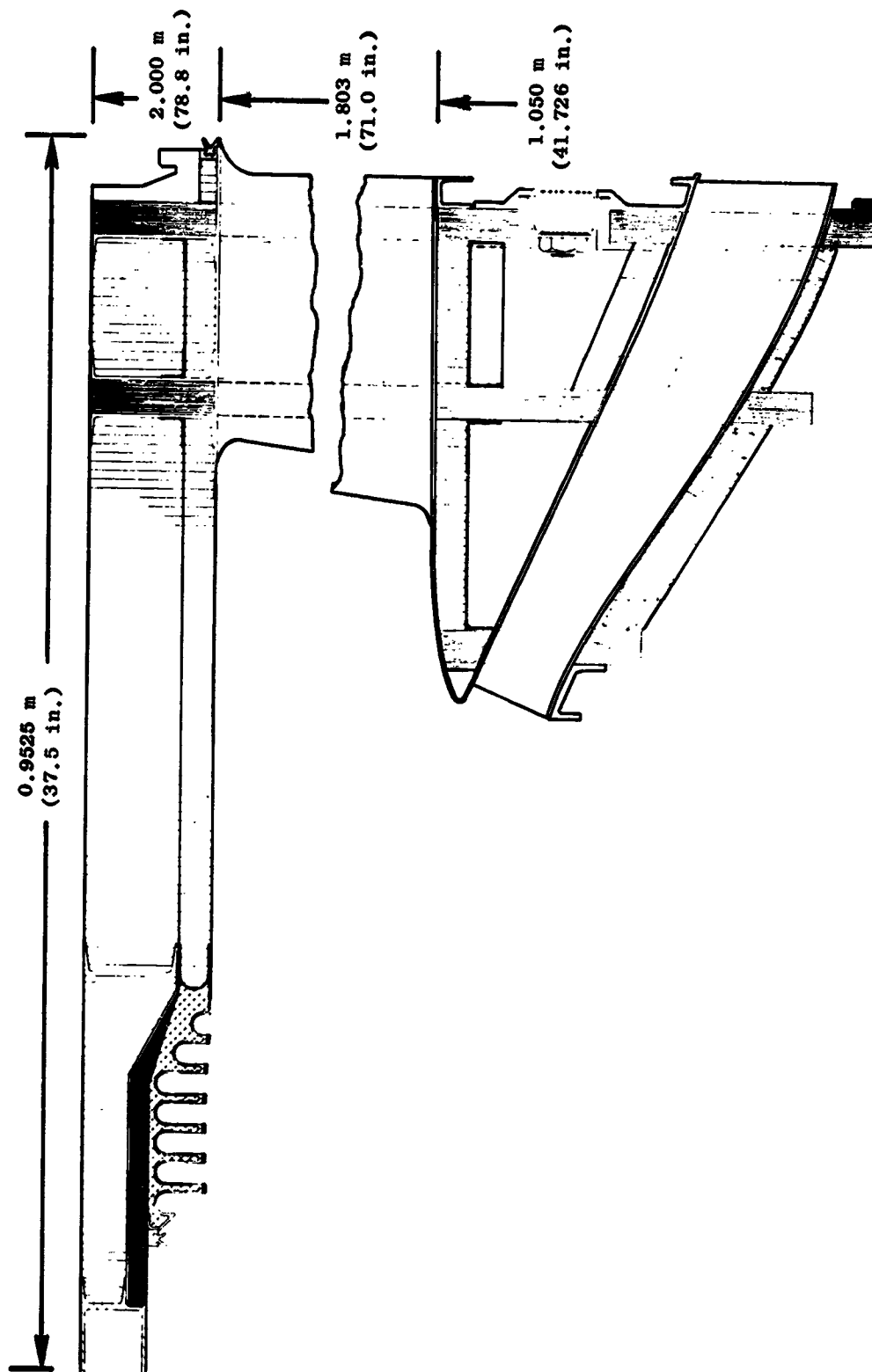
Figure 9-3. QCSEE Composite Frame.

2.000 m (78.8 in.)

1.803 m (71.0 in.)

1.050 m (41.726 in.)

0.9525 m (37.5 in.)

change can be accomplished by simply adding filler material until the desired shape is attained. The fan core OGV structure is a separate bolted-on sub-assembly and a separate design will be used. The only difference between the OTW experimental engine and OTW flight engine that affects the frame is a shift of the mounting system to the outer casing which requires a resizing of the frame structure.

In summary, preliminary design of the QCSEE composite fan frame is complete with no indication of any major problems. A detail discussion of the frame design and analysis is presented in the following paragraphs.

9.2 DESIGN REQUIREMENTS

9.2.1 Loads

The engine, including all nacelle and aircraft furnished components attached to or mounted on the engine and supported through the engine mounts, shall be designed to withstand, within the limits specified, loads defined in Conditions I through VI listed in Table 9-I in addition to the normal range and combination of steady-state pressure, thermal, thrust, and torque loads. Table 9-II summarizes the bearing loads on the frame for 1g down, 1 radian/sec, and one composite fan blade out conditions for both UTW and OTW composite frames. Air loading on the bypass vanes is shown in Figure 9-4.

9.3 STRUCTURAL DESCRIPTION

The UTW and OTW fan frames are structurally identical, and the following comments apply to both except as noted. The QCSEE frame is an all composite, static structure formed from integration of several separate structures. As seen in Figure 9-1, the outer casing of the frame is an integration of the nacelle with the frame outer shell. This casing provides part of the external nacelle flowlines as well as the internal fan flow lines. Fan blade tip treatment and containment is provided by the grooved, felt-filled structure integrated into the forward portion of the outer casing. Positioning of the fan and core engine relative to the integral nacelle/outer casing is provided by 33 bypass vanes which also serve as the fan bypass stator vanes. Therefore, the stator vanes serve as structural supports and provide flow turning of the fan flow discharge. Flow turning of the fan flow into the core is provided by an independent set of outlet metallic guide vanes attached to the forward flange of frame hub. The hub of the frame is connected to the splitter through six equally spaced struts. The inner shell of the outer casing, and regions of the splitter, and the pressure faces of the bypass vanes are perforated to provide acoustic suppression within the frame structure.

The fan core OGV preliminary design is a brazed and machined fabrication. The island splitter on the UTW engine will be of formed sheet metal with stator vanes penetrating the skins and brazed to them. The stator vanes will be supported at the hub through brazed joints into a machined inner casing bolted to the fan frame. Both island and stator vane air loads will be transmitted through this shell to the fan frame. This fan core OGV stator stage serves to turn the fan blade airflow in the new axial direction prior to entering the fan frame.

291

Table 9-I. QCSEE Engine Loads.

Limit Loads

For any one of the following load conditions, all stresses shall remain within the material elastic limits.

Condition I: (Flight and Landing) - See load diagram, Figure 2-2.

Condition II: (Gust Load) - An equivalent load from a 51.44 m/sec (100 knot) crosswind acting at any angle within a plane 1.5708 radians (90 degrees) to the axis of the engine, zero-to-maximum thrust.

Condition III: (Side Load) - A 4g side load combined with 1/3 the equivalent load as defined in Condition II, zero-to-maximum thrust.

Ultimate Loads

The engine shall not separate from the aircraft when subjected to Conditions IV, V, and VI and for static loads equivalent to 1.5 times the loads specified as limit loads in metal parts, and 3.0 times the loads specified as limit loads in composite parts.

Condition IV: (Flight-Engine Seizure) - The seizure loads are due to the fan and engine basic gas generator decelerating from maximum to zero engine speed in one second.

Condition V: (Crash Load) - The crash load is defined as 10g forward, 2.25g side, and 4.5g down at maximum thrust or up to zero thrust.

Condition VI: (5-blades Out) - The engine shall be capable of withstanding unbalance loads caused by the loss of 5 adjacent fan blades at maximum rpm (composite blades only).

292

Table 9-II. QCSEE Frame Radial Bearing Loads.

1g Down

	UTW		OTW	
Bearing No.	Radial Load		Radial Load	
	Newtons	Pounds	Newtons	Pounds
1	3,425	770	4,822	1,084
2	1,099	247	1,882	423
3	364	82	364	82
4	823	185	823	185

1 radian/sec

Bearing No.	Radial Load		Radial Load	
	Newtons	Pounds	Newtons	Pounds
1	27,397	6,159	69,232	15,564
2	27,397	6,149	69,232	15,564
3	1,699	382	1,739	391
4	9,559	2,149	9,906	2,227

1 Fan Blade Out

Bearing No.	Radial Load		Radial Load	
	Newtons	Pounds	Newtons	Pounds
1	235,627	52,971	226,458	50,910
2	82,852	18,626	58,454	13,141
3	7,491	1,684	7,451	1,675
4	28,989	6,517	19,359	.,352
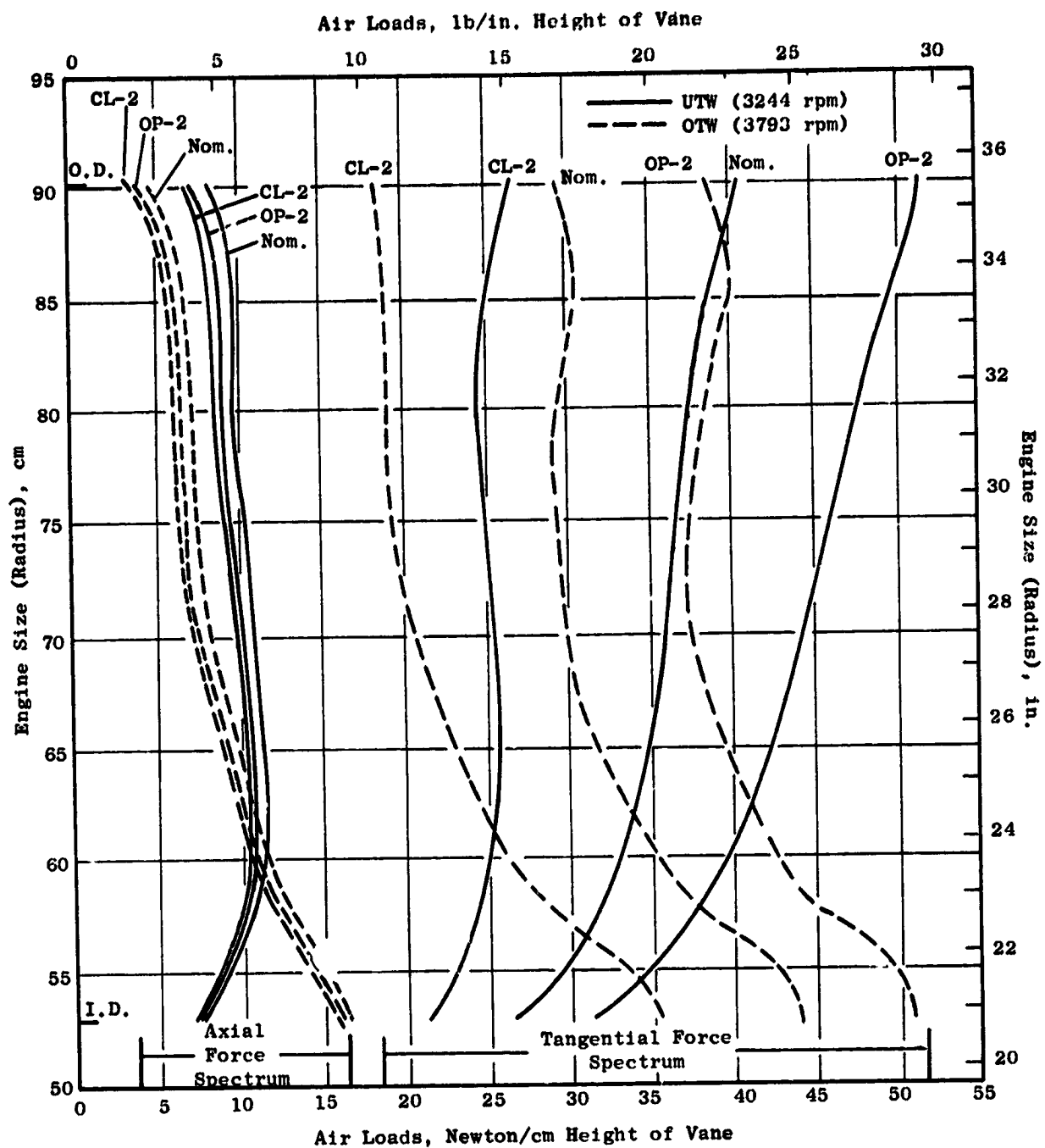
Figure 9-4. QCSEE Fan Design Bypass OGV/Frame Aero Design Air Loads - Closed 2°, Open 2°, and Nominal Vanes.

The frame mechanical design also provides the normal penetrations and accessory mounting positions required of other components. Also required is firewall-type protection between component parts and any fuel or lubricant. This additional objective required that all lube carrying frame passages be metallic lined and sealed.

Oil containment has been achieved by introducing a 360° metallic liner attached to the hub of the frame structural rings. This liner provides the major interface for all penetrations into the fan sump area. These penetrations include oil in, oil scavenge, PTO shaft, fan speed sensors, fan VP drive mechanism, seal drain lines, and the scavenge pump drive shaft shown in Figures 9-5, 9-6, and 9-7 for the $T_{2.5}$ temperature sensor; six total pressure and temperature rakes; and several static pressure taps.

Fan frame fabrication will be tailored to include the many penetration lines at specified steps in the manufacturing cycle. Each frame penetration will be sealed at the interface with the oil shield by an O-ring or other gaskets.

The lines will be of a sheet metal and machined ring welded fabrication with local bosses at each O-ring to support the required clamping force. The scavenge tube and the other penetration lines will be welded sheet metal or formed tubing fabrication with the required end connections for the O-ring seals.

9.4 STRUCTURAL FUNCTIONS

The QCSEE frame is required to perform the following major structural and aerodynamic functions:

- Provides the main engine forward attachment points for thrust, vertical and side loads sustained during flight and ground handling.

- Supports the fan thrust bearing.

- Supports the fan radial load bearing.

- Supports the variable pitch system.

- Supports the reduction gear.

- Supports the compressor thrust bearing.

- Supports the inlet.

- Supports the aft outer and aft inner fan cowl.

- Supports the core compressor at the forward casing flange.

- Supports the fan hub outlet guide vanes.

- Provides the mounting position for the accessory gearbox.

Attachment points for all of the above structures are shown in Figure 9-8.

295
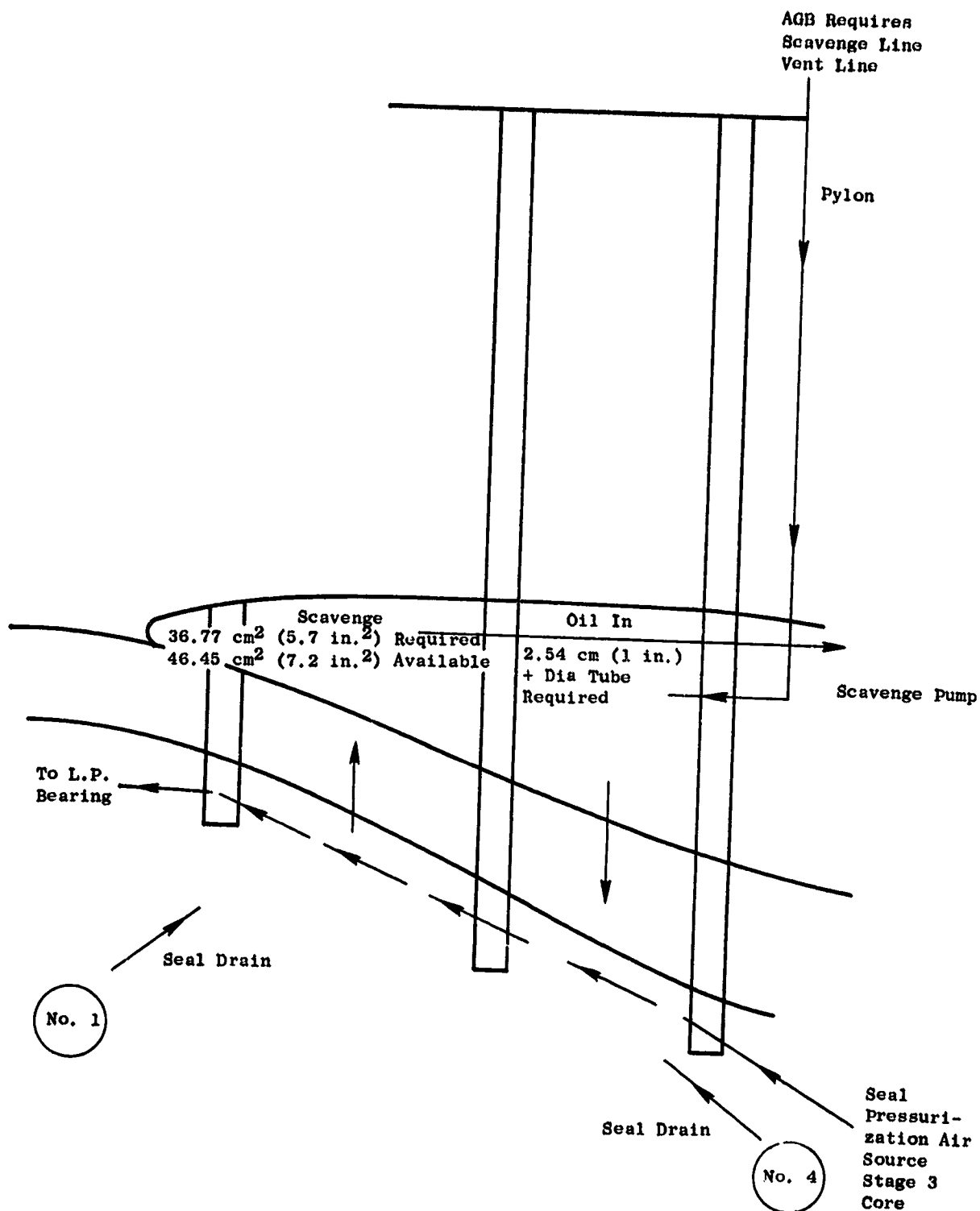
Figure 9-5. Fan Frame Service Areas.

The following labels appear in the figure:

AGB Requires
Scavenge Line
Vent Line

Pylon

Scavenge
36.77 cm^2 (5.7 in.^{2}) Required
46.45 cm^2 (7.2 in.^{2}) Available

Oil In
2.54 cm (1 in.)
+ Dia Tube
Required

Scavenge Pump

To L.P.
Bearing

Seal Drain

No. 1

Seal Drain

No. 4

Seal
Pressuri-
zation Air
Source
Stage 3
Core
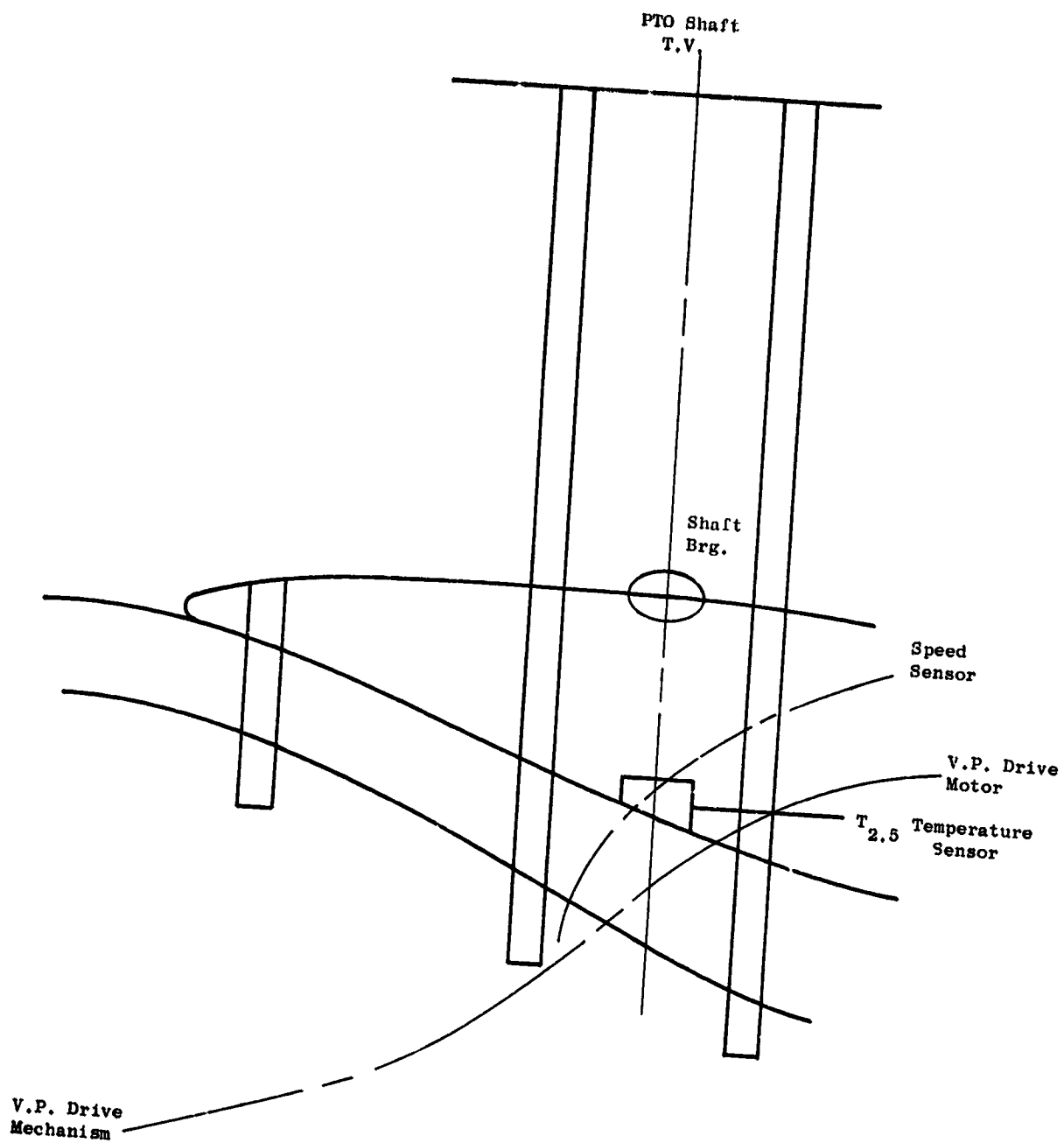
Figure 9-6. Fan Frame Service Areas.
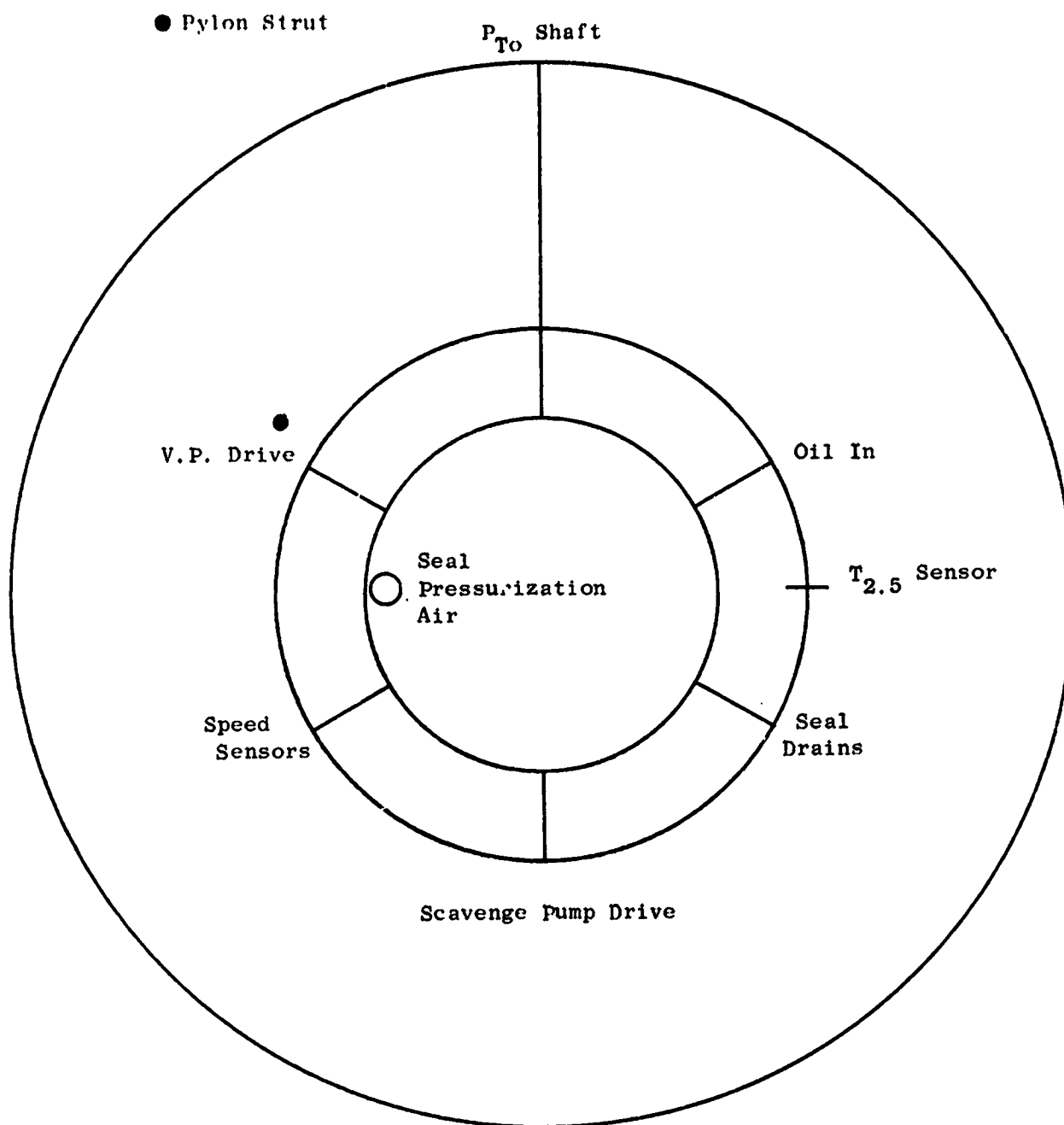
Figure 9-7. Fan Frame Service Areas.
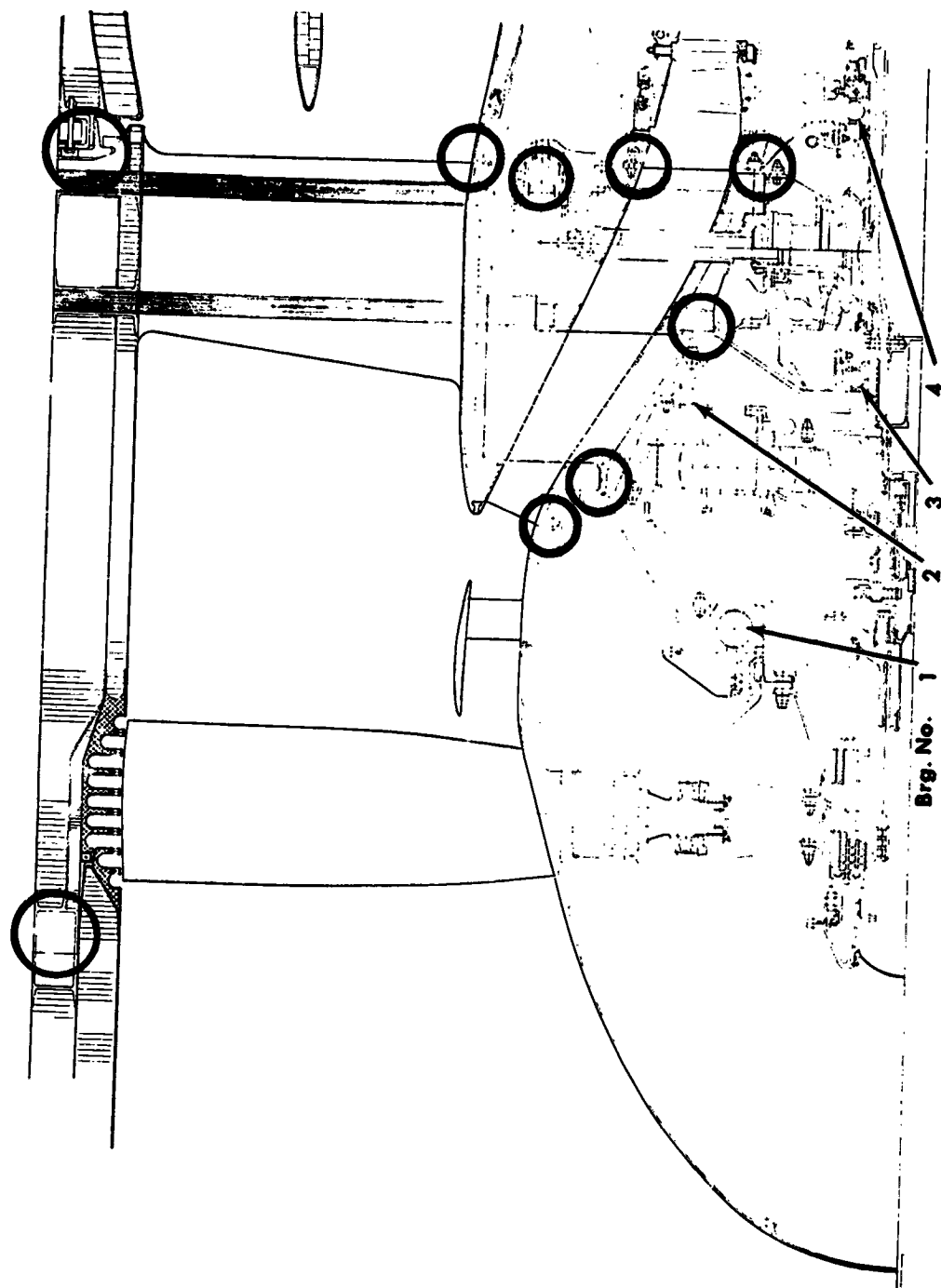
Figure 9-8. QCSEE Composite Frame.

Brg. No. 1 2 3 4

9.5 STRUCTURAL CONCEPT

The overall structural concept used in the frame consists of three basic elements (i.e., structural wheels, shear panels, and reinforcing flanges) with each element designed to perform specific load-carrying functions. The large wheel-like structures are joined together with shear panels which form the bypass and core flowpaths. The frame is then locally reinforced with flanges in the outer casing, splitter, and hub areas as needed. All of the above mentioned structural elements are shown in Figures 9-8, 9-9, and 9-10.

The structural wheel satisfies several load transfer requirements. First, it transfers tensile and compressive radial loads through the struts from one casing ring to another. Second, it transfers both normal and bending ring loads throughout the ring structure. Third, it transfers any forward overturning bending moments that exist in the strut from one casing shell to another.

The shear panels are bonded to the four sides of each wheel cavity and serve as the basic load-carrying members between wheels. The panels perform the following functions. First, they transfer shear forces between wheels imposed on the frame by a forward overturning bending moment. Second, they transfer radial tensile and compressive forces between casings imposed on the struts by a tangential bending moment. Third, they transfer axial tensile and compressive forces between wheels. Fourth, they serve as the airflow surfaces within the frame cavities.

The reinforcing flanges located in either end of each strut or vane perform two basic load-carrying functions: first, they transfer tangential bending moments out of the struts and into the forward and aft rings, and second, they transfer tensile and compressive axial loads between wheels.

This, then, is the basic design concept applied to the QCSEE frame. Completion of the preliminary analysis of the QCSEE composite frame indicates that a three-wheel frame concept is adequate to carry all imposed loads. The forward wheel is a flat-spoked wheel comprised of splitter ring, a hub ring, and six spokes. The middle and aft wheels are flat-spoked wheels comprised of an outer casing ring, a splitter ring, a hub ring, six spokes integrally connecting the hub and the splitter rings, and 33 spokes integrally connecting the outer casing and the splitter rings. The shear panels are bonded to the interior of each wheel cavity, and the panels form the airflow surfaces. "L" flanges are bonded to the inner and outer rings and flowpath panels. This structural concept not only provides a frame with high efficient joints, but also results in a structure which is relatively easy to fabricate and repair and requires a minimum amount of tooling. Structural soundness is enhanced by transferring loads by bonding in many small increments rather than in a few large increments.

The multiplicity of parts does not cause high costs because they are stamped out very economically by inexpensive dies and, after layup in a mold, are all bonded simultaneously into a sound, integrated structure. Metal engine

300
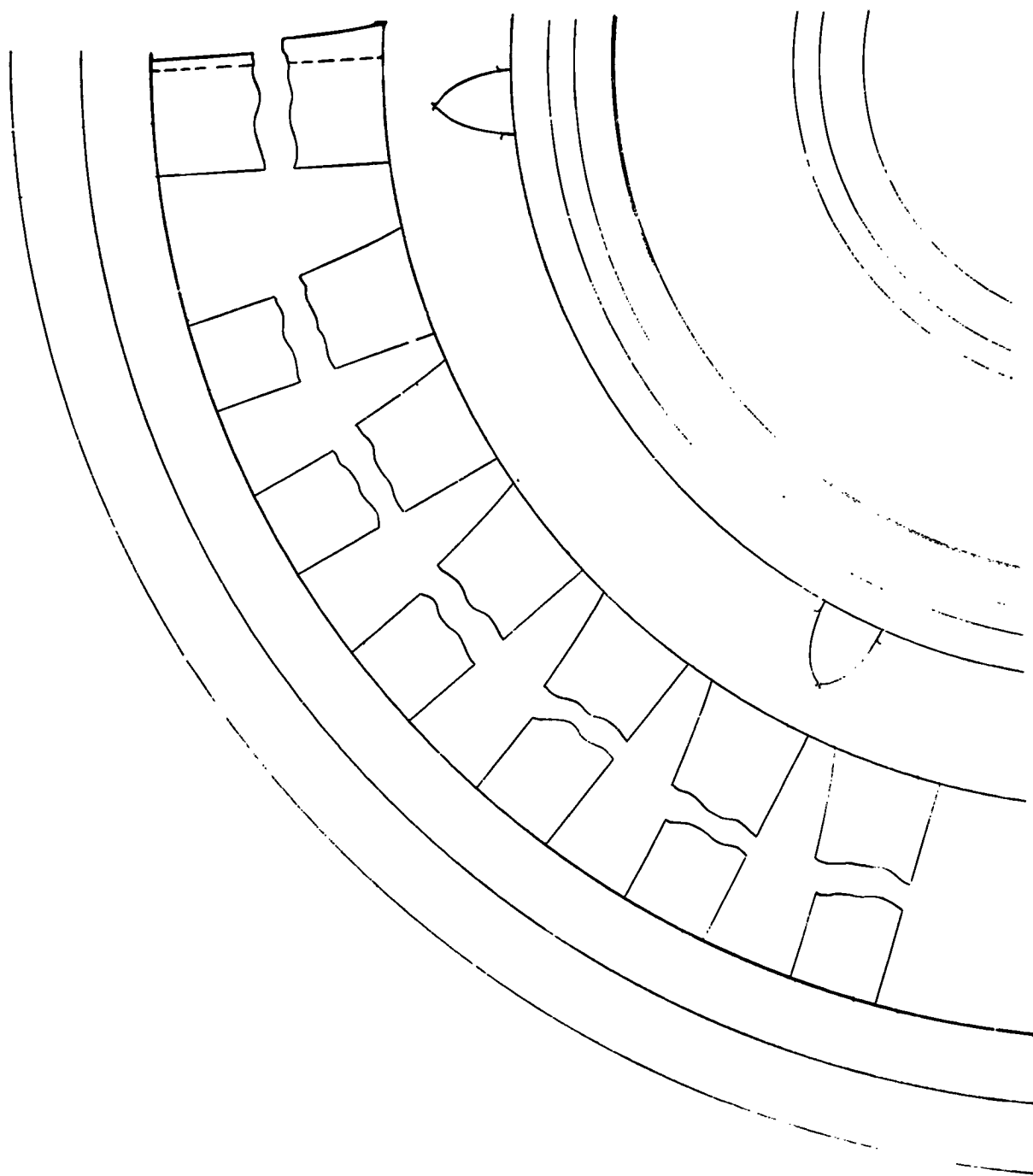
Figure 9-9. Fan Frame, Looking Aft.
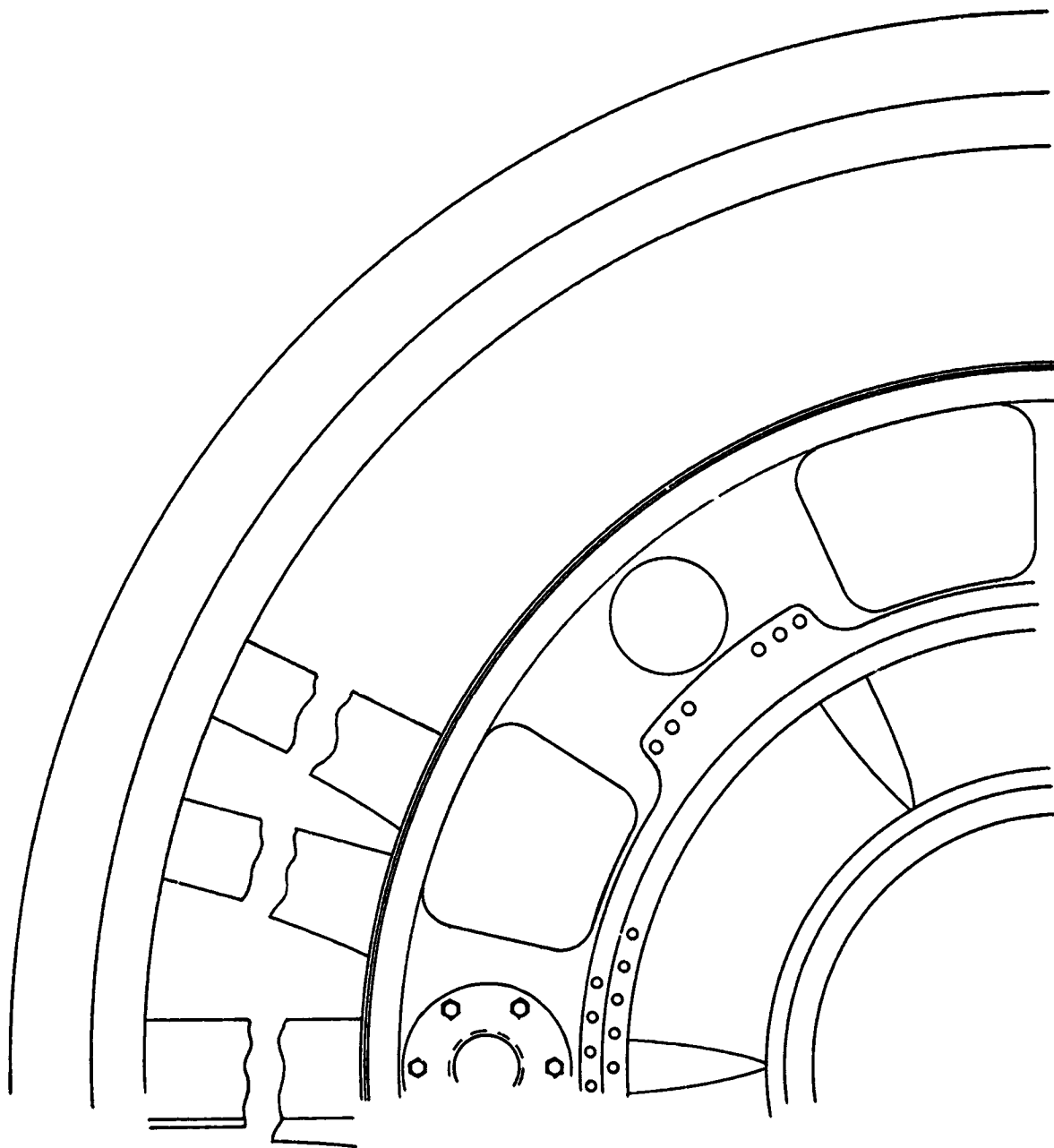
Figure 9-10. Fan Frame, Looking Forward.

mount parts and metal brackets are attached to the composite by bonding and mechanical fastening. The aft splitter ring will be provided with three engine-mount attachment points. The first attachment point is located at the 0° (12 o'clock) position on the aft splitter ring and consists of a metal uniball which supports vertical and side loads. At 45° down from either side of the   al uniball are metal brackets which support all thrust loads of the engine. The inner hub of the frame has flanges for attachment of fan rotor bearing supports, stationary reduction gear bearing supports, the low pressure turbine shaft forward bearing support, and the core rotor forward bearing support.

The nacelle and fan casing, including acoustic treatment, are integral with the frame from the bypass vanes forward to the inlet. The high strength and stiffness in the frame provide the nacelle support and also supports the stator, radial drive gear boss, and other equipment. The entire wall thickness of the fan case and nacelle is utilized to provide fan shroud stiffness and t   upport the blade containment member. The full-depth honeycomb is lighter and   ss expensive to fabricate compared to the conventional double structure. The joints normally required in a metal frame design are reduced, which further reduces weight, tooling, and fabrication costs. This concept is particularly well suited to composite materials due to their low density and easy "bonda-bility." Slotted tip treatment and a small area of frangible honeycomb are provided over the fan blade. The blade FOD containment provisions consist of unimpregnated Kevlar-49 felt wrap, located in a cavity on the outside of the tip treatment structure. This felt is kept in a place by closure of the cavity after the felt is installed. Although this material has never been used for this particular application, it is now being successfully used in ballistic armor and has high promise as a very efficient containment material. The actual demonstration of containment using this concept is, however, not a part of the QCSEE program. A detailed view of the design is shown in Figure 9-11.

Sound suppression features are integral with the casing structure and consist of sound-treated composite flowpath walls backed by honeycomb of specific cell size and depth. The exact configuration varies with location.

9.6 DESIGN ANALYSIS

The first step of the analysis procedure was to establish an iterative design analysis cycle for the composite frame. Figure 9-12 illustrates the design analysis cycle. As seen in the figure, this cycle reflects the design optimization parameters embodied in a typical composite static structure. Refinement of each structural component is accomplished by cycling each component through the above mentioned process until its ply orientation, geometry, and cost have been optimized for the particular loading environment.

The optimization procedure was initiated by assuming practical orientations and thicknesses for all of the component parts of the basic design. Next, a finite element model of the QCSEE composite frame was constructed and is shown in Figures 9-13, 9-14, and 9-15. Due to the simplistic nature of the design philosophy embodied in the frame, wheels (curved beams and straight beams), and skins (plates), the computer model quite accurately represents the actual frame structure. This similarity is shown in Figure 9-13.
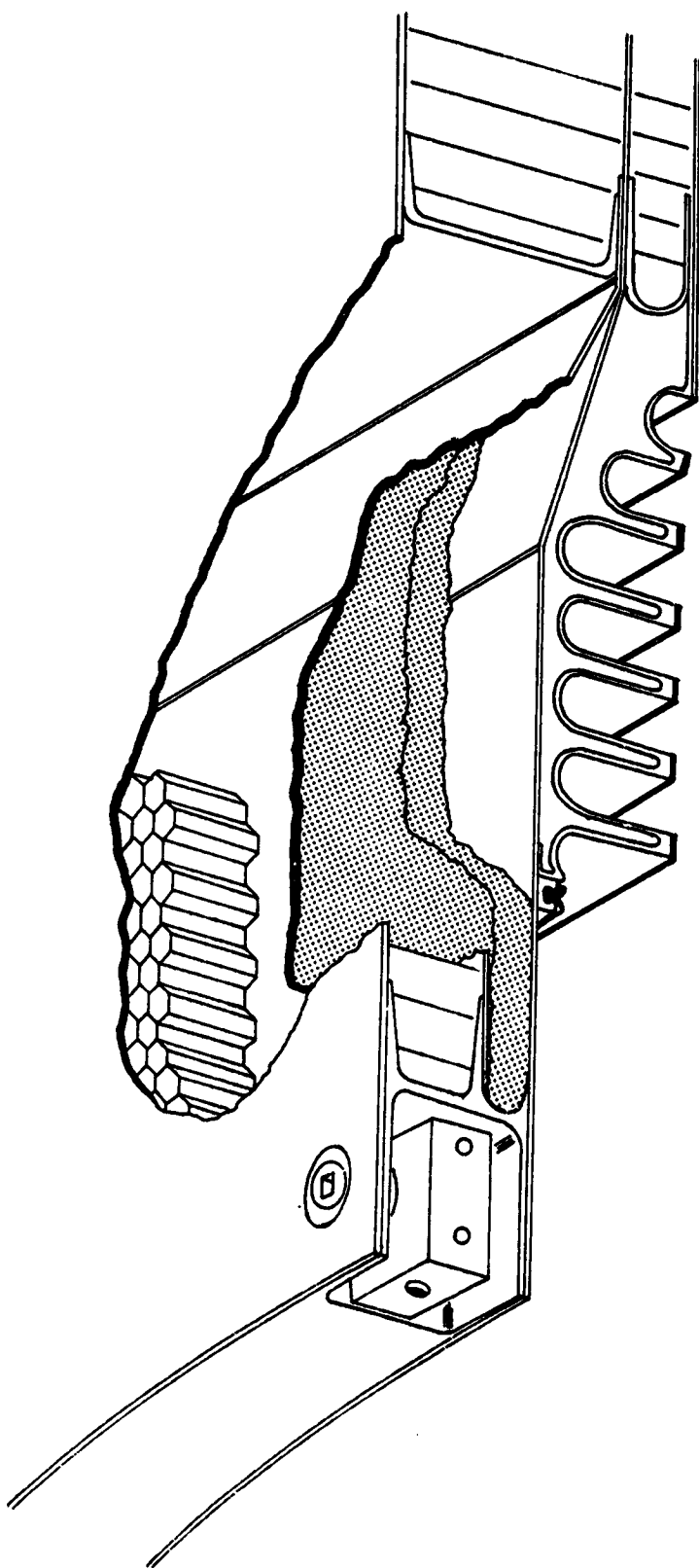
Figure 9-11. Fan Blade Containment Ring.
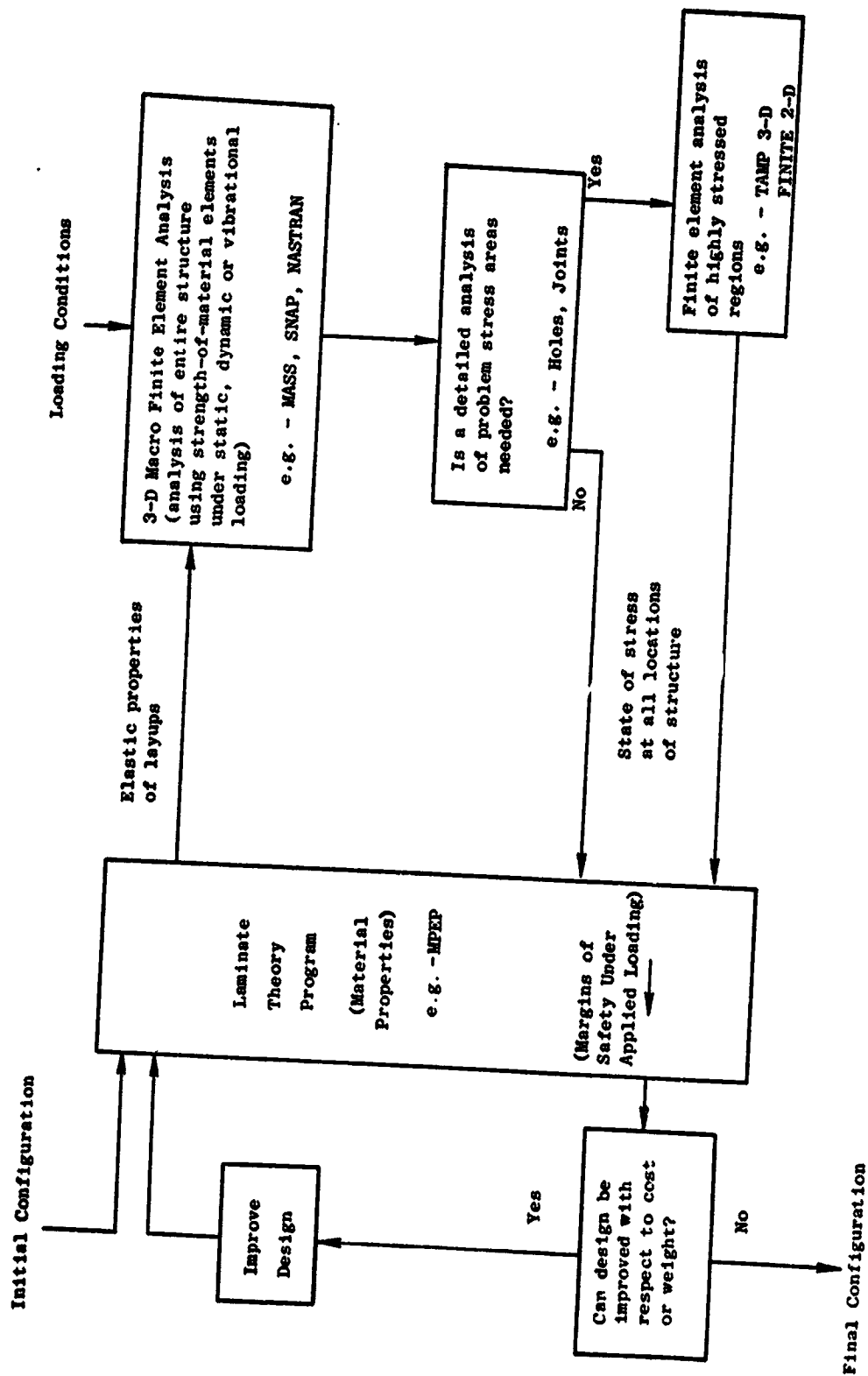
Figure 9-12. Process for Iterative Structural Computer-Aided Design (PISCAD).
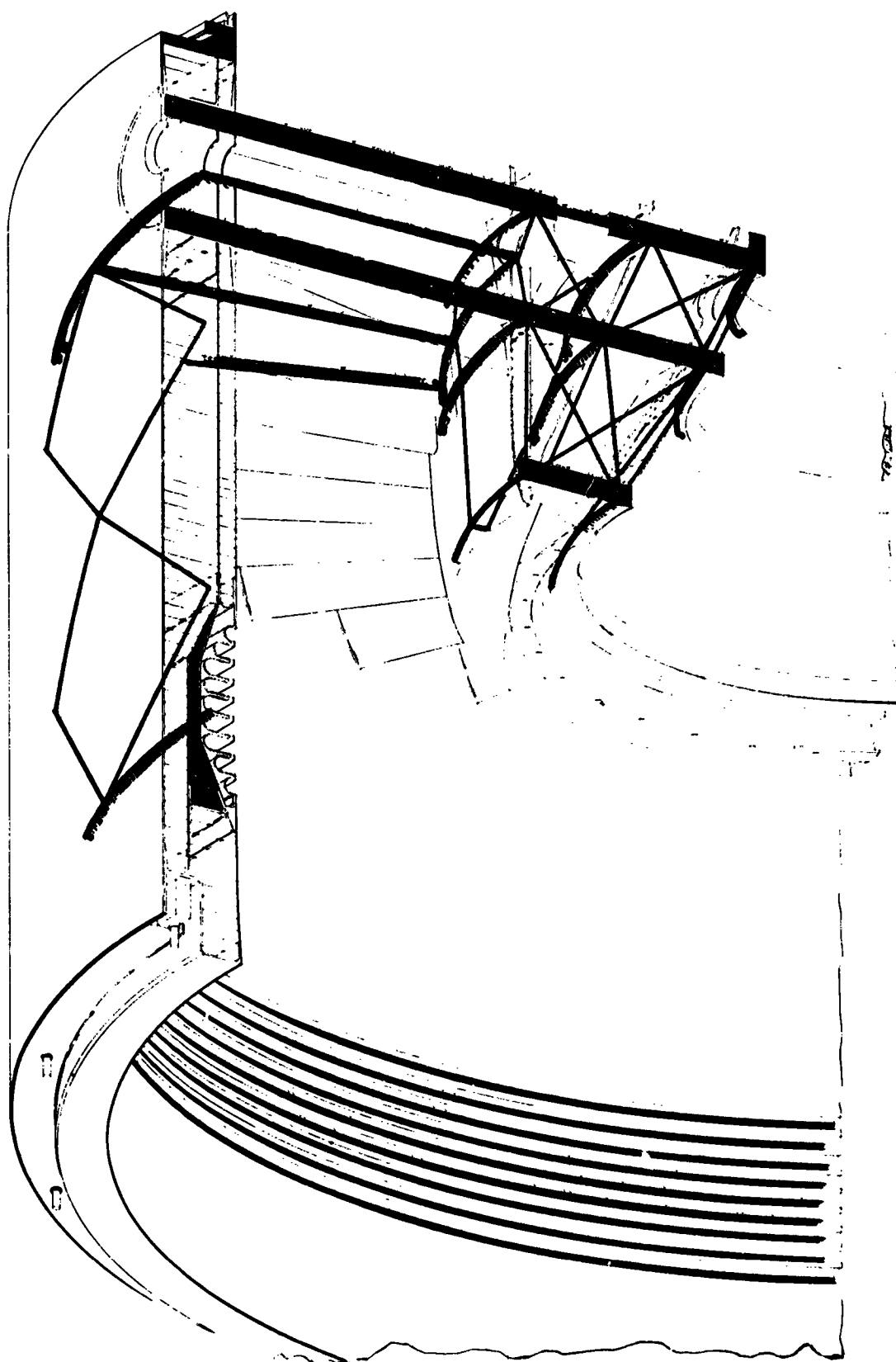
Figure 9-13. Computer Analytical Model of Composite Frame.
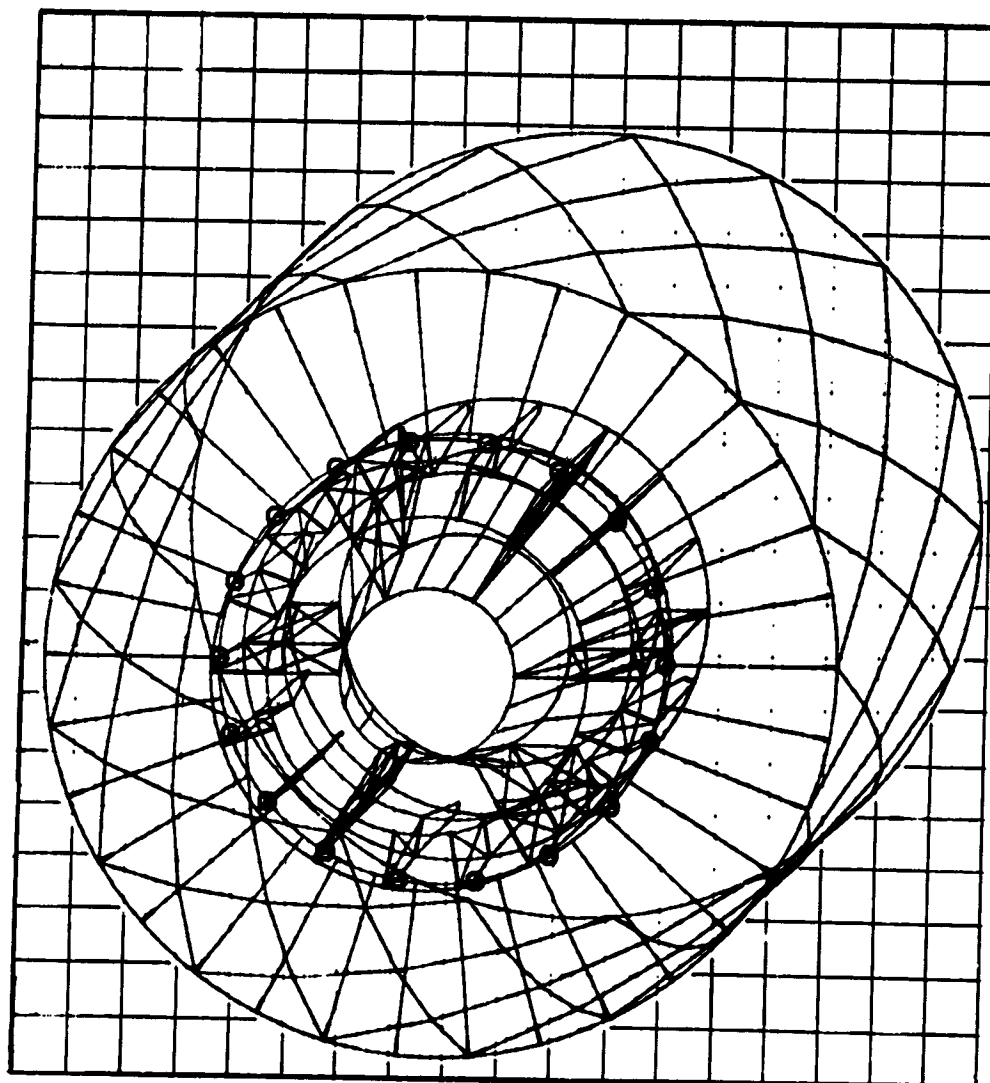
Engine 6:00 Position (Aft Looking Forward)

Figure 9-14. Finite Element Model – Composite Frame.
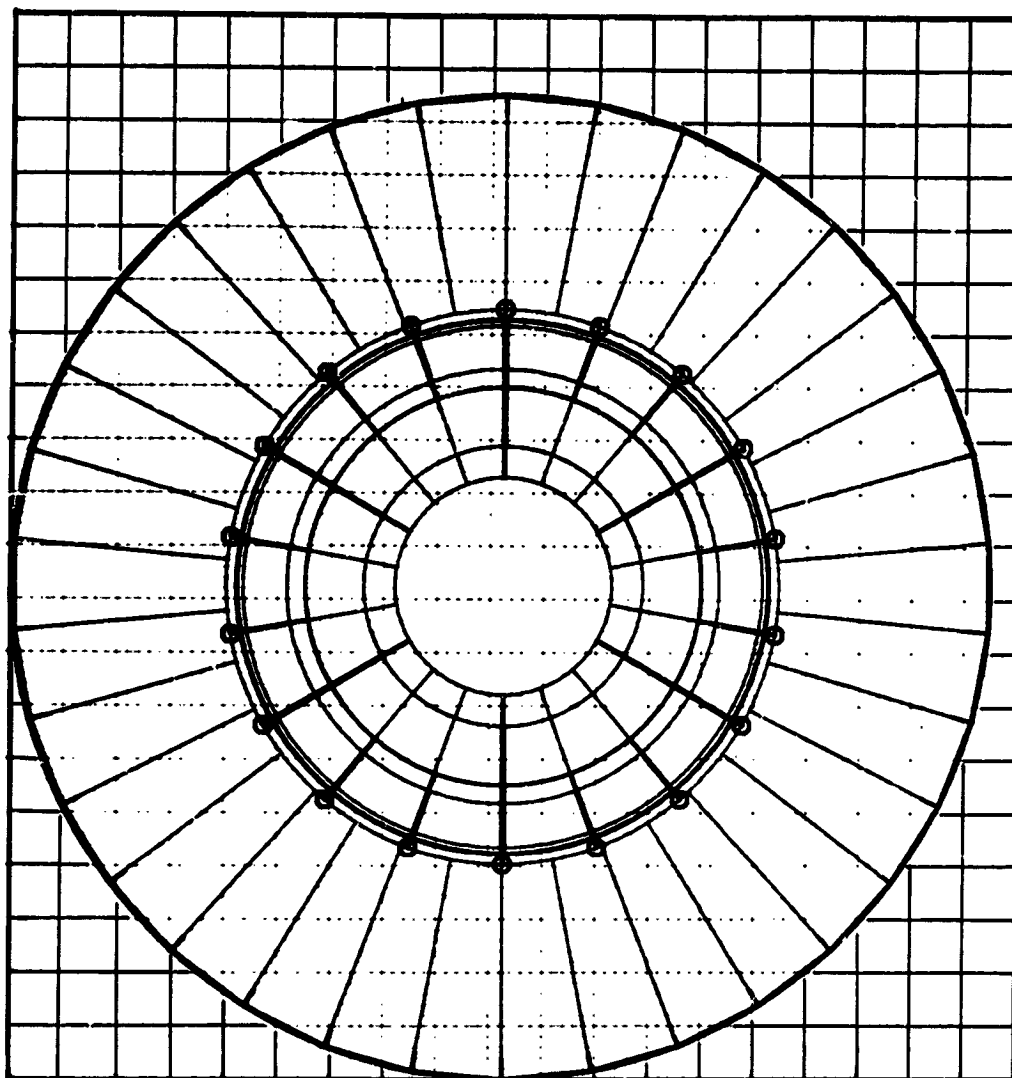
Engine 6:00 Position (Aft Looking Forward)

Figure 9-15.   Finite Element Model - Composite Frame.

The next step of the analysis procedure was to establish the most severe loading environments for the frame. The frame structure in conjunction with the engine mounts, must withstand the maneuver loads as imposed by the conditions as depicted in Table 9-I. The frame must withstand these loads and maintain structural integrity without permanent deformation. In addition, this structure must be capable of transmitting mount loads equivalent to 3.0 times the worst possible combination of maneuver loads without experiencing collapsing, even though the members may acquire permanent deformation. All ultimate load conditions occur at a room temperature environment. Investigation of the mission requirements yielded two critical loading cases.

The first case is Condition II (gust loading). Design conditions require the frame to withstand three times the loads of a 51.44 m/sec (100 knot) crosswind acting at any angle within a plane perpendicular to the axis of the engine at zero-to-maximum thrust. This condition sizes the outer nacelle shell and bypass vanes.

The second case is Condition VI (blade out). five-blade-out condition requires the frame to withstand the unbalance load resulting from a five composite blade-out condition on the fan rotor which causes a dynamic, 1/rev radial load on the No. 1 bearing support. This condition sizes the core struts, hub, and splitter.

Internal loads, stresses, and deflections in the frame incurred by the above mentioned load conditions were analyzed using the MASS computer program and the finite element model of the frame illustrated in Figure 9-14. Maximum frame component stresses and bond shear stresses for Conditions II and VI are shown in Tables 9-III and 9-IV. The maximum radial deflection of the fan casing over the fan was 0.086 cm (0.034 in.). Running clearance is 0.254 cm (0.1 in.). Geometry and material properties of the various composite frame components selected for the preliminary QCSEE frame design are shown in Table 9-V.

9.6.1 Weight

A preliminary weight analysis of the QCSEE composite frame was computed using the final model of the preliminary analysis. This weight breakdown is shown in Table 9-VI.

9.7 SUPPORTING TEST DATA

The composite frame must attach to, and be detachable from, various structures at a large number of locations. Also, the composite frame employs a large number of structural joints that are integrally bonded rather than mechanically fastened together. Therefore, in order to obtain a successful composite frame, specimens, subcomponents, and components representative of various structural frame components shall be required for testing. The purpose of the specimens and subcomponents is to allow the designer to determine the effect of geometry, fiber orientation, and environmental exposure on the allowable design stress levels in these specific components. This method permits refinement and improves the efficiency of each component

Table 9-III. Frame Component Stresses.

Load Case(1) No.	Location	Stress N/m²	(psi)	Allowable Stress N/m²	(psi)	Temperature °K	°F
2	Bypass Vane	402.9×10^6	(58,430)	565.4×10^6	(82,000)	338.7	(150)
6	Fwd Core Spoke	687.06×10^6	(99,650)	841.2×10^6	(122,000)	450	(350)
6	Fwd Core Spoke	690.4×10^6	(100,136)	930.8×10^6	(135,000)	450	(350)

(1) Case 2 - 154.33 m/sec² (300 knot) crosswind gust load + max. maneuver.

Case 6 - 5 composite blade out

Table 9–IV. Bond Shear Stresses.

Load Case[1] No.	Location	Design Stress[2] N/m²	(psi)	Allowable Stress N/m²	(psi)
2	Vane/Splitter	6.05×10^6	(878)	10.34×10^6	(1500)
6	Panel/O.R. Fwd "Wheel"	7.48×10^6	(1085)	10.34×10^6	(1500)
6	Panel/Spoke Fwd "Wheel"	8.06×10^6	(1169)	10.34×10^6	(1500)
6	Panel/I.R. Fwd "Wheel"	4.81×10^6	(698)	10.34×10^6	(1500)

(1) Case 2 – 154.33 m/sec² (300 knot) crosswind gust load + max. maneuver

Case 6 – 5 composite blade out + max. maneuver

(2) Design Stress – $\underline{3}$ x actual for flight and actual for emergency conditions

311

Table 9-V. Geometry and Material Properties of Various Composite Frame Components.

Item	Thickness		Material	Lay-Up Pattern
	cm	(in.)		
Outer Nacelle Shell	0.0889	(0.035)	Hybrid[1]	$0°_1$, $\pm 45°_2$, $90°_2$
Bypass Vane Panels	0.127	(0.050)	Graphite	$0°_4$, $\pm 45°_2$, $90°_2$
Core Shells and Panels	0.254	(0.100)	Hybrid[1]	$0°_{10}$, $\pm 45°_3$, $90°_4$
Core Spoke	2.54	(1.000)	Graphite	$0°_{160}$, $\pm 45°_{20}$
Bypass Spoke	2.54	(1.000)	Hybrid[1]	$0°_{160}$, $\pm 45°_{20}$
Rings	2.54	(1.000)	Graphite	$0°_{93}$, $\pm 45°_{23}$, $90°_{21}$
Rings	0.635	(0.250)	Hybrid	$0°_{25}$, $\pm 45°_{15}$, $90°_{10}$

(1) Hybrid represents either ultra high modulus graphite or boron combined with intermediate modulus graphite

312

Table 9-VI. QCSEE Composite Frame Weight Breakdown.

	Weight	
	kg	(lb)
Composite "Wheels", Rings, and Panels	120.2	(265)
Honeycomb	13.15	(29)
Composite Reinforcing Flanges	21.8	(48)
Adhesive	4.53	(10)
Inlet Flange	8.6	(19)
Sump Shield	2.7	(6)
Containment	20.9	(46)
Core OGV's	16.8	(37)
Total Weight	208.68	(460)

under evaluation. The subcomponent test regions are shown in Figure 9-16. The component test structure shall consist of a sector of the fan frame. This specimen shall be comprised of all structural elements required to fabricate an entire core frame with mounts.

The element test program to verify predicted mechanical properties for the orientations planned for the various frame components is currently in progress as is an investigation of the effects of hot Skydrol on the selected material system.

9.8 DIFFERENCES BETWEEN THE UTW AND OTW FRAMES

There are only two basic differences between the OTW composite experimental frame and the UTW composite frame. First, the axial contour of the inner nacelle shell above the fan tip is straight for the OTW frame and curved for the UTW frame. Second, the island structure of the fan core OGV assembly structure for the OTW is integral with the frame splitter, but separate for the UTW frame. In the flight version, the mount system for the OTW flight frame has two mounts located on the outer casing of the frame at 3 o'clock and 9 o'clock; whereas, the UTW flight frame has three mounts located on the splitter of the frame.

The fan core OGV for the OTW engine, while having 156 vanes as compared to 96 vanes on the UTW engine, will be similar in design. The fan core OGV design and the frame flow splitter will be designed so that either of the two fan frames can be used with each of the OGV designs.

314
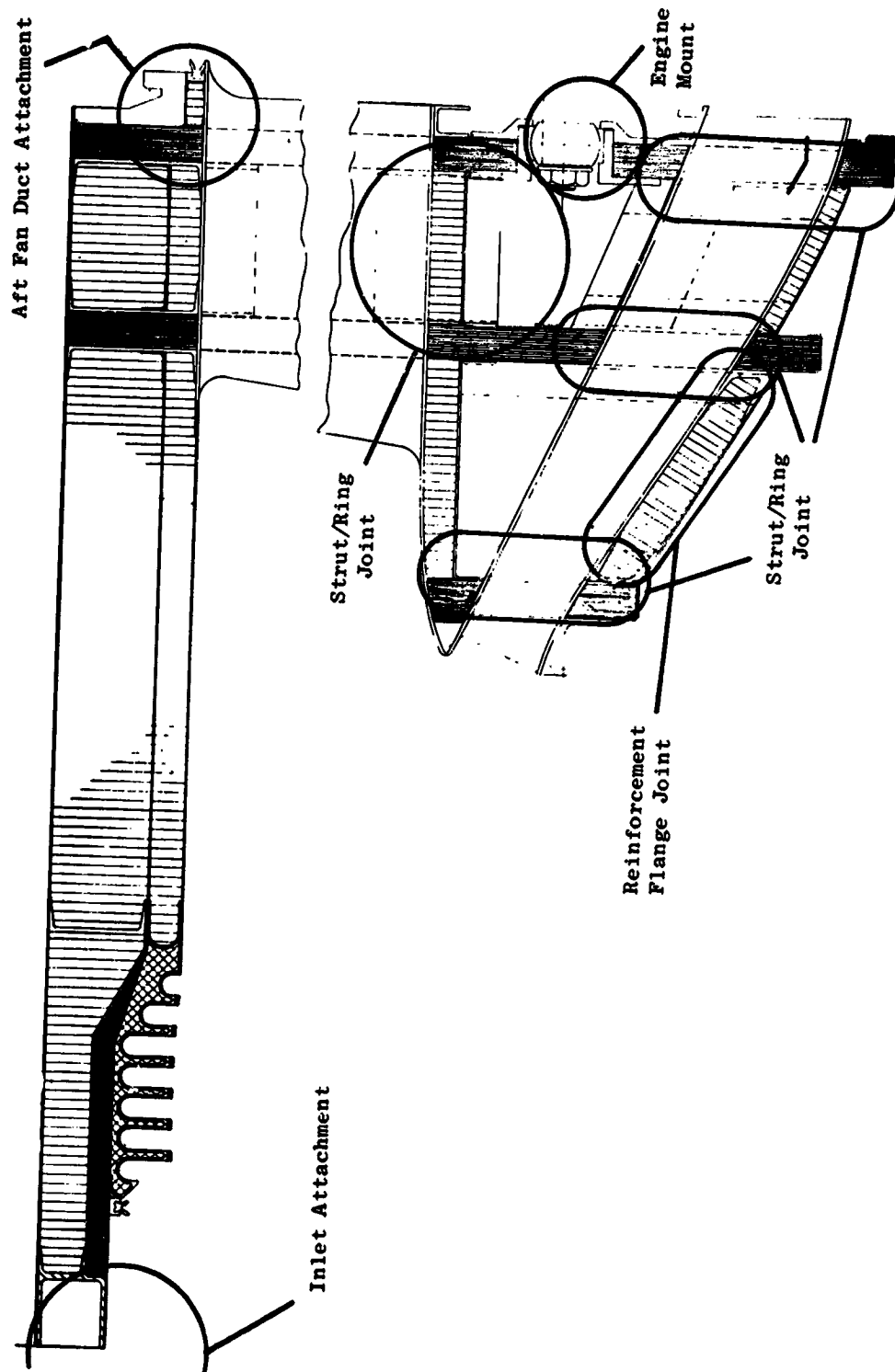
Figure 9-16. Subcomponent Test Regions.

315

SECTION 10.0

REDUCTION GEAR DESIGN

10.1 SUMMARY

The Main Reduction Gear sets for the UTW and OTW QCSEE Engines are being designed and developed by the Curtiss-Wright Corporation, Woodridge, N.J. The designs represent a further development of the first-stage reduction gearing used in the Curtiss-Wright YT49 turboprop engine, see Figure 10-1.

Each gearset is arranged in an epicyclic star configuration. The power turbine drives a sun gear which drives a ring gear through a set of star gears. These star gears are mounted on spherical roller bearings which are in turn mounted on a fixed carrier. This arrangement provides the required gear ratios and results in a compact lightweight design.

Gear stresses are kept within industry approved limits for the flight design. Somewhat higher stresses will be encountered during a small part of the experimental testing. This higher stress level only occurs during fan mapping and is within limits previously found acceptable by both Curtiss-Wright and General Electric. Scoring will be prevented by using controlled low inlet oil temperatures. The contact ratio of the gears is maintained at a value of 2, further reducing stress since two gears are generally in contact and sharing the load (Note: for analysis of gear stresses, credit was not taken for the contact ratio for conservatism). This high contact ratio also reduces vibration and noise.

A bearing test program is included to ensure satisfactory star gear bearing operation prior to testing in the gear box.

In summary, both the UTW and OTW reduction gears are based on proven concepts and conservative design, augmented by improved technology. This approach is expected to result in a compact, lightweight, reliable design.

10.2 DESIGN REQUIREMENTS

The main reduction gear for the QCSEE Engine was designed in accordance with General Electric Specification M50TF1611-S1 modified to meet the engine requirements as they became established. The reduction gears have been designed for the flight duty cycle and then checked for satisfactory operation in the experimental engine ground test cycle. In addition to the general engine requirements covered in Section 2.0, specific requirements have been established for the reduction gear as presented in Table 10-I.

316
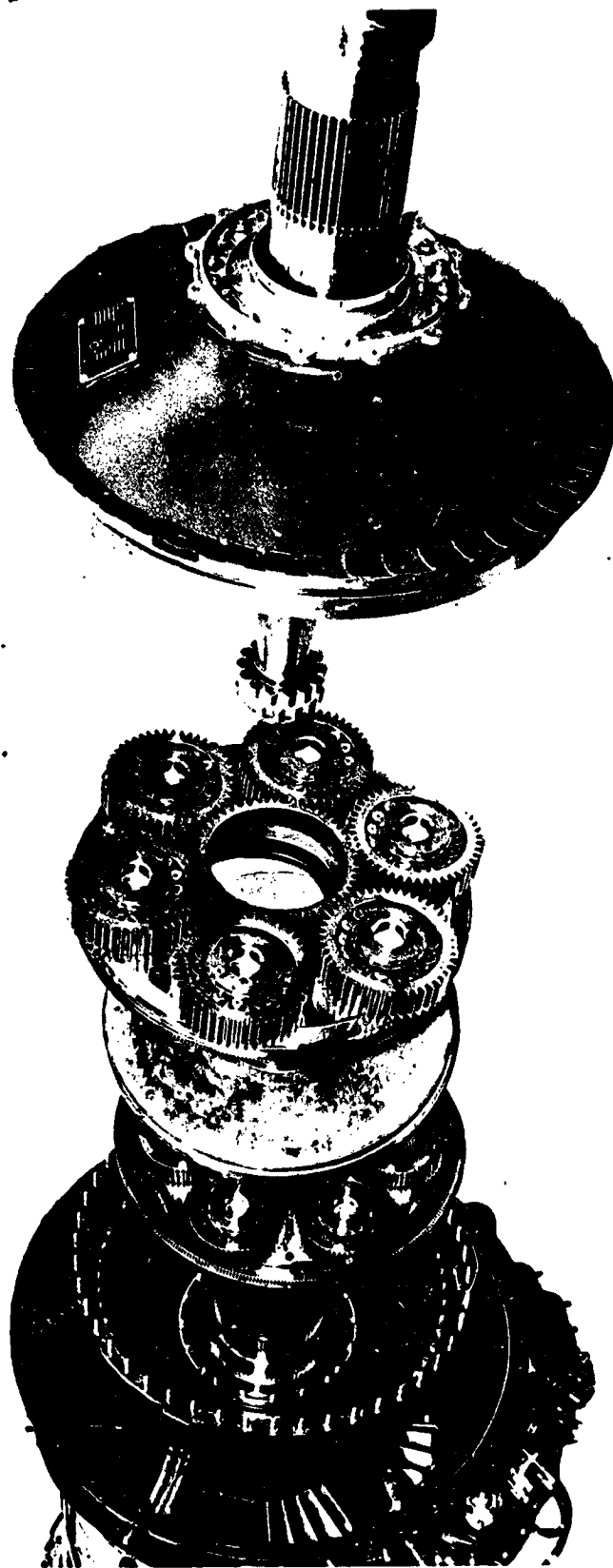
Figure 10-1. YT49-W-1 Reduction Gear.

317

Table 10-I. Design Requirements.

- UTW Gear Ratio = 2.4648
- OTW Gear Ratio = 2.0617
- TBO of 6000 Hours Minimum
- Bearing B1 Life - Over 6000 Hour.
- Minimum Noise
- 36,000 Hour Life
- Min. Efficiency of 99.2% (100% Speed and Power)
- Experimental Test Cycle Capability
- Weight = 77.2 kg (170 lb) for Flight Design

Reduction gear power and speed requirements for the flight duty cycle are presented in Table 10-II.

Table 10-II. Reduction Gear Requirement for Flight Duty Cycle.

Item	Condition	Time %	O.T.W.				U.T.W.				
			Oil In	Power Input		Output Speed	Oil In		Power Input		Output Speed
				KW	HP	rpm	°C	°F	KW	HP	rpm
1	Idle	6.89	*	1290	1721	2586	92	195	990	1326	2100
2	Take Off	2.71		12900	17214	3861	94	200	9900	13256	3143
3	Climb	22.22		10100	13593	3667	99	205	8410	11288	3212
4	Cruise	31.11		7150	9584	3614	110	230	6810	9137	3237
5	Descent	22.22		430	575	1361	130	266	323	433	1084
6	Approach	6.67		7220	9668	3167	98	207	6060	8117	3074
7	Reverse	0.18		12900	17214	3861	91	195	6180	8280	3447
8	Idle	6.89		1290	1721	2586	91	195	990	1326	2100

* To be supplied during detail design

In addition the gearset shall be capable of operating for the alternate experimental duty cycle defined in Table 2-III with the following power levels and speeds:

100% Power = 12,890 kw (17,214 hp) for OTW   100% N_f = 3861 rpm for OTW
100% Power = 9900 kw (13,256 hp) for UTW   100% N_f = 3143 rpm for UTW

10.2.1 Lubrication

Lubrication requirements for the UTW reduction gear for the anticipated duty cycle have been established with MIL-L-23699 oil as shown in Table 10-III.

Operating Condition	Oil Flow		Oil Pressure	
	cm^3/sec	(gpm)	N/m^2	(psi)
1. Idle	113	17.9	152000	22
2. Take Off	151	24.0	276000	40
3. Climb	150	23.8	262000	38
4. Cruise	145	23.0	255000	37
5. Descent	113	17.9	152000	22
6. Approach	139	22.1	234000	34
7. Reverse	148	23.5	262000	38

Table 10-III. Lubrication Requirements for UTW Reduction Gears.

Lubrication requirements for the OTW reduction gears will be supplied prior to completion of detail design.

10.2.2 Envelope

The UTW and OTW reduction gears shall occupy the same envelope. The envelope for the UTW reduction gear is in accordance with Drawing No. 4013157-225, Figure 10-2.

10.2.3 Interfaces

All interfaces shall be in accordance with Drawing No. 4013157-225; the interfaces of OTW and UTW gear sets shall be common (see Figure 10-2).

10.3 GEAR RATIO SELECTION (UTW AND OTW)

General Electric originally proposed a single reduction gear design for both the UTW and OTW engines, having a compromise gear ratio. At NASA request, the approach was modified to individual gearsets having an optimized ratio for each engine.

UTW and OTW gear ratios were selected to match the fan design speeds to the rpm of the F101 low pressure turbine. The turbine design speed limits are as follows:

F101 Takeoff (8000 hrs life)	7710 rpm
Max demonstrated (5 min)	8867 rpm
Calculated disk burst	9405 rpm

The selected QCSEE engine gear ratios, fan rotor speeds, and resulting LPT speeds are tabulated below:

| | | SLS, 33° C (90° F), TO | |
	Gear Ratio	Fan rpm	LPT rpm
UTW	2.4648	3157	7781
OTW	2.0617	3863	7964

The selected gear ratios operate the low pressure turbines at or near their design corrected speed ($N/\sqrt{T_{49}}$) to remain near peak efficiency, while observing the constraints of physical speed capability, and integral number of gear teeth.

10.4 REDUCTION GEAR DESIGN FOR UTW AND OTW

An epicyclic star gear arrangement was chosen to perform the speed reduction and power transmission for both the UTW and OTW engines. The star arrangement uses concentric internal and external gears with a series of idlers (star gears) between them. It is these idlers that distribute the load to many teeth in both input and output members. This permits both members to utilize many teeth to carry the load in lieu of one as is done in a single mesh. This feature greatly reduces the face width required in each gear.

In addition to its compactness, the star gear is the only epicyclic gear train capable of producing the required gear ratios. The idlers rotate about their own axes, unlike planetary gears that rotate around the sun gear as well as their own axes. This feature eliminates the centrifugal field created by rotation about the sun gear thus allowing the star gears to use lighter bearings than in a corresponding planetary gear arrangement. Six star (or idler) gears are used in the UTW engine and eight star gears are used in the OTW engine.

10.4.1 Description of Gear Configuration, UTW and OTW

Both the UTW and OTW arrangements are of similar configuration and are interchangeable as units. Although differences occur in face width, number of idlers, bearings, and carriers, all interfaces are the same and both fit within the same envelope.

320
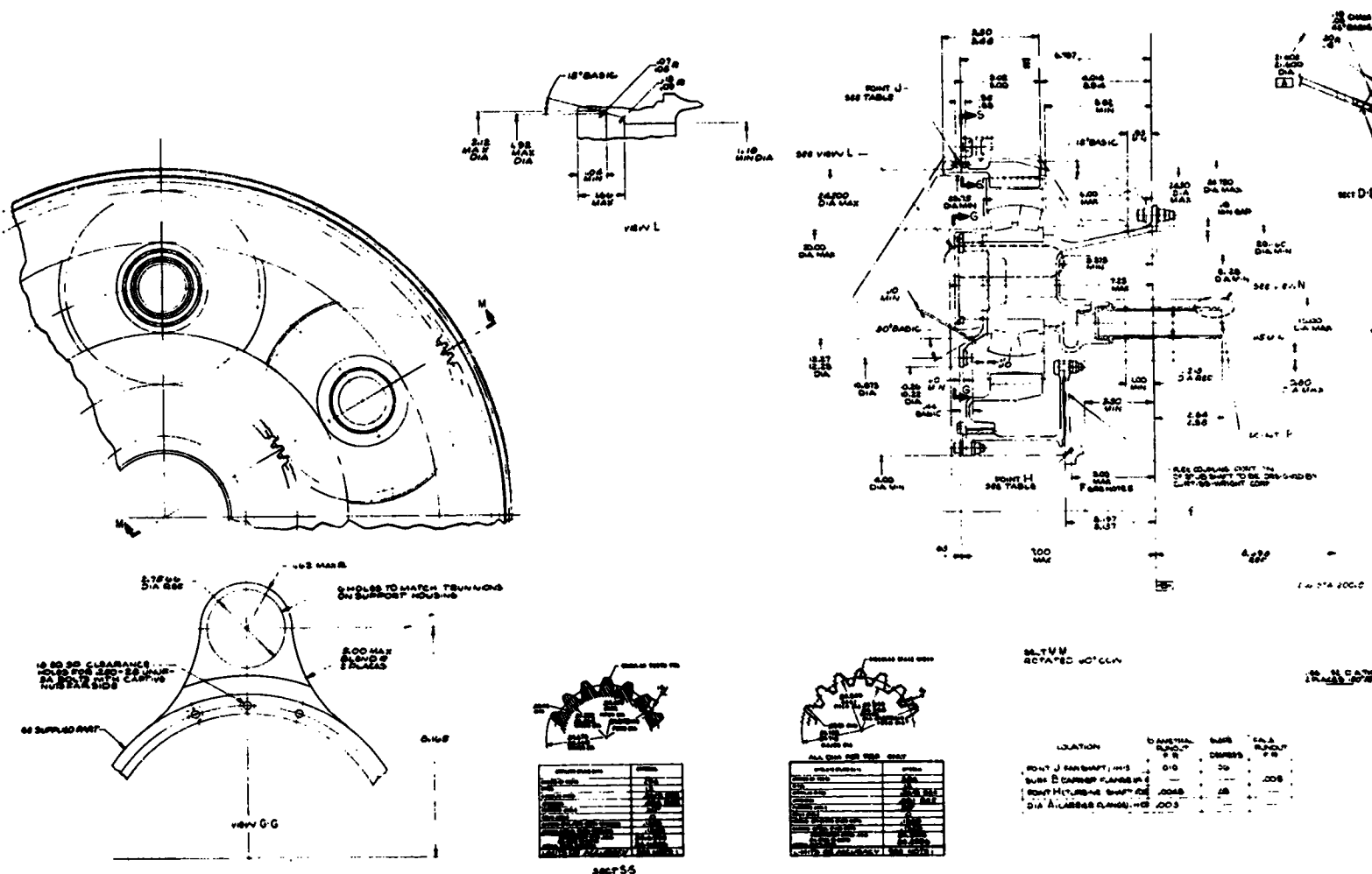
Figure 10-2. UTW Reduction Gea

UTW Reduction Gear Assembly.

321

The following description applies to both the UTW and the OTW gearset.

As shown in Figures 10-3 (UTW), 10-4 (OTW), and 10-5 (typical star arrangement), the power turbine shaft drives the sun gear through a flexible diaphragm and a side-fit flexible spline. The sun gear drives a series of star gears mounted on spherical bearings on a stationary carrier. Each of the star gears meshes with the ring gear which transmits power to the fan shaft through a flexible side-fit spline.

This arrangement provides a modular design that is easily installed without complete engine disassembly.

10.4.2 Design Approach

In order to ensure that all members share the load, certain special features are required.

● **Flexibility** - Both the input and output ends of the system are flexibly mounted to prevent engine deflections from influencing the gear operation.

● **Controlled Gear Deflections** - The rims of the sun and ring gears are contoured so that their deflections match the deflection in the star gears.

● **Self Aligning Star Gears** - Double-row spherical roller bearings are used to allow the star gears to align themselves with the sun and ring gears and thereby minimize the effects of carrier deflections.

● **Nonfactoring Hunting Teeth** - This combination of numbers of teeth results in minimum vibration, low noise, and long life.

● **Modular Concept** - Install and remove as a unit.

10.4.3 Reduction Gear Design Conditions

Table 10-IV shows the key gear and bearing design conditions for the UTW and OTW reduction gears and the related Curtis-Wright YT49 turboprop engine first-stage reduction gears.

Figure 10–3. QCSEE Main Reduction Gear – UTW.
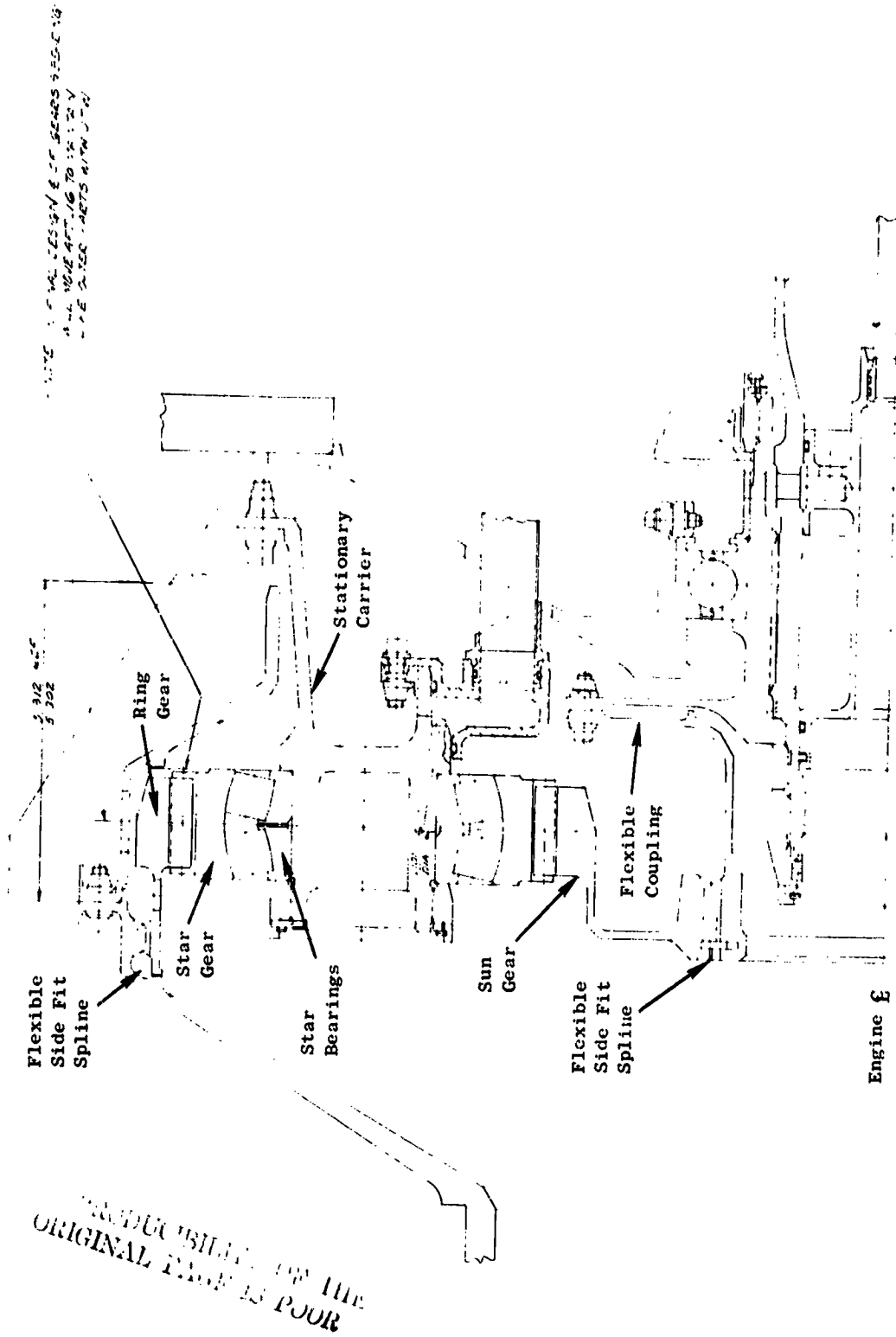
Figure 10-4. Preliminary Design, Main Reduction Gear – OTW.

325
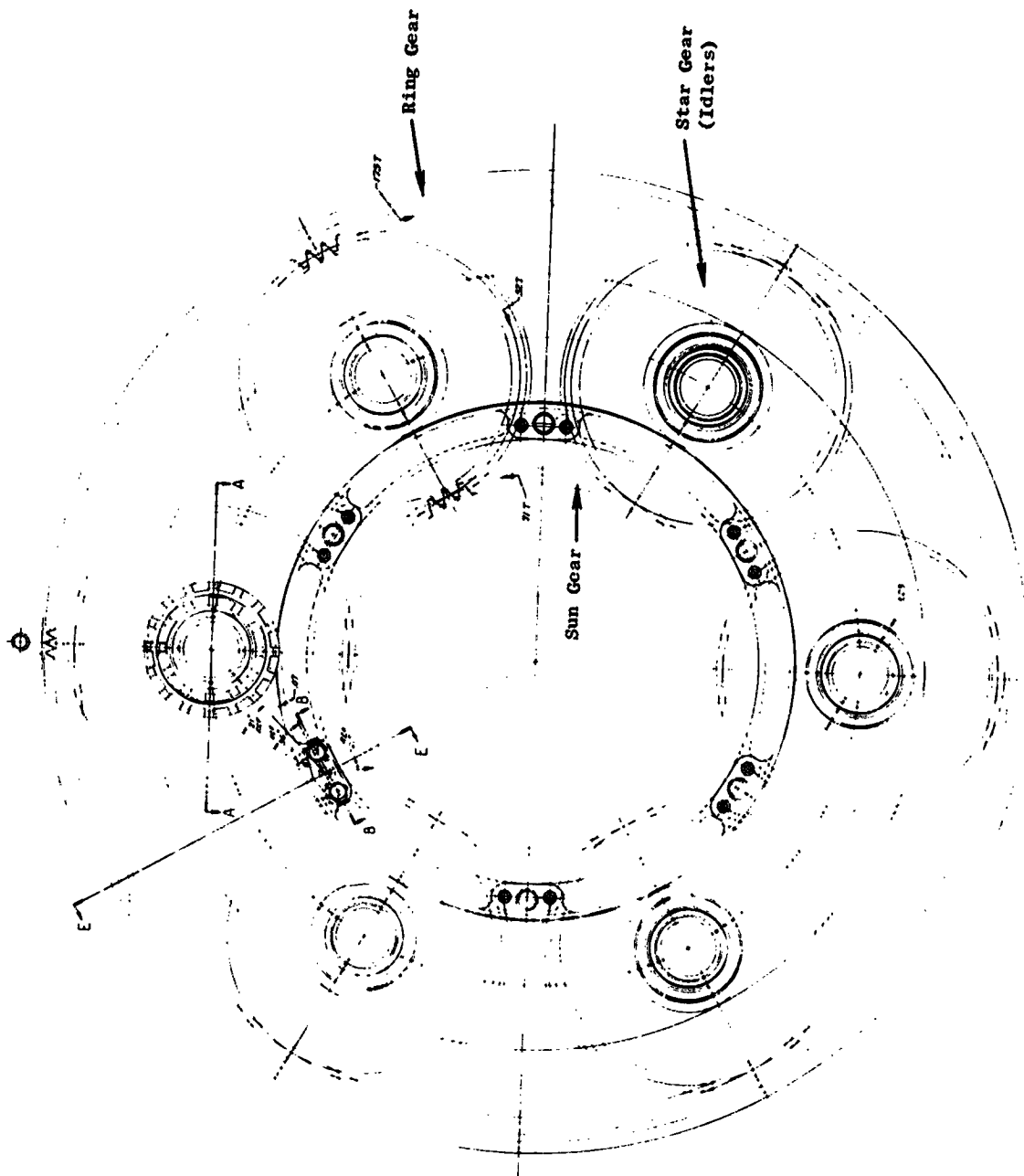
Figure 10-5. Star Arrangement – UTW.

Ring Gear

Star Gear (Idlers)

Sun Gear

Table 10-IV. Reduction Gear Design Conditions.			
Takeoff Condition = 100% Speed, 100% Power			
	UTW	OTW	YT49
● Turbine Power	9,900 kw (13,256 hp)	12,900 kw (17,214 hp)	7,468 kw (10,000 hp)
● Turbine Speed (rpm)	7,747	7,962	7,940
● Pitch Line Velocity	945 m/sec (19,118 fpm)	119.3 m/sec (23,488 fpm)	88.68 m/sec (17,459 fpm)
● Star Gear Speed (rpm)	10,577	14,998	9,500
● Bearing Load	33,900 N (7,627 lb)	26,800 N (6,035 lb)	27,963 N (6,297 lb)

Pitch Line Velocity

To ensure proper lubrication of the high pitch line velocity gears, spraybars are used to distribute oil uniformly across the gear face. The angle of the jet is oriented to obtain maximum oil penetration into the gear teeth. This means of lubricating gears with high pitch line velocity has been successfully applied to several of General Electric's engine accessory gearboxes.

High Speed Bearings

To ensure successful operation of the star gear bearings, a bearing development test program has been initiated. Since the speed of the OTW bearings is higher than that of the UTW bearings, the OTW bearing has the more critical operating conditions.

Low Noise

In order to minimize noise, the following has been incorporated into the design:

- Precision AGMA Quality 13 Gears

- Contact ratio of 2

- Seven plus pitch gears

- 20° pressure angle

- Modified involute at tip and root

- Hunting teeth

This combination results in a minimum of dynamic forces thus reducing both vibration and noise.

10.4.4 Materials

Table 10-V lists the materials used in the gear set. All materials have been used in similar applications before and should present no surprises. All parts will use the same materials in the flight design except the carrier where titanium would be used to reduce weight. Steel will be used in the demonstrator to reduce cost.

Table 10-V. Gear Set Materials.

● Sun Gear	AMS 6265	–	Carburized
● Star Gear	AMS 6265	–	Carburized
● Ring Gear	AMS 6470	–	Nitrided
● Carrier Support	AMS 6415	–	RC32-36
● Bearing			
– Inner Race	AMS 6490	–	CEVM M-50
– Rollers	AMS 6490	–	CEVM M-50
– Cage (Steel)	AMS 6414	–	Silver Plated

10.4.5 Reduction Gear Design

Tables 10-VI and 10-VII show the significant geometry of both the UTW and OTW gearing. Several features should be noted from the tables. The diametral pitch is the minimum consistent with the load to reduce noise. Root radii are kept as large as possible to minimize stress concentration. The contact ratio is maintained at 2. This results in smooth, low-noise, vibration-free gearing.

Contact and Bending Stress

Tables 10-VIII and 10-IX show the calculated gear contact and bending stresses for both the flight cycle and the experimental engine ground test cycle. The American Gear Manufacturers Association (AGMA) method of calculating these stresses was used. Allowable stresses based on AGMA and Curtis-Wright experience are included for reference. It will be noted that the flight stresses are within the limits set by AGMA for infinite life. However, the maximum stress during demonstrator testing exceeds the AGMA limits in some cases. This is acceptable since they are only required for one hour and are within the limits of Curtiss-Wright experience. These stresses have also been checked by General Electric special stress analysis and found within General Electric experience.

328

Table 10-VI. Gear Data UTW.

	Sun	Star	Ring
● No. Teeth	71	52	175
● Diametral Pitch	7.5321	7.5321	7.5321
● Press. Angle (deg)	21	21	21
● Pitch Dia.	23.9 cm (9.4263 in)	17.5 cm (6.9038 in)	59 cm (23.2339 in)
● Center Dist.	20.7 cm (8.165 in)	20.7 cm (8.165 in)	20.7 cm (8.165 in)
● Tooth Thick	0.525 cm (0.2065 in)	0.535 cm (0.2105 in)	0.575 cm (0.2066 in)
● Back Lash	0.01-0.015 cm (0.004-0.006 in)	0.01-0.015 cm (0.004-0.006 in)	0.01-0.015 cm (0.004-0.006 in)
● Root Radius	0.117 cm (0.046 in)	0.135 cm (0.053 in)	0.089 cm (0.035 in)
● Contact Ratio (min)	2.0	2.0	2.0

Table 10-VII. Gear Data OTW.

	Sun	Star	Ring
● No. Teeth	81	43	167
● Diametral Pitch	7.1884	7.1884	7.1884
● Press. Angle (deg)	21	21	21
● Pitch Dia.	28.6 cm (11.2682 in)	15.2 cm (5.9819 in)	59.1 cm (23.2319 in)
● Center Disk	(8.625 in)	(8.625 in)	(8.625 in)
● Tooth Thick.	0.537 cm (0.2116 in)	0.517 cm (0.2254 in)	0.537 cm (0.2116 in)
● Back Lash	0.01-0.015 cm (0.004-0.006 in)	0.01-0.015 cm (0.004-0.600 in)	0.01-0.015 cm (0.004-0.006 in)
● Root Radius	0.125 cm (0.049 in)	0.145 cm (0.057 in)	0.0965 cm (0.038 in)
● Contact Ratio (min)	2.0	2.0	2.0

Table 10-VIII. Gear Contact Stress Data.

		Max. Contact Stress					
		Sun		Star		Ring	
UTW		MN/cm^2	(ksi)	MN/cm^2	(ksi)	MN/cm^2	(ksi)
	Flight Cycle	874	127	867	126	557	81
OTW							
	Flight Cycle	881	128	877	127	614	89
	Test Cycle	1043	151	1038	151	726	105
Allowable Gear Contact Stresses							
	AGMA	1025	149	1025	149	1025	149
	C-W Experience (Mature Design)	1103	160	1103	160	1103	160

Table 10-IX. Gear Bending Stress Data.

		Max. Bending Stress					
		Sun		Star		Ring	
UTW		MN/cm^2	(ksi)	MN/cm^2	(ksi)	MN/cm^2	(ksi)
	Flight Cycle	249	36.1	240	34.9	191	27.7
	Test Cycle	348	50.1	336	48.8	267	38.8
OTW							
	Flight Cycle	218	31.7	195	28.3	169	24.5
	Test Cycle	306	44.3	273	39.6	237	34.3
Allowable Gear Bending Stresses							
	AGMA-10^{10} Cycles	404	58.6	270	39.1	329	47.7
	C-W Experience (Mature Design)	414	60.0	414	60.0	414	60.0

330

Scoring

The AGMA method for determining scoring was used. Table 10-X shows the maximum allowable oil inlet temperatures that are required to prevent scoring for the UTW and OTW experimental engines ground test cycle. A maximum scoring index of 149° C (300° F) was used. Although AGMA scoring data indicate this falls within the medium risk range, both General Electric and Curtiss-Wright experience indicate that scoring does not occur in high quality gearing at this scoring index. Table 10-XI shows the scoring index for the UTW engine with the flight duty cycle.

Gear Efficiency

Table 10-XII shows the calculated gear efficiency at various flight conditions for the UTW reduction gears. These efficiencies meet the requirement of 99.2% efficiency. The OTW data are not shown; however, it also meets the specification criteria. Also shown in this table are the losses attributed to the components and windage. It should be noted that only about half of the losses are in gears while the bearings and windage make up the remainder.

Heat Rejection

Table 10-XIII shows the heat generated due to the inefficiencies in the OTW gears and the effect of this heat on the temperature of the oil supplied to the gearing. These temperature rises plus the maximum allowable inlet temperature do not exceed the capabilities of either MIL-L-7808 or MIL-L-23699 oils.

Table 10-XIV shows the total reduction gear oil flow required for takeoff. It should be noted that 20% additional oil is being supplied for margin. The other operating conditions will receive oil proportional to core speed. Oil flows at the other flight conditions have been checked (Table 10-III) and found adequate.

Bearings

Figure 10-6 shows the bearing chosen to support the star gears. It has the following features:

- Double-Row Spherical Roller Bearing

- Integral Gear and Outer Race

- "Conventional" Inner Race, Roller, and Cage

- Oil Feed Through Center of Inner Race

Table 10-X. Gear Scoring Index for the Experimental Test Cycle.

Ground Test Conditions		UTW				OTW			
		ΔT		Approx. Max.		ΔT		Approx. Max.	
% Fan Speed	% Fan HP	°C	(°F)	°C	(°F)	°C	(°F)	°C	(°F)
105	100	50	91	99	209	66	118	84	182
100	140	66	119	83	181	85	154	64	146
100	130	63	113	86	187	80	145	69	155
100	110	55	100	94	200	71	128	79	172
100	100	52	93	98	207	66	119	83	181
90	80	44	80	105	220	58	104	91	196
75	50	33	59	113	241	42	76	110	224
30	10	12	22	137	278	16	29	134	271
Max. Permissible Scoring Index Tf = 149°C (300°F)									

Table 10-XI. UTW Gear Scoring Index for the Flight Duty Cycle.

Flight Conditions	ΔT		Approx. Max. Allow. Oil In	
	°C	(°F)	°C	(°F)
Idle	10	18	139	281
Takeoff	52	93	98	207
Climb	46	82	104	218
Cruise	39	70	110	230
Descent	5	9	144	291
Approach	36	65	113	235
Reverse	36	64	114	236
Idle	10	18	139	281
Max. Permissible Scoring Index Tf = 149°C (300°F)				

332

Table 10-XII.	Preliminary Overall UTW Reduction Gear Efficiency and Losses for Selected Flight Conditions.						
	Power Losses						
	Bearings		Gears		Churning and Windage		Overall
Condition	kw	(hp)	kw	(hp)	kw	(hp)	Eff. %
Takeoff	9.8	13.17	32.4	43.40	16.2	21.70	99.36
Climb	9.8	13.08	29.2	39.06	14.6	19.53	99.35
Cruise	7.9	10.57	22.6	30.38	9.1	12.15	99.38
Descent	5.3	7.11	9.7	13.02	7.6	3.52	99.36

Table 10-XIII. Preliminary Heat Rejection - OTW.						
					ΔT	
Condition	kw	(hp)	J/sec	Btu/min	°C	(°F)
Takeoff	11100	14,900	94500	5,383	33	58.7
Climb	10020	13,410	87400	4,963	30	54.2
Cruise	7800	10,430	65500	3,721	23	41.7
Descent	10800	14,470	30800	1,750	12	20.8

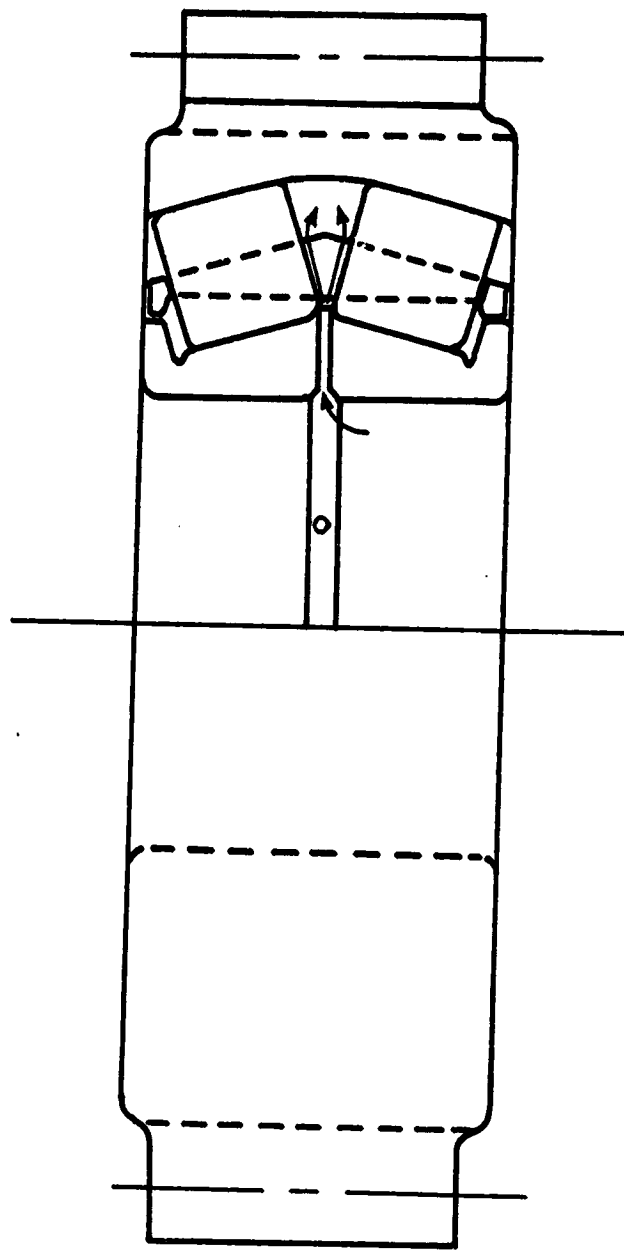| Table 10-XIV. Total Oil Flows for Reduction Gears at Takeoff.				
	UTW		OTW	
	cm^3/sec	(gpm)	cm^3/sec	(gpm)
Required Flow	1260	20	1890	30
Flow to be Supplied	1515	24	2270	36

Figure 10-6. Star Gear Bearings.

This bearing was chosen as the prime candidate based on past experience of similar bearings in the Curtis-Wright YT49 turboprop engine first-stage reduction gears and the recommendations by SKF Corporation. Other bearing manufacturers consulted were Torrington, Food Machinery Corporation, and FAG in Germany. Only SKF and FAG showed interest. SKF was chosen since they meet the Buy American policy.

Table 10-XV shows the average loads and speed used to determine the bearing B_1 life. The results indicate that the bearings can meet requirements of both the flight and experimental duty cycle. However, the OTW bearing does not yet meet the life objective. Investigations are underway to determine what changes can be made to increase the bearing life. Two means of accomplishing the requirement are: (1) determine a more realistic duty cycle, and (2) change the internal geometry of the bearing.

Table 10-XV. Bearing Data.

Type: Double-Row Spherical Roller Bearing
Mat'ls: Outer Race/Gear - AMS 6265 Carburized
Inner Race and Rollers - M-50 Tool Steel

	OTW	UTW
Bearing P/N (SKF)	22,312	22,314
Flight Cycle		
Cubic Mean Load	18,100 N (4,066 lb)	23,500 N (5,295 lb)
Mean Speed (rpm)	11,357	8,573
B_1 Life (hr)	6,384	6,155
Test Engine Cycle		
Cubic Mean Load	20,600 N (4,623 lb)	25,900 N (5,817 lb)
Mean Speed (rpm)	9,406	6,629
B_1 Life (hr)	3,838	5,455

10.5 SUPPORTING DATA

Both the UTW and OTW main reduction gears are further developments of the 1st stage of Curtiss-Wright's YT49 engine. The same personnel that designed that gear system are now designing the QCSEE gear system.

The YT49 engine was designed, built, and tested during the mid 1950's.

Listed below is a summary of the YT49 engine testing:

- Bench Tests   290 hours

- Factory Engine Tests   1960 hours

- Flight Test in B17 and B47
  Flight Test Beds   150 hours

The YT49 was in the same general physical size class as the QCSEE gear sets. The UTW gear set is a small extension of the original YT49 design, while the OTW design extends beyond the UTW. Listed in Table 10-XVI is a comparison of the three gear sets.

Table 10-XVI. Comparison of YT49, UTW, and OTW Gear Sets.			
	YT49	UTW	OTW
● Input Power	7457 kw (10,000 hp)	9900 kw (13,256 hp)	12,850 kw (17,214 hp)
● Gear Ratio	2.7	2.465	2.062
● Sun rpm	8000	7747	7962
● Star rpm	9570	10,577	14,998
● Ring rpm	2992	3143	3862
● Output Torque	23,700 Nm (17,500 lb ft)	29,700 Nm (21,965 lb ft)	31,300 Nm (23,194 lb ft)

From this chart, it can be seen that the difference between the YT49 and the UTW unit are relatively small. In the case of the OTW, it is evident that the star gears are operating at an rpm that is higher than previous experience. As a result of this high speed, a special investigation was made to determine whether or not this should be an area for special testing. This investigation revealed that it is necessary to take into account the roller end loads. This problem has been solved for tapered roller bearings by the Timken Bearing Company and Boeing Vertol jointly by direct lubrication of the roller ends. Listed in Table XVII is a comparison of roller bearings for the YT49, UTW, OTW, and the tapered roller bearing.

Table 10-XVII. Roller Bearing Comparison.				
	Spherical Roller			
	YT49	UTW	OTW	Tapered Roller
DN x 10^6	0.72	0.74	0.90	1.4
rpm	9571	10577	14996	15700
Bore, mm	75	70	60	89

In summary the QCSEE main reduction gears are based on proven concepts (YT49), improved technology (high contact ratio), and conservative design (low stress).

337